Technische Universität München

TUM School of Natural Sciences

Identification of context-specific mRNA translation regulators in human cells by functional genomics

Geraldine Y. V. Rodschinka

Vollständiger Abdruck der von der TUM School of Natural Sciences der Technischen Universität München zur Erlangung des akademischen Grades einer

Doktorin der Naturwissenschaften (Dr. rer. nat.)

genehmigten Dissertation.

Vorsitzende:	Prof. Dr. Cathleen Zeymer
Prüfer der Dissertation:	1. Prof. Dr. Danny Nedialkova
	2. Prof. Peter Murray, Ph.D.
	3. Prof. Dr. Julian Stingele

Die Dissertation wurde am 29.08.2022 bei der Technischen Universität München eingereicht und durch die TUM School of Natural Sciences am 24.10.2022 angenommen.

Table of contents

Abstract

Protein synthesis must be tightly regulated to meet cellular needs and to avoid the production of aberrant polypeptides. Genetic defects that compromise the function of the mRNA translation machinery often leads to human diseases with tissue-specific pathology. To begin defining the underlying mechanisms, we established an experimental platform for functional genomics by inducible CRISPRi in human induced pluripotent stem cells (hiPSC) during and after their differentiation into neuronal and cardiac lineages, as well as in the commonly used HEK293 human cell line. By targeting 262 human genes with functions related to mRNA translation in pooled screens, we find that nearly all ribosomal proteins and core translation initiation and elongation factors are essential in all these cellular contexts. By contrast, the loss of ribosome recycling and translation-dependent quality control factors leads to phenotypes that are strongly context-dependent. Silencing subsets of these genes is detrimental in specific cell types but advantageous in others, particularly during cell state transitions. The depletion of proteins that detect and rescue stalled ribosomes elicited the largest phenotypic variation in our screens. This selective essentiality does not correlate with their abundance in cells or the readthrough efficiency of model stalling substrates upon their depletion. Instead, we find that their loss triggers context-specific cellular response pathways. Profiling ribosome occupancy in cells that are sensitive to the perturbed expression of ribosome rescue factors enabled us to identify some of their endogenous human mRNA substrates. Our findings underscore the importance of cellular context for deciphering the molecular mechanisms of translational control in metazoans, and provide a framework for investigating these mechanisms in physiologically relevant human cell culture systems.

Chapter 1 – Introduction and Background

1.1. The protein homeostasis network regulates protein abundance and integrity

Gene expression has to be tightly regulated to ensure cellular function. Initially, gene expression was thought to be mainly regulated through epigenetic mechanisms and gene transcription on the desoxyribonucleic acid (DNA) level. However, over the last decades it has become clear that messenger ribonucleic acid (mRNA) translation is yet another major hub that has to be orchestrated to produce functional proteins[1]. mRNA levels correlate only poorly with protein abundance and can be dynamically adjusted through translational and post-translational mechanisms to fine-tune proteomes in different cell contexts[2-10].

The human genome comprises ~25,000 predicted protein-coding genes, of which roughly 10,000 to 13,000 are expressed in an average cell[11,12]. Several gene sets are described as “housekeeping“, meaning they have a basic conserved function, which is essential to maintain cell viability. Across different cell types, the levels of “housekeeping“ proteins can vary dramatically, and additional distinct protein species have to be expressed[13]. Protein quantity as well as functionality have to be fine-tuned to the needs of specific cell types to enable their specialized functions[13,14]. Therefore, the question arises on how cells with distinct proteomic needs achieve regulation and maintenance of functional protein pools in multicellular organisms.

Protein biogenesis and breakdown are tightly regulated in the highly complex protein homeostasis (proteostasis) network (**Figure 1.1**)[15,16], which is pivotal for maintaining proteome integrity and cellular health[17]. The malfunction of the proteostasis network or its decline during aging is linked to the build-up of misfolded proteins in neurodegenerative diseases such as Alzheimer’s or Parkinson‘s Disease[18-20]. The proteostasis network consists of macromolecular machineries for protein synthesis, co- and post-translational protein folding, and regulated protein disposal via degradation[21]. All branches are highly interconnected and overseen by ~2000 core factors in human cells[17,22,23].

In the first steps of a protein's life, an mRNA is translated into a nascent polypeptide chain, which has further to be folded and often also targeted its correct location in the cell. These processes involve the core mRNA translation machinery, as well as ribosome-associated complexes that facilitate co-translational folding and organelle targeting. Nascent polypeptide chains can begin to form secondary structures in the ribosomal exit tunnel[24,25] and are further

processed and assembled co-translationally after they emerge from the ribosome[26]. For many proteins, it is anticipated that final folding only takes place after the nascent polypeptide chain is released and with the help of molecular chaperones[16]. The number of chaperones is highly variable between organisms and developed through functional and compartmental specialization. In humans both, co- and post-translational folding, are facilitated through 88 chaperones and 244 regulatory co-chaperones that prevent and correct misfolding events[21,27,28]. In comparison, yeast only encodes 64 and drosophila 219 chaperones and co-chaperones[29,30].

In multicellular organisms, protein levels have to be carefully orchestrated on a cell-to-cell basis depending on the set of genes that are expressed, and adapted to stimuli from other cells or the environment[31], which is achieved by regulating protein synthesis and degradation. Degradation is facilitated through two major systems: the ubiquitin-proteasome system (UPS) and the autophagy-lysosomal pathway[32-35]. Together, they assure degradation and recycling of proteins that are misfolded or no longer needed by the cell.

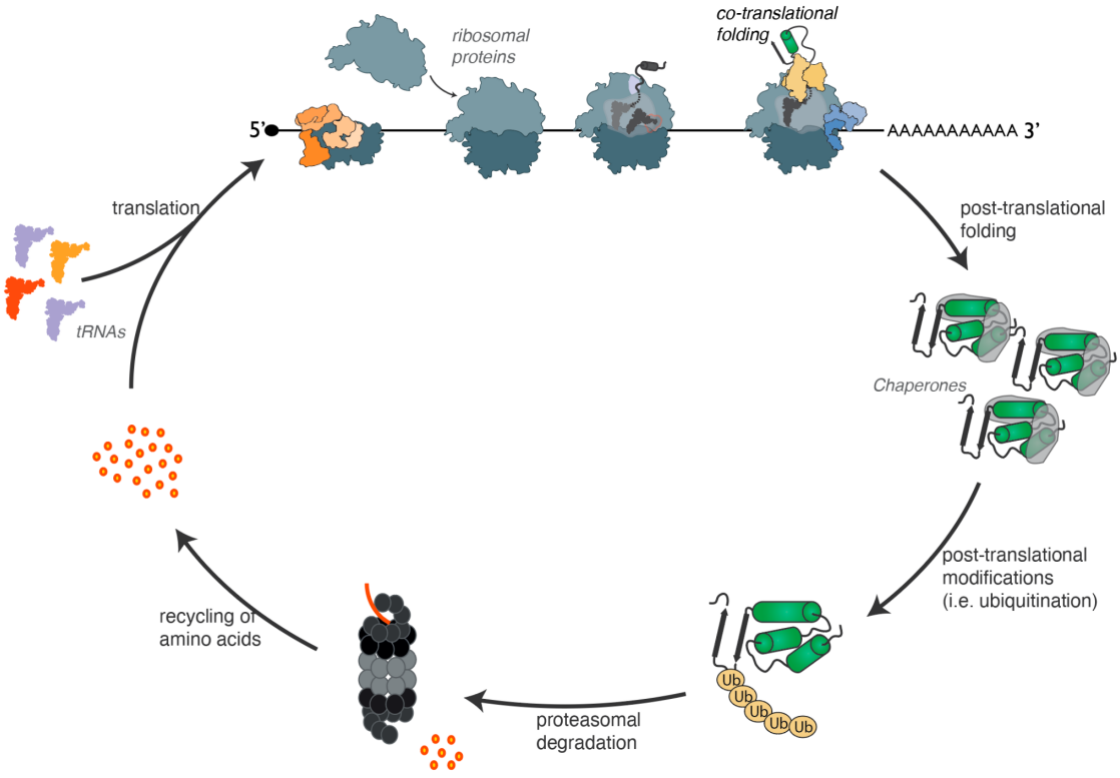

Figure 1.1. ***Graphical depiction of the proteostasis network.***
The proteostasis network coordinates protein synthesis, folding and degradation to establish and maintain a balanced and functional proteomes in cells. The ribosome translates mRNA into a polypeptide chain, which is co- and post-translationally folded with the help of molecular chaperones. Faulty or unneeded proteins are marked with ubiquitin (Ub) for proteasomal degradation and amino acids are recycled for protein synthesis.

Most proteins in eukaryotic cells are degraded via the UPS[36,37]. A prerequisite for this pathway is the ubiquitination of substrates, which is mediated by a cascade of ubiquitin-activating (E1) enzymes, ubiquitin-conjugating (E2) enzymes, and ubiquitin ligases (E3)[38,39]. The UPS core component, the multi-subunit 28S proteasome, then recognizes ubiquitylated proteins, unfolds them, and degrades them[40-43]. For this, the UPS depends on chaperones that enable the unfolding of aggregated proteins to enable their degradation[44]. In case the UPS fails to degrade ubiquitylated proteins, these proteins can be targeted to the autophagy- lysosomal pathway in a chaperone-dependent manner[45-47]. In contrast to the UPS, the autophagy-lysosomal pathway can directly engulf protein aggregates[48]. Although these two pathways degrade distinct protein substrates, they are also highly interdependent[34,49].

Taken together, the proteostasis network is a highly flexible and adaptive system, which enables the cell to adapt protein levels during development and stress conditions and by that ensures cellular fitness. Although the major players of the proteostasis network are fairly well characterized, less is known about how cells regulate and maintain proteostasis as an interactive network and balance context-specific needs in different cell types and tissues.

1.2. The core mRNA translation machinery

1.2.1. The ribosome

A protein's life begins at the ribosome, the first major hub of the proteostasis network (**Figure 1.2**). Ribosomes are defined as "housekeeping" molecular machines that are highly conserved across all organisms, sharing above 60% coding sequence homology among eukaryotes[50,51]. The mammalian ribosome is composed of four ribosomal RNAs (rRNAs) and 80 ribosomal proteins (80S ribosome), which are subdivided into ribosomal proteins of the small (40S) subunit (RPS) and the large (60S) subunit (RPL).

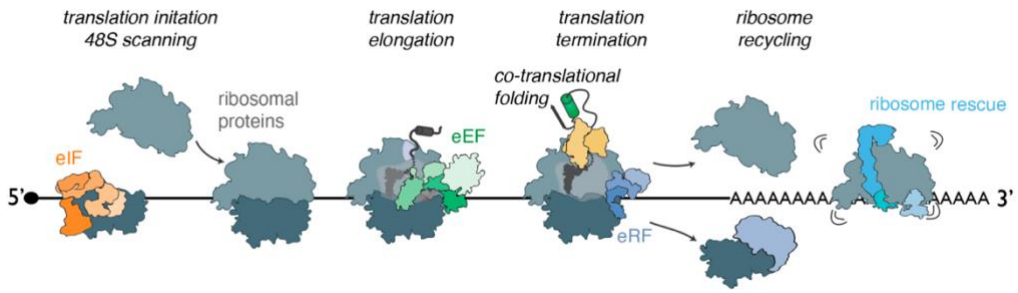

Figure 1.2. Graphical depiction of the major steps of mRNA translation in eukaryotic cells. mRNA translation begins with the binding of the 48S preinitiation complex to the mRNA. The 48S complex consists of translation initiation factors (eIF), the initiator tRNA-iMET-CAT and the 40S ribosomal subunit. The pre-initiation complex scans along the mRNA until it recognizes a AUG start codon and assembles the 80S ribosome for mRNA translation. During translation elongation, elongation factors (eEF) transport tRNAs to the ribosomal A site, a peptide bond is formed and the ribosome moves one codon further. At the same time, ribosome-associated chaperones assist the co-translational folding of nascent chains. When translating ribosomes encounter a stop codon, translation termination factors (eRF) release the nascent chain and recycle the ribosomal subunits. When ribosomes stall on faulty mRNAs, ribosome rescue factors can recognize and rescue them and target the nascent polypeptide chains and mRNA for degradation.

Ribosomes produce tens of millions of protein molecules per eukaryotic cell[52] with an average mRNA decoding speed of six amino acids per second[53]. The mRNA is decoded by small transfer RNA (tRNA) molecules[54], which pair with their cognate anticodon to mRNA nucleotide triplets and deliver amino acids to the ribosome for their incorporation into the polypeptide chain[55,56]. There are three binding sites for tRNA on the ribosome: the aminoacyl tRNA (A site), the peptidyl tRNA (P site) and deacylated tRNA (exit/ E site)[57,58]. After peptide bond formation in the peptidyl-transferase center, the nascent polypeptide chain is pushed through the ribosomal exit tunnel, which can accommodate ~40 amino acids and where small protein domains can already begin to fold[59]. Nascent chains continue to fold co-translationally upon their emergence from ribosomes in a process that is modulated by ribosome surface proteins and ribosome-associated chaperones in a translation rate-dependent manner[60].

1.2.2. Translation initiation

Translation initiation is the major hub for regulating protein synthesis. In eukaryotes, this process requires at least 12 core proteins (initiation factors, eIFs) that form multi-subunit protein assemblies[61,62]. Translation initiation is highly conserved from yeast to humans, which has enabled the identification of the key regulatory aspects of this pathway using budding yeast as a model system[63]. In a first step, eIF2B, a guanine nucleotide exchange factor, activates eIF2-GDP to eIF2-GTP so it can form a complex with the tRNA-iMet-CAT[64,65]. The 43S pre-initiation complex (PIC) then forms by assembling the small ribosomal subunit together with eIF5, eIF3, eIF1 and eIF1A[66-68]. At the mRNA, the eIF4F complex – consisting of eIF4E, eIF4G and eIF4A – binds at the 5´ 7-methylguanosine cap (m7G cap) and the poly(A) binding protein (PABP) at the 3´ poly(A) end of the same mRNA through eIF4G[69]. eIF4A – an RNA helicase – unwinds the mRNA so that eIF1 and eIF1A, that are bound to the P and A site of the 40S subunit, open up a space to facilitate 43S PIC binding close to the m7G cap and by that forming the 48S PIC[70,71]. When the 48S PIC is bound to an mRNA, it "scans" along the 5´untranslated region (UTR) for an initiation codon (AUG) in an ATP-dependent manner (**Figure 1.3**). Generally, a scanning 48S PIC recognizes the first AUG that it encounters. Start codon recognition is enhanced by the presence of a Kozak consensus sequence (GCCPuCCAUGG)[69,72]. AUG codons lacking a Kozak sequence can sometimes be skipped by "leaky scanning", which is used as a mechanisms for autoregulation function[73-76] or the production of protein forms with different organellar localization sequences (**Figure 1.3**)[77]. Upon AUG recognition, the 48S PIC undergoes conformational changes to a "closed" state. The tRNA-iMet-CAT binds the PIC P site and halts the scanning process for eIF2-GTP hydrolysis in an eIF5-dependent manner[78,79]. eIF2-GDP becomes destabilized and released from the complex, promoting the recruitment of eIF5B-GTP and the 60S ribosomal subunit[80]. Further GTP hydrolysis and release of eIF5B-GDP facilitates 80S ribosome formation and is the rate-limiting step for transitioning from translation intiation to translation elongation[81].

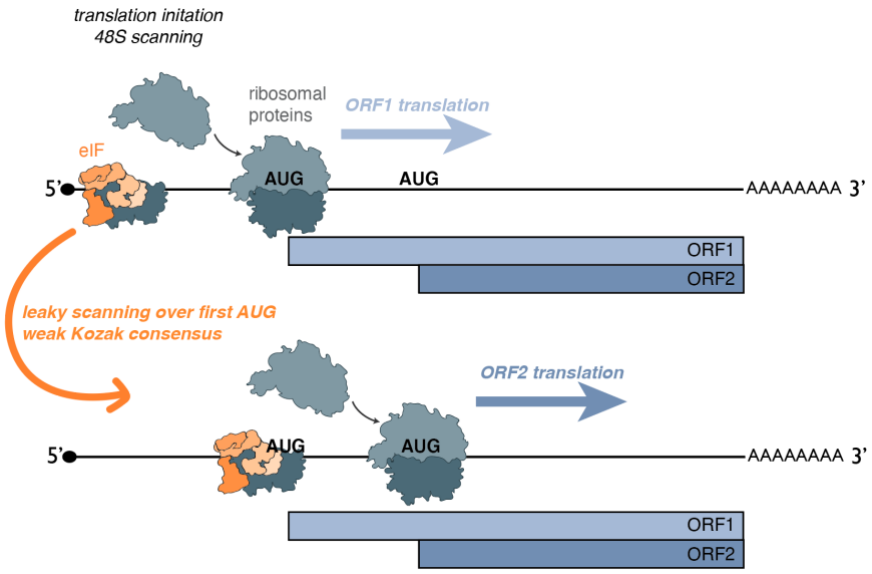

Figure 1.3. Ribosomes can skip start codons through leaky scanning.
The 48S preinitiation complex scans along the mRNA until it recognizes a start codon and assembles the 80S ribosome, which can start translating the mRNA. When the sequence surrounding an AUG codon is weakly matched to the Kozak consensus the 48S PICcan omit it and continues mRNA scanning until it encounters another start codon. This allows the translation of alternative open reading frames (ORF).

1.2.3. Translation elongation

Upon release of eIF5B-GDP from the 80S ribosome, translation elongation factors (eEFs) deliver the cognate elongating tRNA to the empty A site of the ribosome[81]. eEF1A is activated upon GTP binding and forms a ternary complex with an aminoacyl-tRNA that can bind an empty A site. Upon correct base pairing between the aminoacyl-tRNA and the A-site codon, eEF1A-bound GTP is hydrolysed, and eEF1A is released from the ribosome[82-84]. The peptidyl and aminoacyl tRNAs are positioned in the peptidyl transferase center with the help of eIF5A. The peptide bond is formed by transferring the nascent chain form the peptidyl-tRNA to the A site aminoacyl tRNA, and repositioning of the ribosome[85-90]. eEF2-GTP then binds to the A site and facilitates tRNA translocation to the canonical E and P sites through GTP hydrolysis[91-94]. These steps are accompanied by large conformational rearrangements and intersubunit rotation. There are three distinct conformational states of the ribosome during this process: an non-rotated, pre-translocation one, where both the A site and P site are occupied by tRNA, a hybrid one, in which the peptide bond is formed and the deacylated peptidyl tRNA adopts a “hybrid” a P/E state, and a rotated, post-translocation state, where the aminoacyl tRNA is located to the P site[95,96].

1.2.4. Translation termination and ribosome subunit recycling

Two structurally conserved GTPases are orchestrating translation: eEF1A and eRF3, which deliver either aminoacyl tRNAs or eRF1 to the A site[97,98]. Both GTPases have a highly similar structure and function, however their function is not redundant[99]. During translation elongation eEF1A delivers cognate aminoacyl tRNAs to the empty A site, which is moved to the peptidyl transferase center by GTP hydrolysis and a new peptide bond is formed between the nascent polypeptide chain and the new delivered amino acid[100]. During translation termination, any of the three stop codons (UAA, UAG, UGA) is recognized by the eRF3-GTP-eRF1 complex[83,101]. eRF1 resembles a tRNA, which can perfectly accommodate into the A site pocked of the ribosome[102]. This process is facilitated through eRF3 GTPase activity and leads to the release of the nascent polypeptide chain in the P site[103-105].

After release of the nascent polypeptide chain, the ribosome subunits have to be split, and the tRNA and mRNA have to be removed from the 40S subunit. Ribosome splitting can be achieved through ABCE1 interaction with the eRF1/eRF3 complex[102,106]. Upon eRF1 binding in the A site, ABCE1 hydrolyses ATP, which results in structural changes that lead to 80S destabilization and subunit dissociation[107-109].

There are several redundant mechanisms for the recycling of the mRNA and tRNA from the split 40S subunit. One of these is via eIF3 binding to the 40S subunit and recruitment of eIF3j, eIF1 and eIF1A[66,110]. In absence of an initiator codon in the P site, mRNA-40S binding is destabilized and the mRNA can dissociate[111]. Alternatively, recycling can be mediated through eIF2D or the DENR/MCTS1 complex, which contains homologous domains of eIF2D[112-115]. It has been proposed that the SUI1 domain of eIF2D/ DENR interferes with the anticodon stem loop in the P site tRNA and by that destabilizes ribosome binding[115].

1.2.5. Translation re-initiation

Nearly 50% of human mRNAs contain a regulatory element called an upstream open reading frame (uORF)[116]. uORFs precede the main ORF of an mRNA and were identified to regulate translation of specific mRNA subsets exemplified in human cells by ATF4[117], a major stress-induced transcription factor[118,119]. uORFs can be read over by leaky ribosome scanning from 5’ to 3’ (**Figure 1.3**) or translated into short polypeptides following 80S ribosome assembly (**Figure 1.4**)[120,121]. Translation re-initiation is thought to be a major process to regulate alternative ORF translation and is highly dependent on ribosome recycling progression and

ORF length[122-124]. In the case of uORF translation, nascent chain synthesis is terminated and the polypeptide chain released. The 40S ribosomal subunit, however, stays associated with the mRNA and scans it for a subsequent start codon downstream (**Figure 1.4**). Re-initiation was hypothesized to be dependent on eIF4F binding[125], as well as on the proteins of the 43S pre-initiation complex[126,127]. Ribosome scanning is facilitated by eIF4F, and re-initiates translation upon encountering a start codon. Alternatively, the non-canonical translation factor eIF2D was hypothesized to bind and stabilize the 40S subunit on the mRNA by sterically hindering eIF1, eIF1A, eIF2, eIF3, and tRNA-iMET-CAT binding to the 40S subunit surface (**Figure 1.4**)[126]. The eIF2D-40S complex can scan along the mRNA and is released to promote downstream re-initiation at the AUG start codon[120,128].

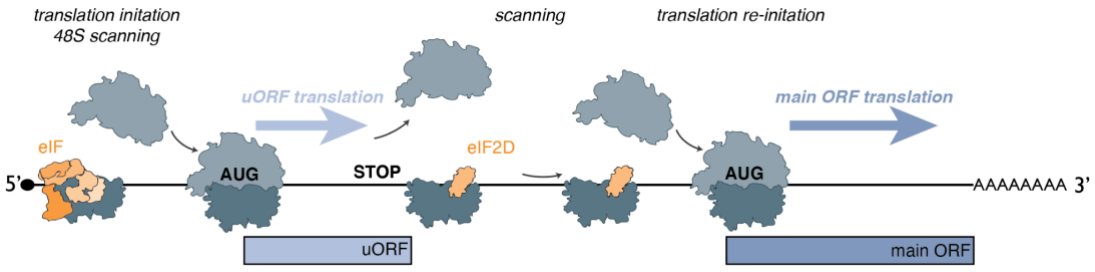

Figure 1.4. Ribosomes can re-initiate translation after uORF translation.
The 48S pre-initiation complex scans the mRNA and starts translation of an upstream open reading frame (uORF). Translation is terminated at the stop codon and the nascent chain and 60S ribosome are dissociated from the mRNA, whereas the 40S remains bound to the mRNA. Translation initiation factor eIF2D (or 43S PIC or DENR/MCTS1) binds the 40S subunit for stabilization and the complex starts scanning the mRNA for a second AUG start codon that encodes the main ORF, where translation can be re-initiated.

DENR/ MCTS1 is a complex that combines the structural and functional domains of the non-canonical translation factor eIF2D[112]. It was recently shown to promote ribosome recycling in yeast[129,130] and additional re-initiation events in human cells[128]. The best described mRNA targets of DENR/MCTS1- translation re-initiation are oncogenes and ATF4[117]. Translation re-initiation via this mechanism, however, seems to be highly specific for uORFs that consist only of a start codon followed by a stop codon[120,128] or very short and defined codons containing the GCG motif in particular. In addition, ribosomes lacking translation factors at the stop codon were shown to be preferentially recycled by DENR/ MCTS1 rather than prepared for translation re-initiation[117,131]. Recent studies in yeast using 40S ribosome profiling showed that deletion of the yeast homologs of DENR or MCTS1 leads to increased ribosome stalling around the stop codon. This suggests that stalled ribosomes are not recycled properly anymore, which can eventually lead to translation re-initiation[130]. It therefore remains unclear whether the DENR/ MCTS1 complex predominantly recycles terminating ribosomes or stimulates translation re-initiation.

1.2.6. Cell context-specific regulation of mRNA translation

Protein synthesis is a fundamental process to maintain cell homeostasis and has to be fine-tuned during organismal development. Several studies showed that the correlation between mRNA and protein levels decreases during development, suggesting a large contribution of mRNA translation regulation to determining protein abundance[3,5]. However, our understanding on how protein synthesis is differentially regulated in stem cells and during development to maintain vital homeostasis is limited.

One suggested mechanism is the formation of "specialized ribosomes"[132]. Such ribosomes are proposed to originate through heterogeneous composition of ribosomal proteins, rRNA, or post-translational modifications of either component and by that regulate translation of specific mRNA subsets in different cellular contexts. This hypothesis arose from several observations, such as the tissue-specific pathology of diseases linked to mutations in ribosomal protein genes[133] and the differential expression profiles of ribosomal protein paralogs in different tissues[134,135]. For instance, RPL3L is highly expressed in human heart and skeletal muscle, which goes along with a decrease in the mRNA levels of its paralog RPL3[134]. In another well-studied example, RPL22 directly destabilizes RPL22L1 transcripts, which are important for hematopoietic development in mice[136,137]. In both cases, the knockdown of one gene can be rescued through translational upregulation of its paralog in many but not all tissues[138,139].

Translation initiation is also mediated by several multi-subunit complexes. A subset of these may have specialized functions during development. The mammalian eIF4F complex, which recruits the 43S PIC to the 5' cap of mRNAs, is highly conserved and consists of three components: eIF4E, eIF4A, and eIF4G. In mammals, each of these components has several paralogs, which can be incorporated into eIF4F only in distinct combinations[140,141]. Some paralogs are expressed ubiquitously in all tissues, whereas others exhibit cell types-specific expression patterns[141,142]. eIF4G3, for example, was shown to be crucial in mouse gametogenesis and tissue-specific chaperone expression[143]. Furthermore, some translation initiation factor family members have regulatory functions in cells[141,142]. One example is eIF4E2, which interacts with ribosome quality control factors to selectively reduce translation initiation on faulty mRNAs[144].

Taken together, these data demonstrate that components of the mRNA translation machinery can be differentially expressed among cell types or their loss can lead to context-specific phenotypes[132]. However, the underlying regulatory mechanisms and the molecular events driving this differential importance remain poorly understood.

1.3. Ribosome-associated mRNA and protein quality control

1.3.1. mRNA surveillance pathways

mRNAs undergo several checkpoints during protein synthesis and are marked for degradation in case of abnormalities. mRNA surveillance mechanisms can be initiated by three main scenarios: when ribosomes are stalled during elongation (no-go decay, NGD); when mRNAs lack a stop codon (nonstop decay, NSD); or when the ribosome encounters a premature stop codon (nonsense-mediated decay, NMD, **Figure 1.5**)[145].

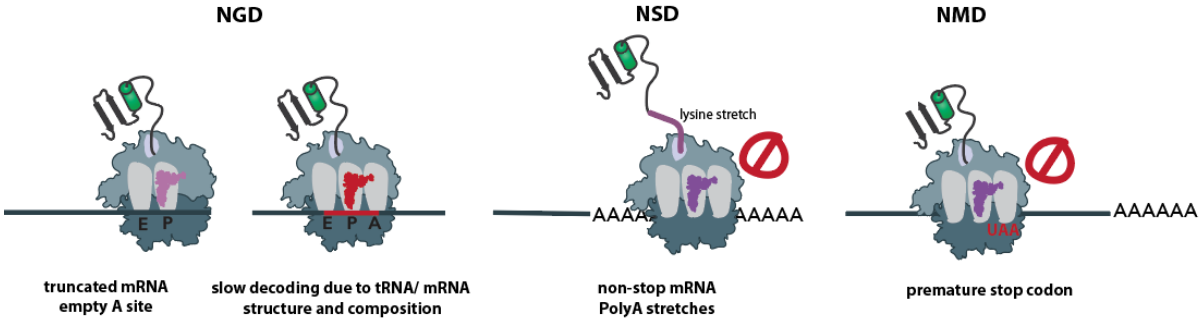

Figure 1.5. Defective mRNAs and slow elongation can cause ribosome stalling and induce mRNA and protein surveillance mechanisms.
Ribosomes slow down translation and possibly arrest upon encountering truncated mRNAs or poly-lysine stretches and highly charged and repetitive sequences. tRNA availability and mRNA secondary structures can also influence decoding speed.

NGD is induced through prolonged ribosome stalling on the mRNA during translation elongation[146,147]. This can be triggered by stable mRNA secondary structure, GC-rich and repetitive sequences on the mRNA, or slow delivery of cognate tRNAs. By contrast, NSD is induced by ribosomes stalled at the 3‘ end of an mRNA, which can result from a missing stop codon or premature mRNA polyadenylation[148,149]. When the ribosomal A site is empty, as in NSD, the HBS1L/PELO complex can be recruited[146,150,151]. PELO, a structural homolog of eRF3, can be positioned in the A site by HBS1L GTPase activity, recruit the ABCE1 complex and disassemble the ribosomal subunits[98,147,152]. Since the HBS1L/PELO complex cannot hydrolyse the peptidyl-tRNA, it remains bound to the 60S subunit and requires the RQC pathway for disassembly (**Figure 1.6**)[153,154]. Initially, yeast factors Hbs1 and Dom34 (yeast homologs of HBS1L and PELO,) were identified by structural comparisons to ribosome termination factors and were primarily linked to mRNA decay pathways in NGD reporter

expression experiments[146,155]. Shortly after, they were identified as ribosome dissociating components during truncated mRNA degradation in dependency of an empty A site in yeast[147,152,156] and mammals[98]. Deletion of Hbs1 or Dom34 does not alter yeast growth[157]. In contrast, deletion of mouse Hbs1L or Pelo is embryonically lethal in mice [158,159].

After ribosome disassembly, mRNA degradation factors are recruited to the faulty mRNA: the DCP2 decapping protein[160], the XRN1 5'-3' exoribonuclease[161,162], the deadenylases PARN and CCR4[163], and the exosome[162,164-167].

Unlike NGD or NSD, NMD is directly linked to the classical translation termination pathway, NMD relies on eRF1 and eRF3 through UPF1[168-170]. NMD is triggered when the ribosome encounters a stop codon that is not efficiently terminating translation[171]. Termination and NMD induction hereby are dependent on stimulating factors and their presence nearby the stop codon. Typically, NMD is triggered in the first round of translation at premature termination codons, where translation termination and/ or re-initiation factors are not available and termination is delayed. One such stimulating factor is a missing connection of termination factor eRF3 with PABPC1. Normally, PABPC1 enhances termination through increased eRF1 and eRF3 recruitment, whereas its absence can trigger NMD[164,172-176]. For this, UPF3b is recruited to the ribosome, followed by UPF2 and UPF1 [177-179], and eRF3, which is positioned in the A site of the ribosome[170]. SMG1, which is regulated through its interaction partners SMG8 and SMG9, phosphorylates UPF1 and causes a conformational activation[180-185]. By that, the ribosomal subunits are disassembled and downstream proteins are removed from the mRNA [186-190]. This allows the recruitment of the SMG5/SMG7/SMG6 complex, which leads to UPF1 dephosphorylation and mRNA degradation through the endonucleolytic activity of SMG6 or the recruitment of DCP2, XRN1, PARN and CCR4 and the SKI-exosome complex via SMG5/SMG7[191]. NMD can also be induced by the presence the exon junction complex (EJC) more than 50 to 55 nt downstream of a premature stop codon[192-195]. In this scenario, SMG6 mediates NMD activity through interaction with EJC[196-198].

1.3.2. Ribosome-associated quality control pathways

Aberrant proteins are mostly misfolded proteins, proteins that have lost their normal function or acquired additional abnormal functions. This can result from mutations, errors during gene transcription, chemical damage, or imbalanced expression of interaction partners. Their accumulation in cells can cause an imbalance of the proteostasis network. Eukaryotic cells have a variety of specialized machineries to detect and degrade faulty proteins[199]. In order to

avoid accumulation and aggregation of toxic polypeptides produced from aberrant mRNAs, several quality control pathways rescue stalled ribosomes and degrade the faulty mRNA and nascent protein chains.

Ribosomes can slow down or even stall while translating truncated mRNA or "hard-to-decode" codon stretches (**Figure 1.5**)[200-202]. A stalled ribosome may cause a ribosome collision if a second ribosome that is decoding the same mRNA catches up. These two ribosomes form so-called collided disomes. Polybasic amino acid stretches or combinations of specific codons decoded by rare tRNAs can cause ribosomal stalling[202,203]. One well established motif is composed of two or more of the rare arginine codon CGA, which is decoded via wobble pairing by a rare tRNA and causes ribosome stalling in yeast[204]. However, CGA codon stretches do not cause translational arrest in mammalian cells because the matching tRNAs are not limiting[205]. So far, only two very specific sequence stretches have been shown to cause ribosome stalling in mammalian cells: poly-lysine stretches encoded by AAA, which ribosomes can encounter in prematurely polyadenylated mRNAs[202,205], and a 26 amino-acid stretch in the "unspliced" XBP1 (XBP1-u) protein, which induces ribosome arrest to enable XBP1 mRNA recruitment to the endoplasmic reticulum (ER) stress[206,207]. This is necessary for IRE1-mediated XBP1 mRNA splicing as part of the unfolded protein response to ER stress.

The pathway that targets nascent polypeptide chains from stalled ribosomes for degradation is termed ribosome-associated quality control (RQC) pathway and is closely linked to mRNA surveillance mechanisms (**Figure 1.6**). The RQC pathway is conserved between yeast and humans and was identified by using a genome-wide loss of function screen in yeast[208,209]. A prerequisite for RQC pathway initiation is a 60S subunit that still contains a nascent chain and a peptidyl tRNA[98,152]. In human cells, the RQC complex recognizes this 60S subunit through NEMF and recruits LTN1[209-212], an E3 ligase that ubiquitylates the nascent polypeptide chain[213]. Subsequently, VCP and its co-factor ANKZF1 bind to the complex, hydrolyse the P site tRNA, and release the nascent polypeptide chain[208,209,214,215]. The ubiquitylated nascent chain is then degraded by the UPS[214]. In case translation fails at an early stage, so that the nascent chain is too short tot emerge from the ribosome exit tunnel, the yeast factor Rqc2 can additionally recruit tRNAs charged with alanine and threonine. These amino acids are added at the C-terminus of the nascent chain to form alanine/ threonine tails (CAT tails). These extensions are thought to help the nascent chain emerge the ribosome out of the ribosomal exit tunnel until Ltn1 can ubiquitylate a lysine residue[211,216-219]. CAT tails further have been observed to accumulate on nascent chains terminated at specific stalling sequences, such as poly-lysine stretches or CGA stretches, and are thought to help to recycle highly charged

nascent chains[217]. More recently, it has been shown that CAT tails not only improve Ltn1-dependent degradation efficiency but also can function as a degron mark for proteasomal degradation when Ltn1 is absent[220]. In human cells, NEMF was recently shown to mediate nascent chain tailing with alanine only, and the regulatory function of these alanine tails remains unclear[221].

Recent work has shown that the interface between two collided ribosomes is recognized a by the E3 ubiquitin ligase ZNF598[222,223]. The yeast homolog of ZNF598, Histone E3 Ligase 2, (Hel2), was originally discovered as a regulator of histone protein levels[224]. Additional whole genome screens using polybasic reporters revealed Hel2 association with ribosomes, and Hel2-dependent nascent chain degradation as part of the RQC pathway[208,222,225]. More recently, the use of flow cytometry-based assays for AAA-encoded poly-lysine stalling reporter readthrough has enabled the dissection of this pathway in mammalian cells[202,205]. Several ribosome quality control factors were tested using this reporter including HBS1L/PELO, ABCE1 and ZNF598, but only ZNF598 depletion improved poly-lysine readthrough. Further *in vitro* assays revealed that ZNF598 mediates the ubiquitination of RPS10 and RPS20 on the small subunit of collided ribosomes, thereby presenting the missing link between ribosome collision and RQC initiation in mammals[202,205]. Nevertheless, neither Hel2 deletion in yeast nor ZNF598 knockout in HEK293T cells impairs cell growth[202,205], suggesting a non-essential function.

After ZNF598-mediated 40S ubiquitylation, ASCC3 has been proposed to then bind and disassemble the stalled ribosome in a ubiquitin-dependent manner, triggering the RQC pathway (**Figure 1.6**)[153,226]. ASCC3 is a helicase that is part of the ASC-1 complex, which is important for DNA repair in the nucleus[227,228]. However, for its function in ribosome rescue, ASCC3 acts on stalled ribosomes independently of the ASC-1 complex[226]. These dependencies are conserved between yeast and human cells[225,229,230]. Alternatively, the yeast endoribonuclease Cue2 can cleave mRNA at stalled ribosomes, allowing Hbs1/Dom34 to recognize the empty A site in the ribosome[231]. This would enable RQC pathway induction through an alternative pathway that is independent of Hel2 or mRNA sequence and structure. So far, endonucleolytic activity has been demonstrated for Cue2 homologs in *Escherichia coli* (SmrB)[232], *Bacillus subtilis* (MutS2)[233] and *Caenorhabditis elegans* (NONU-1)[234], but not for the human homolog N4BP2.

More recently, EDF1 was identified as another factor specifically recruited to collided ribosomes[235,236]. EDF1 and ZNF598 facilitate recruitment of the GIGYF2/eIF4E2 complex,

which inhibits translation initiation on the problematic mRNA by outcompeting eIF4E binding[144,235-238]. Translation can thus be transiently inhibited until ribosome stalling is resolved. If stalling persists, the mRNA is targeted for degradation[109,239]. GIGYF2 knockout does not influence the growth of cultured HEK293T cells but it is perinatal lethal in mice[144,237,240]. Deletion of yeast homologs Smy2p and Syh1p does not influence growth[241]. Furthermore, Smy2p and Syh1p facilitate mRNA decapping and degradation but do not reduce translation initiation, suggesting that their function differs between single-cell eukaryotes and mammals[237].

Several quality control steps are essential for efficient protein synthesis, which suggests that also quality control pathways have to be highly regulated. In that regard, the GTPases GTPBP1 and GTPBP2 were recently described to function as ribosome quality control factors in the mouse brain[242]. The loss of either of these proteins elicits neurodegenerative phenotypes upon tRNA defects, their function in ribosome rescue pathways was suggested to be redundant[242,243]. However, the two proteins displayed different properties in *in vitro* translation elongation assays[244].

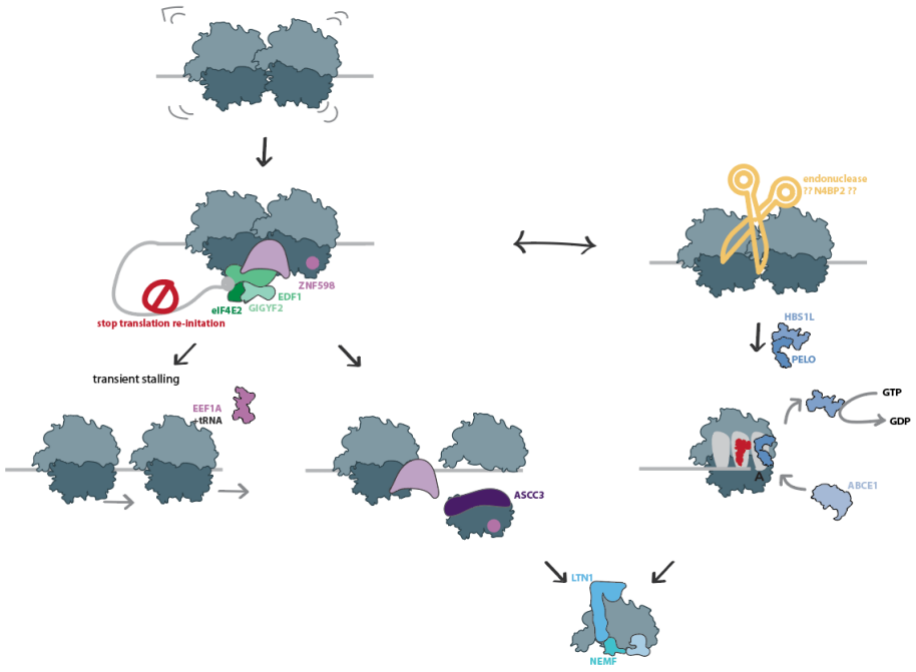

Figure 1.6. Models for ribosome collision-induced RQC.

These recent discoveries suggest that collided ribosomes are a major signal for triggering co-translational quality control and may act as an interaction hub for factors that modulate translation initiation and induce cellular stress response pathways[245]. Our current understanding of ribosome and mRNA quality control pathways, however, so far mostly stems

from *in vitro* assays, stalling reporter studies, and work in yeast and immortalized human cell lines. Most ribosome quality control factors are dispensable in these settings, but are highly essential in embryonic – and especially neurological – development, which suggests that they may have cell context-dependent functions. For example, conditional knockouts of Hbs1L or Pelo in neuronal and dermal cells in mice suggests that these genes are essential during development only of specific cell types within a tissue, and become dispensable after differentiation[246,247]. Since translation requirements profiles vary between cell types and change during development[248-250], it is conceivable that also ribosome and mRNA regulation and quality control pathways are dynamically modulated to ensure proteostasis. Moreover, our understanding of the endogenous stalling events that trigger these pathways is very limited. Recent data from selective ribosome profiling in yeast suggests that Hel2 engages with secretory ribosome-nascent chain complexes, which may help prevent mistargeting of secretory proteins[251]. By contrast, another study has shown that Hel2 mainly binds at the 3' end of mRNAs around the stop codon[252]. Moreover, disomes seem to occur less frequently in yeast cells lacking Hel2[253]. These data underscore the complexities associated with identifying endogenous substrates of ribosome and mRNA quality control pathways.

1.3.3. Cellular responses to defective mRNA translation

When stalled ribosomes are not resolved or faulty mRNAs are not degraded efficiently, downstream stress responses are activated to promote cell survival or induce apoptosis. Persistent ribosome stalling leads to activation of the integrated stress response (ISR) and to global downregulation of translation initiation through eIF2α phosphorylation[64,119,254,255]. There are four eIF2α kinases in mammalian cells, which are activated by different stressors. Heme deprivation sensed by heme-regulated inhibitor (HRI), viral infection is sensed by protein kinase RNA-activated (PKR), ER stress is sensed by PKR-like endoplasmic reticulum kinase (PERK), and amino acid deprivation is sensed by general control nonderepressible 2 kinase (GCN2)[119]. In contrast, yeast only encodes one eIF2α kinase - Gcn2[256]. This protein is thought to sense amino acid deprivation by directly binding to stalled ribosomes[257,258]. eIF2α phosphorylation globally shuts down mRNA translation, but selectively induces translation of specific mRNAs[254]. ATF4 is one major transcription factor that becomes more efficiently translated upon stress through uORF-based regulation in mammalian cells[259]. It then activates stress response genes to restore proteostasis[260,261]. These include amino acid biosynthesis and transport genes, autophagy factors, ER chaperones, and genes involved in redox balance[262]. If this fails to restore proteostasis, apoptosis is induced by the upregulation of CHOP and ATF3[119].

Alternatively, cellular stress responses can commonly be activated by mitogen-activated protein kinase (MAPK) signaling pathways[263]. MAPK activation is organized in an extensive and complex regulatory network MAP kinase kinase kinases (MAP3Ks) sense cellular stress signals and activate downstream MAP2Ks, which themselves activate MAPKs[264]. There are two major MAPK that have been linked to translation: p38 and the c-Jun N-terminal kinase (JNK), which are stress-activated protein kinases that determine cell fate by promoting pro-survival and pro-apoptotic gene expression, respectively[265-267]. p38 is a cluster of four kinases: p38-α (MAPK14), p38-β (MAPK11), p38-γ (MAPK12) and p38-δ (MAPK13). P38-α and p38-β are ubiquitously expressed, whereas p38-γ and p38-δ have cell type-specific expression patterns and possibly elicit more specialized functions[268]. p38 activates MK2, an AP-1 transcription factor that regulates cell cycle and survival genes[269]. JNK groups three kinases: JNK1 (MAPK8), JNK2 (MAPK9), and JNK3 (MAPK10) with at least ten isoforms[270]. JNK1 and JNK2 are ubiquitously expressed and seem to have a redundant function, whereas JNK3 seems to function neuron-specific[271-273]. JNK is supposed to phosphorylate c-Jun, which causes activation of AP-1 transcription factors and the subsequent induction of consequential apoptosis-related genes[274-277]. ZAKα is an essential MAP3K that acts upstream of p38- and JNK-dependent stress response mechanisms[278-282]. ZAKα can phosphorylate the MAP2Ks MKK3 and MKK6 to activate p38[283-286], or MKK4 and MKK7 for JNK activation[287]. When this is triggered by compounds that bind to and interfere with translating ribosomes, the resulting response is often referred to as a “ribotoxic stress response” (RSR)[288].

The ISR and RSR pathways are thought to be organized in a sequential order depending on stress duration and persistence of ribosome collisions (**Figure 1.7**)[264,265]. This hierarchical organization model is based on recent studies showing that these cellular stress response pathways can be activated to a different extent upon induction of ribosome collisions by treating cells with low doses of translation elongation inhibitors such as cycloheximide, anisomycin, and emetine (**Figure 1.7**)[149,236,245,265]. RQC and ribosome rescue pathways normally trigger ribosome disassembly and degradation of the nascent chain and mRNA. However, when ribosome stalling persists, ZAKα can bind the collided ribosomes and coordinate downstream responses either through recruitment of GCN2, which activates the ISR, or through p38/JNK-based RSR activation[265]. However, it is unknown how cells assess ribosome stalling severity, and what the molecular mechanisms are that mediate the transition from quality control pathways to the ISR or the RSR.

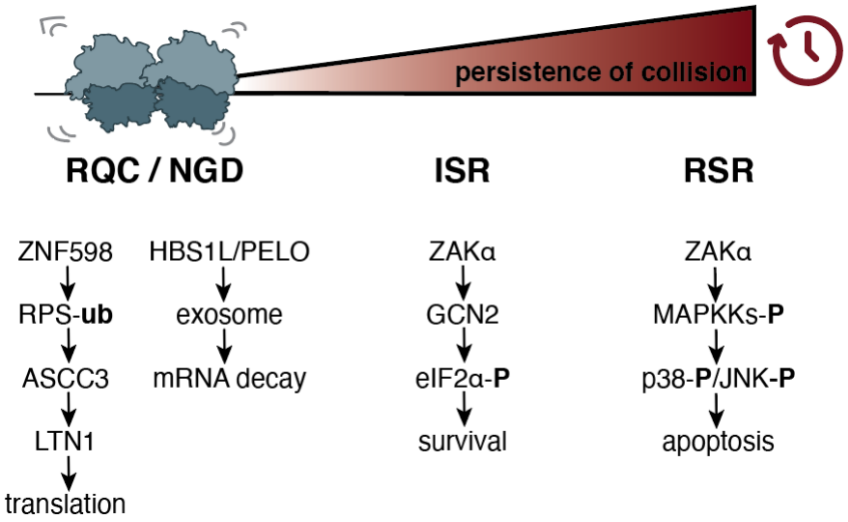

Figure 1.7. Simplified model for temporal stress pathway activation upon ribosome collision.
In the first instance, RQC and NGD pathways are activated. RQC is activated through ZNF598 binding, RPS ubiquitination and ribosome subunit disassembly by ASCC3. LTN1, the key component of the RQC complex, ubiquityles the nascent chain for degradation and ribosome recycling so that translation can progress. NGD is activated through mRNA cleavage, ribosomes are disassembled through HBS1L/PELO, and the truncated mRNA is degraded through the ski-exosome complex. If stalling is persistent, the ISR is activated through stress kinases that bind to the ribosome and eIF2α phosphorylation (-p). This leads to global translation shut-down and targeted translation of survival genes. In the final instance, the RSR is activated through an interconnected MAPkinase cascade. ZAKα (MAP3K) binds collided ribosomes, phosphorylates MAP2Ks and further activates p38 (MAPK) for cell cycle regulation or JNK (MAPK) to induce apoptosis.

1.4. Dysregulated mRNA translation and human disease

mRNA translation is a highly conserved process that is essential in all organisms. Metazoans face the challenge to adapt the regulation of this process to distinct proteome needs in specific cell types. During organismal development, cells fine-tune translational mechanisms to establish and maintain cell identity and tissue homeostasis[249]. Therefore, it is not surprising that genetic defects in translation factors have been linked to human diseases. Translation dysregulation has been linked to immunodeficiencies, metabolic and neurological disorders, and cancer[289-292]. Diseases that are caused by defects in ribosome biogenesis and function are collectively referred to as ribosomopathies. They often arise through ribosomal haploinsufficiency which surprisingly elicit tissue- and even cell type-specific phenotypes[293-295]. Diamond-Blackfan anemia is one of the most common ribosomopathies. It is frequently caused by heterozygous mutations of ribosomal protein genes, and primarily manifests in impairment of erythropoiesis and skeletal development[133,296]. Most other ribosomopathies also impact only specific cell populations: Shwachman-Diamond syndrome causes deficiencies in pancreas and bone marrow[297], Treacher Collins syndrome impairs facial development[298], chromosome5q syndrome impairs hematopoiesis[299], and North American Indian child-hood cirrhosis decreases liver function[300]. Two major hypotheses are currently considered to explain these tissue-specific disease phenotypes. One of these is connected to the theory of “specialized ribosomes”, which suggests that the composition of ribosomes can differ between tissues or cell compartments and this can serve to regulate the translation of specific mRNAs[132]. The other hypothesis is that ribosomal protein imbalance causes global mRNA translation dysregulation, p53-mediated cell cycle arrest and apoptosis[296,301-303]. This is more likely to cause strong phenotypes in rapidly dividing cells such as hematopoietic cells than in other tissues[304-307].

In addition to ribosomal protein gene defects, mutations in several genes encoding translational quality control factors, e.g. *GIGYF2*, *ZNF598* and *LTN1*, are linked to neurological disorders such as Parkinson’s disease, amyotrophic lateral sclerosis, autism spectrum disorder, and intellectual disabilities[308-311]. Mouse models with disease-linked *LTN1* mutations recapitulate a deficiency of motor and sensory neuron development[311]. Neurons are morphologically distinct from other cell types, since their dendrites and axons constitute separate functional and polarized compartments in which local mRNA translation is required to fine-tune responses to incoming stimuli[312,313]. During neurodevelopment, protein expression levels are only lowly correlated with mRNA levels[4], but instead they need to rapidly adapt and

reprogram through translational regulation to determine cell fate[249,314]. Furthermore, neurons have been shown to slow down general translation events but also reduce proteasomal activity, which makes them highly prone to aggregation if the proteostasis network is imbalanced[19,315,316]. Deregulation of this network and distinct local translation patterns may make neurons highly vulnerable to even small alterations of the translation machinery. Similarly to ribosomopathies, however, the mechanisms behind the tissue-specific translational response remain unclear. Due to the complexity and interconnectivity of the proteostasis network, it is conceivable that multiple factors contribute to selective cellular vulnerability upon dysregulated mRNA translation and quality control.

1.5. Human induced pluripotent stem cells: a model system to study cell context-dependent molecular mechanisms

A major obstacle to defining the molecular mechanisms behind tissue-specific vulnerability to perturbed mRNA translation is the lack of physiologically relevant model systems. In mice, the loss of most translation-associated factors is embryonic or perinatal lethal, which means the investigated protein has to be depleted in a conditional knockout in a specific tissue. This is very costly and time-consuming, and it also severely limits the experimental approaches that can be used to characterize the resulting molecular events. Cultured human cell lines have been used for decades to study fundamental molecular mechanisms. However, most commonly used cell lines are either immortalized by transformation or derived from cancer cells. They are thus nearly always aneuploid and have aberrant gene expression, extensive chromosomal rearrangements, and unstable genomes[317]. Due to this, their responses to genetic defects may differ from those in cells with a normal karyotype and physiology[318].

The recent development of robust and efficient protocols for the derivation and targeted differentiation of human induced pluripotent stem cells (hiPSC) offers a genetically tractable system for dissecting cell context-specific regulation. Pluripotent stem cells have the capability to differentiate into specialized cell types from all three germ layers. They undergo asymmetric cell division, where only one of the daughter cells is entering cell reprogramming and the other remains pluripotent[319]. In 2006, Takahashi and Yamanaka identified four crucial transcription factors – Oct3/4, Sox2, c-Myc, and Klf4 – whose expression allows the reprogramming of terminally differentiated human cells into hiPSCs[320]. These cells exhibit the key characteristics of embryonic pluripotent stem cells, such as the ability to self-renew and differentiate into all three germ layers. Since then, countless protocols have been established to perform targeted differentiation of hiPSC into a wide variety of cell types by transcription factor overexpression or with small molecules and growth factors[321]. Typical growth factors include fibroblast growth factors (FGFs)[322], modulators of Wnt family members[323], transforming growth factors (TGFβ) and bone morphogenic proteins (BMPs)[324], which have to be carefully combined and titrated to induce the desired cell fate[321]. A resource of publicly available, high-quality hiPSC lines for use in academic research was recently provided by the Human Induced Pluripotent Stem Cells Initiative (HipSci), which reprogrammed and characterized several hundreds hiPSC lines derived from donors with a healthy genetic background[325].

1.6. Functional genomics with CRISPR-Cas9

Recent advances in the field of genome engineering adapted the bacterial defense system against foreign nucleic acids, called CRISPR/ Cas, to efficiently target and modify genomic DNA of various organisms[326,327]. The most commonly used CRISPR system relies on Cas9 from *S. pyogenes,* a DNA nuclease that can be targeted to a genomic locus of interest by a single guide RNA (sgRNA). In eukaryotic cells, this leads to a double-strand break (DSB), which triggers endogenous DNA repair mechanisms[328]. A sgRNA is composed of a variable CRISPR RNA (crRNA) and a constant transactivating CRISPR RNA (tracrRNA), which form a hairpin structure that guides Cas9 to complementary DNA sites[329]. The variable crRNA can be modified to target a locus of interest and normally consists of 20 nucleotides. Targeted sites also require a protospacer adjacent motif (PAM) – 5'-NGG for Cas9 system – so that the DNA is recognized and cleaved[330]. Subsequently, eukaryotic cells repair the DSB through non-homologous end joining, which often causes small deletions or insertions and can lead to disruption of the targeted gene[331]. Alternatively, if a repair template is provided, the cells can use it for homology directed repair, which enables the insertion of specific mutations or even complete genes into a target locus of the human genome[332]. Although the necessity of a PAM sequence somewhat limits targeting approaches, it outcompetes other genomic engineering approaches through its simple experimental workflow, high specificity, and minimal off-targeting effects[333].

Since its discovery, the classical "cutting" CRISPR/Cas9 system has been repurposed in many ways[334]. One of these is to act as a transcriptional repressor, which was achieved through deactivation of the endonucleolytic activity of Cas9 ("dead" Cas9, dCas9). The dCas9 still a target DNA locus in complex with a sgRNA, but instead of cleaving it, it sterically blocks gene transcription[335]. The efficiency of this system, called CRISPR interference (CRISPRi), is enhanced through fusing dCas9 to a Krüppel-associated box (KRAB) domain, which triggers epigenetic silencing of the target site by recruiting the chromatin modifiers KAP1 and HP1 (**Figure 1.8**)[336,337]. CRISPRi is highly efficient in inhibiting gene expression and exhibits much lower off-target effects when compared to RNA interference[338]. The main advantage of CRISPRi apart from potent and precise inhibition of gene transcription, is the lack of DSB induction. DSBs can activate the p53-mediated proteasomal degradation of several proteins including RPS27A, and might introduce large genomic alterations of genetically healthy cells[339]. CRISPRi also enables studying the function of genes that are essential for cell viability[339].

Constitutive expression of KRAB-dCas9, however, does not allow for controlling the timing or extent of gene repression. This can be important since disease-related phenotypes are highly cell context-dependent and can arise only in specific developmental stages.

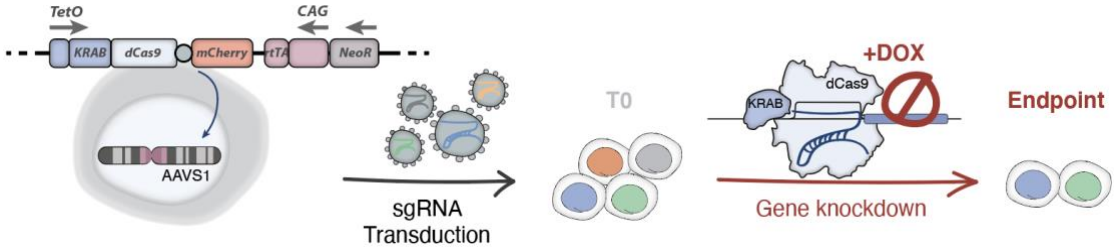

Figure 1.8. inducible CRISPRi system for whole genome target screenings.
The inducible CRISPRi expression cassette is stably integrated into a genomic safe harbor (*AAVS1* locus) of the human genome by TALENs engineering. KRAB-dCas9 expression is regulated by an array of TetO promoters and is induced by doxycycline. KRAB-dCas9 is additionally linked to mCherry, but becomes separated during translation by a 2A skipping sequence (grey dot). Neomycin resistance (NeoR) for clone selection is expressed through the endogenous *AAVS1* locus and rtTA, which is necessary for the TetO promoter, is expressed from a constitutive CAG promoter. In a separate step, an individual sgRNA or a pool of different sgRNAs can be introduced by lentiviral transduction at low multiplicity of infection to ensure that each cell receives only one sgRNA construct. After antibiotic selection of transduced cells, addition of doxycycline induces KRAB-dCas9 expression, leading to transcription repression of the targeted gene. Final sgRNA levels can be compared to a non-induced culture that was treated the same way as the induced screen population by NGS. Screening scores are calculated by analyzing the top three sgRNAs per target.

Furthermore, disease-related phenotypes are commonly caused by partial reduction of protein activity for essential genes rather than a complete loss. Inducible CRISPRi can be used to overcome both bottlenecks. In this system, KRAB-dCas9 is expressed from a tetracycline-inducible promoter from a cassette that is stably integrated in a “safe harbor” genomic locus (**Figure 1.8**)[340]. To use inducible CRISPRi for screening approaches, a pool of sgRNAs that target coding genes of interest is introduced into the cells under conditions where each cell receives only one sgRNA that targets a single gene. KRAB-dCas9 expression is then induced by doxycycline addition to the culture medium for a defined period of time. Afterwards, the pool of surviving cells (endpoint) and the starting pool (T0) are harvested, the sgRNA locus is amplified, and the resulting library is sequenced by next generation sequencing (NGS). Most commonly, T0 is defined as the initial transduced pool of sgRNAs into the CRISPRi cells harvested before doxycycline-mediated induction of KRAB-dCas9. However, general cell passaging and maintenance or differentiation might bias sgRNA. This can be circumvented by splitting the initial cell pool and maintaining two cultures - one with and one without doxycycline, for the duration of the screen, and preparing sgRNA libraries of both cultures at the screen endpoint. By comparing sgRNA frequency in these two datasets, we can identify genes that were positively or negatively selected in the presence of doxycycline. In this set-up, KRAB-dCas9-mediated knockdown is tunable, reversible, and above all, inducible at any time point of cell culture. This enables protein depletion in a time-sensitive manner, as well as in post-mitotic cells[339].

In two proof-of-principle studies, a focused and a genome-wide CRISPRi screen were recently performed in HiPSC-derived neurons[341,342]. For this, KRAB-dCas9 was integrated into the genome of a hiPSC line under a constitutive promoter. The cells were also engineered to contain a doxycycline-inducible NGN2 expression cassette. This lineage-specific transcription factor directs hiPSC differentiation into excitatory neurons[343,344]. Because neuron derivation results from *isogenic*, *integrated* and *inducible* NGN2 expression, the cells are commonly called i^{3}Neurons[344]. To target KRAB-dCas9 to genes of interest, genes encoding specific sgRNA were delivered into the iPSC by lentiviral transduction. During continuous sgRNA and KRAB-dCas expression, neuronal differentiation was then induced by the addition of doxycycline to the culture medium. Samples were collected at several time points after NGN2 induction to query gene importance at different stages of neuronal differentiation. However, since gene knockdown already begins prior to the start of neuronal differentiation, knockdown phenotypes that would only arise at early neuronal stages (such as in progenitors) or in mature neurons cannot be investigated in this experimental set-up.

Another aspect to consider is that genome-wide approaches need large amounts of cells to reach sufficient coverage and achieve sensitive readouts of sgRNA dropout. This can be especially problematic for hiPSC-derived cells, as most hiPSC differentiation protocols are optimized for small-scale culture. Genome-wide studies also often use only three to five sgRNAs per gene, which might lead to inefficient KRAB-dCas9 targeting and gene knockdown, especially since sgRNA design can be critical for CRISPRi efficiency. Dedicated computational pipelines can be used to improve CRISPRi sgRNA design by taking into account chromosome accessibility (from MNase-seq or ATAC-seq data) or previously validated sgRNAs[345]. However, most of these data are derived from screens in transformed cell lines. Chromatin accessibility patterns, in particular, might vary in different cellular states and alter sgRNA targeting efficiency. By contrast, in a focused (targeted) screen, the number of distinct sgRNA per genes and cells per sgRNA can be increased to optimize the sensitivity of phenotype detection.

1.7. Research strategy and scope of the thesis

Proteostasis dysregulation has detrimental consequences for cellular and organismal fitness and is often linked to diseases with tissue-specific pathology. However, the size and complexity of the proteostasis network is a challenge for systematic studies to determine its interconnectivity and cell context-dependent functions. Most of our current knowledge about the molecular mechanisms regulating proteostasis in eukaryotes originates from work in budding yeast. Studies in mammals have almost exclusively relied on gene knockout in transformed cultured mammalian cells that exhibit high genomic instability and aberrant gene expression. These limitations complicate conclusions about the essentiality and interdependencies of proteostasis regulators. Loss of many of these proteins is not lethal in yeast or in commonly used cell culture lines. In contrast, gene knockouts in mice are almost always lethal at very early stages of embryonic development. Although this can be circumvented by conditional gene inactivation in certain tissues, this very targeted approach also dismisses information about their cell-context dependent function within an organism.

The overarching goal of my doctoral project is to define the components of the mRNA translation machinery that are essential for cellular fitness in physiologically relevant settings, and to identify cell context-specific mechanisms of translational control. It relies on the powerful combination of hiPSC-based models with functional genomics by CRISPRi to investigate gene function in isogenic human cells with a healthy genetic background and in the commonly used HEK293 human cell line. By depleting 262 proteins of the core translation machinery in focused CRISPRi screens, we identified core- and context dependent-essential regulators of proteins synthesis in human cells. After extensive validation of a subset of targets, we focused on the molecular mechanisms that underlie cell context-specific essentiality of ribosome quality control factors. We identified cellular stress response pathways activated in their absence and discovered new endogenous targets and modes of action for these factors in human cells. This discovery-oriented project provides new insights into how core protein synthesis factors help meet distinct proteome demands in different metazoan cells types and an experimental framework for determined the molecular basis of cell context-specific regulatory processes.

Chapter 2 – Results

2.1. Establishing a CRISPRi screening platform to investigate cell context-dependent functions of human genes

2.1.1. Derivation and characterization of neuronal progenitors, mature neurons, and cardiomyocytes from hiPSC

One obstacle to studying the regulation of molecular processes in different mammalian cell types is the lack of culture models with normal karyotypes and isogenic background. Most commonly used cultured cell lines have diverse genetic backgrounds and were immortalized by transformation or derived from cancer cells with aneuploid genomes. Such cell lines are not suited for studying protein synthesis and folding, since both of these processes are strongly perturbed by aneuploidy and uncontrolled cell growth[346,347]. Pluripotent stem cells provide a powerful model system to circumvent many of these problems. When derived from healthy individuals, these cells represent a normal physiological state, have a stable diploid genome, and divide indefinitely in culture without the need for transformation[348]. Combining robust stem cell models with an inducible CRISPRi approach enables gene knockdown at any time point, circumventing secondary effects that can arise during long cell cultivation periods or differentiation[340]. Accordingly, fine-tuning of both components is crucial to maximize experimental efficiency and biological relevance.

To investigate cell type-specific variations of the mRNA translation machinery, we first established reproducible protocols for targeted differentiation of hiPSC into dividing neuronal progenitor cells (NPC) and post-mitotic neurons, which were previously used to study neuronal diseases such as Parkinson's disease and amyotrophic lateral sclerosis[349,350]. We used the commercially available reference hiPSC line kucg-2, which is derived from an individual with a healthy genetic background and has been extensively characterized by the HipSci consortium[325] as the basis for all our experiments. Recent CRISPRi screens in hiPSC-derived neurons relied on the i^{3}Neuron approach, in which neurons are directly derived from hiPSC by doxycycline-inducible mNGN2 expression[341,342]. However, we opted for a small molecule-based approach for NPC and neuron derivation[349] because it has several advantages. First, it produces proliferating NPC that can be expanded and stably propagated in culture for ~40 passages[349]. Second, it enables the use of the TetO promoter to induce the expression of KRAB-dCas9 rather than mNGN2. This allows us to control the timing of gene repression by

inducible CRISPRi and perform it before, during, or after the differentiation process, which increases our understanding of developmental defects and defects arising in differentiated cells.

We derived NPC from hiPSC by embryoid body formation triggered by the addition of small molecules to the culture medium that drive cell differentiation into the neuronal lineage (**Figure 2.1 A**). These molecules induce Wnt and hedgehog signaling pathways (CHIR99021 and PMA), which promotes dorsal and ventral brain development, and inhibit the growth factor BMP/ TGF-β pathways (dorsomorphin and SB431542)[351,352]. After seven days of priming, cells are plated to obtain ventral NPC that are capable of differentiating into cells of the neural tube and the neural crest[349]. At this stage, the NPC culture is still heterogeneous and must be purified by sequential digestion of the different cell types for two more passages. After purification, the resulting homogeneous NPC culture can be passaged for several weeks or further differentiated into motor neuron-like cells. For this, NPC are patterned by inhibiting proliferation with retinoid acid (RA) while enhancing hedgehog signaling by adding of PMA and neuronal survival with neutrophins (BDNF, GDNF). After six days, primed neurons are maturated by inhibiting gliogenesis with TGF-b3 and adding compounds that promote neuron survival (dbcAMP, BDNF, GDNF)[349,353].

For cardiomyocyte (CM) differentiation, cells were primed in medium containing Wnt signaling activator (CHIR99021), growth factors that promote lateral mesoderm differentiation (ActivinA, FGF2b, BMP4) and a mix of insulin/transferrin/selenium (ITS) to promote survival and supply cells with antioxidants (**Figure 2.1 B**)[354]. After one day of priming, growth factors were removed to stop Wnt signaling induction. One day later, Wnt signaling was actively inhibited with C59 to decrease proliferation and cells were maturated for another 12 days. Nine days after starting the derivation of CM, cells were deprived of glucose for 24 hours and incubated in the presence of lactic acid instead. Since cardiomyocytes, but not other cell types, can switch their energy metabolism, this step reduces the survival of non-CM cells in the culture[355].

To assess cell purity after differentiation, we measured mRNA levels of cell type-specific genes by performing mRNA-seq of two independent differentiations per cell type (**Figure 2.1**). This analysis showed a decrease in mRNA levels for proliferation-related genes (KI67 and PCNA) in neurons and CM but not in NPC (**Figure 2.1 C**). The mRNA levels of pluripotency marker genes (NANOG and POU5F1/OCT4) decreased in all differentiated cultures by a thousand-fold (**Figure 2.1 D**). The NPC marker gene PAX6 was upregulated 250-fold in comparison to hiPSC, while the neuronal markers MAP2 and CHAT were upregulated 30 and

250-fold in the mature neuron cultures. In addition, the cardiac marker gene TNNT2 and NKX2-5 were specifically upregulated in CM cultures by 250 and thousand-fold. Collectively, these data demonstrate that hiPSC-derived cultures do not express pluripotency marker and robustly express characteristic cell identity marker genes (**Figure 2.1 D**). We then assessed culture purity after hiPSC differentiation by immunofluorescence staining of marker proteins. hiPSC and NPC cultures homogeneously expressed POU5F1 and PAX6, respectively, while most cells in CM cultures were positive for cTNNT2 (**Figure 2.1 E**). Furthermore, nearly all neurons were positive for the pan-neuronal marker MAP2, while a subset also showed staining for the motor neuron-specific transcription factor ISL1 (**Figure 2.1 E**). Together, these data demonstrate the successful derivation of homogeneous populations of NPC, neurons, and CM from hiPSC.

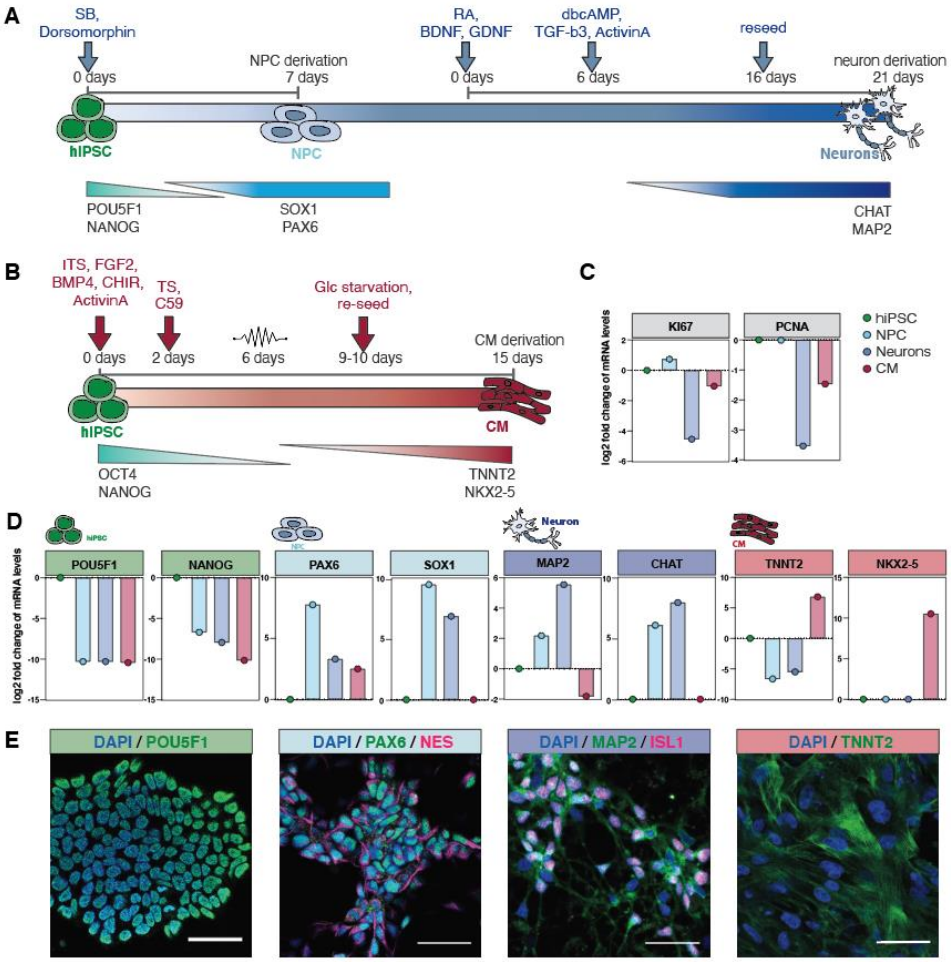

Figure 2.1 Robust and efficient protocols for the derivation of neuronal progenitor cells, neurons, and cardiomyocytes.
(A) Schematic representation of the neuronal differentiation protocol based on Reinhardt et al.[349], including commonly used cell type-specific markers to check culture identity and homogeneity. SB = SB43154. RA = retinoic acid. BDNF and GDNF = brain and glial cell-derived neurotrophic factor. TGF-b3 = transforming growth factor beta-3 (B) Cardiomyocyte (CM) differentiation protocol based on Zhang et al.[354], including common CM marker. mRNA-seq log2 fold expression changes of (C) common proliferation and (D) cell type marker compared to hiPSC. p-value cut-off 0.05 (E) Marker staining of hiPSC, NPC, neurons and CM. Scale bar: 50µM

2.1.2. Inducible CRISPRi cassette engineering into hiPSC

We next inserted an inducible KRAB-dCas9 expression cassette into the *AAVS1* "safe harbor" locus of kucg-2 hiPSC cells with a previously established protocol[340]. The cassette encodes a KRAB-dCas9-2A-mCherry sequence (TetO promoter), an rtTA complementing the TetO-system (CAG promoter) and a neomycin resistance cassette, which is expressed from the endogenous AAVS1 locus (**Figure 2.2 A**). Plasmids with TALEN homology arms and the KRAB-dCas9 cassette were co-transfected into kucg-2 hiPSC cells. After selection with neomycin, colonies that originated from a single cell were picked for evaluation of cassette insertion by PCR on genomic DNA (**Figure 2.2 B**). For this, primers were designed to bind the flanking region of the AAVS1 locus, which was targeted for insertion (primer pair A), and an additional third primer for binding of the inserted CRISPRi cassette (primer pair B). PCR amplification creates a ~300bp product when no insertion has occurred and a ~500 bp product when the cassette was inserted in the AAVS1 locus. The presence of both bands in a PCR indicates that the cassette was inserted in one allele only.

Using this strategy, we obtained monoclonal hiPSC lines with heterozygous insertions of the inducible CRISPRi cassette into the AAVS1 locus. Western Blot analysis of hiPSC lines before and after doxycycline treatment showed that all clones we tested expressed the KRAB-dCas9 fusion protein only upon doxycycline treatment (**Figure 2.2 C**). We continued our remaining characterization and experiments with clone C2. Karyotype analysis of cells from this line revealed a healthy karyotype, ruling out large genomic arrangements as a result of the genetic engineering (**Figure 2.2 D**). We then derived an NPC line from the CRISPRi hiPSC line following the protocol outlined in **Figure 2.1 A**. In addition, a HEK293 CRISPRi cell line generated by an identical engineering strategy was kindly provided by Dieter Edbauer (DZNE, Munich), enabling us to assess the effects of gene knockdown in this commonly used human cell line.

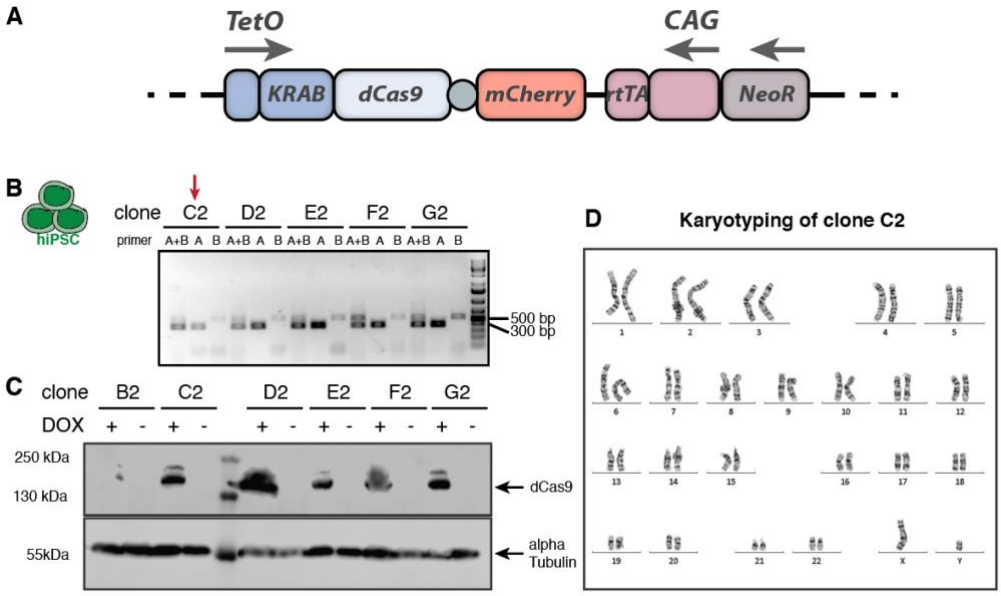

Figure 2.2. Engineering and validation of hiPSC-CRISPRi cell line.
(A) KRAB-dCas9 is expressed from an array of tetracycline-inducible promoter (TetO) together with mCherry, which becomes separated by a 2A skipping sequence (grey circle). A CAG promoter drives the expression of rtTA, which is necessary for the Tet-ON system. A neomycin cassette is expressed through the internal promoter of the AAVS1 locus for selection. The Inducible CRISPRi cassette was co-transfected with TALENS homology arms into hiPSC, selected with neomycin and single colonies were picked for validation by (B) screening PCR. Primer pair A produces a PCR product of the wild type *AAVS1* locus, Primer pair B produces a PCR product for a successful inserted CRISPRi cassette. (C) Single clones were expanded and induced with doxycycline. Doxycycline-induced KRAB-dCas9 expression of various clones was tested via Western Blot in hiPSC. (D) Karyotyping results of G-band analysis for hiPSC clone C2.

Stem cells and cancer cells are characterized by high proliferation rates[317], whereas proliferation decreases during the differentiation process[21,53]. To quantitatively compare growth phenotypes between our cell types, we assessed cell doubling times of the engineered cell lines[345]. For this, growth rates of the HEK293 CRISPRi line, as well as the CRISPRi hiPSC and hiPSC-derived NPC were quantified by measuring the number of viable cells two and four days after seeding. For all contexts, we observed slower division rates after two days, which accelerated after longer cultivation without in-between passaging. The mean cell doubling times were very similar between hiPSC and HEK293 cells (21 and 24 hours), whereas the average cell doubling time of NPC was longer (31 hours, **Figure 2.3**). For unbiased comparison of cellular growth phenotypes after gene knockdown, we opted for measuring phenotypes after a period of time that would represent the same doubling time for different cell lines. This resulted in equal doxycycline induction times for hiPSC and HEK293 cells, and 1.5-times longer doxycycline induction for NPC.

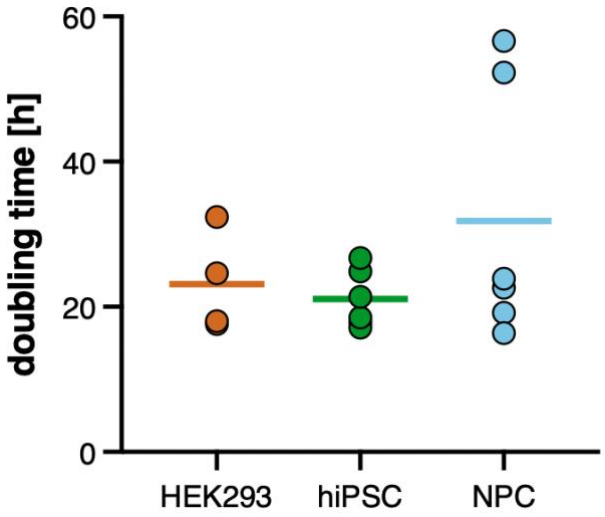

Figure 2.3. Doubling times of HEK293, hiPSC and NPC CRISPRi lines.
Cell doubling times were assessed by cell count evaluation after two and four days of culture in three biological replicates.

2.1.3. The TetO promoter is silenced upon hiPSC differentiation, which can be prevented by continuous culture in doxycycline

Next, we tested the induction efficiency of hiPSC-derived cell types by using the fluorescent signal of mCherry, which is expressed from the same mRNA as KRAB-dCas9, separated through a P2A skipping sequence (**Figure 2.2 A**). We cultured the cells for two cell doublings with doxycycline and used freshly harvested cells for flow cytometry analysis. KRAB-dCas9 induction was highly efficient in hiSPC and HEK293, whereas very few NPC and neurons expressed mCherry (**Figure 2.4 A**). We tried to overcome low induction rates by using TB9-DOX – a doxycycline analog that was shown to have higher stability and TetO promoter induction rates in the mouse brain[356]. Using 2 µM TB9-DOX to induce KRAB-dCas9 expression did not decrease the number of mCherry-positive cells in comparison to 2 µM doxycycline in the hiPSC CRISPRi line, but also did not recover induction efficiency in differentiated cells (**Figure 2.4 B**). Thawing fresh NPC stocks, by contrast, increased the fraction of mCherry-positive cells to 70%, which decreased again over several passages (**Figure 2.4 C**). To ensure that the engineered cassette was not removed from the AAVS1 locus by recombination, we re-selected the NPC line with G418, but this did not increase the number of mCherry-positive cells after doxycycline induction.

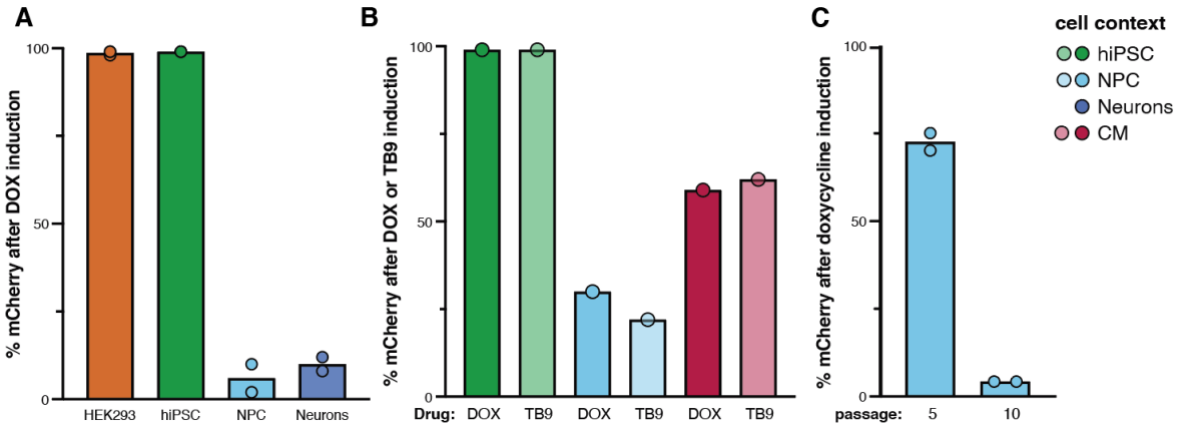

Figure 2.4. KRAB-dCas9 induction is reduced for differentiated cells.
(A) KRAB-dCas9 induction rates of HEK293 cells, hiPSC, NPC and neurons were assessed by measuring the number of mCherry-positive cells after two days of doxycycline treatment using flow cytometry. (B) KRAB-dCas9 induction rates of hiPSC, NPC and cardiomyocytes (CM) that were induced by either doxycycline (DOX) or TB9-DOX (TB9) were assessed by measuring the number of mCherry-positive cells after two days of doxycycline treatment or CM derivation using flow cytometry. (C) KRAB-dCas9 induction rates of NPCs that were freshly thawed or maintained in culture for 10 passages were assessed by measuring the number of mCherry-positive cells after two days of doxycycline treatment using flow cytometry.

These observations suggested that the CRISPRi cassette could be silenced in differentiated cells. To test this, we performed targeted bisulfite sequencing of both promoters in the cassette (TetO array for KRAB-dCas9 and CAG for rtTA expression, **Figure 2.2 A**, **2.5**). We observed high CpG methylation levels only of the TetO promoter in NPC, CM, and neurons, whereas in hiPSC it remained unmethylated (**Figure 2.5 B**). CAG promoter methylation remained at very low levels, suggesting that its occasional methylation does not influence inducibility of the KRAB-dCas9 construct through a decrease in rtTA levels.

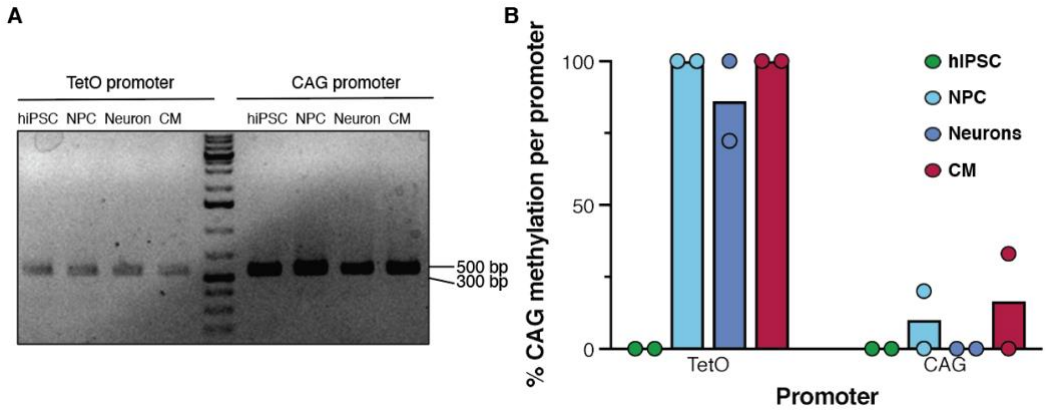

Figure 2.5.The TetO promoter becomes methylated upon hiPSC differentiation.
(A) PCR amplification products, which were amplified for all cell types to perform a bisulfite conversion and analyze methylation by Sanger Sequencing of two technical replicates. (B) Quantification of CpG methylation for both promoters in hiPSC and differentiated cell types.

We next asked whether deriving NPC from hiPSC in the continuous presence of doxycycline would prevent TetO promoter silencing. Since the cells did not contain any sgRNA, continuous production of KRAB-dCas9 is unlikely to affect cell growth or viability, and cells constitutively expressing KRAB-dCas9 are commonly used for functional genomics[338,341]. The system still remains inducible, however, since doxycycline withdrawal from culture medium leads to rapid shut-off of KRAB-dCas9 expression[340]. Indeed, after differentiation and NPC purification in the presence of doxycycline, the fraction of mCherry-positive NPC increased to 90% and did not decline over several passages (**Figure 2.6 A**). Surprisingly, removal of doxycycline for even a single passage reduced this fraction to 20% (**Figure 2.6 A**). Therefore, we continued to maintain the NPC in a medium containing doxycycline. When neurons were derived from this new NPC line, 60% of them were positive for mCherry when doxycycline was present throughout the differentiation protocol and 40% when doxycycline was removed at the start of neuronal derivation from NPC (**Figure 2.6 B**, compare "diff" and "surv"). Similarly, about 60% of CM were mCherry-positive when derived in the presence of doxycycline, and 50% when doxycycline was only added after CM derivations (**Figure 2.6 B**).

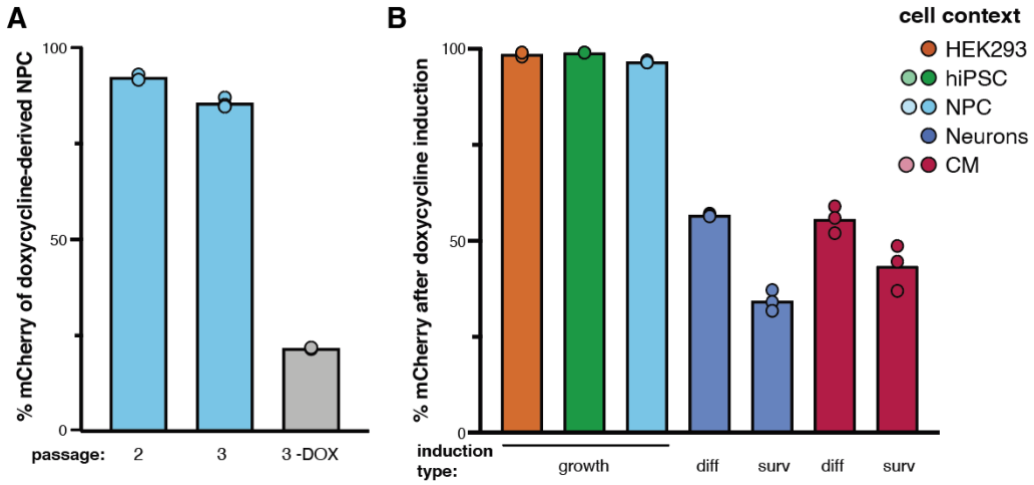

Figure 2.6. The continuous presence of doxycycline in culture medium prevents TetO promoter silencing upon hiPSC differentiations.
(A) Percent of KRAB-dCas9 induction efficiency in NPC derived and cultured with doxycycline and remaining mCherry levels after one passage when doxycycline is removed. (C) Percent of KRAB-dCas9 induction efficiency in doxycycline induced hiPSC and HEK293 cells, in NPCs derived and cultured with doxycycline and differentiated neurons and cardiomyocytes (CM) derived without doxycycline and with continuous doxycycline treatment in three technical replicates. diff = differentiation, surv = survival.

2.1.4. Optimized lentiviral transduction increases the efficiency of CRISPRi in NPC

Since NPC had to be cultured in the presence of doxycycline to prevent TetO promoter silencing, this would lead to an immediate knockdown of target genes upon lentiviral transduction of sgRNA-containing constructs. This can be problematic for pooled screens, because sgRNAs targeting essential genes could quickly drop out of the pool already during puromycin selection for cells that have integrated the sgRNA expression construct. Therefore, we asked whether the transduction and selection period, and with that the KRAB-dCas9 induction time, can be shortened. For this, we tested variations of the published lentiviral transduction protocols[340]. We quantified transduction efficiency by measuring GFP fluorescence, since the GFP gene is delivered on the same lentiviral construct as the sgRNA (**Figure 2.7 A**). We kept the lentiviral transduction and puromycin selection period to a minimum by using a reverse transduction approach, and we shortened the selection period while adjusting puromycin concentrations (**Figure 2.7 A**). These optimizations increased initial transduction rates from 25% to 35% and resulted in 75 to 90% of GFP-positive NPC after only two days of puromycin selection (**Figure 2.7 B**). 24 hours after transduction, the NPCs are re-seeded either with or without doxycycline and selected using puromycin, which means we use the same pool of transduced cells for the knockdown experiments and a non-induced control. Removal of doxycycline showed that mCherry levels decrease rapidly, which suggests a fast shutdown of the TetO promoter and hence KRAB-dCas9 expression in the cells (**Figure 2.6 B**). We also applied this optimized transduction protocol to hiPSC as well, since due to its higher efficiency, we did not need to add TransduceIT, a reagent that enhances transduction efficiency, which increased cell viability.

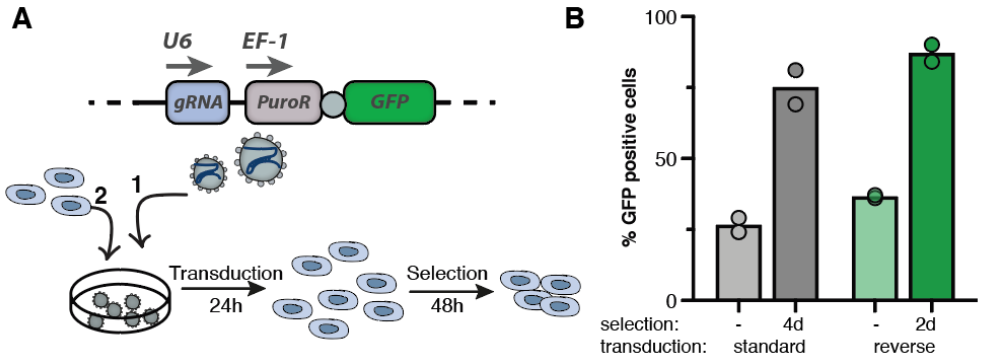

Figure 2.7. Reverse transduction improves sgRNA construct delivery into NPC.
(A) Scheme of the reverse transduction protocol and the sgRNA expression construct. sgRNAs are expressed from a mouse U6 promoter. The EF1α promoter drives expression of puromycin for selection and GFP for flow cytometry analysis. The two open reading frames are separated by a T2A skipping sequence (gray circle). Cells are seeded on plates already containing lentivirus, and medium is exchanged 24 hours post-transduction with medium containing puromycin for 48 hours. (B) Percentage of GFP-positive NPCs measured prior to puromycin selection (-) or after two days (2d) or four days (4d) of puromycin selection following standard or reverse transduction.

2.1.5. Optimization of the CRISPRi sgRNA library preparation workflow yields homogeneous representation of individual sgRNAs

Pooled CRISPRi screens are performed by delivery of a sgRNA pool, which contains sgRNAs targeting a gene set of interest. Each gene is usually targeted by several sgRNA sequences to maximize efficient knockdown probability. sgRNA pools are usually obtained as custom-made oligo pools and then cloned and packaged into lentiviruses. In order to properly assess sgRNA selection patterns upon knockdown in cells, all sgRNAs must be represented in roughly equal proportions in the pool. However, each of the steps in sgRNA library preparation can introduce bias and lead to an over- or underrepresentation of specific sgRNAs in the pool.

We designed a sgRNA library targeting protein synthesis-associated genes that contained 2680 individual sgRNAs and 320 non-targeting controls. We first attempted to use a published protocol for cloning the commercially synthesized sgRNA oligo pool into a lentiviral expression vector. The protocol relies on PCR amplification of sgRNA sub-pools, restriction digestion, and ligation into a sgRNA backbone plasmid[340]. The first sgRNA pool that we ordered contained different adaptors to distinguish between various gene subgroups, namely RPS, RPL, translation initiation, elongation, and termination factors, mRNA stability factors, and a final mixed group of genes regulating protein biogenesis, folding, and ribosome-associated quality control. However, PCR-dependent amplification and restriction digestion were extremely inefficient, which led to a large background signal resulting from inefficient ligation. We worried that this might lead to biases in the sgRNA distribution and high numbers of empty plasmids in the final library; hence, we decided to change our strategy and insert the sgRNAs by Gibson Assembly into the final construct. This eliminated the possibility to prepare sgRNA subpools, but it dramatically increased cloning efficiency. NGS of the final cloned sgRNA library showed a homogeneous count distribution of nearly all sgRNAs that were designed for the screen as well as high sequence content scores, which means that all four bases were equally distributed (**Figure 2.8**).

Taken together, this optimization of the workflows for hiPSC differentiation, inducible CRISPRi, and sgRNA library preparation provided a highly reproducible platform for further experiments to investigate the cell context-specific gene functions.

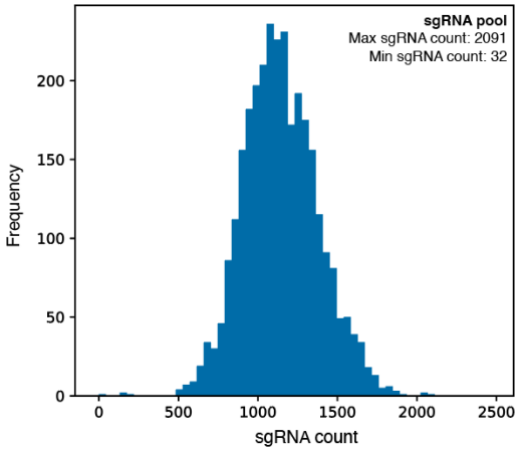

Figure 2.8. sgRNA sequence representation in the final plasmid library.
A synthetic pool of 3000 sgRNAs was cloned into a lentiviral backbone using our optimized Gibson Assembly approach. sgRNA abundance in the library pool was analyzed by NGS.

2.2. Pooled CRISPRi screens in human stem cell-derived models identify core and context-essential regulators of mRNA translation

2.2.1. Pooled inducible CRISPRi screens in hiPSC and hiPSC-derived cells are highly reproducible

Metazoans consist of highly diverse cell types with distinct proteomes. Accordingly, up to one quarter of the core translation machinery is differentially expressed in diverse mammalian cell types[302], suggesting some of these proteins may function in a cell type- or tissue-specific manner. How the protein biogenesis machinery is tuned to these different proteome demands is unknown, and the importance of proteins from the core translation machinery for fitness in diverse mammalian cell types has not been examined systematically so far.

To define mRNA translation regulators with differential importance in different cell contexts, we performed pooled inducible CRISPRi screens in hiPSC and hiPSC-derived NPC, neurons, and CM, as well as in the common aneuploid human cell line HEK293. We targeted a total of 262 genes associated with protein synthesis, including ribosomal proteins, translation initiation and elongation factors, mRNA stability and decay factors, co-translational chaperones, and mRNA and ribosome quality control factors. We also included eight genes encoding markers of stem cells and different neuronal cell populations. We used the CRISPRia Design Pipeline[345] to design a sgRNA library containing nine sgRNAs per gene and 300 non-targeting sgRNAs. We included publicly available chromatin accessibility information from DNase and FAIRE-seq data from the human embryonic cell line H1,as well as SNP data from our kucg-2 hiPSC cell line during sgRNA prediction. The resulting library, containing 3000 individual sgRNA sequences, was synthesized as an oligonucleotide pool by Twist Bioscience, and cloned in a lentiviral expression vector using our optimized Gibson assembly-based approach. After preparing lentiviral stocks, we transduced hiPSC, NPC, and HEK293 CRISPRi cells at an initial transduction rate of ~30% and a coverage of 1000 cells per sgRNA. This was done to minimize the chance that a single cell will be simultaneously transduced with two lentiviral constructs and thus express two different sgRNAs. We then selected transduced cells with puromycin. Each culture was subsequently split in two, and KRAB-dCas9 expression was induced by addition of doxycycline to one half of the cells for a period of time that corresponds to ten cell doublings. In parallel, we cultured the other half of the cellular pool in the absence

of doxycycline for the same period of time. These non-induced samples were used to normalize sgRNA read counts from the screen compared to KRAB-dCas9-expressing cells. hiPSC and NPC were further differentiated into mature cardiomyocytes and neurons to perform either differentiation or survival screens (**Figure 2.9 A**). After harvesting cells, genomic DNA was extracted and sgRNAs were amplified by PCR. Screening results were analyzed using the ScreenProcessing pipeline[345]. In this workflow, reads from different samples are aligned to sgRNA sequences and counted, and sgRNA dropout rates are compared to the respective non-induced CRISPRi cells. The analysis pipeline calculates phenotype scores, which represent the mean sgRNA change of the top three sgRNAs per gene, and a Mann-Whitney p-value, which compares changes of all nine targeting sgRNAs compared to the non-targeting sgRNAs[345]. A dropout of a certain sgRNA means that the knockdown of its target is negatively selected in the culture. There are two possible reasons for sgRNA dropout, which we cannot differentiate in pooled screens: gene knockdown can lead to increased cell toxicity followed by rapid cell death, or decreased cell proliferation. In contrast, sgRNA counts can also increase in the pool, which means that the gene knockdown enhances cell fitness by increasing proliferation in dividing cells or survival in post-mitotic cell types.

Data from CRISPRi screens have to be carefully evaluated for reproducibility and off-target effects. Therefore, initial quality control measurements of the screening data are crucial to assure that biases from the experimental methodology are minimized. We therefore evaluated our screening results by examining the correlation between replicates and the distribution of non-targeting controls. Over the screen duration of ten cell doublings HEK293 cells, hiPSC and NPC exhibited extensive sgRNA dropout rates, which highlights the importance of many genes in our target set cellular fitness (**Figure 2.9 B**). Single gRNA phenotype scores were highly reproducible between biological replicates, with a Pearson's correlation of ~0.9 for all dividing cells and during neuronal and CM derivation. The correlation between replicates was lower in post-mitotic cells survival screens (Pearson's R = 0.68 for CM and R = 0.18 for neurons, **Figure S 5.1**). This is probably due to the inherent variability of targeted differentiation protocols, as well as the smaller fraction of CM and neurons, in which KRAB-dCas9 expression can be induced (**Figure 2.6 D**, **S5.1**), as well as the lack of dilution effects due to the absence of cell division. We also found that non-targeting sgRNAs had nearly no phenotypic effects, as the distribution of their phenotype scores was very narrow and centered around zero, with little correlation between replicates in any screening set-up (Pearson R <= 0.06). These data confirm the high specificity and reproducibility of CRISPRi in our experimental set-up.

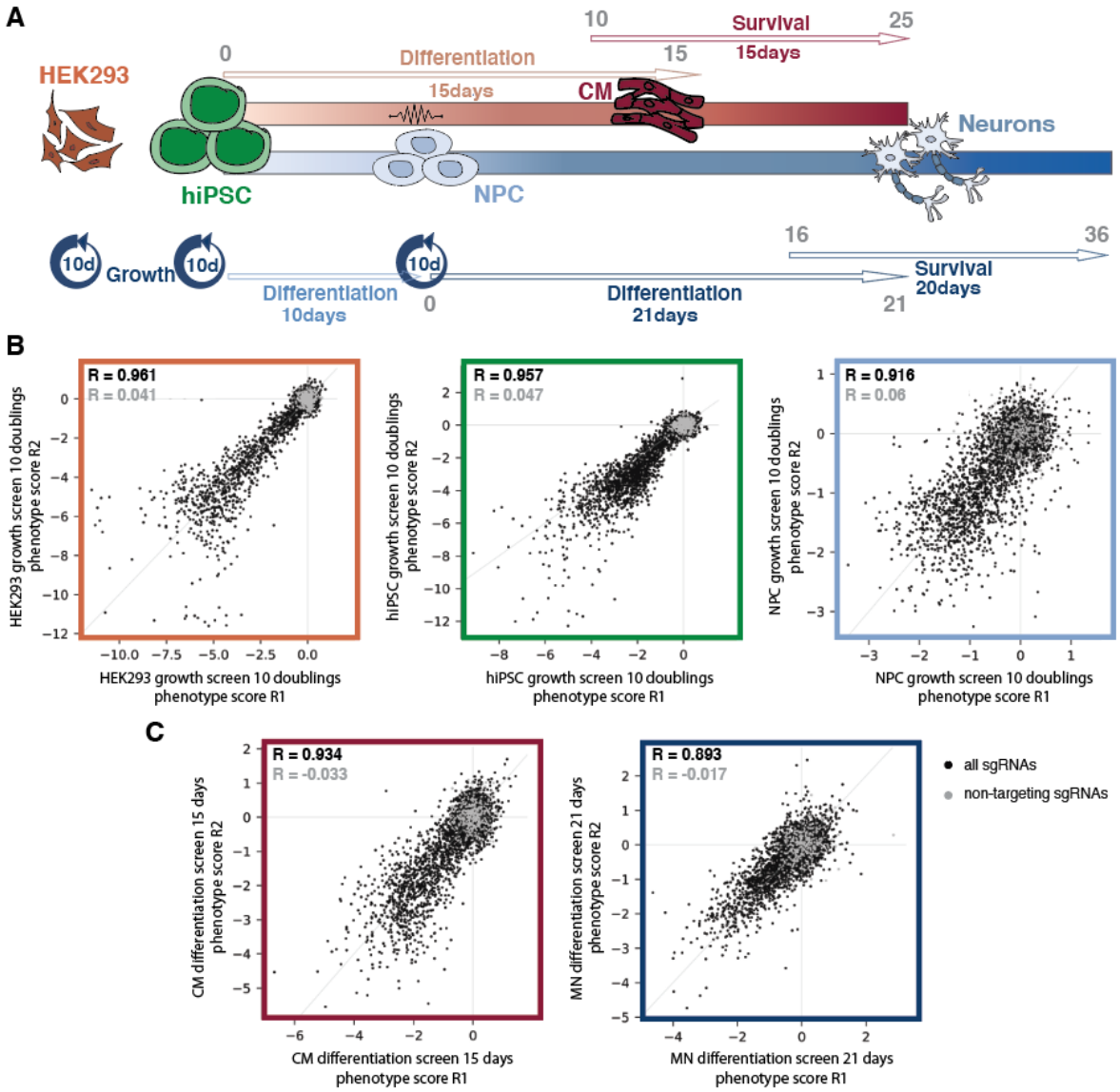

Figure 2.9. Replicate correlation analysis of CRISPRi screens in different cellular contexts.
(A) Scheme of cell differentiation and screening types and their doxycycline induction time points (gray numbers) in different cell types. Differentiation was performed in the presence of doxycycline (differentiation screens) or in the absence of doxycycline (growth screens for mitotic cells or survival screens for postmitotic cells). Correlation plots of two independent biological replicates for growth screens (B) and differentiation screens (C) (black: targeting sgRNAs; gray: non-targeting sgRNAs). R = Pearson's correlation. All correlation plots are in Figure S **5.1.**

We also plotted phenotype scores against the Mann-Whitney p-values in a volcano plot. We observed that a substantial fraction of targets passed our p-value threshold in all cell contexts, whereas only one out of 300 non-targeting controls showed a significant change in sgRNA counts in neurons (**Figure 2.10 A**, **B**). In HEK293 cells, the knockdown of 171 genes resulted in a negative growth phenotype, while the absence of 15 genes enhanced cell growth, and 76 genes did not elicit a statistically significant phenotypic difference. In comparison, in hiPSC cells, repression of 206 genes elicited a negative phenotype, 7 showed a positive phenotype,

and only 49 genes did not elicit a significant phenotype. Phenotypic effect sizes were smaller in non-dividing cells because of lack of proliferation combined with longer protein half-lives[357]. Despite higher inter-replicate variability, we detected statistically significant negative phenotypes for 120 genes in neurons and 112 genes in CM (**Figure 2.10 C**). Taken together, these analyses show that most genes we targeted are efficiently and reproducibly repressed in our pooled CRISPRi screen set-up.

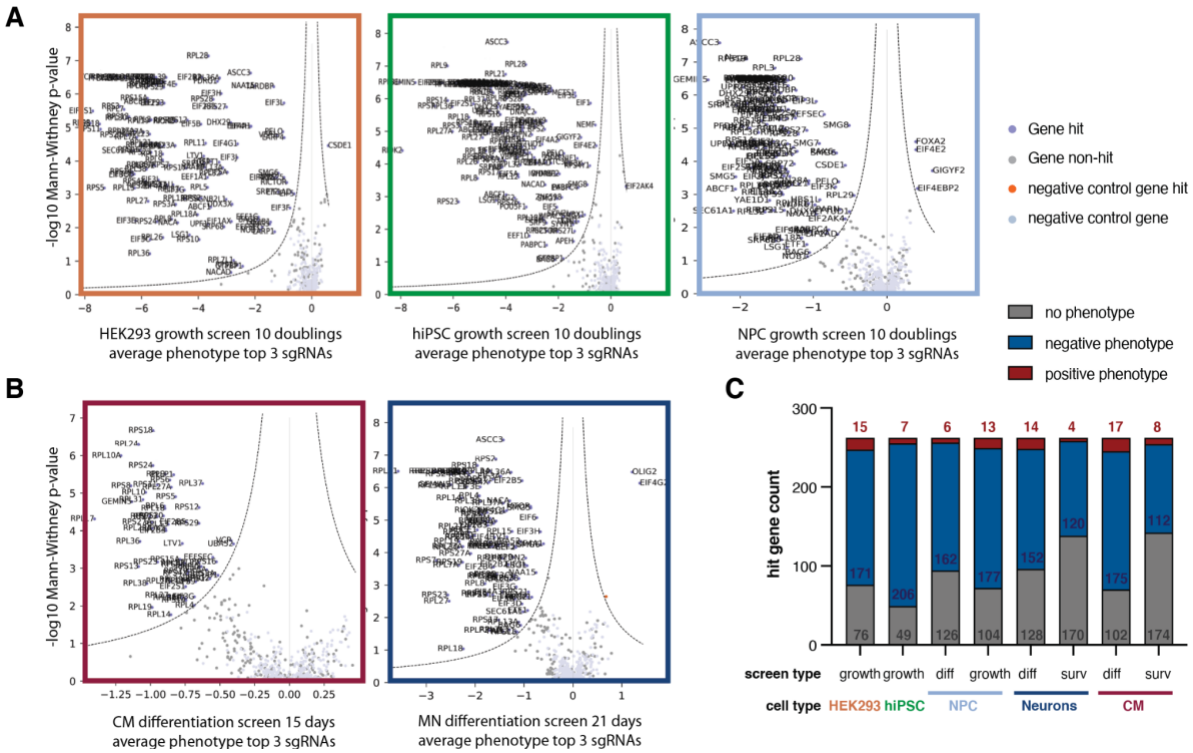

Figure 2.10.Phenotypic effect size in CRISPRi screens differs according to cellular context. Phenotype scores per gene calculated with the ScreenProcessing pipeline[345] in dividing HEK293, hiPSC and NPC CRISPRi lines (A) and differentiated cardiomyocytes (CM) and neurons (B). Positive, negative and neutral growth phenotypes were assessed by the sgRNA dropout rates for each cell context and screen type with a Mann-Whitney p-value cutoff of <0.1 (C) diff = differentiation, surv = survival.

Essential genes are generally defined as genes that orchestrate basic biological processes required to maintain cell homeostasis and are thereby indispensable for cell viability[358]. For our screens, we defined genes as essential when gene knockdown resulted in a negative phenotype score with a significant Mann-Whitney p-value ($p<0.1$). Since this essentiality can be cell context- or tissue-specific[359], we further subdivided genes into core essential (constitutive determinants of cell viability in all cell contexts), and context-essential (with variable impact on fitness in different cellular contexts).

To identify core essential genes, we compared knockdown phenotypes in our CRISPRi screens between different cell contexts and also with publicly available data sets. We found that 84 out of the 262 genes we targeted are core-essential in all cell contexts we tested. We detected a larger number of common gene hits upon excluding postmitotic cells, which is most likely due to higher rates of sgRNA dropout when cells divide. If we narrow our analysis to dividing cells only cells, we increase sensitivity to a total of 147 core-essential genes, which goes up further to 168 genes by only evaluating dividing cells with a healthy genetic background (hiPSC and NPC, **Figure 2.11 A**).

Next, we compared our data with publicly available data sets from genome-wide screens in cancer cell lines (DepMap2, https://depmap.org/portal/) and hiPSC-derived i^{3}Neurons (**Figure 2.11 B, C**)[342]. DepMap2 contains gene essentiality data of whole genome CRISPR knockout screens for 17,634 genes in 563 cell lines (Achilles data set). We found a large overlap in genes essential in hiPSC and HEK293 datasets and inDepMap2 data (**Figure 2.11 B**). Importantly, we detected 32 additional genes that are essential in hiPSC but not in HEK293 or cancer cell lines, the importance of analyzing gene essentiality in healthy genetic backgrounds.

In the published genome-wide CRISPRi screen in i^{3}Neurons, only 25 of the genes we targeted in our screen were found to elicit a negative phenotype (**Figure 2.11 C**). By contrast, our temporally controlled KRAB-dCas9 induction set-up led to a large increase in sensitivity, and also allowed us to identify genes that are only essential during but not after neuronal differentiation.

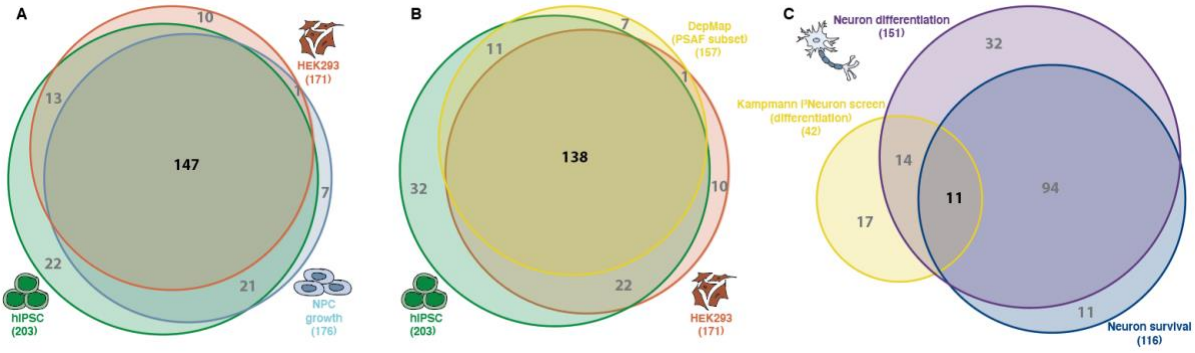

Figure 2.11. Comparison of essential gene sets identified by inducible CRISPRi screens with published data.
(A) Essential gene hits that overlap between growth screens of hiPSC, NPC and HEK293 cells. (B) Overlap between hiPSC, HEK293 cells and gene subset of DepMap2 essential gene list (https://depmap.org/portal/). (C) Overlap of our neuron survival and differentiation screen with the PSAF gene subset of a neuron differentiation screen from Tian et al.[342].

2.2.2. CRISPRi-induced phenotypes vary among distinct functional groups of mRNA translation regulators

We next asked whether cells were more susceptible to the loss of some functional components of the translation machinery than others, which could reveal the essentiality or specialized function of these factors, depending on the cell context. For this, we clustered all screening hits into four functional groups: ribosomal proteins (RPs), translation factors, ribosome-associated factors and mRNA binding and stability factors (**Figure 2.12**). Generally, we found that most ribosomal proteins, translation factors and ribosome-associated proteins showed high sgRNA dropout rates in dividing cells (phenotype scores of -10 to -7), which decreased in differentiated cells (phenotype scores of -4 to -1). Furthermore, factors for mRNA stability and ribosome quality control generally displayed a lower phenotype strength compared to the other functional groups. The number of genes with significant phenotypes upon gene knockdown decreased in differentiated cells, e.g. from 84 of 93 RPs in hiPSC (90%) to 67 of 93 RPs in cardiomyocytes (72 %). In hiPSC, 70% of the translation factors (53 out of 75), 71% of ribosome-associated proteins (42 out of 59) and 54% of mRNA stability factors (27 out of 50) were essential. A similar trend of protein essentiality between functional groups was observed in all cell contexts (**Figure 2.12**).

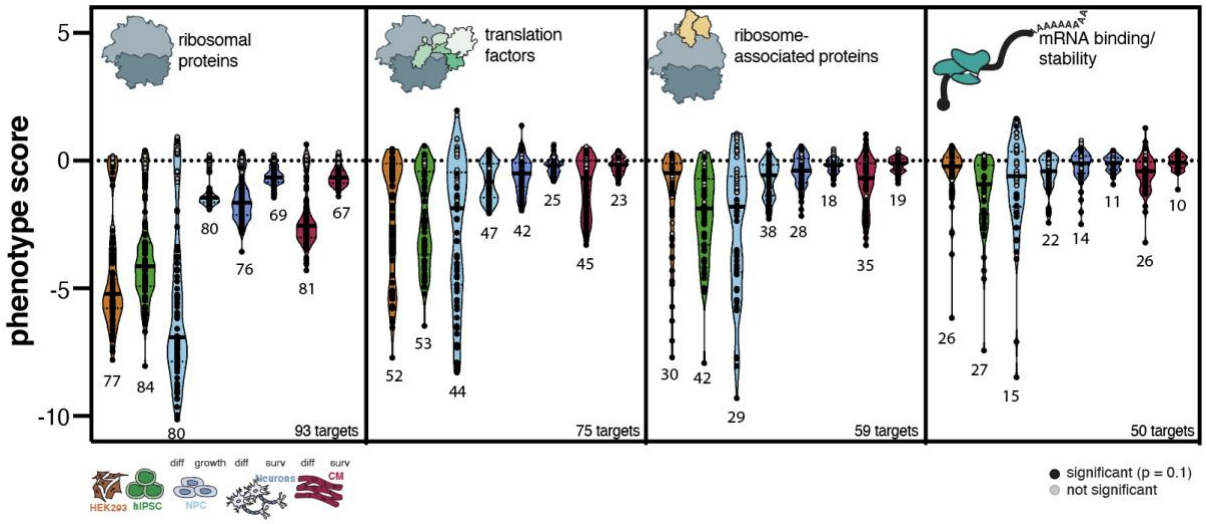

Figure 2.12. The consequences of gene repression are highly variable between different functional groups.
Gene phenotypes were calculated with the ScreenProcessing pipeline, genes were clustered into five functional groups, and phenotypes were plotted per cell type. Numbers indicate significant gene hits per cell context.

2.2.3. Genes encoding canonical ribosomal proteins are core-essential in human cells

Next, we investigated the conserved essentiality of each factor within the different cell contexts. We included two timepoints of the NPC growth screens to compare whether the phenotypes induced by gene knockdown are time-dependent. For this, we evaluated sgRNA dropout after 10 and 17 cell doublings. At the later time point, phenotype scores increased from -3 to -10, while the correlation between samples slightly decreased from R = 0.9 to R = 0.61 (**Figure S 5.1**). At the single gene level, we observed high similarity between both samples with a stronger sgRNA dropout or enrichment in NPCs that were cultured for 17 cell doublings (**Figure S 5.1**). This shows that phenotype effect size but not gene hit identity is time-dependent in this screen set-up.

We next evaluated the consequences of ribosomal protein gene knockdown in different cellular contexts. 75 out of 94 core ribosomal proteins were essential in dividing cells, and 59 elicited significant negative phenotypes under all screen conditions. RPL41 was the only canonical ribosomal protein, which was negatively selected in HEK293 cells, but not in hiPSC nor NPC. RPL41 was shown to be overexpressed in aneuploid and cancer cells, and suggested to enhance cell proliferation by stabilizing ATF4 and ATF4-mediated transcription of “survival signals”, whereas its downregulation increased cell death[360,361]. This specialized function of RPL41 has not been described in cells with a healthy genetic background may indicate that the fitness only of transformed cells is dependent on RPL41 (**Figure 2.12**, **2.13**). However, since a significant negative phenotype was detectable in NPC after 17 cell divisions, it is also possible that RPL41 is not efficiently depleted of silenced in hiPSC.

Several human ribosomal protein genes have paralogs (**Figure 2.13**). Paralogs originate from a gene duplication are called similarly to the canonical ribosomal protein, e.g. RPL3 and RPL3 “like” (RPL3L). They are often expressed in specific tissues and have been suggested to regulate ribosome specialization[134]. However, their function is difficult to assess by classical CRISPR knockout approaches due to their high sequence similarity, which makes it difficult to design sgRNAs that disrupt only one paralog. This is possible by CRISPRi, however, because gene repression is achieved by targeting transcriptional start sites (TSS). Indeed, we observe that canonical ribosomal protein gene are essential, while their the paralogs are nearly always dispensable for cell fitness (RPL3/3L, RPL10/10L, RPL26/26L1, RPL36A/36AL, RPL39/39L). Furthermore, when different predicted TSS of one gene are targeted by specific sgRNAs, we observed that in most cases only one of them is essential (RPL13A, RPL22, RPS30, RPS3).

In some cases, targeting the alternative TSS elicits a phenotype only in one of the differentiated cell types, which indicates that they might have specific functions during development. As an example, previous studies have shown that RPL22 and RPL22L1 can substitute each other in case of deficiencies in most tissues[136], which we confirmed in our screening results, as neither of these knockdowns elicited a negative phenotype (**Figure 2.13 A**). Interestingly, the knockdown of RPL22 improves the proliferation or differentiation of hiPSC to NPCs and to CM depending on which TSS is targeted. This suggests a potential shift in the use of TSS under different cell conditions that may regulate the transcription of these genes during development.

Similarly, for RPS4, repressing the copy on the X-chromosome (RPS4X) elicited strong negative phenotypes in all cell lines, while the essentiality of the two gene copies on the Y-chromosome (RPS4Y1 and RPSY2) between cell contexts (**Figure 2.13 B**). HEK293 cells did not show any selection, which was expected since they are derived from female kidney cells and lack a Y-chromosome. In contrast, in hiPSC, NPCs and neurons, which are male, RPS4Y1 knockdown elicited context-specific phenotypes.

Taken together, these data show that acute depletion of canonical ribosome proteins is nearly always detrimental in human cells, while some ribosomal protein gene paralogs may have specific functions at distinct stages of cell differentiation.

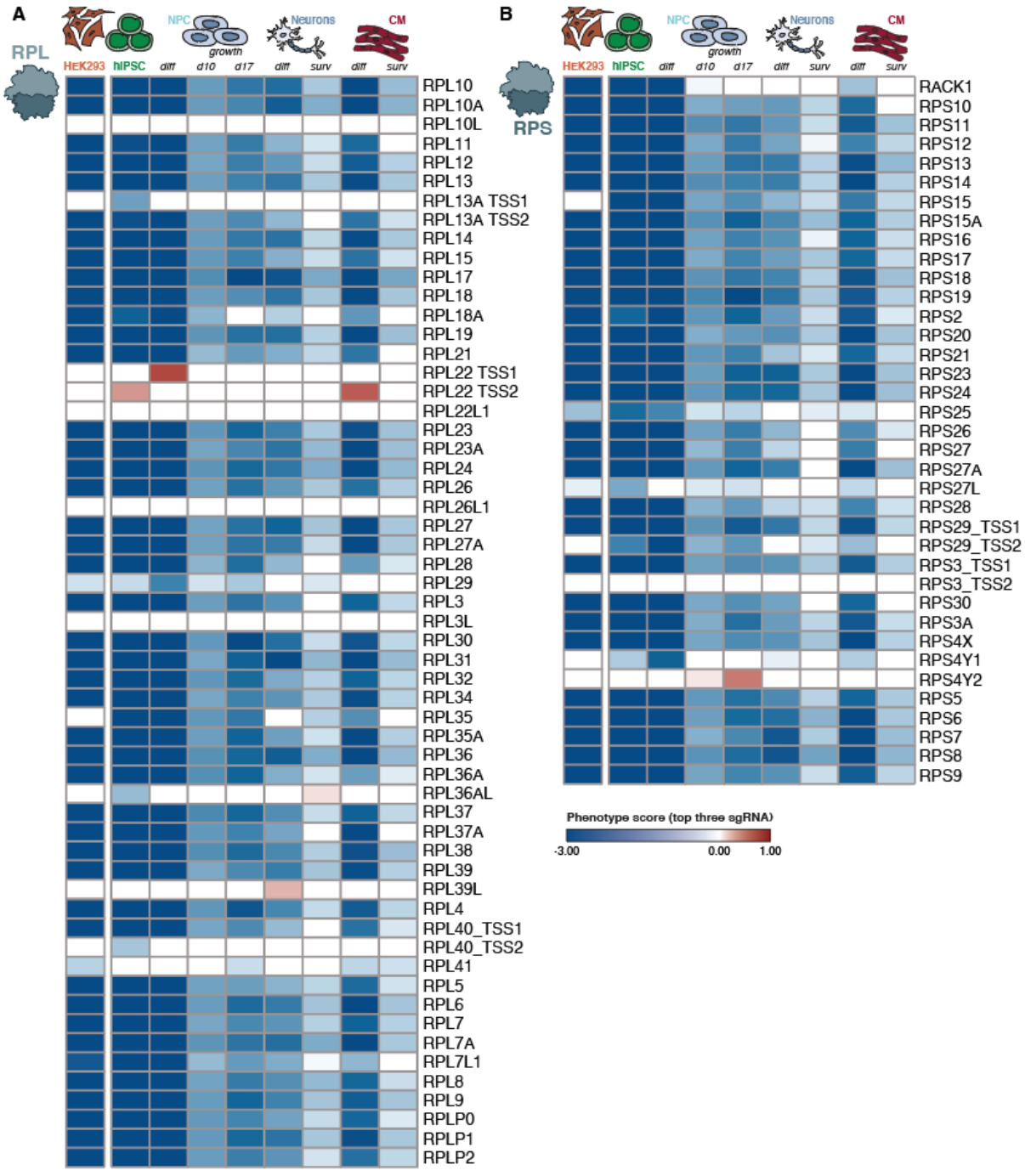

Figure 2.13. Phenotype scores of ribosomal protein gene knockdown across cell contexts
Proteins of the large (A) and small (B) ribosomal subunits. d = cell doublings, diff = differentiation, surv = survival, CM = cardiomyocytes.

2.2.4. Paralogs and alternative transcriptional start sites increase functional redundancy of translation factors

Translation initiation is the rate-limiting step of protein synthesis and therefore must be tightly regulated to maintain homeostasis. Like ribosomes, translation initiation factors are often organized into multi-subunit complexes. Furthermore, many translation initiation factor-coding genes also have paralogs EIF1AX/ EIF1AY, EIF3C/ EIF3CL, EIF5A/ EIF5AL1) and alternative TSS (EIF4G2, EIG4G3, EEF2). Under these circumstances, it is possible that translation initiation is particularly finely adjusted under different physiological conditions. Hence, we compared phenotype scores between cell contexts on a single gene level (**Figure 2.14**). As seen for ribosomal proteins, many translation initiation factors have one essential canonical form, while the other paralog or transcript isoform is dispensable for cellular fitness in the contexts we tested.

The PIC complex, which is formed by EIF1, EIF1A, EIF3, and EIF5, is essential for cap-dependent translation. Consequently, these complex components are consistently negatively selected in the screens, except for EIF1, which is only negatively selected in HEK293 cells, hiPSC, and during hiPSC differentiation to NPC. This suggests that EIF1 might be essential only in rapidly dividing cells but become dispensable when proliferation is reduced. The components of EIF2B, which activate the tRNA-iMet-CAT for translation initiation, were also negatively selected in all cell contexts and are core-essential. The EIF4F complex is composed of EIF4E, EIF4A and EIF4G, which all have several variants with highly variable composition and changes during development[140,141]. Interestingly, we observe that phenotypes upon loss of EIF4A components are the most variable ones of all translation initiation factors. Only EIF4A1 and EIF4A3 are consistently negatively selected in all cell contexts, hence their function is core-essential. EIF4A2 and EIF4G2 have two TSS to regulate cell fate. Their predominant form shows a highly negative phenotype score across cell types but seems to be protective during the neuron differentiation.

The core translation elongation complex comprises EEF1A and EEF1B, which both are encoded by several paralogs (e.g. EEF1A1/1A2) or have an alternative TSS. Accordingly, EEF1A and EEF2 were the only core essential translation elongation factors in our screen (**Figure 2.14**), The knockdown of most other translation elongation factors elicited strong negative phenotypes in HEK293, hiPSC, and NPC, but had smaller consequences in neurons and CM. This suggests that a decrease in proliferation and global protein synthesis rates may also decrease the essentiality of translation elongation factors.

Knockdown of the key translation termination factors, ERF3A and ABCE1, was highly negatively selected in hiPSC and HEK293 cells, while only ABCE1 showed consistently negative phenotypes in all cell types. It was previously shown that the expression of ERF3A and ERF3B varies between tissues: ERF3A is found ubiquitously, and ERF3B expressed predominantly in the mouse brain[362]. However, we did not observe negative pehnotypes of ERF3B knockdown in neurons. It is possible that ERF3B loss can be compensated by ERF3A in our culture-based experimental system.

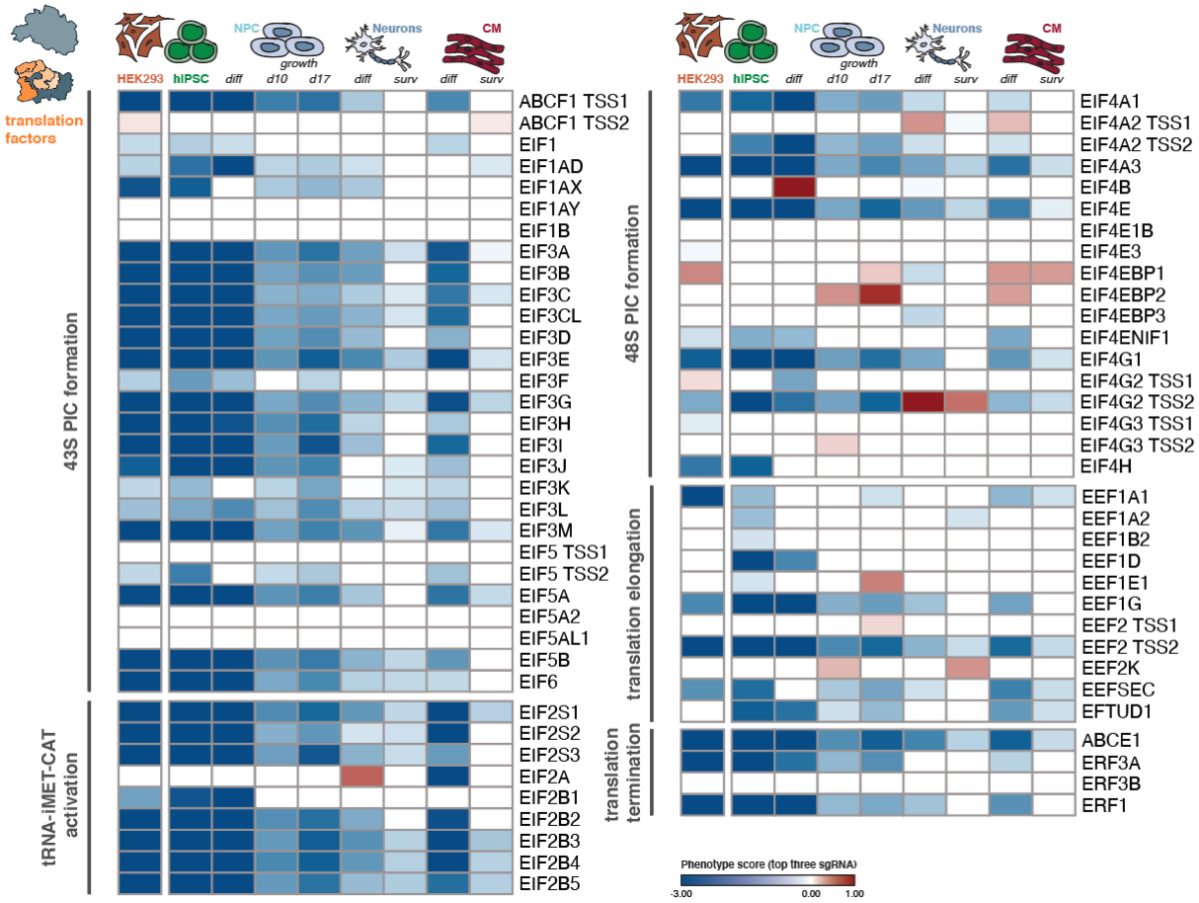

Figure 2.14.Phenotype scores of translation initiation, elongation, and termination factors across cellular contexts.
d = cell doublings, diff = differentiation, surv = survival, CM = cardiomyocytes.

2.2.5. Factors for mRNA binding and stabilization are essential in cells with a normal karyotype

During mRNA translation, numerous proteins have to maintain mRNA stability and degrade mRNAs in case of defects. Their malfunction can perturn homeostasis. In our screens, the depletion of proteins that mediate mRNA stability had high variable consequences in different cell lines, with sometimes surprising differences in the phenotypes elicited by loss of individual protein complex subunits (**Figure 2.15**).

Interestingly, we found two RNA-binding proteins – LARP4B and CSDE1, which were non-essential in hiPSC but their loss elicited positive phenotypes during NPC derivation. CSDE1 and LARP4B are key regulators of mRNA stability that modulate cell proliferation, differentiation, and apoptosis by controlling translation initiation events on specific mRNAs[363-365]. Their dysregulation is also associated with tissue-specific diseases in humans. For example, lower expression levels of CSDE1 were found in Diamond-Blackfan anemia[366], while its complete loss was strongly associated with neurological diseases such as Autism Spectrum Disorder[367]. By contrast, GEMIN5, a highly conserved RNA-binding protein that coordinates splicing, localization, translation, and mRNA stability[368-370], is highly essential in all cell contexts we tested (**Figure 2.15**).

Intriguingly, the three main ribonucleases in our screens ERI1, SLFN14, and ZC3H12A showed very similar phenotypic patterns. They were non-essential in hiPSC (except ERI1), strongly positively selected in NPC, and negatively selected during CM differentiation. ZC3H12A has been shown to positively regulate the derivation of glia cells from NPC[371] and to induce apoptosis in human CM[372]. These data show that our CRISPRi screens faithfully recapitulate known cell context-specific phenotypes.

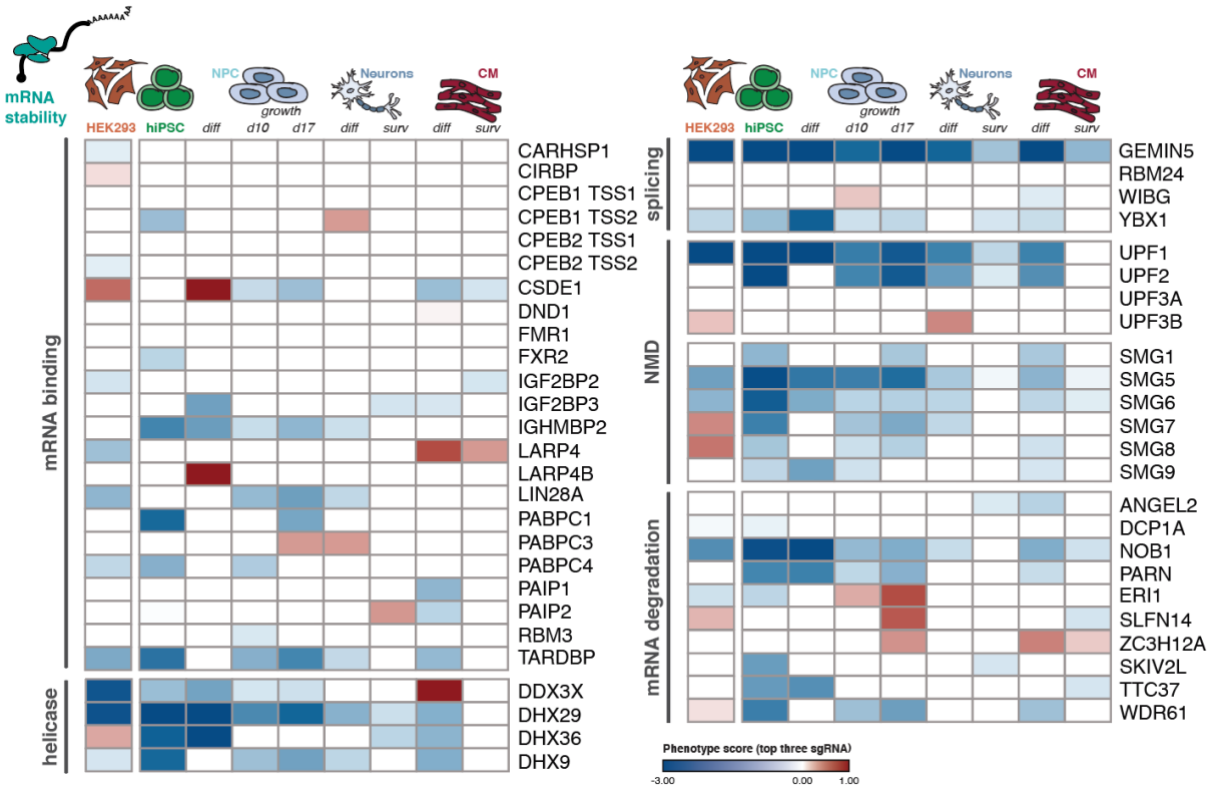

Figure 2.15. Phenotype scores of genes encoding mRNA stability factors.
d = cell doublings, diff = differentiation, surv = survival, CM = cardiomyocytes.

The NMD pathway provided another surprising example of context-specific phenotypes. The core components of the NMD pathway, the helicase UPF1 and the endonuclease SMG6, showed consistent negative phenotypes in all cell types. Depletion of SMG proteins was highly detrimental in hiPSC and NPC, while HEK293 depleted of SMG7 or SMG8 were positively selected in the screen. A central component of the NMD pathway, SMG1, did not elicit significant phenotypes in several cell contexts, including in HEK293 cells and NPC (after 10 cell doublings, **Figure 2.15**). Therefore, we investigated individual sgRNA dropout phenotypes from the screen (**Figure 2.16**) and observed that in NPCs only two sgRNAs gave consistent negative phenotypes (sgRNA5 and sgRNA8). By contrast, in HEK293 exactly the same sgRNAs elicited a positive phenotype. However, in both cases, the phenotype strength varied among biological replicates, which means that after Mann-Whitney p-value evaluation of phenotype strength for all nine sgRNAs, these knockdown phenotypes are not statistically significant. These data highlight that the essentiality of genes that are not identified as hits in a screening set-up has to be carefully re-evaluated and validated. We note, however, for most of the gene targets that we investigated in more detail, we did not observe such phenotypic discrepancies (**Table S 5.1**).

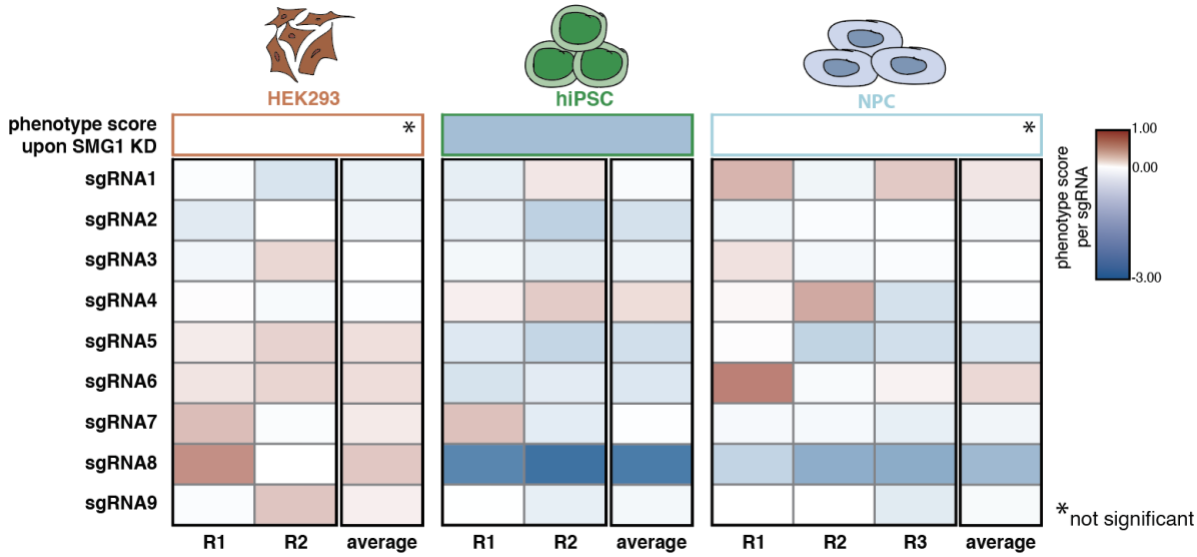

Figure 2.16. SMG1 is essential in hiPSC and NPC, but its loss may enhance HEK293 growth.
Evaluation of individual sgRNA phenotypes of the ninesgRNAs that target SMG1 and as an average of the two screen replicates (R1 and R2).

2.2.6. The loss of proteins of the ribosomal quality control pathways elicits phenotypes that are highly cell context-specific

Many proteins act co-translationally to orchestrate a variety of processes including nascent chain folding, protein translocation, and protein modification. Since ribosomes are highly abundant complexes with high turnover rates, they are continuously synthesized. Their initial assembly is orchestrated in the nucleus but is finalized in the cytoplasm. Correspondingly, the main factors mediating cytosolic ribosome biogenesis - LSG1, LTV1 and RIOK2 - were core essential in our screens (**Figure 2.17**). This observation corroborates our findings that ribosomal protein genes are core-essential. It also suggests that although ribosomal proteins have relatively long half-lives in postmitotic cells (~7-8 days)[315], new ribosomes must be continuously synthesized and assembled to maintain cellular homeostasis.

Most factors for co-translational folding are essential for cellular fitness in all contexts we tested (**Figure 2.17 A**). Interestingly, DNAJC2 and HSPA14, which are thought to function as co-translational chaperones, are essential in dividing cells with a normal karyotype (hiPSC, and NPC), but not in the aneuploid HEK293 cell line. Factors that regulate mRNA localization are also highly essential in all cell contexts. Loss of the Nascent Polypeptide Associated

Complex Subunit Alpha (NACA) elicits strong negative phenotypes all cell contexts, while the highly similar proteins NACA-like protein (NACA2) and NACA-containing domain (NACAD) show cell context-selective importance (**Figure 2.17 A**). Both components of the N-terminal acetyltransferase complex A (NATA) - the catalytic protein NAA10 and the auxiliary protein NAA15[373,374] - are core essential. In contrast, loss of their paralogs NAA11 and NAA16[375,376], respectively, which were shown to partially compensate for their loss when overexpressed, does not lead to significant phenotypes in the screens. These data suggest that NAA10/ NAA15 dysfunction cannot be rescued by their paralogs under physiological settings, probably because these genes are epigenetically silenced in most tissues[376].

Many proteins stimulate translation by binding or modifying proteins of translation initiation complexes (**Figure 2.17 B**). MTOR, a major regulator of translation and proliferation[377], was highly negatively selected in the screens. However, the direct interaction partner (RICTOR) or downstream targets of MTOR (RPS6KA2, RPS6KB2, RPS6KL1) were not. Furthermore, members of the EIF2AK family, which are the major stress sensors in the cell and mediate eIF2α phosphorylation[378], showed highly diverse phenotypes. Depletion of GCN2 (EIF2AK4), which senses amino acid deprivation[126], surprisingly promoted growth in HEK293 and hiPSC, but was detrimental in NPC. The GIGYF2/ EIF4E2 complex was previously shown to associate with mRNAs on which ribosomes collide to prevent further rounds of translation by inhibiting initiation[235,236]. The loss of these two proteins elicited phenotypes that were highly concordant, confirming their functional association. Interestingly, GIGYF2/EIF4E2 loss was detrimental in hiPSC and during the derivation of NPC, but elicited a positive phenotype in NPC. Finally, the knockdown of EIF2D, which has been suggested to orchestrate translation re-initiation events, did not lead to significant phenotypes under any of our screening conditions (**Figure 2.17 B**). By contrast depletion of DENR or MCTS1, which work in a complex and contain homologous structural domains to EIF2D, had negative phenotypic consequences in hiPSC and most hiPSC-derived cells. Surprisingly, the knockdown of these genes elicited a strong positive phenotype during CM differentiation (**Figure 2.17 B**). These data suggest that in human cells, the endogenous mRNA substrates of EIF2D and DENR/MCTS1 might differ.

Cell context-dependent phenotypes also frequently resulted from loss of proteins involved in the recognition and resolution of collided ribosomes. In hiPSC, almost all of these factors are essential for cell fitness, confirming our ability to effectively deplete them by CRISPRi. However, we found that only a few of them are core essential, e.g. ASCC3 (**Figure 2.17 B**). Interestingly, loss of the other components of the ASC-1 complex we targeted - ASSC2, and TRIP4 - did not give rise to detectable phenotypes in most cellular contexts, except a modest

growth defect in hiPSC lacking TRIP4 and a modest growth advantage during neuron derivation (**Figure 2.17 B**). Notably, HEK293 cells are less affected by loss of these factors, and only show mild negative phenotypes upon loss of a subset of proteins, namely NEMF, PELO and ZNF598. Furthermore, factors that act downstream of ribosome disassembly (LTN1, NEMF, ANKZF1, and TCF25), have less pronounced phenotypes than their upstream effectors (GTPBP1, HBS1L, PELO, ZNF598, ASCC3) in hiPSC. This suggests that recognition and disassembly of stalled and/or collided ribosomes is essential for cellular fitness, whereas defects in downstream steps such as 60S recycling and nascent chain degradation by the RQC complex are better tolerated under the conditions of our screen.

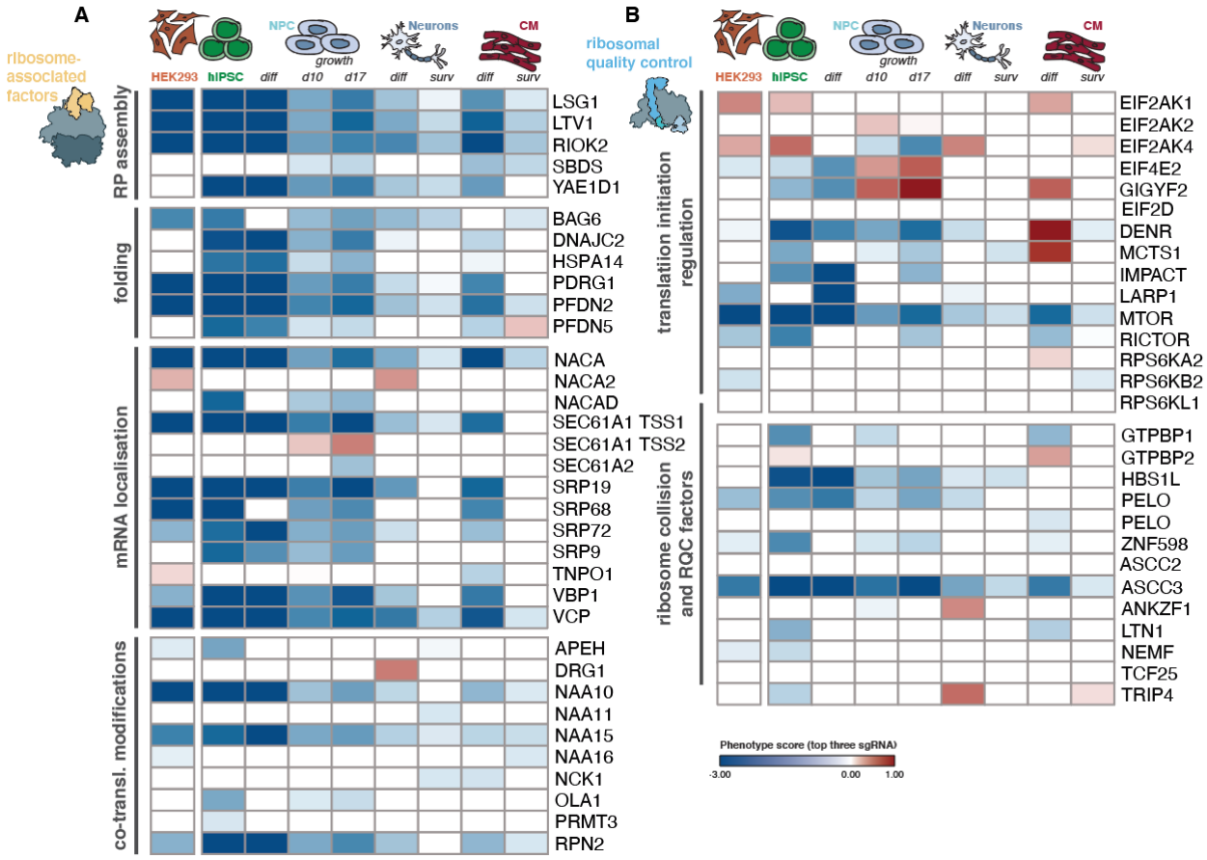

Figure 2.17. Phenotype scores of genes that directly associate with ribosomal proteins.
d = cell doublings, diff = differentiation, surv = survival, CM = cardiomyocytes.

Due to the large differences in the phenotypic consequences of representing genes from the ribosome collision and quality control among different cell lines, we focused our validation experiments as well as downstream investigations on those factors.

2.3. Targeted CRISPRi validates screening results and identifies common responses to perturbations in ribosome collision surveillance

2.3.1. Pooled screening phenotypes are highly reproducible in single knockdown experiments

CRISPRi exhibits low false-positive and false-negative rates and result in fewer off-target effects than RNAi in mammalian systems[333]. Its use as a large-scale screening platform is a powerful tool for the exploratory assessment of biological processes and gene function. However, screening data need careful evaluation and downstream validation to ensure the accuracy of the results obtained.

After we successfully performed pooled CRISPRi screens, we chose 22 genes for validation by single sgRNA knockdown validation and further investigations of the mechanisms underlying cell the cellular phenotypes resulting from gene repression. These genes mostly encoded factors implicated in the recognition and resolution of collided ribosomes. The strongest phenotypes we observed were in dividing cells, which typically have higher protein synthesis rates than postmitotic cells. Therefore, we focused most of our follow-up experiments on hiPSC, NPC, and HEK293 cells.

We previously observed that the phenotype analysis using the ScreenProcessing pipeline could miss genes because their p-value (Mann-Whitney) is calculated as an average of the nine sgRNAs we designed per gene target (**Figure 2.16**). This can lead to false-negative results, because for some genes or cell contexts, only a fraction of these sgRNAs may efficiently reduce gene transcription. For this, we first investigated individual sgRNA scores of each of our selected genes. We found that most of the dropout / enrichment rates for sgRNAs were consistent among several sgRNAs targeting the same gene (**Table S 5.1**). However, for GTPBP1, we found that the screening phenotypes were not significant in HEK293 cells although two sgRNAs gave very strong negative phenotypes (sgRNA 2 and 9, **Figure 2.18**). Because some sgRNAs were also weakly positively selected (e.g. sgRNA 6 and 7), the calculated average phenotype score for the GTPBP1 gene in HEK293 was negative (-2.48), but had a Mann-Whitney p-value of 0.14, which did not pass our significance threshold. When we compared sgRNA scores in hiPSC and NPC, we saw that the same two sgRNAs also led

to strong negative phenotypes (**Figure 2.18**). Due to the consistent dropout rates of sgRNA2 and sgRNA9, we reasoned that GTPBP1 is also essential in HEK293 cells.

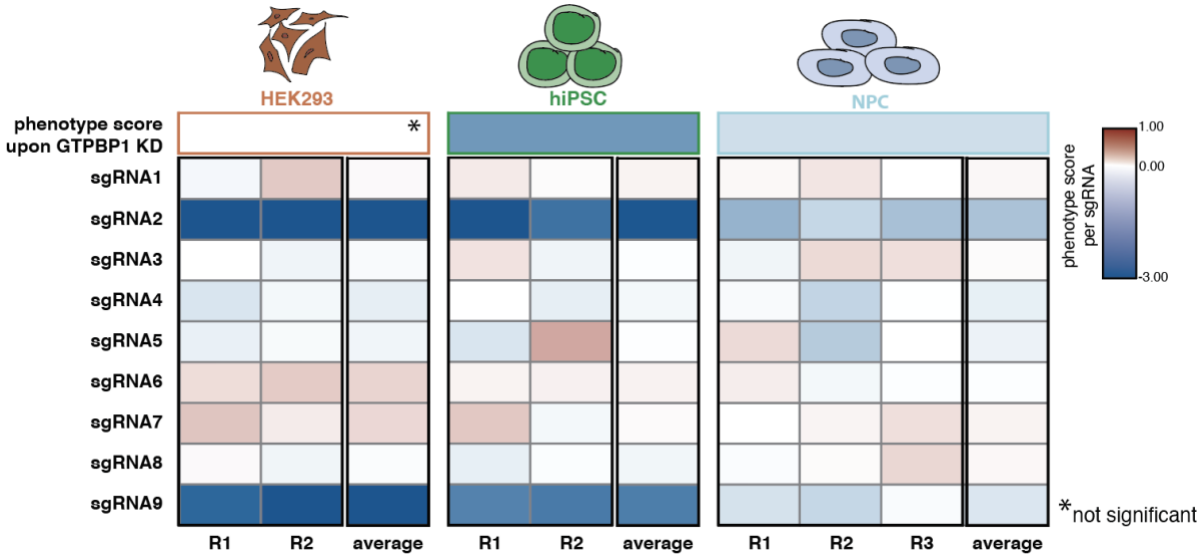

Figure 2.18. GTPBP1 is essential in HEK293, hipSC, and NPC.
Evaluation of individual sgRNA phenotypesselection of the nineall nine single sgRNAs that target GTPBP1 individually and as an average of the two screen replicates (R1 and R2).

We validated our pooled screens using a single sgRNA knockdown approach. sgRNAs were selected based on their screen phenotype scores and individually inserted into the lentiviral expression vector (**Figure 2.7 A**). hiPSC, NPC, and HEK293 cells were then transduced and cellular phenotypes were evaluated by comparing the percentage of GFP-positive cells after doxycycline induction relative to the GFP-containing fraction in uninduced cells every four cell doublings by flow cytometry (**Figure 2.19 A**). We chose genes whose loss elicited strong negative phenotypes (GTPBP1), no phenotypes (GTPBP2), and cell context-specific phenotypes (HBS1L) in our screens. We observed that upon GTPBP1 knockdown, GFP levels rapidly decreased and almost completely disappeared after eight cell doublings in hiPSC and HEK293 cells, whereas they decreased at slower rates in NPC. GTPBP2, which did not show any phenotype in the screens, also did not change growth rates in hiPSC or HEK293, but slightly decreased NPC proliferation at late timepoints beyond the last one we used for NPC screens. Upon HBS1L knockdown, the number of GFP-positive cells decreased rapidly in hiPSC, more slowly in NPCs, and not at all in HEK293 cells. Using this assay, we tested growth phenotypes for 22 genes from the screen, and our results were consistent with the screening phenotypes (**Table S 5.2**, **S5.3**, **S5.4**, **Figure S 5.2**).

To confirm that the lack of cellular phenotypes is not due to inefficient gene repression or protein depletion, we selected cells with puromycin and measured the mRNA levels of target genes by quantitative RT-PCR after three cell doublings (**Figure 2.19 B**), and protein levels by Western Blot after five cell doublings (**Figure 2.19 C**). Since cells depleted for GTPBP1 were rapidly lost from culture, we decreased the knockdown duration to two doubings for this target. We observed that upon gene knockdown, mRNA and protein levels were strongly decreased for all targets. Importantly, this was the case also for genes whose loss did not lead to significant phenotypes in our pooled screens (e.g. GTPBP2, **Figure 2.19 C**). We also confirmed that upon HBS1L depletion, the abundance els of its interaction partner PELO also decreases (**Figure 2.19 C**), in line with published data[379].

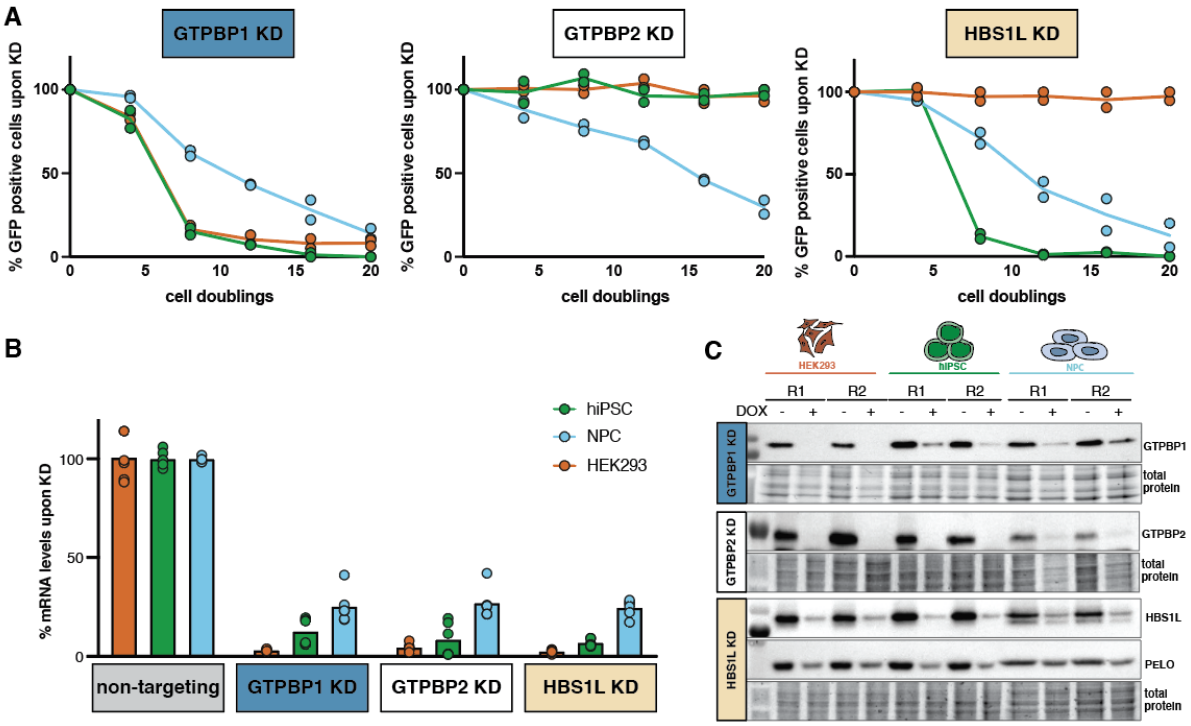

Figure 2.19. Single gene knockdown experiments validate screening phenotypes.
(A) Growth curves of GTPBP1, GTPBP2 and HBS1L (left to right) knockdown (KD) in hiPSC, NPC and HEK293 cells. GFP-positive cells were measured by flow cytometry everyfour cell doublings for a total of 20 cell doublings, and normalized to GFP % in non-induced control samples. At least 10,000 cells were analyzed per measurement. (B) To measure remaining mRNA levels, gene knockdown was induced for two (GTPBP1) and three cell doublings (GTPBP2, HBS1L) before RNA extraction. B2M was used as a reference gene for relative mRNA quantification. mRNA levels were normalized to the levels in corresponding non-targeting control (n=2) with three technical replicates. (C) Western Blot analysis of protein abundance lafter two (GTPBP1) or five cell doublings (GTPBP2, HBS1L) compared to non-induced controls containing the same sgRNA. Experiments were performed in two biological replicates (R1 and R2).

Taken together, the validation experiments led us to conclude that the screening phenotypes were highly reliable. We confirmed the cellular fitness effects for 19 of the 22 genes we selected for validation. We could not reproduce the mild positive screening phenotypes we

observed in hiPSC and HEK293 for the eIF2AK family in the pooled screens (**Table S 5.2**, **S5.3**). We tested different initial transduction rates and cell seeding densities, but in all cases the fraction of GFP-positive cells in induced samples remained very similar to that in uninduced controls. This suggested that our experimental set-up for single sgRNA validation might not be sensitive enough to capture weak positive selection in highly proliferative cells.

We also probed whether differences in protein abundance among cellular contexts could account for the distinct importance of ribosome collision and quality control factors. For that, we performed quantitative proteomics of the CRISPRi cell lines at the MPI-B Mass Spectrometry Core Facility. This revealed highly similar protein levels in all cell types, with the exception of ZNF598, which was more abundant in HEK293 than in hiPSC or hiPSC-derived cultures (**Figure 2.20 A, B**).

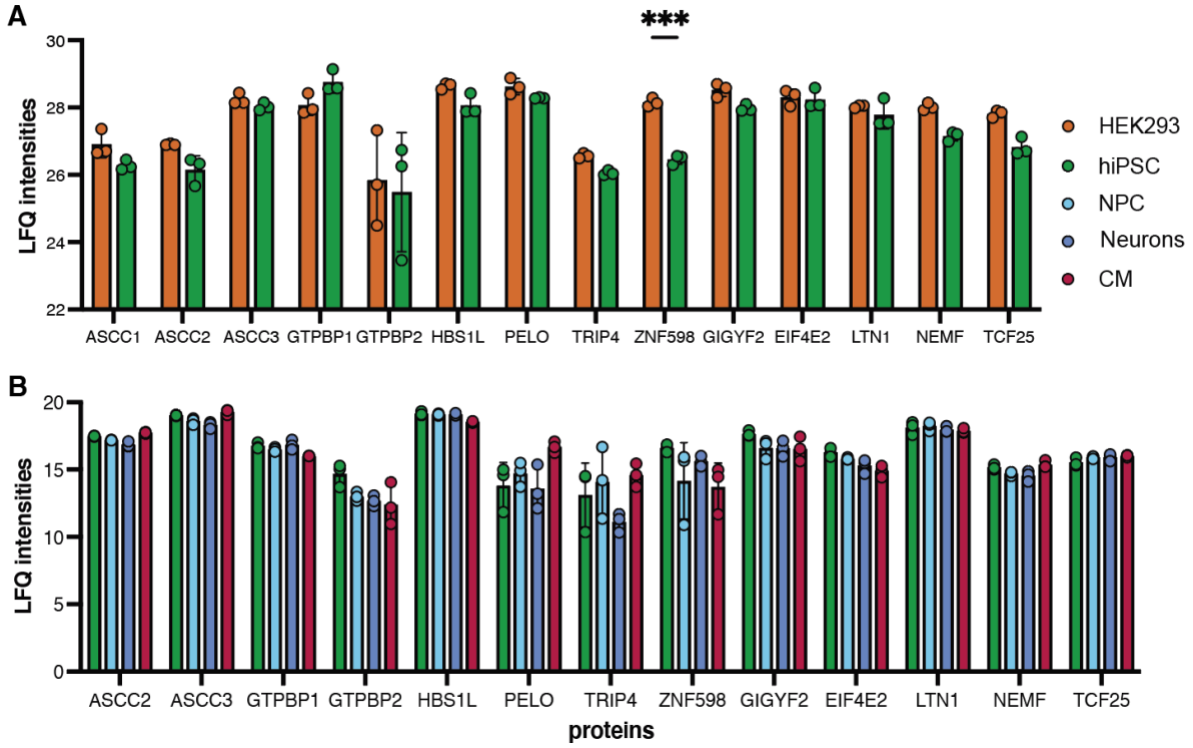

Figure 2.20. Protein abundance does not correlate with growth phenotypes upon protein depletion. Normalized LFQ intensities per protein derived from quantitative mass spectrometry comparisons between (A) hiPSC and HEK293 cells, and (B) hiPSC and hiPSC-derived cell types. T-test significance p=0.01.

Taken together, these data show that the phenotypes from pooled CRISPRi screens are highly reproducible in single sgRNA experiments. Furthermore, they suggest that the differences in phenotypic importance among cell contexts are not caused by differences in mRNA or protein stability or differences in expression levels.

2.3.2. Global translation changes are cell context specific

We next analyzed how gene knockdown impacts cell cycle progression, cytotoxicity, and global translation in different cellular contexts. Knockdown duration depended on the phenotype's appearance, so we individually chose the time point at which >75% of the knockdown cells were still viable. When the phenotypes were cell context-specific, we harvested all cells after the same amount of cell doublings. Consequently, we harvested GTPBP1 after two doublings, HBS1L after five doublings, and knockdowns without a phenotype after five doublings (GTPBP2), as we previously confirmed protein depletion at this time point (**Figure 2.19**). These targets were chosen as representative examples for different knockdown phenotypes and essentialities between cell contexts. Therefore, investigating their gene knockdown effects on proliferation and cell viability should be informative on general molecular mechanisms that influence cellular states.

To identify cell cycle progression defects, we stained cells with propidium iodide (PI), measured fluorescent intensity by flow cytometry, and analyzed the proportion of cells in each cell cycle phase with the Watson Pragmatic Algorithm[380]. Cell cycle profiles were compared to those in cells containing a non-targeting (NT) sgRNA in which KRAB-dCas9 expression was induced for five cell doublings. This analysis did not reveal any major changes in cell cycle progression for most of our targets (**Figure 2.21**, **S5.3**), except for GTPBP1 in HEK293, where a higher proportion of cells remained in the G2 phase (**Figure 2.21 A**). For other targets and cell contexts (**Figure 2.21 B**, **C**, **S5.3**), the fraction of cells in different cell cycle phases was comparable equally distributed compared to the NT control.

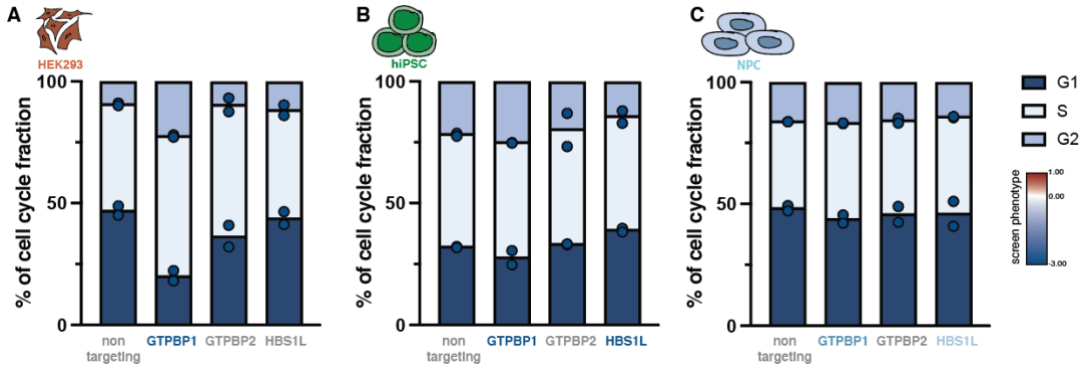

Figure 2.21. Cell cycle progression is not impaired upon knockdown of GTPBP1, GTPBP2, or HBS1L. Gene knockdown (KD) was induced for two (GTPBP1), and five cell doublings (GTPBP2, HBS1L) in biological replicates. Cells were harvested at 75% viability after knockdown, stained with propidium iodide and analyzed by flow cytometry. Proportions of cells per cell cycle phase (G1, S and G2) were determined with the Watson Pragmatic Algorithm. Fraction of cells in G1, S and G2 phase upon knockdown of ribosome collision factors with different screening phenotype strengths in (A) HEK293 cells, (B) hiPSC and (C) NPC. At least 10,000 cells were analyzed per biological replicate. Experiments were performed in two biological replicates. Color of gene label indicates pooled screening phenotypes.

We then investigated whether cells lacking NGD/ NSD factors accumulated toxic by-products by translating dysregulated mRNAs, or whether they simply reduced proliferation and translation in order to rebalance protein synthesis. For this, we measured cellular lactate dehydrogenase (LDH) levels, which are often used to assess cytotoxicity and early apoptotic processes. LDH is a soluble enzyme in the cytoplasm of cells and is released into the culture medium after membrane damage[381]. We measured LDH in supernatants from the same knockdown cultures used for cell cycle analysis, and normalized LDH levels to NT control cells. This means, as before, we induced gene knockdown to the point where cells reached 75% viability. LDH quantification showed that HEK293 cells did not elucidate any changes in LDH levels, regardless of their phenotype strength (**Figure 2.22 A**). For genes and cell contexts with very strong and early negative phenotypes, such as GTPBP1, LDH release was detectable for hiPSC but not HEK293 cells (**Figure 2.22 A**, **B**). Genes with later phenotypes showed only mildly increased LDH levels (HBS1L), and genes whose knockdown had no phenotype did not trigger LDH release. NPCs, similar to HEK293 cells, did not increase cell toxicity (**Figure 2.22 C**). These observations were consistent for all gene ribosome collision and quality control genes we tested (**Figure S 5.4**), and indicate that an early negative phenotype is generally associated with cytotoxicity in hiPSC, but not in other cell contexts (**Figure 2.22 B**).

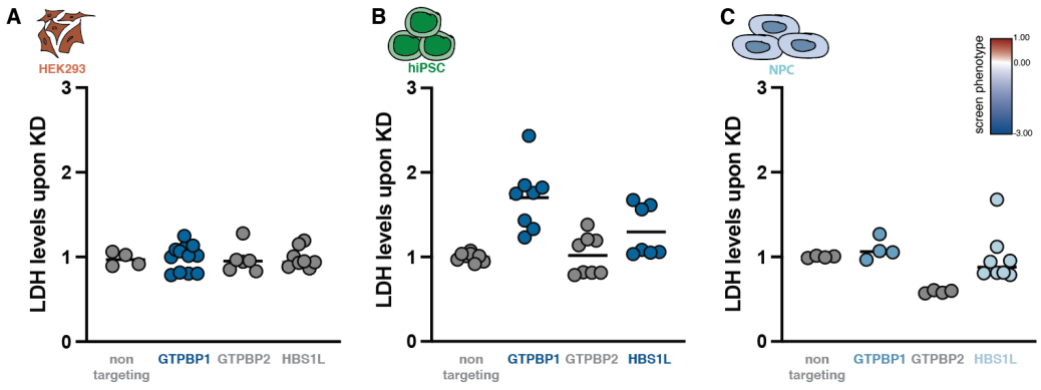

Figure 2.22. Early negative phenotypes are linked to cytotoxic stress.
Gene knockdown (KD) was induced for two (GTPBP1), and five cell doublings (GTPBP2, HBS1L) in biological replicates before measuring cytotoxicity with LDH. LDH levels in the medium of four technical replicates were measured by a colorimetric quantification using a CytoTox Assay Kit (Promega) and normalized to a non-targeting sgRNA control cell population (A) HEK293 (B) hiPSC, (C) NPC. Color of gene label indicates pooled screening phenotypes.

HEK293 cells and NPCs did not change the level of LDH or the progression of the cell cycle, but maintained the characteristics of stable proliferation. Therefore, we investigated whether cells change proliferation by adapting global translation. We used L-Homopropargylglycine (HPG), a methionine analog containing an alkyne moiety, to monitor global protein synthesis by its incorporation into nascent chains, which can be quantified by chemoselective ligation of

an azide fluorophore and subsequent analysis by flow cytometry[382]. As before, we induced gene knockdown until cells reached 75% viability, cultured them in medium without methionine for 30 minutes, and added HPG-containing medium for another 30 minutes before harvesting. We observed that HPG incorporation in HEK293 cells was generally not altered by gene knockdown (**Figure 2.23 A**), while global protein synthesis decreased by 20-40% in hiPSC for most knockdowns (**Figure 2.23 B**, **S5.5**). Interestingly, HPG incorporation increased after GTPBP1 or HBS1L knockdown by 50% in NPC (**Figure 2.23 C**).

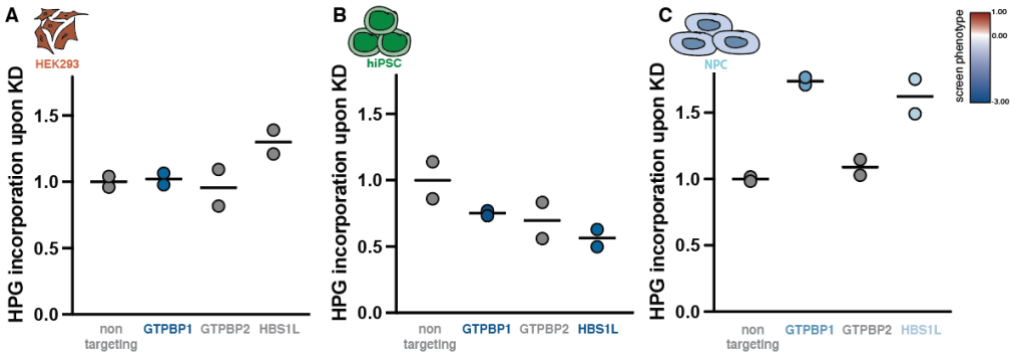

Figure 2.23. Global translation decreases upon loss of NSD/NGD factors in hiPSC.
Gene knockdown (KD) was induced for two (GTPBP1), and five cell doublings (GTPBP2, HBS1L) in biological replicates before HPG incorporation into the nascent chain. HPG was incorporated for 30 minutes in the nascent chain and a picolyl-azide was added by click chemistry after fixation. At least 10,000 cells were analyzed by flow cytometry and HPG incorporation changes were normalized to a non-targeting control for HEK293 cells (A), hiPSC (B) and NPC (C). Color of gene label indicates pooled screening phenotypes.

2.3.3. Cell context-dependent phenotypes do not correlate with differences in stalling reporter readthrough

We next examined the effect of gene repression in different cellular contexts on mRNA surveillance. Translation defects that trigger ribosomal quality control can occur on truncated mRNAs, polybasic amino acid stretches, or during translation of highly repetitive or structured mRNA stretches[199]. Most studies on ribosome stalling detection and resolution rely on the use of a flow cytometry-based reporter to quantitatively assess stalling. The reporter contains N- and C-terminal fluorescent proteins, separated by a FLAG-stalling reporter (SR) sequence[202]. The FLAG-SR is flanked by viral 2A sequences, which induce ribosome peptide skipping during translation and therefore separate newly synthesized peptides from each other[383]. When no stalling sequence is present, the three proteins should be synthesized in equimolar amounts. When sequences that trigger ribosome arrest are inserted in the FLAG-SR region, only the N-terminal fluorescent protein should be produced. Stalling readthrough can thus be analyzed under different conditions by quantifying changes in the ratio of N-terminal to C-terminal fluorescent protein abundances[202,226,237].

We adapted previously established reporters by exchanging the N-terminal GFP with a BFP and the C-terminal RFP with a mOrange cassette, so that fluorescent signals would not overlap with our KRAB-dCas9 (mCherry) or sgRNA (GFP) expression constructs (**Figure 2.24**). Furthermore, we optimized the expression of the construct by several sequence modifications. First, we exchanged the first P2A for a T2A sequence, since this has been shown to improve skipping in triple-gene constructs[384]. Second, we exchanged the expression promoter from the strong CMV (which is inactive in stem cells) to the moderate UbC promoter, to equalize construct expression levels in all cell contexts [385,386]. Third, we incorporated our reporter construct into a lentiviral backbone, which enables us to stably insert and express the reporter in a scalable manner by titrating lentiviral transduction rates. This helps ensure that each cell receives only one copy of the reporter construct. Finally, we inserted previously established SR sequences, namely a poly-lysine stretch encoded by AAA codons (K20-SR), an XPB1 stalling sequence (XBP1-SR), and a non-stop mRNA construct that is stabilized with a MALAT1 3' UTR hairpin structure (nonstop-SR, **Figure 2.24 B**, **C**, **E**)[202,237]. We also generated the corresponding control reporter, which contained no stalling sequence, or a stop codon MALAT1 3' UTR hairpin (**Figure 2.24 A**, **D**). Similarly to proliferation assays, we measured mOrange and BFP fluorescence after expressing all stalling reporters for two cell doublings at 75% cell viability after inducing gene knockdown. As an example, we induced the knockdown of ZNF598 by doxycycline treatment for three cell doublings, transduced those cells with the stalling constructs at a 40% infectivity rate, and cultured them for two additional doublings. This resulted in a ZNF598 knockdown duration of five cell doublings at the time of analysis.

After optimization of the construct, we asked whether our set-up allows us to reproduce published reporter expression and readthrough changes after knockdown of ZNF598 and GIGYF2 [202,237]. We induced ZNF598 knockdown for the K20- and XBP1-SR reporter and GIGYF2 knockdown for the nonstop-SR expression in HEK293 cells, and analyzed the reporter readthrough compared to a non-targeting control (**Figure 2.24**). We observed an increase in the mOrange: BFP ratio upon knockdown for both the K20- and the XBP1 stalling constructs, which means that, in accordance with published data, the readthrough of these stalling sequences is increased in the absence of ZFN598 (**Figure 2.24 B**, **C**). For the nonstop construct, we observed a slight decrease in the mOrange: BFP ratio (**Figure 2.24 D**). Both results are consistent with recent findings[202,226,237] and suggest that our modified reporters were functional. Interestingly, HEK293 cells also showed changes in mOrange levels in the non-stalling reporter expression after knockdown, which led to an increase in the mOrange: BFP ratio (**Figure 2.24 A**, **D**, **S5.6**). Since 2A sequences have been shown to induce ribosome

collisions in yeast[265], this could mean that low levels of ribosome stalling may already appear in control reporters. To avoid biases from potential stalling at 2A sequences, we normalized the median fluorescent intensities of the stalling to the non-stalling reporter for each gene knockdown.

Previous work suggests that mRNAs that trigger ribosome stalling are targeted for degradation, which in our set-up would lead to a decrease in the BFP signal[237]. This is problematic because we cannot differentiate between fluorescence intensity changes due to mRNA stability or ribosome arrest. To confirm that the changes result from increased mOrange signal rather than changes in mRNA stability and hence also BFP signal, we plotted the fluorescent fold change of both fluorophores in comparison to a non-targeting control (**Figure 2.24 F**). This analysis revealed that only the mOrange signal changed upon gene knockdown, suggesting that increased readthrough did not derive from changes in mRNA abundance of the reporter.

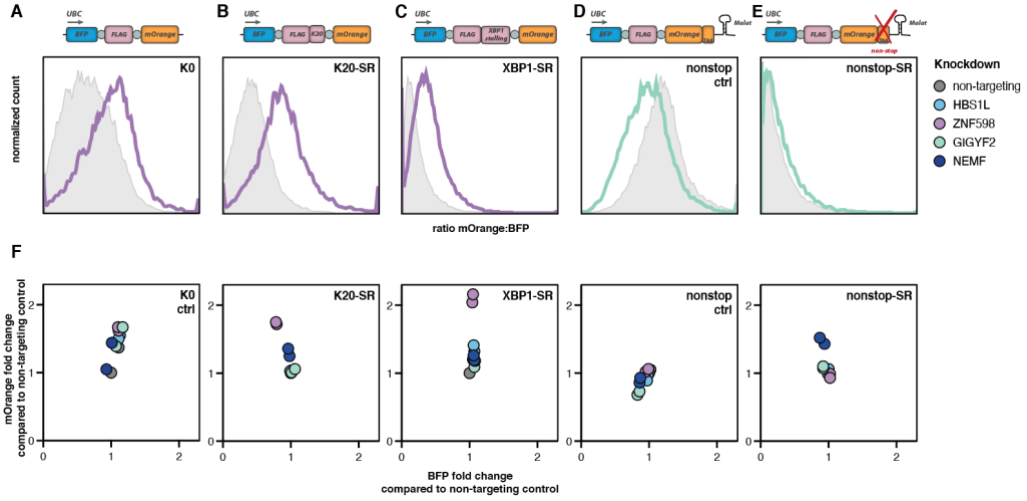

Figure 2.24. Fluorescent reporters reveal gene knockdown effects on stalling readthrough in HEK293 cells.
Schematic of stalling and control reporter constructs used in this thesis: no stalling control (K0), poly-lysine stretch (K20), XBP1 stalling, stop codon-containing control and non-stop construct(A to E). Fluorescent intensity of BFP and mOrange was measured in 30,000 cells by flow cytometry and the resulting ratio was plotted using Flowjo for ZNF598 (A to C) or GIGYF2 (D to E) knockdown in HEK293. (F) Median fluorescent intensity changes of individual fluorescent proteins produced from reporter constructs were compared to the non-targeting control for the indicated gene knockdowns in HEK293 cells. Experiments were performed in biological replicates, histograms depict one representative replicate.

ZNF598 and ASCC3 were shown to influence reporter readthrough and therefore ribosome collisions in HEK293 cells[202,226]. However, it is unclear whether and how other factors of the ribosome collision and quality control pathways influence ribosome stalling in different cell contexts. For this, we systematically analyzed the effect of depleting twelve proteins on stalling reporter readthrough in HEK293 cells, hiPSC and NPC (**Figure 2.25**, **S5.6**). We observed that

the ratio of mOrange:BFP in the K20-SR only increased after ZNF598 and ASCC3 knockdown in hiPSC and HEK293 cells (**Figure 2.25 A**). In NPCs, we also observed such an increase, but only before normalization to the K0 non-stalling control (**Figure S 5.6**). These data show that ZNF598 and ASCC3 are important for translation arrest at AAA-encoded polylysine stretches. Readthrough of XBP1-SR increases upon the knockdown of ZNF598 and ASSC3 in HEK293 and hiPSC, while this effect decreases in NPC after normalization (**Figure 2.25 B**). Surprisingly, XBP1-SR was also increased in hiPSC and NPC but not HEK293 after knockdown of HBS1L and PELO. This suggests that in addition to the known effects of ZNF598 and ASCC3, the HBS1L/PELO complex also influences ribosome pausing in this stalling sequence in some cellular contexts. In contrast, the effects of gene knockdown on nonstop reporter stabilization were detectable in several gene knockdown contexts, but only in HEK293 cells (GIGYF2, NEMF, GTPBP1, GTPBP2 and LTN1), and with much more modest effect sizes (**Figure 2.25 C**). These data suggest that HEK293 cells, but not hiPSCs or NPCs, increase protein synthesis without a stop codon after the suppression of RQC factors.

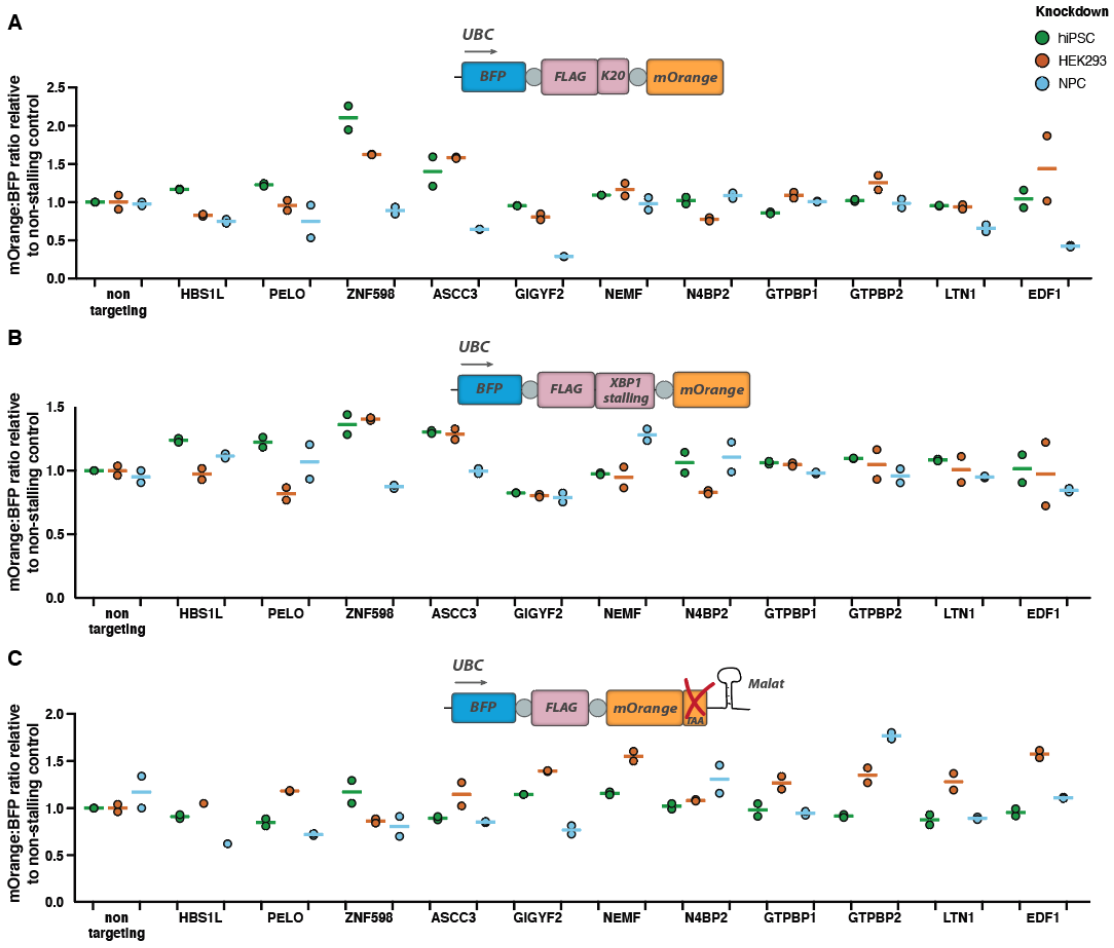

Figure 2.25. Nonstop-SR readthrough in HEK293 cells depleted for ribosome quality control factors. Stalling readtrhough of reporters containing an AAA-encoded poly-lysine stretch (K20-SR, (A)), XBP1 stalling (XBP1-SR, (B)), and nonstop-SR (C). Fluorescence intensity was quantified by flow cytometry in 30,000 cells and the resulting ratio was normalized to the respective non-stalling control (n=2 biological replicates).

We next asked whether our inability to detect changes in stalling readthrough in some cellular contexts could be due to reporter construct expression levels since we used the moderate strength promoter UbC, and a low lentiviral transduction rate to limit multi-copy integration events. To test how expression levels change the readout of these reporter assays cause phenotypic differences, we transduced stalling constructs with high infectivity (>90%) into HEK293 cells, which we hoped would result in the integration of several reporter copies in one cell, and compared stalling readthrough efficiencies to our low-infectivity set-up (**Figure 2.26**). We observed that potentially higher expression levels did indeed increase stalling readthrough for some of our targets (GIGYF2 and EDF1), but led to diminished effects in others (NEMF) or to increased variation between replicates. By applying this approach to the other stalling constructs, we observed similar trends for the K20-construct, but not the XBP1-SR was not affected. Taken together, these data suggest that reporter expression levels can greatly influence the interpretation of gene essentiality for stalling readthrough, possibly by titrating out cellular components present in limiting amounts.

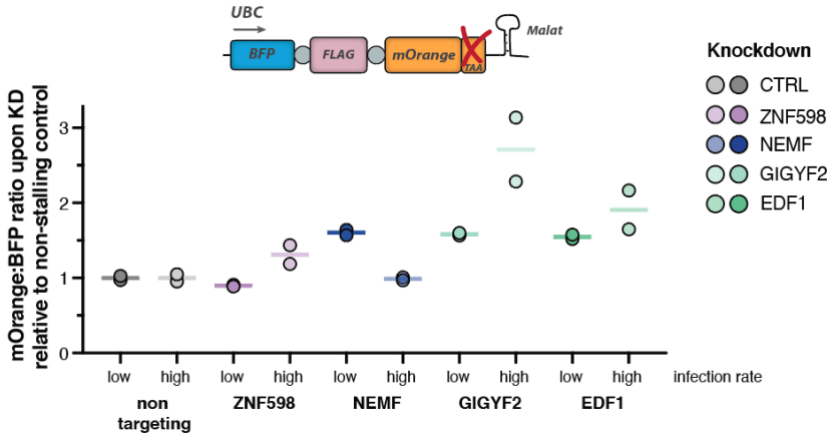

Figure 2.26. Differences in reporter expression levels change stalling readthrough in HEK293 cells depleted for ribosome quality control factors.
Each reporter construct was transduced in parallel with a low (30%) and a high (90%) initial transduction efficiency. Median fluorescent intensity of BFP and mOrange was measured by fluorescent quantification of 30,000 cells using the flow cytometer and the resulting ratio was normalized to the respective non-stalling control.

2.3.4. Human cell lines exhibit different sensitivity to translation elongation inhibitors

We next asked whether cells exhibit differential sensitivity to loss of ribosome quality control factors because their overall sensitivity to ribosome stalling and collisions is different. We used anisomycin and emetine, two translation elongation inhibitors commonly used at low dose to

induce ribosome collisions, to investigate the activation of the ISR and RSR pathways[223,235,236,265]. For this, we titrated both drugs in the range of commonly used concentrations and monitored eIF2α and p38 phosphorylation by Western blotting (**Figure 2.27**). Interestingly, the anisomycin concentration sufficient for inducing RSR was 25-fold lower in HEK293 cells than hiPSC by as seen for p38 phosphorylation levels. p38 phosphorylation was expectedly abrogated at high anisomycin concentrations (25 mg/l), which stall the ribosome rather than inducing collisions. eIF2α phosphorylation, by contrast, showed less prominent differences, which might be masked by strong background phosphorylation signals in untreated cells (**Figure 2.27 A**). Surprisingly, emetine treatment did not trigger phosphorylation of neither p38 nor eIF2α in hiPSCs, while in HEK293 cells the same factors became phosphorylated at emetine concentrations as low as 0.01 mg/l (**Figure 2.27 B**). These data suggest that in hiPSC and HEK293, the RSR is induced already at very low concentrations of anisomycin. The striking differences in the response of the two cell lines to emetine and anisomycin also suggest that translation elongation inhibitors cannot be used interchangeably to study cellular responses to ribosome collisions.

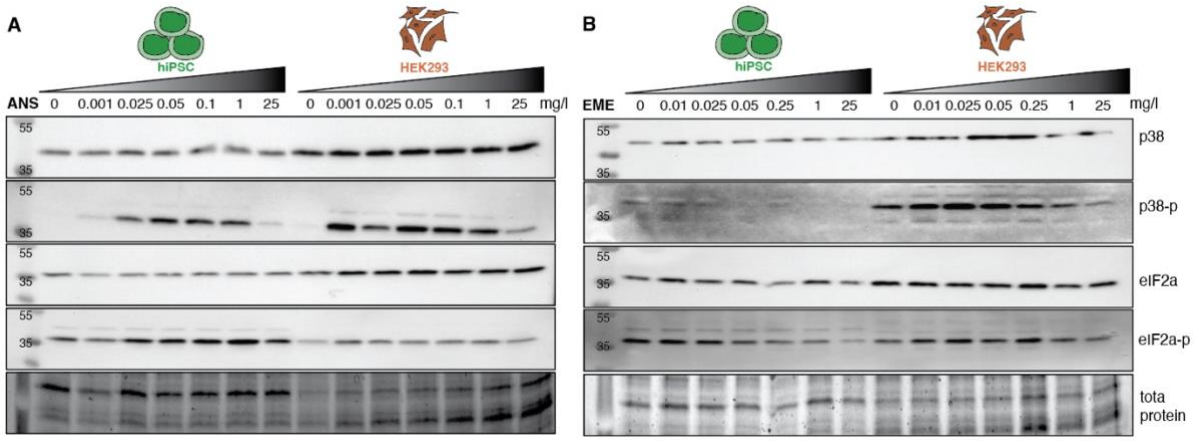

Figure 2.27. hiPSC and HEK293 exhibit differential sensitivity to translation elongation inhibitors. (A) Treatment of cells with anisomycin (ANS) or (B) Emetine (EME) with increasing concentrations for 15 minutes at 37°C. Ribotoxic stress response was measured by eIF2α and p38 phosphorylation, total protein stain of one representative blot.

2.4. Molecular consequences of depleting ribosome surveillance factors in human cells

Persistent ribosome stalling can trigger several response pathways in the cell. First, the NGD / RQC pathways are activated to disassemble ribosomal subunits and degrade the nascent chain. The current consensus is that stalled ribosomes are ubiquitylated by ZNF598 binding and further disassembled through ASCC3 in a ubiquitin-dependent manner. Subsequently, the RQC complex removes the nascent chain and recycles the large ribosomal subunit. Alternatively, it is hypothesized that an endonuclease can trigger NGD by cleaving mRNAs between collided ribosomes, leading to HBS1L/PELO-dependent ribosome splitting and mRNA degradation (**Figure 1.5**). Our pooled screens showed highly diverse cellular responses to ribosome collision factors between hiPSC with a normal karyotype and a healthy genetic background, and the aneuploid HEK293 line. hiPSC exhibited strong negative phenotypes upon depletion of ASCC3, ZNF598, HBS1L, and PELO, while HEK293 cells only showed midler growth defects for ZNF598, ASCC3, and PELO, an none for HBS1L (**Figure 2.19**, **2.28 A**). The RQC factors that work downstream of the ribosome disassembly pathway did not show strong phenotypes in any of the cell contexts we tested (**Figure 2.17**), which is why we did not investigate them further. In this chapter, we focused on identifying the mechanisms that lead to cell context-specific phenotypes upon loss of ribosome stalling and surveillance factors.

2.4.1. The essentiality of ribosome surveillance factors differs in HEK293 and hiPSC

First, we validated the screening results with single knockdown growth assays and quantitative RT-PCR for HBS1L, PELO, ASCC3 and ZNF598 **Figure 2.19**, **2.28 B**, **C**). For this, we induced the KRAB-dCas9-mediated gene knockdown and measured the percent of GFP-positive cells every four cell doublings (**Figure 2.19**, **2.28 C**). We observed that the knockdown of HBS1L did not alter GFP-positive cell counts in HEK293 cells (**Figure 2.19**, **2.28 C**), while depletion of ASCC3, PELO, and ZNF598 decreased GFP-positive cells by 25% - 50% over the total of 20 cell doublings (**Figure 2.28 C**). For hiPSC, the fraction of GFP-positive cells decreased to only 25% already after eight doublings upon knockdown of HBS1L, ASCC3, and ZNF598, and to zero at twelve cell doublings. The PELO knockdown showed similar, but delayed, loss of GFP-positive cells in hiPSC. Furthermore, we performed quantitative RT-PCR

analysis of each knockdown after three cell doublings to investigate gene target downregulation. For all knockdown conditions, we observed robust target down-regulation at the mRNA level (**Figure 2.28 B**). We then analyzed changes in cell cycle progression after gene knockdown, but we could not find a correlation with phenotypic differences between cell contexts (**Figure S 5.3**). Interestingly, we found that in both hiPSC and HEK293, ZNF598 knockdown arrests cells in S / G2 phase, while knockdown of HBS1L, ASCC3, and PELO did not alter cell cycle progression (**Figure S 5.3**). Collectively, these data suggest that the strong phenotypic differences upon gene knockdown in these two cell lines do not result from differences in mRNA stability and do not correlate with defects in cell cycle progression.

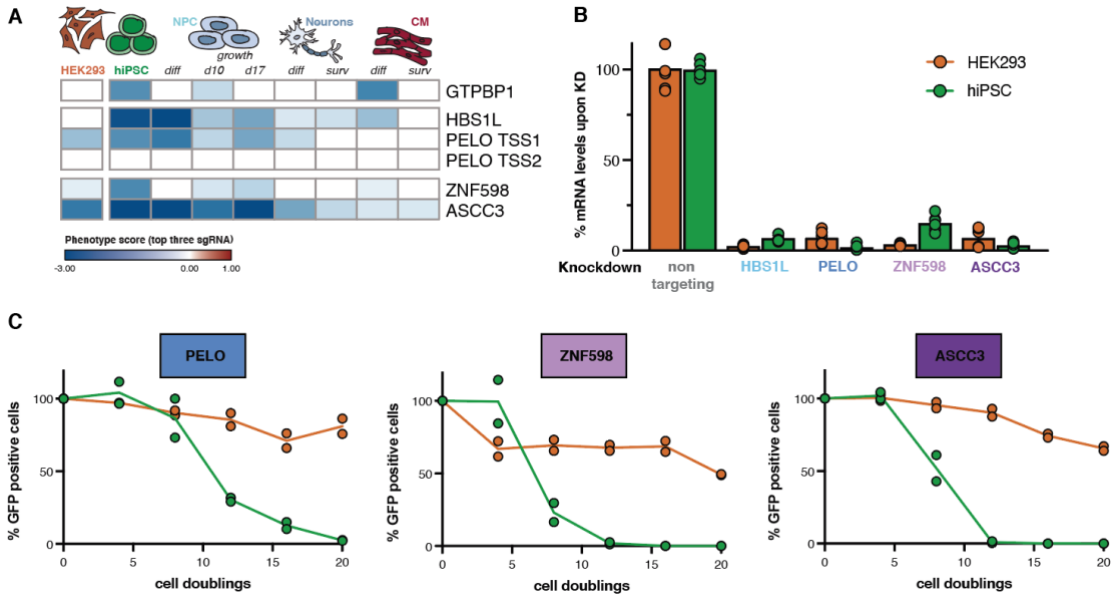

Figure 2.28. HBS1L/ PELO, ZNF598 and ASCC3 influence cell viability in a cell context-dependent manner.
(A) Phenotype scores of the top three sgRNAs of biological replicates from the pooled CRISPRi screen with a Mann-Whitney p-value of 0.1 for the gene knockdown of GTPBP1, HBS1L, PELO, ZNF598 and ASCC3. (B) To measure remaining mRNA levels, gene knockdown was induced for three cell doublings before RNA extraction. B2M was used as a reference gene for relative mRNA quantification and normalized to the corresponding non-targeting control in three technical replicates. (C) Growth assay of two biological replicates in HEK293 cells and hiPSC after gene knockdown. GFP-positive cells were measured by flow cytometry after the time period of four cell doublings for a total of twelve cell doublings and normalized to non-induced control. At least 10,000 cells were analyzed per measurement.

2.4.2. Ribosome rescue genes exhibit distinct interaction profiles in different cellular contexts

Due to the vast phenotypic differences in HEK293 cells and hiPSCs, we hypothesized that interaction profiles could differ between cell contexts and trigger different molecular response mechanisms. To test this, we investigated genetic interactions among ribosome collision and quality control factors and with other known interaction partners. For this, we adapted a dual

sgRNA construct (**Figure 2.29 A**)[387] to simultaneously knock down two genes in different cellular contexts, and we performed growth assays by measuring the percentage of GFP-positive cells every four cell doublings on a total of 20 cell doublings (**Table S 5.5**, **S5.6**, **S5.7**). We validated dual gene knockdown after three cell doublings by quantitative RT-PCR for all targets (**Figure S 5.2**). Finally, using the fraction of GFP-positive cells of both individual and double knockdowns, we calculated the difference between observed and expected phenotypes, which allowed us to identify buffering or synergistic genetic interactions[388]. An interaction was defined as buffering when the observed growth phenotype after simultaneous knockdown of two genes was greater than the expected growth phenotype. When the observed phenotype was lower than the expected phenotype, we defined the interactions as synergistic. In simpler words, buffering effects suggest that two genes function in the same pathway, while a synergistic interaction suggests that genes function in separate or complementary pathways. Therefore, the elimination of factors from two alternative pathways that recognize or disassemble collided ribosomes would result in a larger decrease in cell fitness than the individual gene knockdowns.

With this approach, we investigated the genetic interaction profiles of GTPBP1 and HBS1L, which are two structurally conserved GTPases involved in mRNA translation. Both proteins are thought to have PELO as their primary interaction partner. We wanted to test whether GTPBP1 can compensate for the loss of HBS1L, by binding and delivering PELO to the empty A site by its GTPase activity and induce ribosome disassembly pathways, as previously suggested by ribosome profiling studies of brains from Gtpbp1 knockout mice (**Figure 2.29 B**)[242]. Taking this model into account, we would expect a synergistic genetic interaction between GTPBP1 and HBS1L, but a buffering interaction between GTPBP1 and PELO. In contrast, Zinoviev et al. found no interaction between GTPBP1 and other ribosomal factors *in vitro*[244]. Hence, we analyzed interaction signatures of the GTPBP1/ HBS1L or GTPBP1/ PELO knockdown after eight cell doublings in HEK293 cells, but only four cell doublings in hiPSC, since here the single knockdowns were almost completely lost from cell populations at eight cell doublings (**Figure 2.19**, **Table S 5.5**, **S5.6**). We observed buffering interactions between GTPBP1 and PELO, but surprisingly also between GTPBP1 and HBS1L in HEK293 cells (**Figure 2.29 C**). In contrast, GTPBP1 and HBS1L seem to act in parallel pathways in hiPSC.

Furthermore, we simultaneously depleted GTPBP1 and EXOSC9, a major component of the exosome complex, since GTPBP1 loss has been shown to lead to mRNA processing defects[389]. Since EXOSC9 was not included in our CRISPRi screens, we designed an

EXOSC9-targeting sgRNA using the CRISPRia Design pipeline and tested its knockdown efficiency in a single knockdown cell line. As in our initial validation experiments, we performed growth assays by inducing KRAB-dCas9 expression with doxycycline and monitored growth every four cell doublings for a total of 20 cell doublings. We observed that the rates of GFP-positive cells rapidly decreased in both hiPSC and HEK293 (**Figure 2.29 D** top). Furthermore, we tested mRNA downregulation by quantitative RT-PCR after three cell doublings. We observed that mRNA levels were greatly decreased in both cell contexts (**Figure 2.29 D** bottom), confirming efficient target downregulation after knockdown. Our comparison of single and double knockdown phenotypes revealed a buffering interaction between these two genes, but only in HEK293 cells (**Figure 2.29 C**).

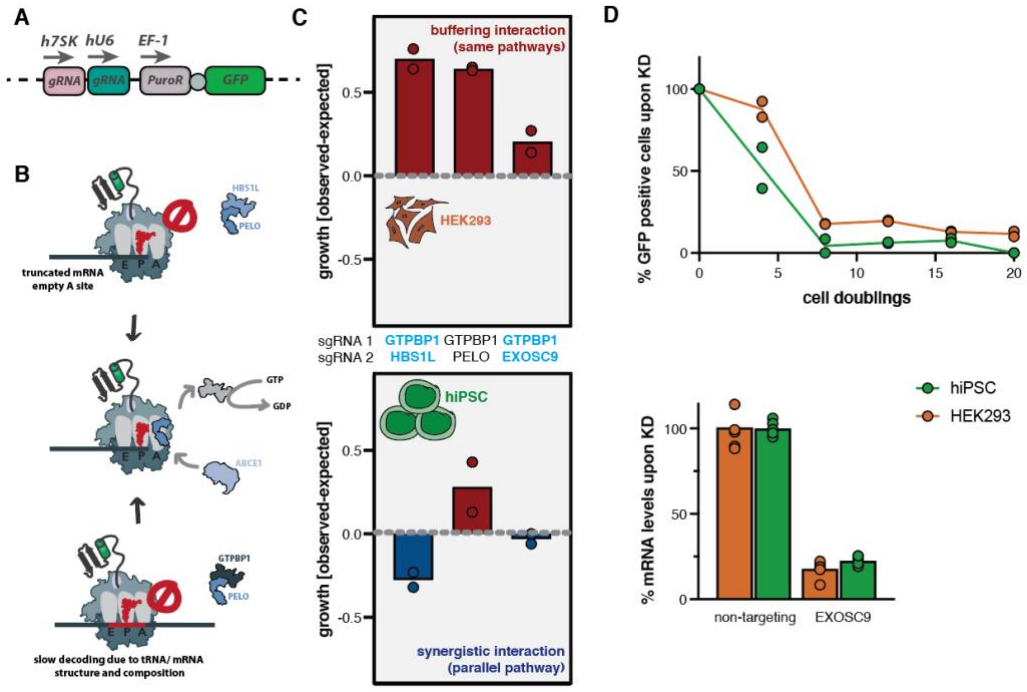

Figure 2.29. Genetic interactions between GTPBP1, HBS1L, PELO, and the exosome.
(A) sgRNA construct for simultaneous knockdown (KD) of two targets. sgRNA expression is driven through H7SK and human U6 promoter. EF1-alpha drives expression of puromycin for selection and GFP for flow cytometry analysis; both are separated by a 2A skipping sequence (grey circle). (B) Proposed model of PELO interaction with either HBS1L on truncated mRNAs or with GTPBP1 on internal ribosome pausing events and the ribosome disassembly mediated by ABCE1. (C) show growth phenotypes for different double knockdown and the corresponding single knockdown phenotypes after four or eight cell doublings of biological replicates. Percent of GFP-positive cells was analyzed by flow cytometry analysis of 10,000 cells in biological replicates and normalized to non-induced control (other time points in Suppl Tables 9.1 to 9.9). The dotted line indicates the expected growth phenotype, which is calculated from a multiplicative model: expected growth = observed phenotype of sgRNA1 * sgRNA2. (D) EXOSC9 sgRNA validation. Growth assay of two biological replicates in HEK293 cells and hiPSC after gene knockdown. GFP-positive cells were measured by flow cytometry every four cell doublings for a total of twelve cell doublings and normalized to non-induced control. At least 10,000 cells were analyzed per measurement (top). To measure remaining mRNA levels, gene knockdown was induced for three cell doublings before RNA extraction. B2M was used as a reference gene for relative mRNA quantification and normalized to the corresponding non-targeting control in three technical replicates and biological replicates.

We next examined genetic interaction profiles of ZNF598, ASCC3, HBS1L, and PELO. Recent studies showed that the yeast endonuclease Cue2 can cleave the mRNA between two collided ribosomes and trigger ribosome disassembly through Hbs1/Dom34[231]. Therefore, we included the human homolog N4BP2 in our experiments, to test its hypothesized function in HBS1L/PELO-dependent ribosome disassembly. Due to the recent discovery of its yeast homolog Cue2, N4BP2 was not included in our pooled CRISPRi screens. Hence, we designed an sgRNA targeting N4BP2 with the same criteria as for EXOSC9 and tested its knockdown efficiency with growth assays and quantitative RT-PCR. We observed no growth defects in either hiPSC or HEK293 cells despite efficient N4BP2 knockdown (**Figure 2.30 A**).

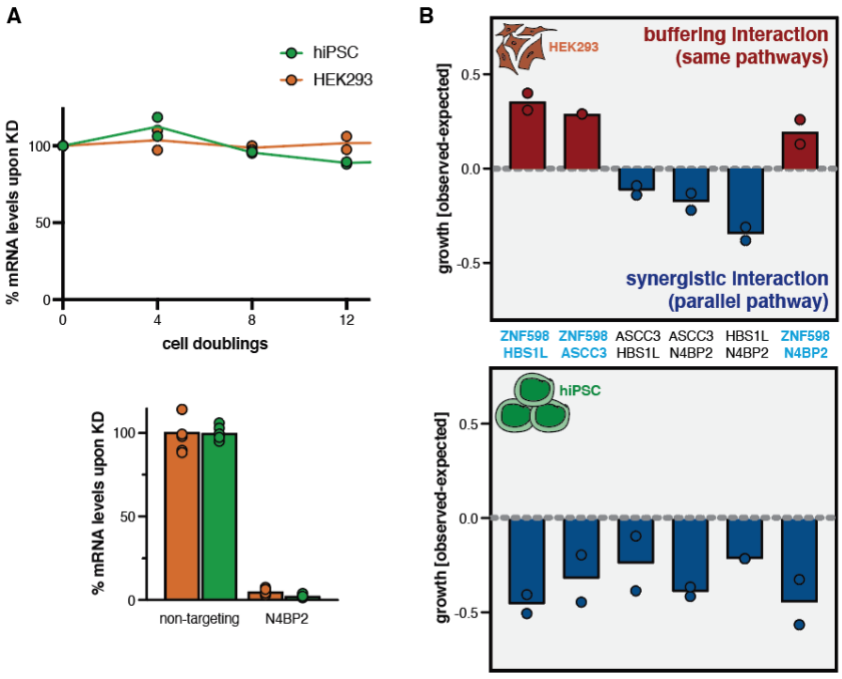

Figure 2.30. Context-dependent genetic interaction profiles among ribosome collision factors.
(A) sgRNA validation for N4BP2 sgRNA. Growth assay of two biological replicates in HEK293 cells and hiPSC after gene knockdown. GFP-positive cells were measured by flow cytometry after the time period of four cell doublings for a total of twelve cell doublings and normalized to non-induced control. At least 10,000 cells were analyzed per measurement (top). To measure remaining mRNA levels, gene knockdown was induced for three cell doublings before RNA extraction. B2M was used as a reference gene for relative mRNA quantification and normalized to the corresponding non-targeting control in three technical replicates and biological replicates. (B) Growth phenotypes for different double knockdown and the corresponding single knockdown phenotypes after four or eight cell doublings of biological replicates. Percent of GFP-positive cells was analyzed by flow cytometry analysis of 10,000 cells in biological replicates and normalized to non-induced control (other time points in Suppl Tables 9.1 to 9.9). The dotted line indicates the expected growth phenotype, which is calculated from a multiplicative model: expected growth = observed phenotype of sgRNA1 * sgRNA2.

After N4BP2 sgRNA validation, we performed combinatorial knockdowns of ASCC3, ZNF598, HBS1L and N4BP2 and calculated their genetic interaction profiles in HEK293 and hiPSC (**Figure 2.30 B**). We previously observed a HBS1L-dependent downregulation of PELO protein levels, which highlighted its connection with HBS1L for complex formation

(**Figure 2.19 C**). Therefore, we assumed that PELO interactions would phenocopy HBS1L interaction profiles and did not include it in our interaction studies. We measured genetic interactions after four cell doublings in hiPSC, because they already showed very early and lethal phenotypes at eight cell doublings (**Table S 5.5**). In contrast, growth phenotypes were delayed or neutral for many targets in HEK293 cells (**Table S 5.6**). Therefore, we calculated the genetic interaction strength after twelve cell doublings (**Table S 5.5**, **S5.6**). Our analysis showed that although the knockdown of N4BP2 did not affect hiPSC or HEK293 growth, it exacerbated the growth defects caused by ASCC3 or HBS1L knockdown in both cell contexts (**Figure 2.30 B**). However, the genetic interaction profile of ZNF598 / N4BP2 differed between hiPSC and HEK293 cells: the two genes further decreased GFP rates in hiPSC and act in parallel pathways but in the same pathway inHEK293 cells. Together, the genetic interaction profiles in hiPSC support the hypothesis that cells can resolve stalled and collided ribosomes either through the ZNF598-ASSC3 branch or alternatively through cleaving mRNA with N4BP2 and disassembling the ribosome through HBS1L/ PELO. However, they also suggest functions of HBS1L and N4BP2 in parallel pathways. Already in yeast, NGD through the exonuclease Xrn1 was shown to be the predominant pathway, while Cue2 phenotypes were only observed when Xrn1 was additionally deleted[231]. This highlights our limitations in defining genetic interactions of pathways that can easily be compensated for by other complexes. The differences between our genetic data and the current understanding of the pathways for detecting and resolving ribosome collisions based on reporter and *in vitro* assays also suggest that these factors might be involved in additional biological processes. They also highlight that genetic interaction profiles in human cells can be highly cell context-dependent.

2.4.3. Loss of ribosome rescue factors perturbs the XBP1 branch of the unfolded protein response

Our current understanding of ribosome collision factors states that ZNF598 senses and mediates ubiquitylation of RPS, which triggers ubiquitin-dependent ribosome disassembly by ASCC3, whereas HBS1L/PELO is suggested to act in NSD / NGD as the parallel pathway for disassembly independent of the other factors. However, our data showed extensive differences in genetic interactions between ZNF598, ASCC3, and HBS1L between cell contexts. Since most of the current knowledge about these pathways is derived from studies with a handful of stalling reporters that mostly have no counterparts in endogenous mRNA sequences (e.g. AAA-encoded K20), we decided to investigate the function of ribosome collision factors on an endogenous substrate. For this, we chose XBP1, which is part of the unfolded protein response (UPR).

Upon ER stress, the UPR becomes activated by three major pathways that sense misfolded proteins in the ER and regulate DNA transcription and RNA translation to restore cellular homeostasis. PERK can build homodimers under ER stress and phosphorylate eIF2α via its cytosolic kinase domain, leading to a decrease in global translation, but an increase in the translation of specific mRNAs such as the ATF4-encoding transcript[390,391]. Second, ATF6 activates the transcription of UPR genes by translocating to the Golgi apparatus, where its cytosolic domain is separated and functions as a transcription factor in the nucleus[392]. The third pathway involves the endoribonuclease IRE1, which activates the expression of the transcription factor XBP1. During normal growth, cells express an "unspliced" XBP1 mRNA, which contains a 26-nucleotide non-conventional intron. The XBP1-u protein contains an "arrest peptide" that pauses ribosomes and recruits the XBP1 mRNA to the ER through SRP binding[207,393,394]. Upon ER stress, IRE1, which has a similar architecture to PERK, is activated by homodimerization , and excises the 26-nt intron from the XBP1 mRNA. This results in the production of a longer XBP1 proteoform without the arrest peptide (XBP1-s). Upon mRNA release from the ER membrane, new rounds of translation can be initiated, resulting in the production of large amounts of XBP1-s. This protein translocates to the nucleus, where it functions as a transcription factor and upregulates a specific subset of "UPR genes", such as the ER chaperone DNAJB9[206,207]. XBP1-s also upregulates PERK and its own gene transcription in an autoregulatory loop (**Figure 2.30**)[395].

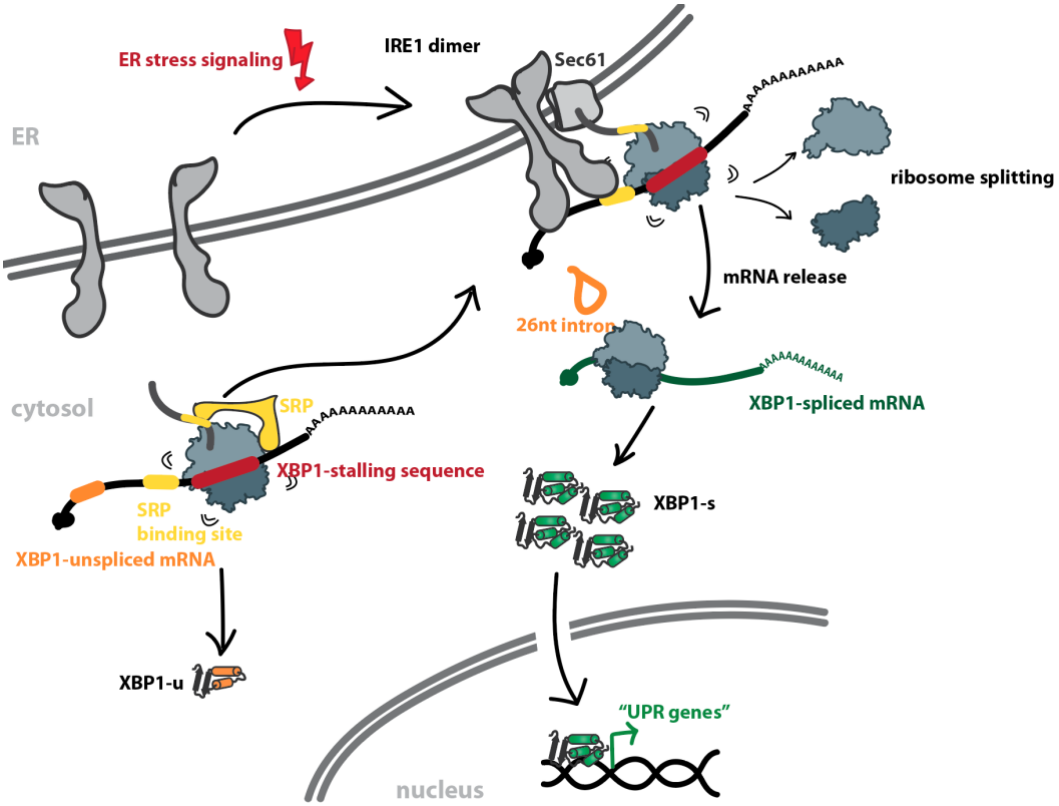

Figure 2.31. Schematic representation of IRE1-mediated UPR regulation via XBP1 mRNA splicing.

We used published stalling sequences in a flow cytometry-based reporter to test the function of ribosome collision factors for the resolution of the XBP1 stalling event (**Figure 2.25**). We observed that readthrough of the XBP1 stalling sequence could be enhanced upon depletion of ASCC3 and ZNF598 in both hiPSC and HEK293. Surprisingly, the loss of HBS1L and PELO also improved XBP1 stalling readthrough in hiPSC. Therefore, we tested whether the phenotypes observed in the overexpression experiments of reporter constructs are reproducible by probing endogenous XPB1-s mRNA and protein levels. We first depleted ZNF598, ASSC3 or HBS1L and then induced ER stress by treating cells s with tunicamycin for six hours. We then examined XBP1 mRNA splicing by quantitative RT-PCR and protein expression by Western blotting (**Figure 2.32**, **2.33**). We also confirmed the efficient depletion of all target proteins for all targets (ZNF598, ASSC3, HBS1L). XBP1-u was almost undetectable in both unstressed and tunicamycin-treated cells, in accordance with prior data showing that XBP1-u is unstable and quickly degraded in a UPS-dependent manner[206,395]. XBP1–s expression was robustly induced by tunicamycin in both hiPSC and HEK293. Its levels were comparably high in HEK293 depleted for ZNF598, ASSC3 or HBS1L (**Figure 2.32 A**). By contrast, the knockdown of all these genes reduced XBP1–s protein levels after six hours of tunicamycin treatment in hiPSC (**Figure 2.32 B**).

We hypothesized that the presence of either ribosome collision factor alone could be sufficient to induce the expression of XBP1-s in HEK293 cells and thereby compensate for the loss of the others. Therefore, we tested whether a simultaneous knockdown of two synergistic pathways could influence XBP1-s protein expression to the same degree as in hiPSC. We used our dual sgRNA expression construct (**Figure 2.29 A**) to simultaneously knock down ZNF598/ASCC3 or ZNF598/HBS1L. Upon tunicamycin treatment, we observed that both double knockdowns did not change the expression of XBP1-s protein in HEK293 cells (**Figure 2.32 A**), while the knockdown of ZNF598/HBS1L reduced the levels of XBP1-s protein in hiPSC (**Figure 2.32 C**). This result, together with the single knockdown assays, suggested that HBS1L can compensate for the function of ZNF598 in XBP1–s expression and vice versa, but a loss of both factors strongly inhibits XBP1–s expression. This result is in line with the synergistic genetic interaction we observed between ZNF598 and HBS1L in hiPSC (**Figure 2.30 B**).

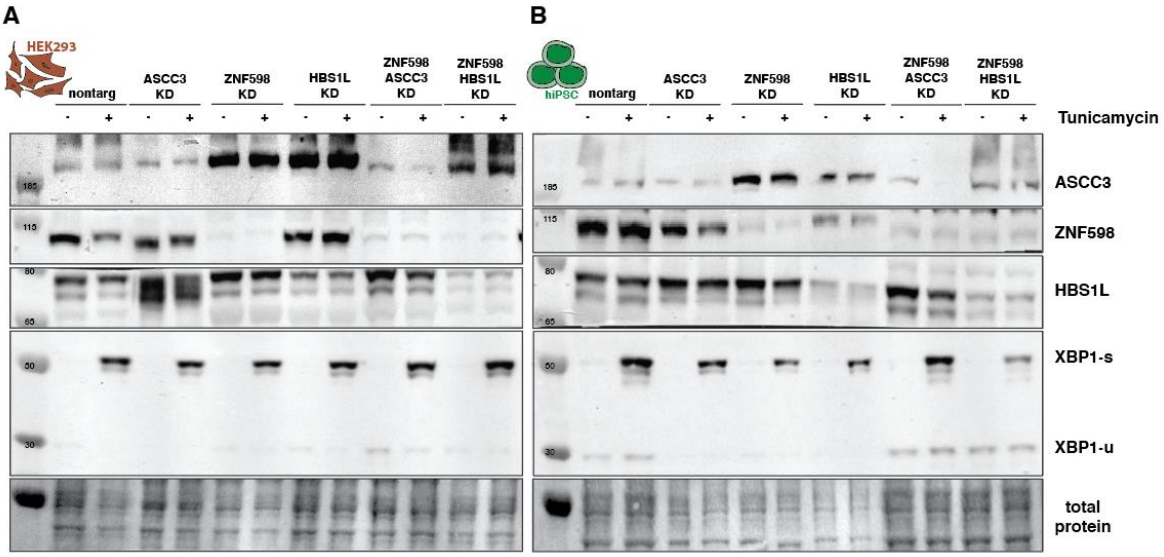

Figure 2.32. XBP1-s protein expression is regulated by ribosome rescue factors in hiPSC.
Gene knockdown (KD) was induced for five cell doublings in the single knockdown and three cell doublings for the double knockdown experiments. Subsequently, cells were treated with 2.5 µM tunicamycin for six hours in non-targeting and gene knockdown cells. Samples were analyzed by Western blot for (A) HEK293 cells and (B) hiPSC with a knockdown of either ZNF598, ASCC3, HBS1L or combinations of these genes.

We next asked whether reduced XBP1-s protein levels were due to defects in IRE1-mediated splicing. For this, we analyzed XBP1 mRNA splicing isoforms and downstream target expression (DNAJB9) by quantitative RT-PCR after depletion of a single or two genes, followed by six hours of tunicamycin treatment (**Figure 2.33**). All gene knockdown conditions showed highly comparable results. We observed that upon tunicamycin treatment, XBP1-s mRNA levels still increased 10- to 25-fold (hiPSC and HEK293 cells) compared to non-stressed cells in both knockdown and non-targeting control cells (**Figure 2.33 A**). Downstream target expression of DNAJB9 was also elevated compared to non-stressed cells. Concordant with lower XBP1-s protein levels in hiPSC upon gene knockdown (**Figure 2.33 B**), DNAJB9 mRNA levels were upregulated by only two-fold upon gene knockdown (compared to four-fold in NT control, **Figure 2.33 B**). Since XBP1-s also binds and activates transcription of its own gene, total XBP1 mRNA levels also increase upon ER stress in NT controls of hiPSC and HEK293. However, this effect decreases in hiPSC depleted of ribosome collision and surveillance factors. (**Figure 2.33 C, D**).

Next, we tested the splicing efficiency of XBP1 mRNA upon ER stress. For this, we compared the expression changes of XBP1-s to total levels of XBP1. Changes in the ratio of XBP1-s/XBP1-total would suggest that XBP1-s mRNA splicing is altered by the loss of ribosome collision factors (**Figure 2.33 E**). This comparison showed that splicing upon gene knockdown remained stable in HEK293 cells compared to NT cells. Interestingly, splicing efficiency

improved in hiPSC, which was correlated with lower levels of XBP1-u in those cells (**Figure 2.33 D**, **E**). The data showed that after the knockdown of the ribosome collision factors, XBP1 mRNA is still efficiently spliced upon ER stress. However, total, unspliced and spliced XBP1 mRNA levels decreased after gene knockdown in hiPSC, suggesting that the self-amplification loop of XBP1 is impaired. This data is in accordance with the decrease in XBP1-s protein levels we detected in tunicamycin-treated knockdown cells by Western blotting (**Figure 2.32**).

In summary, these results demonstrate that ribosome surveillance factors are essential for efficient XBP1-s protein expression upon ER stress in hiPSC but not in HEK293 cells.

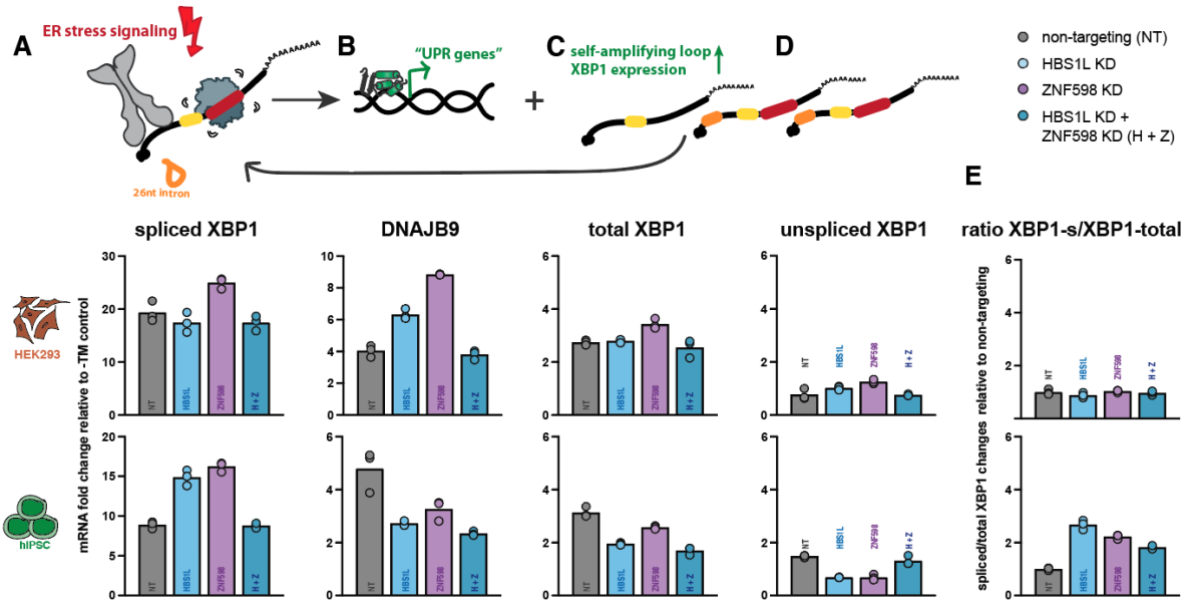

Figure 2.33. XBP1-s autoregulatory mechanisms are impaired upon loss of ribosome collision factors in a cell context-dependent manner.
Gene knockdown (KD) was induced for five cell doublings in the single knockdown and three doublings in double knockdown experiments. Subsequently, cells were treated with 2.5µM tunicamycin for six hours. Samples from hiPSC or HEK293 were analyzed by quantitative RT-PCR for HEK293 cells and hiPSC with a knockdown of either ZNF598, HBS1L or ZNF598/HBS1L. Samples were analyzed by quantitative RT-PCR for spliced XBP1 (XBP1-s)(A), downstream DNAJB9 expression (B), total XBP1 levels (C), unspliced XBP1 (XBP1-u), and the splicing efficiency (ratio of XBP1-s to total XBP1)(E). B2M was used as a reference gene for relative mRNA quantification and normalized to the corresponding non-targeting control in three technical replicates.

2.4.4. A RING domain ZNF598 mutant stably associates with polysomes and reduces global translation rates

We hypothesized that knockdown experiments of ribosome collision factors might not be sensitive enough to monitor transient endogenous interactions in cell culture. Alternative pathways could take over to induce ribosome disassembly, which means that the loss of a collision factor would be compensated for and subtle changes in ribosome pausing and collision would be masked. Therefore, our objective was to increase our readout sensitivity for ribosome stalling events by overexpressing a double C29S/ C32S RING domain mutant of ZNF598 (ZNF598^{mut}, **Figure 2.34 A**), which was previously shown to inhibit activation of the RQC pathway[229]. We presumed that ZNF958^{mut} may still be able to bind to its substrates (stalled ribosomes), but would not be able to mediate ubiquitination of ribosomal proteins because of impaired E2 recruitment. In this way, ZNF958^{mut} may mark problematic mRNA translation events more stably than the wild-type protein.

We stably integrated a ZNF598^{mut} expression construct either in wild type cells or in a ZNF598 knockdown background by lentiviral transduction. To test the effect of ZNF598 knockdown or ZNF598^{mut} overexpression on polysome distribution in cells, we performed sucrose gradient analysis of cellular extracts (**Figure 2.34**). Polysome profiles did not show changes in HEK293 cells (**Figure 2.34 B**), but a strong decrease in polysomes relative to the monosome was seen in hiPSC depleted of ZNF598 and/or overexpressing ZNF598^{mut} (**Figure 2.34 C**). This suggests that hiPSC but not HEK293 cells change global translation rates in the presence of ZNF598^{mut}. We next analyzed the distribution of ZNF598 and ZNF598^{mut} along the gradient by Western blotting. Endogenous ZNF598 was only found in the soluble protein fraction of gradients, whereas ZNF598^{mut} migrated into polysome fractions from both HEK293 and hiPSC (**Figure 2.34 B**, **C**). These data support our hypothesis that ZNF598^{mut} is more stably bound to the ribosomes it targets for disassembly.

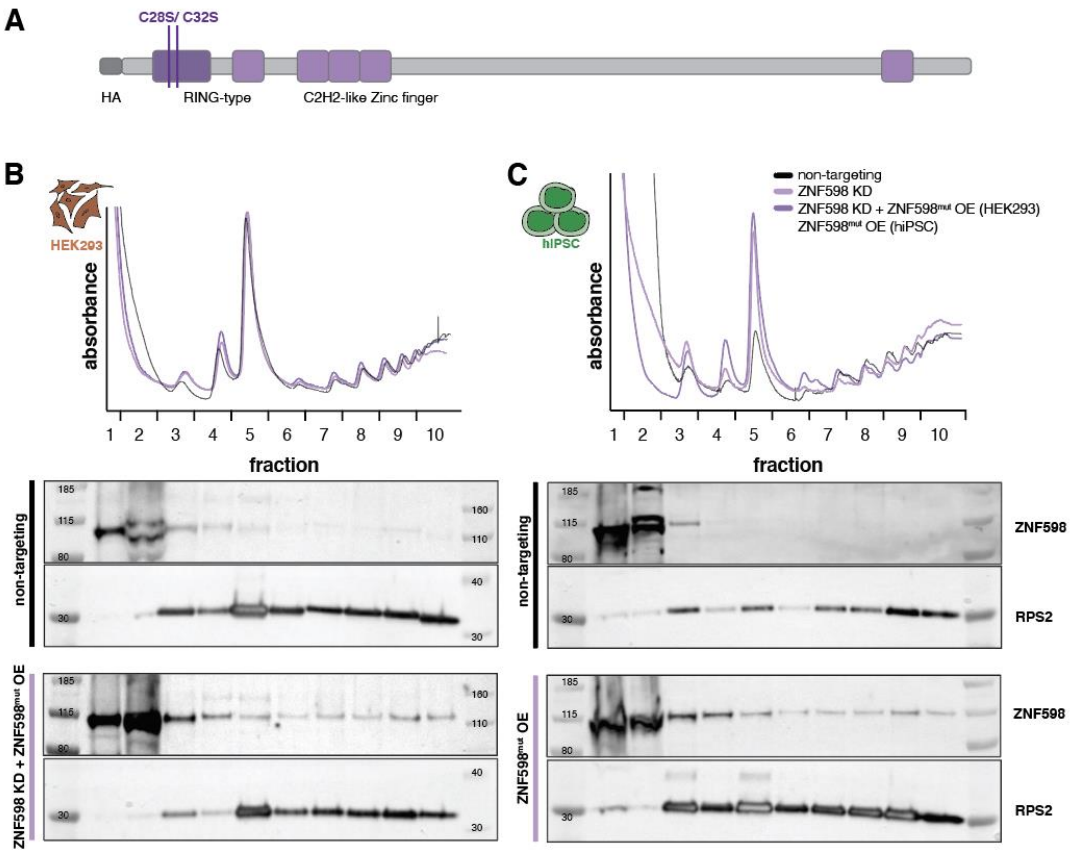

Figure 2.34. ZNF598^{mut} associates with polysomes in hiPSC and HEK293 cells.
(A) ZNF598 C29S/C32S double mutant (ZNF598^{mut}) construct with N-terminal HA tag. (B,C) Polysome profiles and Western Blot analysis of ZNF598 wild type, ZNF598 knockdown and ZNF598^{mut} expression cells. ZNF598 knockdown was induced for four cell doublings and ZNF598^{mut} was expressed for two cell doublings in hiPSC. in HEK293 cells, the ZNF598^{mut} was expressed while additionally knocking down ZNF598 WT. Cell lysate were separated on a sucrose gradient (10-50%) and fractions collected for Western Blot analysis. Polysome profiles and ZNF598 association in polysomes for (B) HEK293 cells and (C) hiPSC. Polysome fractions correspond to loaded lanes on the Western blot. Experiments depict one representative biological replicate.

Since we observed changes in polysome profiles after ZNF598 knockdown and ZNF598^{mut} overexpression in hiPSC, we probed global translation changes after depletion of ribosome collision factors by HPG incorporation. We induced gene knockdown for four cell doublings for ZNF598, five cell doublings for HBS1L, PELO, and ASSC3 and overexpressed ZNF598^{mut} for two cell doublings (**Figure 2.35**). The results showed that the incorporation of HPG did not change in HEK293 cells, but translation remained globally stable (**Figure 2.35 A**). In hiPSC, HPG incorporation was generally decreased, which means that translation was down-regulated after loss of ribosome collision factors (**Figure 2.35 B**). Furthermore, we tested translation changes in the ZNF598^{mut} overexpression construct and found that its translation levels resembled those of ZNF598 knockdown experiments in hiPSC and a 50% down-regulation in HEK293 cells, suggesting that its E3 ligase function is responsible for translation changes. These results were consistent with data from polysome profiles, showing that the

monosome-to-polysome ratio changed in hiPSC after the loss or RING domain perturbation of ZNF598 (**Figure 2.34 B**). However, we found no support for the previously reported increase in global translation after ZNF598 knockout in HEK293T cells[396]. This could be due to the fact that ZNF598 is not completely depleted by CRISPRi. It is also possible that phenotypes in knockout cells can be due to secondary effects, since we found that ZNF598 is essential for cellular fitness in HEK293 (**Figure 2.28**). Furthermore, ZNF598^{mut} expression led to stronger ribosome association and stronger translation inhibition phenotypes, suggesting that its use to investigate endogenous substrates could be advantageous over knockdown experiments.

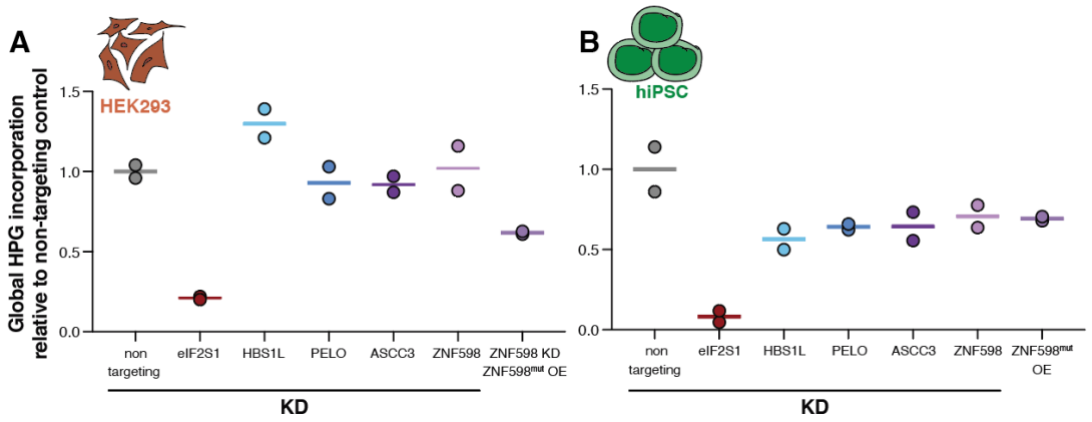

Figure 2.35. Global translation in hiPSC is decreased upon ribosome collision factor knockdown. Gene knockdown (KD) was induced for two (eIF2S1), four (ZNF598), and five cell doublings (HBS1L, PELO, ASCC3) in biological replicates before HPG incorporation into the nascent chain. ZNF598^{mut} was expressed for two cell doublings, with the additional knockdown of endogenous ZNF598 in HEK293 cells. HPG was incorporated for 30 minutes in the nascent chain and a picolyl-azide was added by click chemistry after fixation. At least 10,000 cells were analyzed by flow cytometry and HPG incorporation changes were normalized to a non-targeting control for HEK293 cells (A) and hiPSC (B).

We also analyzed cell cycle progression after ZNF598 knockdown and ZNF598^{mut} expression by propidium iodide staining (**Figure 2.36**). We observed that hiPSC accumulated cells in S phase and HEK293 cells were enriched in G2 phase, indicating a defect in cell cycle progression after loss of ZNF598. ZNF598^{mut} overexpression, similar to knockdown, reduced the percentage of cells that were arrested in the G1 phase. HEK293 cells are arrested in the G2/M phase, in which cells grow, synthesize proteins and finally undergo mitosis (**Figure 2.36 A**). hiPSC specifically accumulated in S phase, where DNA is replicated to form a normal set of diploid chromosomes (**Figure 2.36 B**)[397]. Together, our data suggest that cell cycle progression and cell proliferation is impaired upon loss or malfunction of ZNF598 independent of the cellular context.

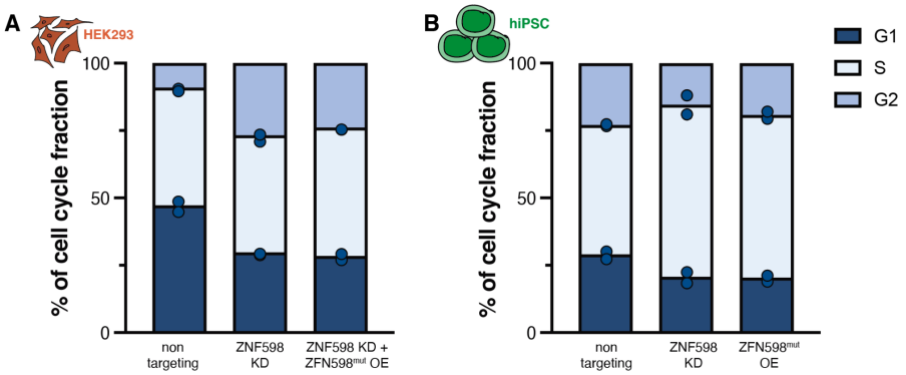

Figure 2.36. Loss or RING domain mutation of ZNF598 leads to alterations in cell cycle progression. Gene knockdown (KD) was induced for four cell doublings in the knockdown experiments. ZNF598mut was stably integrated into hiPSC and HEK293 cells and expressed for two days in the presence (hiPSC) or absence (HEK293 cells) of endogenous ZNF598. Cells were harvested at 75% viability after knockdown, stained with propidium iodide and analyzed by flow cytometry. Proportions of cells per cell cycle phase (G1, S and G2) were determined with the Watson Pragmatic Algorithm. Fraction of cells in G1, S and G2 phase upon knockdown of ribosome collision factors with different screening phenotype strengths in (A) HEK293 cells, and (B) hiPSC. At least 10,000 cells were analyzed per biological replicate. Experiments were performed in two biological replicates.

2.4.5. ZNF598^{mut} inhibits XBP1-s synthesis and downstream XBP1-mediated UPR pathways

We next tested the effect of ZNF598^{mut} overexpression on XBP1-s synthesis following ER stress. For this, we knocked down endogenous ZNF598, overexpressed ZNF598^{mut}, and treated cells with tunicamycin for six hours (**Figure 2.37**). Western Blot analysis showed efficient depletion of the ZNF598 protein in both HEK293 and hiPSC. Furthermore, the expression of ZNF598^{mut}, which can be distinguished from endogenous ZNF598 by its N-terminal HA-tag, was much higher than the endogenous ZNF598 protein levels in hiPSC (**Figure 2.37 B**), while it was present in comparable amounts to the endogenous protein in HEK293 (two bands in **Figure 2.37 A**). These results are in accordance with the higher levels of ZNF598 we detected in HEK293 cells by quantitative mass spectrometry (**Figure 2.20 A**). Therefore, to ensure that the remaining endogenous expression levels of ZNF598 do not influence phenotypes in HEK293 cells, we performed ZNF598^{mut} overexpression in the context of endogenous ZNF598 knockdown.

In HEK293 treated with tunicamycin, ZNF598^{mut} overexpression led to a modest decrease in XBP1-s compared to non-targeting control or ZNF598 knockdown (**Figure 2.37 A**). Strikingly, however, ZNF598^{mut} overexpression completely abolished XBP1-s protein production in

hiPSC (**Figure 2.37 B**). These data suggest that the RING domain mutant acts in a dominant-negative manner and inhibits binding of other ribosome collision factors.

Recent studies showed that collided ribosomes can be bound by several factors that trigger co-translational stress response pathways[398]. Models suggests that under normal conditions, ribosomes are disassembled, and the nascent chain and mRNA are degraded. When not resolved, the collided ribosomes are bound by ZAKα to coordinate different stress responses. GCN2 induces eIF2α phosphorylation to induce ISR, or ZAKα activates MAP kinase cascades (p38 or JNK phosphorylation) to induce RSR. Therefore, we hypothesized that the absence of ribosome collision factors would immediately trigger downstream stress responses. Therefore, we investigated eIF2α and p38 phosphorylation levels after loss and malfunction of ZNF598 (**Figure 2.37**). In our Western Blot analysis, no changes in eIF2α or p38 phosphorylation patterns were observed in HEK293 cells and only ZNF958^{mut} overexpression with additional knockdown of endogenous ZNF598 increased eIF2α phosphorylation (**Figure 2.37 A**). This was also the only condition under which we could observe changes in global translation in HEK293 cells (**Figure 2.37 A**). On the contrary, we observed increased eIF2α phosphorylation after ZNF598 knockdown in hiPSC and no increase in p38 phosphorylation. ZNF598^{mut} expression eIF2α expression and phosphorylation almost completely disappeared and p38 phosphorylation increased (**Figure 2.37 B**). These observations were concordant with global downregulation of translation (**Figure 2.35 B**). Together, these data suggest that ISR pathways are activated upon loss of ZNF598, and the RSR pathway upon its RING domain malfunction (ZNF598^{mut}).

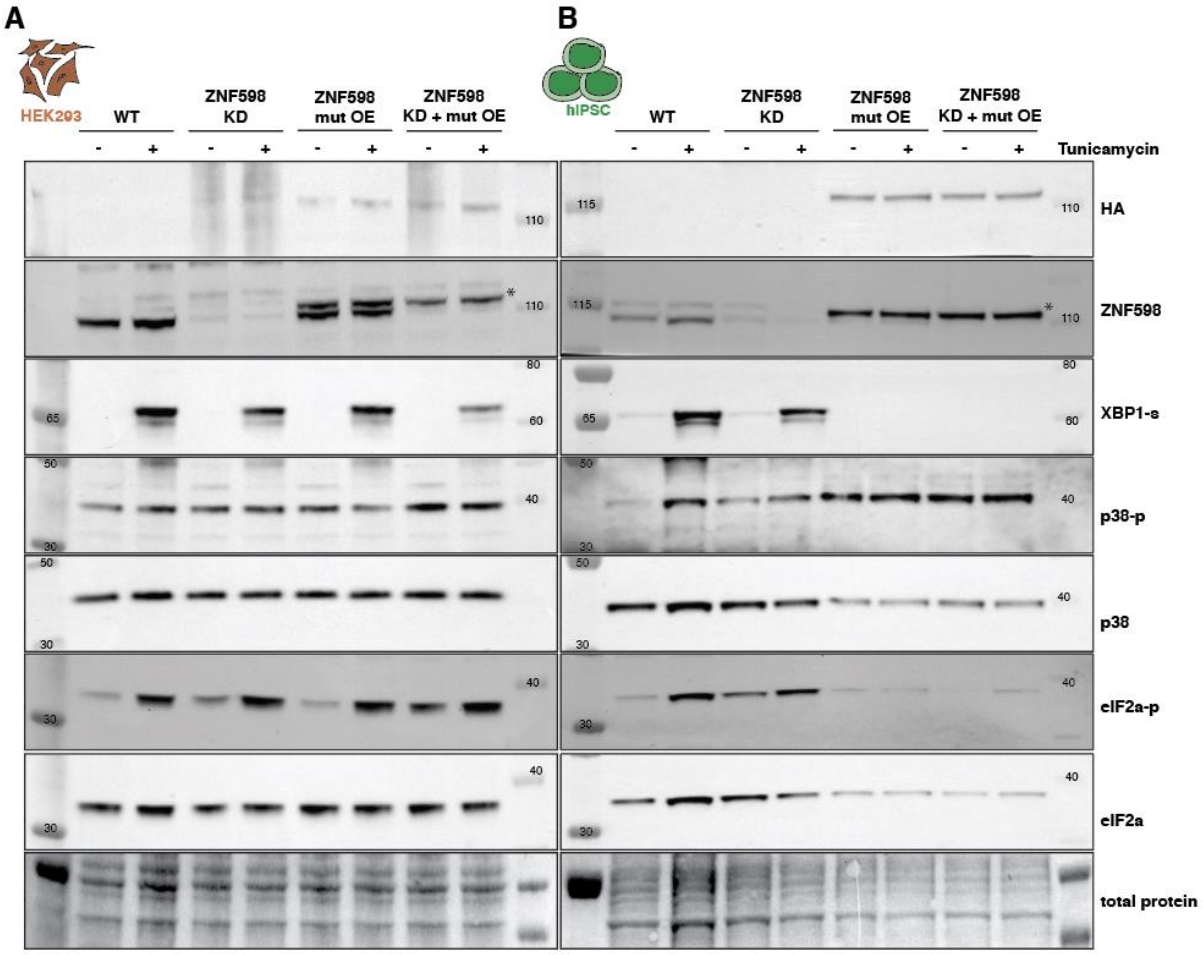

Figure 2.37. ZNF598^{mut} overexpression inhibits XPB1-s protein production upon ER stress and induces RSR.
Gene knockdown (KD) was induced for five cell doublings in the single knockdown experiments. ZNF598^{mut} was stably integrated into hiPSC and HEK293 cells and expressed for two days in the presence or absence of endogenous ZNF598. Subsequently, cells were treated with 2.5 µM tunicamycin for six hours in non-targeting and gene knockdown cells. Samples were analyzed by Western blot for HEK293 cells (A) and hiPSC (B) with a knockdown of either ZNF598, ZNF598^{mut} overexpression or combination of both. Images are from a representative biological replicate.

Next, we analyzed changes in the XBP1 transcript levels in these samples by quantitative RT-PCR upon ZNF598^{mut} overexpression (in hiPSC) or ZNF598^{mut} overexpression combined with endogenous ZNF598 knockdown (in HEK293 cells). The expression of ZNF598^{mut} in hiPSC and HEK293 cells decreased the splicing of XBP1 (**Figure 2.38 A**). As some XBP1-s protein was still detectable in tunicamycin-treated HEK293 expressing ZNF598^{mut} (**Figure 2.37 A**), the levels of DNAJB9 and total XBP1 mRNAs were still increased in comparison to unstressed cells. By contrast, DNAJB9 and XBP1 mRNA levels did not increase after tunicamycin treatment in hiPSC expressing ZNF598^{mut} (**Figure 2.38 B**, **C**) and unspliced XBP1 levels were lower than in unstressed cells for both cell contexts (**Figure 2.38 D**). However, XBP1 splicing is still highly efficient in the presence of ZNF598^{mut}, as the ratio of XBP1-s to total XBP1 in the knockdown and ZNF598^{mut} overexpression cells was 1.5 – 2-fold higher than in controls for

both HEK293 and hiPSC (**Figure 2.38 E**). These results suggest that after splicing of pre-existing XBP1 mRNAs, their release from the stalled ribosome at the ER is impaired by ZNF598^{mut}, and the spliced mRNA cannot be translated to produce the XBP1-s protein. This inhibits downstream target expression (i.e. DNAJB9) and the autoregulatory loop that amplifies XBP1 mRNA levels.

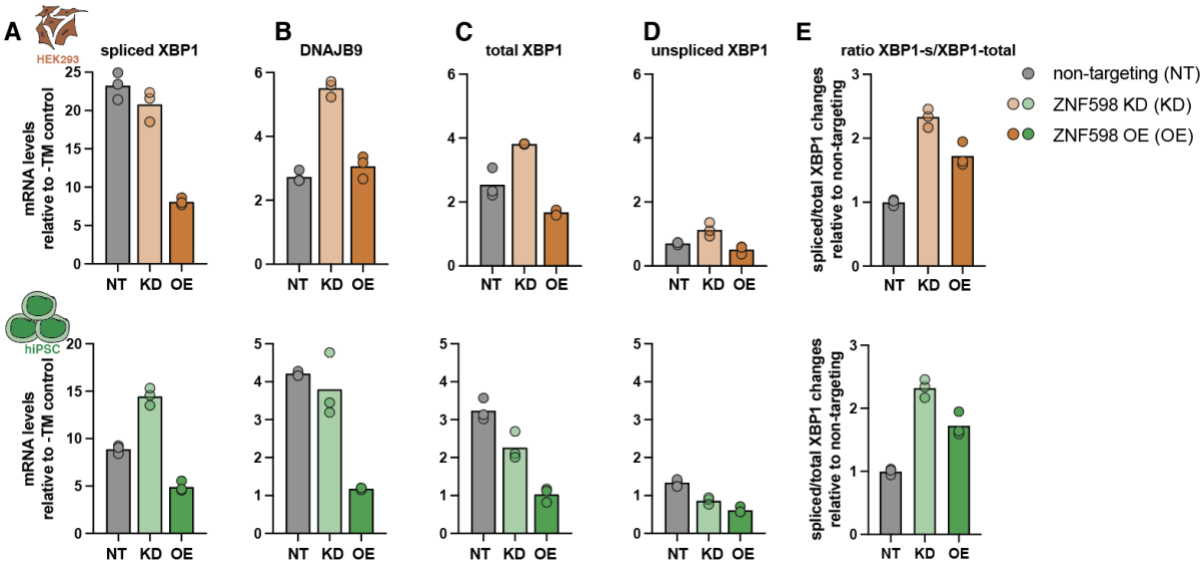

Figure 2.38. ZNF598 RING domain mutations do not impair XBP1 mRNA splicing but inhibit XBP1-s target expression.
Gene knockdown (KD) was induced for four cell doublings in the single knockdown experiments. ZNF598^{mut} was stably integrated into hiPSC and HEK293 cells and expressed for two days in the presence (hiPSC) or absence (HEK293 cells) of endogenous ZNF598. Subsequently, cells were treated with 2.5µM tunicamycin for six hours. Samples were analyzed by quantitative RT-PCR for spliced XBP1 (XBP1-s)(A), downstream DNAJB9 expression (B), total XBP1 levels (C), unspliced XBP1 (XBP1-u), and the splicing efficiency (ratio of XBP1-s to total XBP1)(E). B2M was used as a reference gene for relative mRNA quantification and normalized to the corresponding non-targeting control in three technical replicates.

2.4.6. Loss of ribosome rescue factors triggers cellular stress responses

Previous studies suggested that in yeast, Hel2 may preferentially interact with ribosomes on mRNAs encoding secretory proteins to regulate their correct localization[251]. We hypothesized that the cell context-specific essentiality of its human homolog ZNF598, as well as other ribosome quality control factors, may result from different endogenous substrate pools in human cells. Therefore, we first compared global mRNA changes in response to knocking down some of these factors in HEK293 cells or hiPSC. We depleted ZNF598 and HBS1L by CRISPRi for four and five cell doublings, or overexpressed ZNF598^{mut} for two cell doublings, and compared mRNA levels to respective non-targeting controls by RNA-seq. We observed that the mRNAs that change significantly in abundance overlapped remarkably well between the knockdown of ZNF598 and HBS1L within the same cell line, but were distinct between HEK293 and hiPSC (**Figure 2.39**). This suggests different molecular responses to ZNF598 or HBS1L loss in different cellular contexts. By contrast, the gene expression changes induced by ZNF598^{mut} expression did not resemble those resulting from ZNF598 knockdown or any other knockdown tested, but they were very similar in both HEK293 and hiPSC. This suggests that cells respond differently to loss or malfunction of ribosome collision-sensing factors. It is conceivable that the RING domain mutation of ZNF598^{mut} leads to its accumulation on the mRNA by impairing its interaction with an E2 ubiquitin ligase, which induces different cellular responses than the loss of the protein.

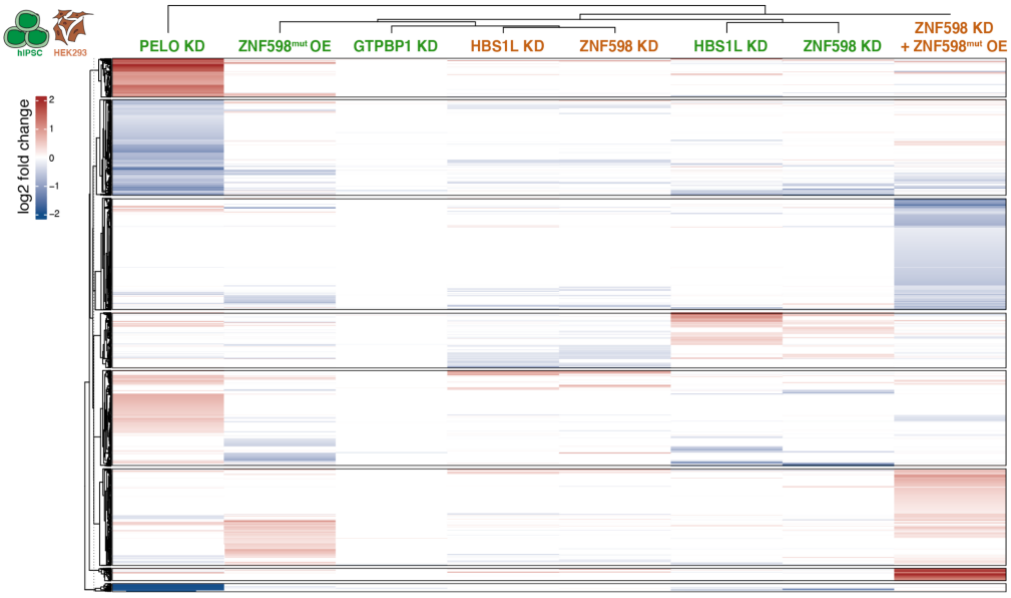

Figure 2.39. Differential gene expression analysis by RNA-Seq reveals cell context-dependent reprogramming upon ribosome collision factor depletion in hiPSC and HEK293.
Heatmap of significant mRNA fold changes (padj< 0.05) compared to respective non-targeting controls or wild type cells (ZNF598mut in hiPSC) calculated with DESeq2 and clustered using pheatmap.

We also performed RNA-seq analysis upon knockdown of PELO and GTPBP1 in hiPSC. We expected an overlap with the response to HBS1L knockdown, since PELO and HBS1L form a complex (**Figure 2.19 C**). GTPBP1, on the other hand, is another GTPase with high structural similarity to HBS1L that may also function in complex with PELO[242]. Interestingly, the knockdown of PELO or GTPBP1 resulted in gene expression changes that were distinct from those we observed upon knockdown of HBS1L or ZNF598 (**Figure 2.39**). Since PELO is the leading force that facilitates ribosome disassembly and possibly can be transported to the ribosomal A site by multiple GTPases, it is conceivable that its loss has different consequences compared to its interaction partner HBS1L. Furthermore, PELO depletion in mice is embryonically lethal at day 7.5 compared to day 8.5 for HBS1L[247].

To gain insights into the cellular pathways activated by gene knockdown, we next analyzed differentially expressed genes (padj<0.05) for Gene Ontology (GO) term enrichment using ClusterProfiler (**Figure 2.40**). This analysis confirmed similar response pathways for ZNF598 and HBS1L knockdown in HEK293 cells. Downregulated genes were involved in ribosome and tRNA biosynthesis, mRNA splicing, and mRNA surveillance pathways. In contrast, genes from some of these pathways were upregulated after HBS1L or ZNF598 knockdown in hiPSC (**Figure 2.40**). Remarkably, the gene expression changes triggered by PELO knockdown in hiPSC showed greater similarities with those induced by HBS1L loss in HEK293 cells than in hiPSC. Since these data were obtained from a sample in which PELO was depleted for three days (**Figure 2.28**). RNA-seq data of a later time point might shift molecular response mechanisms and have to be investigated in further detail. Finally, GTPBP1 knockdown led to the differential expression of only very few mRNAs, with very few GO terms enriched among them (**Figure 2.40**). When comparing single genes, we observe changes in many genes involved in neurogenesis and gastrulation such as CTNNB1, SFRP1, or OTX2, which would present a possible link to its hypothesized function in rescuing stalled ribosomes specifically in the brain[242].

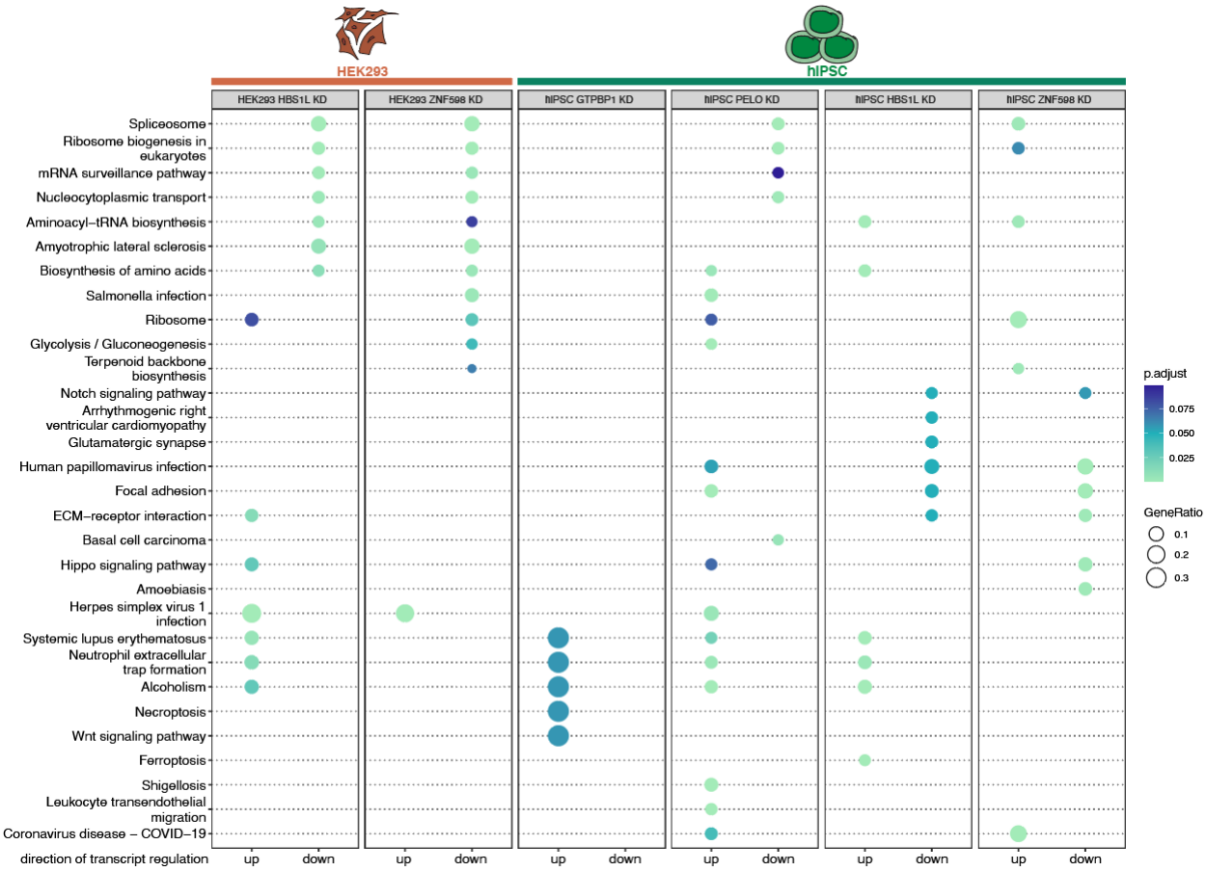

Figure 2.40. Ribosome collision factor knockdown triggers different response pathways in HEK293 and hiPSC.
Gene knockdown (KD) was induced for two (GTPBP1), three (PELO), four (ZNF598) or five (HBS1L) cell divisions and RNA-Seq libraries were prepared from two biological replicates. Data were analyzed in comparison to the corresponding non-targeting control using DESeq2. GO term enrichment analysis of biological functions in genes with significant differential expression (padj<0.05) was performed with ClusterProfiler and GO categories with padj<0.1 were plotted for upregulated (up) and downregulated (down) genes in HEK293 (left) or hiPSC (right).

The GO term enrichment analysis of the response to ZNF598^{mut} overexpression, by contrast, showed a large overlap between the genes with significant differential expression in hiPSC and HEK293 cells (**Figure 2.41**). Splicing and mRNA surveillance pathways were upregulated, as already partially observed after ZNF598 knockdown in hiPSC. Additionally, many pathways that regulate cell metabolism were downregulated.

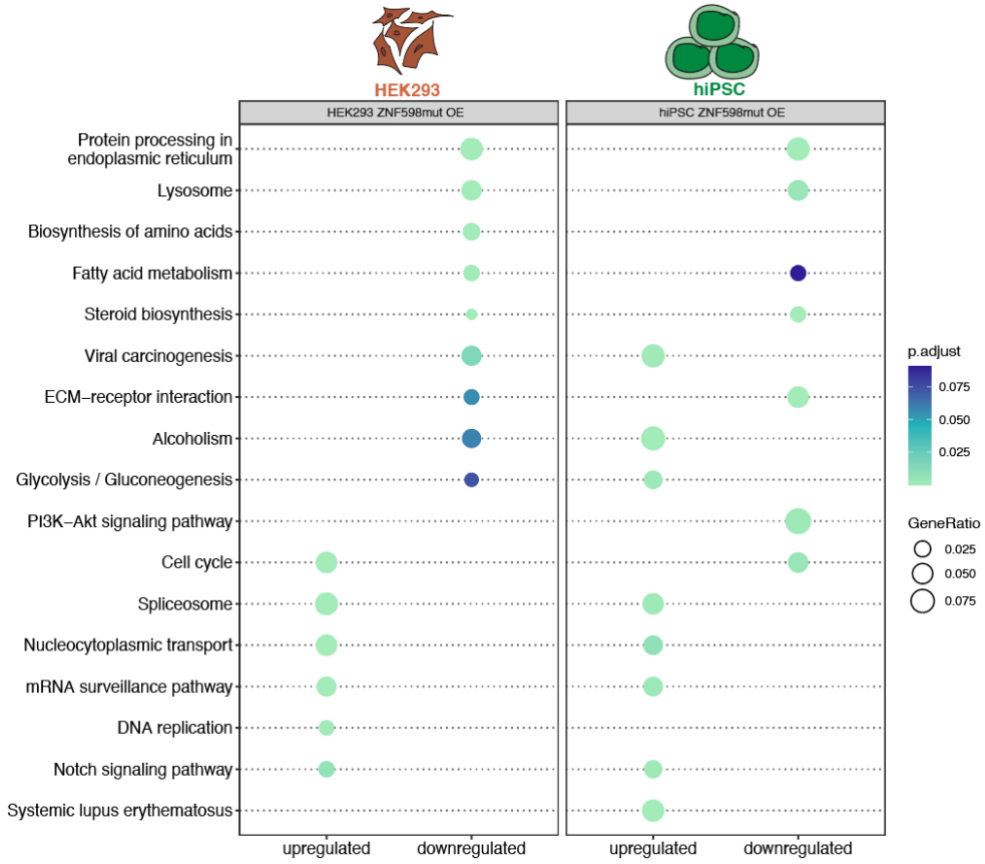

Figure 2.41. GO term enrichment analysis reveals similar responses to ZNF598^{mut} expression in HEK293 and hiPSC.
After ZNF598 knockdown (only in HEK293 cells) and/or ZNF598^{mut} expression, RNA-Seq libraries were prepared from two biological replicates. Data were analyzed in comparison to the corresponding non-targeting control using DESeq2. GO term enrichment analysis of biological functions in genes with significant differential expression (padj<0.05) was performed with ClusterProfiler and GO categories with padj<0.1 were plotted for upregulated (up) and downregulated (down) genes in HEK293 (left) or hiPSC (right).

In the mouse brain or epidermis, conditional knockout of HBS1L and/or PELO was found to upregulate genes related to the mTORC1 pathway[246,247]. Our HBS1L knockdown cells showed a minor upregulation of MTOR (log_2 fold change of 0.2), but none of its downstream targets or interactors (**Figure 2.42**). This suggests that in the human cell lines we profiled, the mTORC1 pathway is not the main mechanism of translational dysregulation. However, since this pathway is mostly regulated via post-translational modifications, further analysis of, e.g., phosphorylation levels of mTORC1 pathway members is needed to establish how this signaling is modulated by HBS1L loss in human cells.

Interestingly, however, we observed that genes associated with the ISR (e.g. ASNS, CHAC1, TRIB3, and HSPA/BIP) were among the top upregulated ones upon depletion of ZNF598 or HBS1L in hiPSC (**Figure 2.42**). Therefore, we analyzed our RNA-seq and ribosome footprint data from matched samples for common genes that are upregulated during the ISR or RSR

pathways in the different knockdown cell lines (**Figure 2.42**). The depletion of HBS1L, PELO, or ZNF598 consistently increased both mRNA and footprint levels for ISR-induced genes in hiPSC. Furthermore, HBS1L knockdown also increased levels of ATF3 and CHOP, which are common markers of apoptosis upon ISR activation. In contrast, the expression of these genes was not significantly altered by ZNF598 or HBS1L knockdown in HEK293 cells. These data, together with the induction of eIF2α phosphorylation (**Figure 2.37**) and the reduced global protein synthesis (**Figure 2.35**), indicate that the loss of ribosome rescue factors triggers the ISR in a cell context-dependent manner.

In contrast to ZNF598 depletion, ZNF598^{mut} expression led to a downregulation of ISR target genes in both HEK293 and hiPSC. Furthermore, it elicited an increase in the expression of genes linked to the RSR and apoptosis, including JUN, PPP1R15A/GADD34, and KLF11 (**Figure 2.42**). Interestingly, this phenotype was conserved between cell contexts. These data suggest that the more stable association of ZNF598^{mut} with translating ribosomes (**Figure 2.27**) inhibits the activation of the ISR and triggers the RSR pathway and apoptosis.

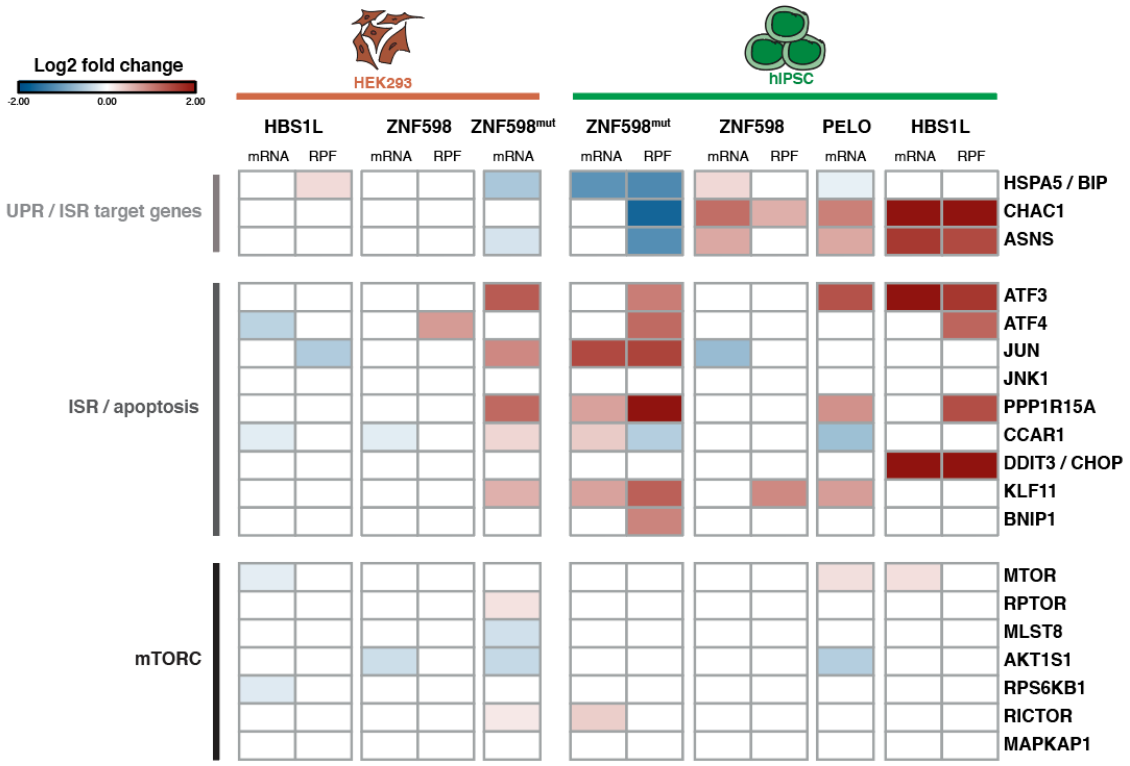

Figure 2.42. Loss of ribosome collision factors induces the ISR, whereas ZNF598 RING domain malfunction induces apoptosis in HEK293 and hiPSC.
Gene knockdown (KD) was induced for three (PELO), four (ZNF598) or five (HBS1L) cell doublings and ZNF598mut was expressed for two cell doublings in biological replicates and matched samples were prepared for RNA-seq and ribosome footprinting libraries. Significant mRNA and footprint fold changes (padj<0.05) in comparison to the respective non-targeting controls (KD) or wild-type cells (ZNF598^{mut} in hiPSC).

The ISR can be activated through four major stress kinases. All of them phosphorylate eIF2α, leading to global mRNA translation shutdown and activation of stress response genes, such as ASNS and CHAC1, through ATF4. To gain insights into whether the gene expression signatures we observed in our knockdown lines were due to activation of the eIF2α-ATF4 ISR axis, we compared our RNA-Seq and ribosome occupancy data with previous results that identified specific targets for each branch of the UPR using Perturb-Seq of human cells subjected to ER stress (**Figure 2.43**)[399]. This study identified a total of 104 genes, which were specifically up- or downregulated dependent on either ATF6, PERK, or XBP1 after treatment with tunicamycin or thapsigargin. HEK293 cells did not show consistent up- or downregulation for any of these groups, which we already observed for our analysis of common markers (**Figure 2.42**, **2.43**). Interestingly, however, PERK-regulated genes in thapsigargin- or tunicamycin-treated human cells showed highly similar expression patterns in hiPSC depleted for ZNF598 or HBS1L. The expression of ZNF598^{mut}, by contrast, elicited a downregulation of ER stress-regulated genes in both cell contexts, which was evident not only for ATF4 targets, but also for ATF6 targets (**Figure 2.43**). These data strongly suggest that the eIF2α -ATF4 axis of the ISR is activated upon loss of ZNF598 or HBS1L in hiPSC.

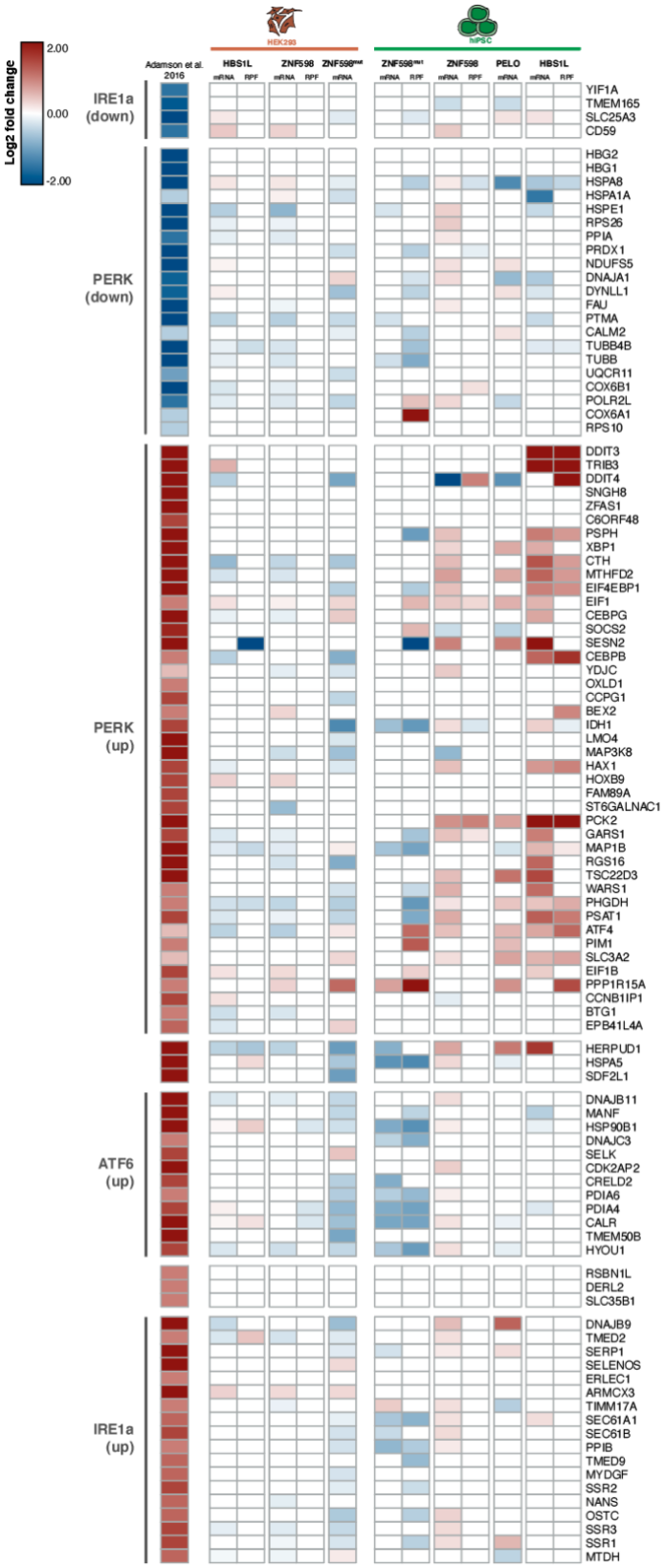

Figure 2.43. Loss of ribosome collision factors induces the eIF2α-aTF4 ISR axis in hiPSC.
Gene knockdown (KD) was induced for three (PELO), four (ZNF598) or five (HBS1L) cell doublings and ZNF598^{mut} was expressed for two cell doublings in biological replicates and matched samples were prepared for RNA-seq and ribosome footprinting libraries. Significant mRNA and footprint fold changes (padj<0.05) in comparison to the respective non-targeting controls (KD) or wild-type cells (ZNF598^{mut} in hiPSC). Data on UPR-dependent gene up- and downregulation in human cells treated with tunicamycin or thapsigargin was obtained from Adamson et al.[399].

2.4.7. ZNF598^{mut} expression in hiPSC leads to ribosome pausing at start codons of mRNAs with short 5'UTR

In yeast, loss of Hel2 was recently shown to decrease the frequency of ribosome collisions, possibly as a result of decreased initiation rates following ISR activation[253]. We found that global protein synthesis was also inhibited in ZNF598-depleted hiPSC (**Figure 2.35**). Accordingly, using ribosome profiling, we did not detect significant ribosome pauses along endogenous mRNAs in samples from ZNF598-depleted hiPSC (data not shown). Given that ZNF598^{mut} associates more stably with translating ribosomes (**Figure 2.34**), we asked whether the use of this mutant would allow us to gain some insights into the endogenous targets of ZNF598 in human cells. For this, we transduced the ZNF598^{mut} expression construct in hiPSC, which are highly sensitive to the depletion of the wild-type protein (**Figure 2.28**). After two days, we harvested the cells along with a wild-type control not expressing ZNF598^{mut} without translation inhibitor pretreatment, and prepared libraries from ribosome-protected mRNA fragments with a length of 19 to 32 nt, corresponding to monosome footprints[265].

We first compared ribosome occupancy around start and stop codons in control versus ZNF598^{mut}-expressing hiPSC. Metagene analysis of read distribution along the coding sequence (CDS) showed the typical signature of high-quality ribosome profiling libraries from mammalian cells that have not been treated with translation inhibitors, i.e. a lack of coverage in UTRs and an accumulation of ribosomes at stop codons[53]. Remarkably, this analysis revealed a substantial increase in ribosome density at or very close to annotated start sites of mRNA transcripts upon ZNF598^{mut} expression (**Figure 2.44 A**). Recent work has shown that in yeast, Hel2 may bind translated mRNAs around the stop codon[252]. However, we found a minor decrease in ribosome occupancy at stop codons upon ZNF598^{mut} expression in hiPSC (**Figure 2.44 B**)[252].

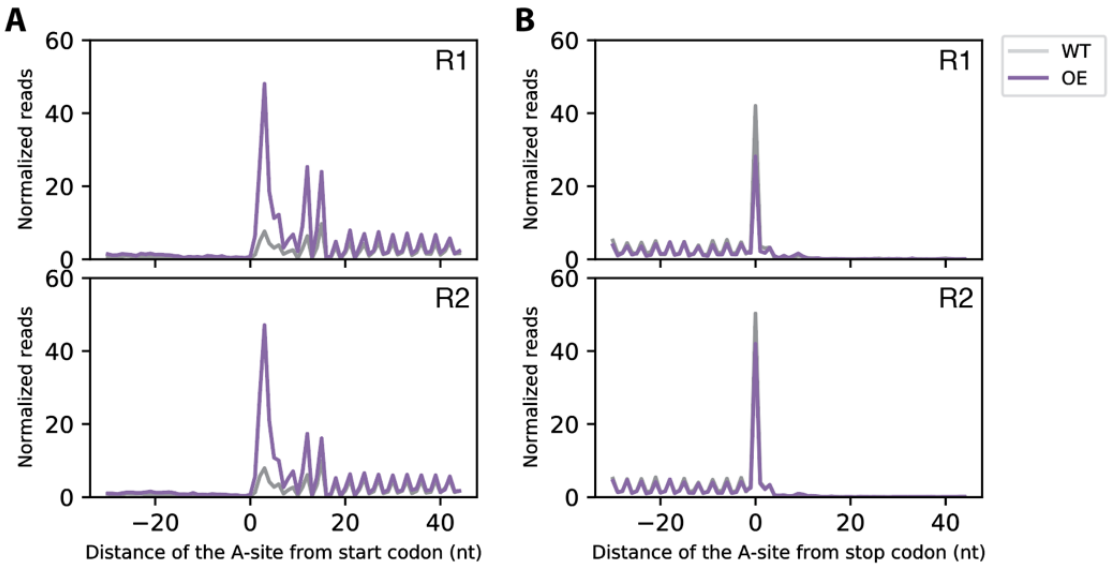

Figure 2.44. ZNF598^{mut} expression in hiPSC leads to increased ribosome density at start codons. Metagene profiles of ribosome occupancy in control (WT) and ZNF598^{mut}-expressing (OE) hiPSC in two biological replicates (R1 and R2). The A site in each footprint read was predicted using a random forest model. Reads were normalized to the average ribosome occupancy per transcript and aligned to the annotated start (A) and stop codon (B).

We next asked whether ribosome pausing at start sites upon ZNF598^{mut} expression was pervasive or occurred only in a subset of mRNAs, and whether ribosomes accumulated at any other sites on endogenous mRNAs. For this, we devised a computational pipeline for the identification of strong pause sites at nucleotide resolution (see Materials and Methods). We first transformed the codon-level coverage per mRNA into z-scores, and then filtered out low-coverage genes to avoid bias. Of the 17601 mRNA transcripts in our reference, 4760 passed our minimal coverage threshold of ≥0.1 reads per codon in all samples. We then identified pause sites as peaks with a z-score >5 in both biological replicates of a given sample. This analysis identified 2500 genes in WT and 2529 genes in ZNF598^{mut}-expressing hiPSC with one or more pause sites, confirming our ability to detect instances of higher-than-average ribosome occupancy.

We considered peaks occurring at the same or adjacent codon in both WT and ZNF598^{mut} as conserved pause sites, and peaks with significantly different z-scores in ZNF598^{mut} versus WT (two-tailed Fisher's exact test $p<0.01$) as sensitive pause sites. Remarkably, pausing strength differed significantly between WT and ZNF598^{mut} in only 342 genes. Of these, 323 genes (94%) displayed increased pausing in cells expressing ZNF598^{mut} (**Figure 2.45**, **Table S 5.8**). We found pauses at 344 sites in these genes, 321 of which (95%) were non-conserved, i.e. did not have a z-score indicative of ribosome pausing in the control. Most notably, the vast majority of ZNF598^{mut}-specific pauses (328; 95%) were within the first 10 codons of the CDS,

of which 222 (64.5%) represented footprints of ribosomes with a start codon in the P site. This was consistent with the results from metagene analysis of ribosome footprint coverage around start sites (**Figure 2.44**).

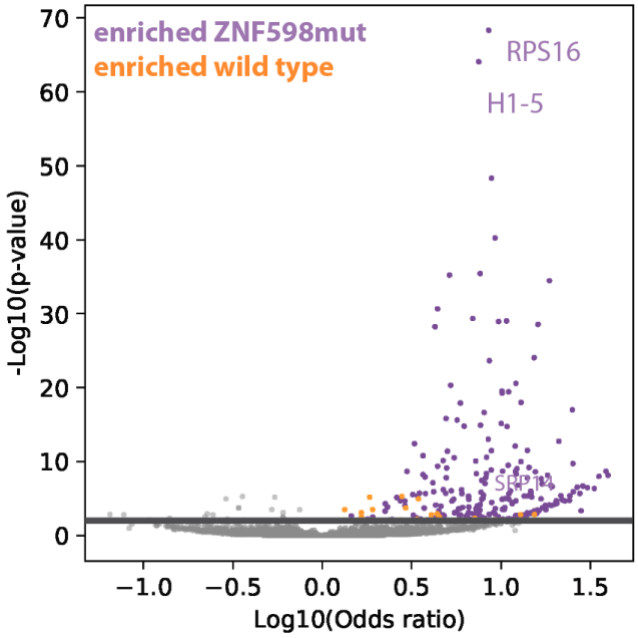

Figure 2.45. Ribosome pausing increases in ZNF598^{mut}-expressng hiPSC.
Volcano plot showing the odds ratio of sensitive pause sites between WT and ZNF598mut-expressing cells and the associated p-value from a two-tailed Fisher's exact test.

To identify common features of mRNAs with pausing sites in the ZNF598^{mut} expressing hiPSC, we analyzed common sequence motifs of those mRNAs (**Figure 2.46 A**). We found a strong enrichment of the Kozak consensus sequence (GCCPuCCAUGG, **Figure 2.46 A**)[69,72], which was supported by increased ribosome occupancy at or around start sites (**Figure 2.44 A**). Since no other sequence motifs were enriched, we analyzed 5' UTR length, which plays a major role in start site selection and translation efficiency of eukaryotic mRNAs[76]. This analysis revealed that transcripts with pauses only detectable upon ZNF598^{mut} expression mostly had 5' UTRs of <100 nt (**Figure 2.46 B**). Taken together, these findings suggest that in human cells, ZNF598 has a previously unappreciated role in relieving ribosome pausing at start codons in a subset of mRNAs with shorter-than-average 5' UTRs.

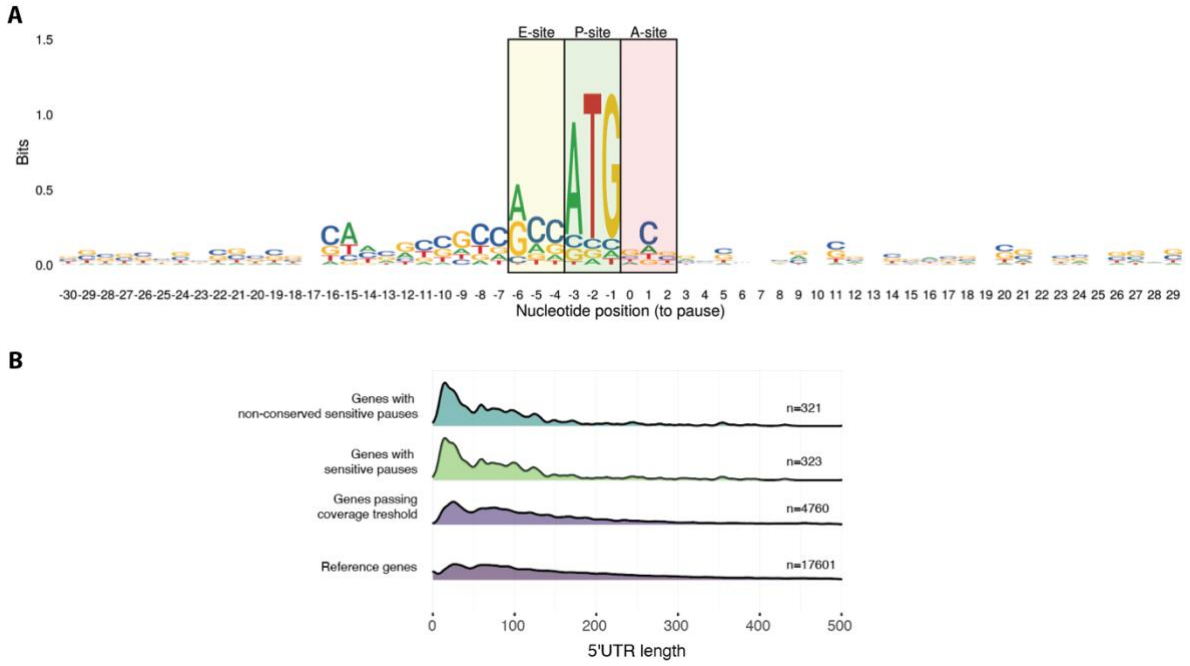

Figure 2.46. Ribosomes pause at start sites of mRNAs with short 5' UTRs ZNF598^{mut}-expressng hiPSC.
(A) Sequence context analysis of mRNAs with sensitive pauses in ZNF598^{mut}-expressing hiPSC using GGseqlogo2. (B) Annotated 5' UTR length distribution in the indicated gene subsets.

Next, we investigated the read distribution of individual mRNA transcripts which showed sensitive pause sites after ZNF598^{mut} expression. Pausing did not change globally, but accumulated within distinct clusters of mRNAs encoding ribosomal proteins, translation initiation factors, splicing and proteasomal factors, SRP components, and many histones (**Table S 5.8**). Interestingly, even though ribosome footprint density drastically increased at the start codon, the read counts and their distribution did not change along the coding sequence (**Figure 2.47 A** to **C**). To find out how pausing impacts protein levels, we focused on the linker histone H1-5, which had a very pronounced increase in ribosome occupancy at the start codon in ZNF598^{mut}-expressing hiPSC (**Figure 2.47 C**). Despite a significant increase in mRNA abundance and ribosome occupancy of this mRNA in ZNF598^{mut}, Western blotting analysis showed an ~20% decrease in H1-5 protein levels (**Figure 2.47 D**). This discrepancy between mRNA and protein levels in the presence of ZNF598^{mut} suggests that accumulation of ribosomes at start sites may reduce protein expression.

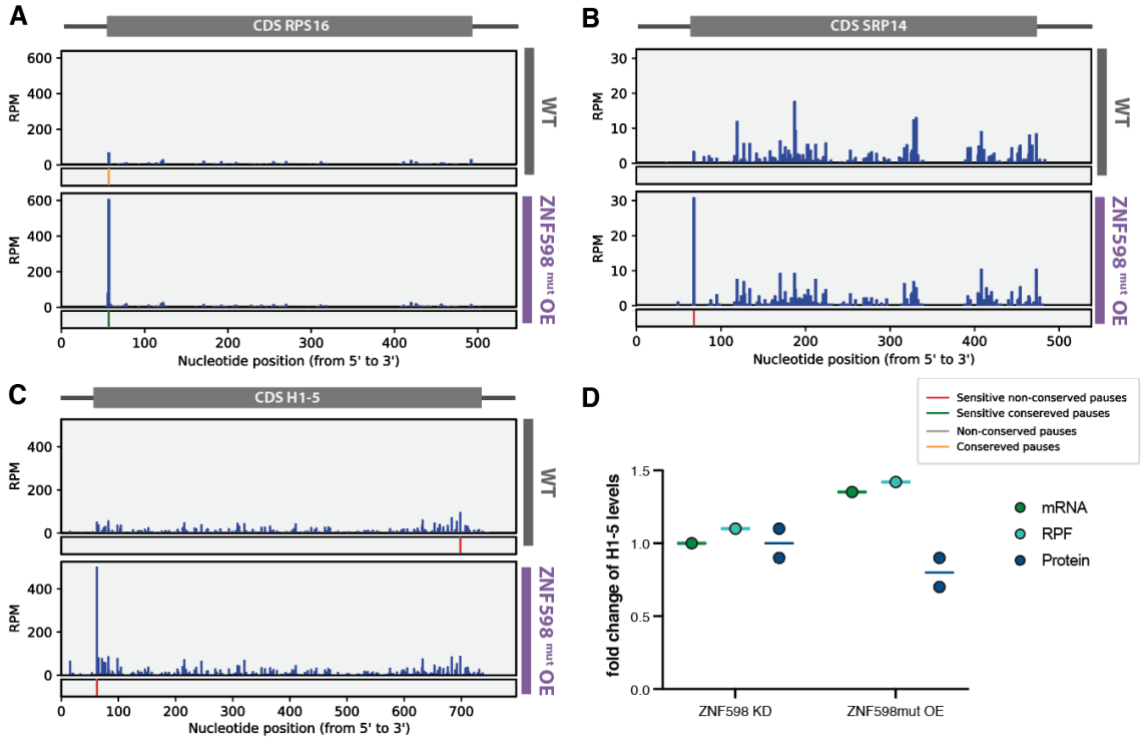

Figure 2.47. ZNF598^{mut} expression leads to ribosome pausing at start codons of mRNAs with short 5' UTRs.
Ribosome footprint profiles at nucleotide resolution of representative genes in wild type (WT) and ZNF598^{mut} -overexpressing (OE) hiPSC. The barcodes below each profile show the position and the type of the pause sites in RPS 16 (A), SRP14 (B) and H1-5 (C). (D) Relative RNA abundance, ribosome occupancy, and protein levels for H1-5 after four cell doublings of knockdown or two cell doublings of ZNF598^{mut} expression in hiPSC compared to either non-targeting controls or wild-type cells. Changes in mRNA abundance or ribosome density were calculated with DESeq2 (padj<0.05). Protein levels were quantified from Western Blot analysis, normalized to total protein and compared to the respective control in two biological replicates.

An impairment of histone protein synthesis is in line with gene expression changes we detected by RNA-Seq data, in which we found CCND2 and HMGCS1 among the most strongly downregulated genes after ZNF598 knockdown or ZNF598^{mut} overexpression. Both are important regulators for the G1/S phase transition and reinforced our observation of cell cycle defects upon ZNF598 perturbation in hiPSC (**Figure 2.36**). Failure to package newly synthesized DNA into nucleosomes can lead to replication stress and induce cellular senescence[397]. Aneuploid and cancer cells are often able to bypass most cell cycle checkpoints at the expense of increased genome instability, which may account for the milder growth phenotype of ZNF598 depletion in HEK293 cells we observed (**Figure 2.27**). In the case of ZNF598^{mut} expression, however, it seems that cells arrest in G2 and further induce apoptosis. In summary, investigating gene function in physiologically relevant cell contexts allowed us to identify endogenous substrates for ZNF598-mediated translational control in human cells and a novel role of this E3 ligase in preventing ribosomal pausing during translation initiation on mRNAs with short 5' UTRs.

Chapter 3 – Discussion

3.1. The inducible CRISPRi system in hiPSC as a screening platform for identifying cell context-dependent human gene function

In this study, we combined inducible CRISPRi[340] with robust hiPSC differentiation protocols[349,354] to identify non-essential, core-essential, and cell context-essential components of the mRNA translation machinery in human cells. So far, many labs successfully performed genome-wide CRISPRi screens in immortalized human cell lines such as HEK293T, HeLa, or K562 cells. Recent screening approaches were expanded to healthy hiPSC and hiPSC-derived neurons, which, however, were limited to protein depletion during the derivation process[341,342]. Genome-wide screens are costly and need substantial cell numbers to start with. Therefore, many labs limit their screens to only ~3-5 sgRNAs per target gene, and some reduce sgRNA coverage to 300-500 cells per sgRNA, or even only screen the “druggable” genome. Unfortunately, published CRISPRi data also showed that sgRNA prediction for many genes can be difficult and, consequently, sgRNAs are not efficiently targeting or knocking down target gene transcription. This would mean that in set-ups with fewer sgRNAs per target, many essential genes may be missed. In contrast, we pursued a focused screening approach by targeting 262 genes. This enabled us to use nine sgRNAs per target and a coverage of 1000 cells per sgRNA while minimizing handling time and experimental costs. By optimizing screening and differentiation protocols, we achieved highly reproducible screening results not only in dividing transformed (HEK293) and non-transformed cells (hiPSC, NPC), but also in postmitotic hiPSC-derived cultures (neurons and CM). This enabled us to investigate for the first time how gene knockdown influences the growth and survival of different isogenic human cell lineages with a healthy genetic background in comparison to a commonly used aneuploid cell culture line. With this powerful comparative approach, we identified numerous human genes that are essential for growth and survival of hiPSC and hiPSC-derived differentiated cells, but were previously thought to be dispensable based one studies in yeast or immortalized human cell lines (**Figure 3.1**). This highlights the need for interrogating protein function and defining molecular mechanisms in physiologically relevant experimental systems.

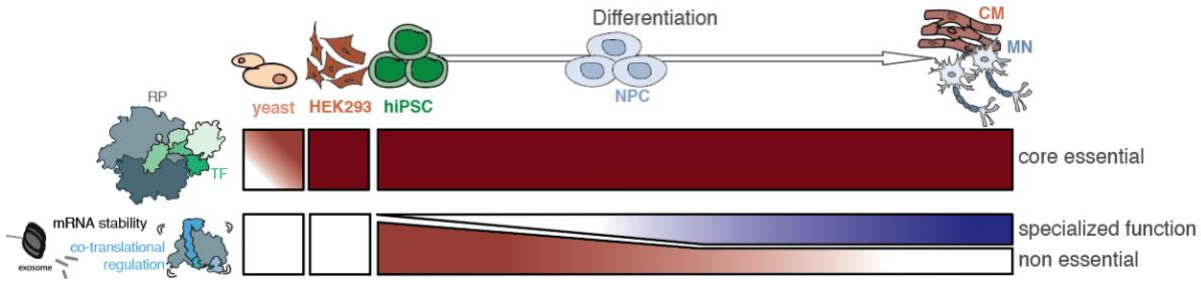

Figure 3.1. Ribosomal protein and translation factors are core-essential, while other factors become more specialized functions in different cell contexts.
We propose that ribosomal proteins and translation factors are core-essential in mammalian cells. This essentiality is not completely conserved to yeast. In contrast, many factors that bind the ribosome and mRNA to assure stability and quality control are not essential in yeast and aneuploid HEK293 cells. Many of them are still highly essential in hiPSC, however, essentiality decreases upon differentiation and specialize their function in differentiated cell types.

We found that ribosomal proteins and translation initiation and elongation factors are core essential across all cell contexts (**Figure 2.13**, **2.14**, **3.1**), which highlights the robustness of our screens even in differentiated cell types. Our data also indicate that none of the core ribosomal proteins are dispensable in any of the cell contexts we tested. Our setup does not exclude the possibility that several subpopulations of ribosomes with a heterogeneous protein composition exist in some cellular contexts, or that ribosome heterogeneity can arise through reversible and/or irreversible post-translational modifications of RPs or rRNAs. Current hypotheses on specialized ribosomes also focus on differential expression patterns across cell types of core RPs with paralogues in the genome[132,134,135]. Interestingly, we observed that the knockdown of most paralogs of core-essential RPs did not elicit detectable phenotypes for most cell contexts and was even beneficial in some (**Figure 3.1**). This suggests that most RP paralogs are not functionally redundant and many may be dispensable for fitness in most cellular contexts. Further biochemical and biophysical experiments are needed to explore in more detail how interchangeable RP paralogs are in human cells.

3.2. Deciphering ribosome quality control mechanisms in physiologically relevant cellular backgrounds

In contrast to the core essentiality of genes encoding ribosomal proteins and translation initiation and elongation factors, we observed that most mRNA and protein quality control regulators are essential in hiPSC but dispensable after hiPSC differentiation and in HEK293 cells. Silencing subsets of these genes is detrimental in specific cell types but advantageous in others, particularly during cell state transitions (**Figure 2.15**, **3.1**). The depletion of proteins that detect and rescue stalled ribosomes elicited the largest phenotypic variation in our screens (**Figure 2.17**). Even though ribosome collision factor loss consistently impaired growth and survival in hiPSC, it led to no or minor fitness loss in HEK293 cells. Indeed, in HEK293T cells, stable knockout lines can be created and maintained without phenotypic changes of the culture[202,226,237]. When comparing stalling readthrough efficiency of reporters, we only observed minor differences between cell contexts. Hence, we propose that phenotypic variability between hiPSC and HEK293 cells upon depletion of ribosome quality control factors arises through differences in the cellular pathways activated in response, rather than through the specialized function of these factors in different cellular contexts. In accordance with this idea, we found that depletion of ribosome quality control factors leads to a global decrease in protein synthesis and is cytotoxic in hiPSC but not in HEK293 cells (**Figure 2.22**, **2.23**). Dysregulated gene expression patterns in aneuploid immortalized cell lines such as HEK293 may therefore make them more resistant to the consequences of defective ribosome quality control.

3.3. XBP1-mediated UPR activation is dependent on ribosome rescue factors

One of the major goals of this work was to obtain a molecular understanding of endogenous ribosome pausing events and the function of ribosome collision-sensing and rescue factors in their resolution in human cells. In order to maintain protein synthesis, stalled ribosomes need to be recognized, disassembled and recycled by the cell[199]. We found that endogenous XBP1 mRNA and protein levels are modulated by ribosome collision factors and suggest a new regulatory function of ZNF598 stress induction (**Figure 3.2**). The most well characterized ribosome stalling sequences in human cells are AAA-encoded stretches of more than four lysines and the XBP1 arrest peptide[202,205]. Both sequence motifs are frequently incorporated in reporter constructs used to investigate the RQC in mammalian cells[202,226]. It is unclear, however, to what extent these exogenous reporters represent natural substrates of RQC pathways. Although ribosomes could encounter poly(A) stretches when translating a faulty mRNA with no stop codon, a stretch of more than three lysines is almost never encoded by an AAA codon run in human genes[200]. High reporter expression levels may also overwhelm cellular quality control pathways, complicating the interpretation of the data. On the other hand, depletion of ribosome collision-sensing and rescue factors leads to the activation of stress responses and a global repression of protein synthesis (**Figure 2.35**, **2.37**)[253], which may help decrease the frequency of ribosome stalling and collision on cellular mRNAs. Thus, our general understanding of endogenous pausing events is limited, and global principles for pausing-induced translational regulation remain elusive.

To gain detailed insights into the function of ribosome collision factors and their function in cells, we probed their importance for the splicing and translation of XBP1 mRNA in response to tunicamycin-induced ER stress. We could show that upon tunicamycin treatment, the XBP1 mRNA is efficiently spliced in the absence of HBS1L or ZNF598, but XBP1-s protein expression is decreased (**Figure 2.32**, **2.33**). Strikingly, despite efficient mRNA splicing, the XBP1-s protein was completely undetectable in hiPSC expressing ZNF598^{mut} (**Figure 2.37**). The C29S/C32S RING domain mutation in ZNF598^{mut} may impair the recruitment of E2 ligases[400], trapping the protein on stalled ribosomes and blocking mRNA release. Recent work in yeast indicates that Hel2 may bind to ribosome-nascent chain complexes (RNCs) to impede mistargeting of secretory proteins. Hel2 was found to bind RNCs in early stages of translation, which was proposed to inhibit the synthesis of toxic hydrophobic regions that are decoded

further downstream of the binding site[251]. However, we found no defect in XBP1 mRNA splicing in tunicamycin-treated cells expressing ZNF598^{mut}, which suggests that mRNA targeting to IRE1 at the ER is still functional (**Figure 3.2**). Taken together, our observations suggest that ZNF598 and possibly also HBS1L are needed to disassemble ribosomes that stalled on XBP1 mRNAs to enable XBP1-s translation, and downstream UPR gene activation (**Figure 3.2**).

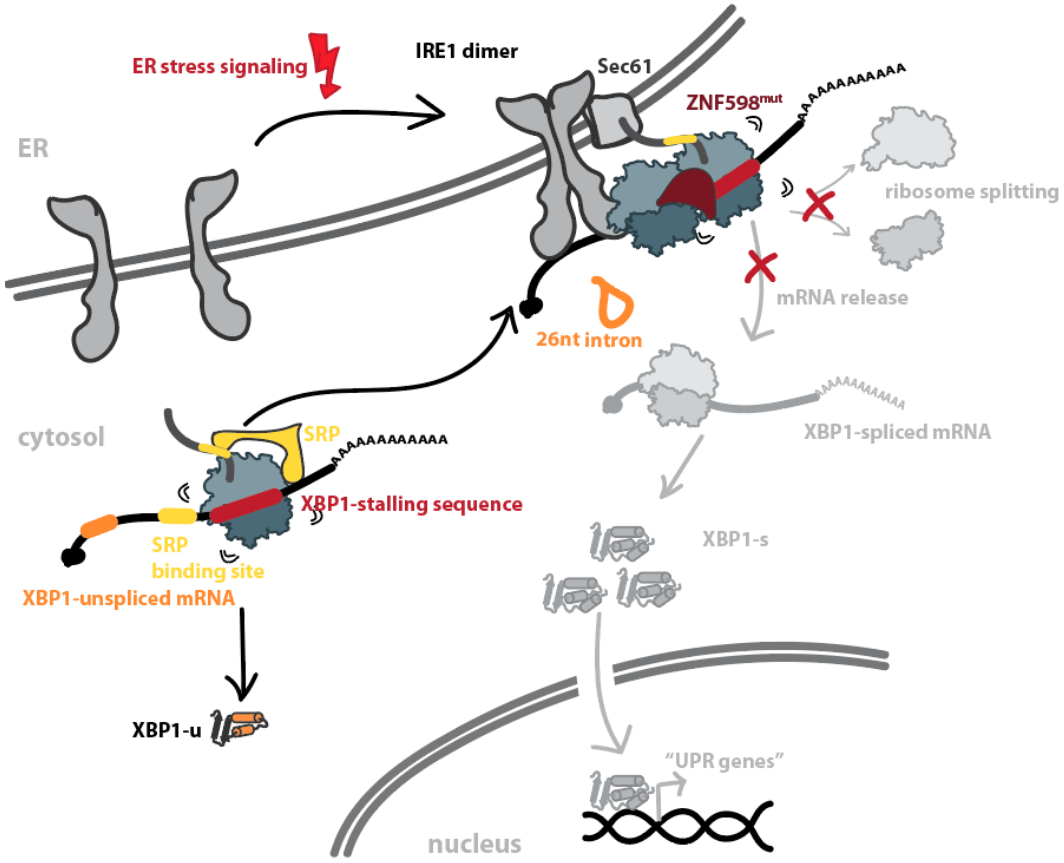

Figure 3.2. Ribosome collision factors modulate UPR responses by enabling XBP1-s mRNA translation.
The XBP1-unspliced (XBP1-u) mRNA is constitutively transcribed in cells. It contains a SRP binding domain, which is followed by a ribosome stalling peptide sequence. When ribosomes pause, the SRP domain is exposed from the ribosomal exit tunnel, bound by SRP and transported to the Sec61 translocon complex at the ER membrane. Upon ER stress induction, IRE1 dimerizes and excises a 26-nucleotide region from the XBP1-u mRNA to yield the XBP1-spliced (XBP1-s) mRNA, which encodes an active transcription factor. In the absence or malfunction of ZNF598 or HBS1L/PELO, stalled ribosomes cannot be disassembled and downstream XBP1-s protein synthesis and UPR gene activation is inhibited.

3.4. Depletion of ribosome rescue factors induces diverse cellular stress response pathways

When errors occur during mRNA translation, cells can initiate different stress response pathways that decrease global protein synthesis rates, facilitate ribosomal subunit recycling, and initiate degradation of faulty nascent chains and mRNAs. Recent studies with conditional knockouts in the mouse brain or epidermis indicate that loss of HBS1L/PELO induces mTOR-mediated downregulation of cell proliferation and translation[246,247,401]. Furthermore, upon induction of ribosome collisions with low doses of translation elongation inhibitors or UV irradiation, GCN2 and ZAKα mediate cellular stress responses by activating the ISR and RSR pathways, respectively[265]. Both stress pathways are proposed to act in sequential order by binding to collided ribosomes and determining cell fate depending on the duration and persistence of the stress, with unresolved ribosome collisions inducing the RSR and apoptosis (**Figure 3.3**). However, it is not well understood how cells assess the severity of co-translational stress and how the transition from RQC to ISR and ISR to RSR pathways is mediated.

Here, we show that in hiPSC, loss of ribosome rescue factors leads to the activation of the eIF2α-ATF4 ISR axis and global translation shutdown. We found that loss of ZNF598 and HBS1L triggered upregulation in mRNA levels and ribosome occupancy of genes that are linked to the PERK-mediated branch of UPR signaling in cells subjected to ER stress[399]. This was in line with increased eIF2α phosphorylation and a global reduction of mRNA translation (**Figure 2.32**, **2.35**). By contrast, we found no significant changes in the expression of genes from the mTOR pathway (**Figure 2.42**). Loss of factors that sense and disassemble stalled ribosomes could lead to misfolding and aggregation of nascent chains destined for the ER, and therefore activate the ISR. However, since the four different eIF2α kinases in human cells have a set of common downstream target genes, which are regulated through ATF4, it remains to be determined which of them is the key mediator of cellular responses to the loss of ribosome collision factors[119]. It is possible that the absence of these factors triggers an interaction of ribosomes with GCN2 to increase eIF2α phosphorylation and promote ATF4 protein synthesis, but an accumulation of misfolded proteins in the ER could also activate PERK. In addition, many cellular signaling pathways rely on post-translational modifications of proteins rather than changes in their expression levels. Therefore, to specifically probe for GCN2, PERK, or mTOR-mediated stress responses, we would need to investigate the phosphorylation status of key members of these pathways.

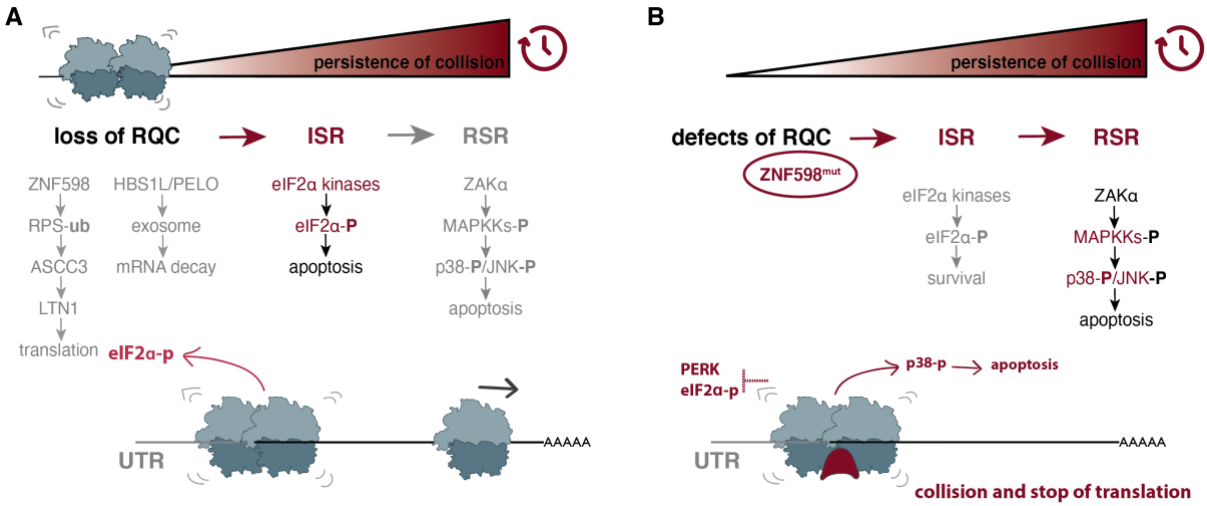

Figure 3.3. Models of stress response pathway induction by different levels of ribosome collision persistence in human cells (based on Wu et al.[265] and this work).
(A) Upon loss of ribosome collision factors ZNF598 or HBS1L, PERK-mediated stress response pathways are activated and lead to eIF2α phosphorylation, and further apoptosis if stress is persistent. (B) RING domain mutations in ZNF598 lead to a downregulation of the ISR/UPR and activate the ribotoxic stress response (RSR).

Furthermore, the expression of the RING domain ZNF598^{mut}, which associates more stably with translating ribosomes (**Figure 2.34**) and likely interferes with disassembly of stalled ribosomes and downstream RQC events, led to increased p38 phosphorylation, down-regulation of UPR gene expression, and up-regulation of the RSR/apoptosis genes (**Figure 2.42**). Recent studies have shown that in yeast cells treated with chemical agents, which induce ribosome stalling, Hel2 attenuates GCN2 binding and that the RQC and ISR are competitive pathways[245]. These findings are in line with our results showing that in hiPSC expressing ZNF598^{mut}, its presence on ribosomes stalled on endogenous mRNAs hinders ISR activation and leads to induction of the RSR and apoptosis instead. The stable association of ZNF598, or the ribosomal conformation it causes, may therefore represent the “persistent stress signal” to activate the RSR (**Figure 3.3**).

3.5. ZNF598 resolves ribosome pausing during translation initiation

Ribosome profiling of ZNF598^{mut}-expressing hiPSC revealed a suppressing and previously unappreciated role of this protein in preventing ribosome pausing during the early stages of translation of a subset of endogenous mRNAs. Translation initiation is generally the rate-limiting step of protein synthesis and needs to be tightly controlled. In yeast, initiation rates can vary by several orders of magnitude for different mRNAs[402,403], whereas elongation rates are more uniform (3 – 5 amino acids per second)[404]. The length of 5'UTR, which is highly variable between species and among different mRNAs in an organism, is one of the major determinants of translation efficiency [117,405]. The average 5' UTR length ranges from 53 nt in yeast to 218 nt in humans, but can extend to more than 2500 nt for some mRNAs in human cells[405]. The 48S PIC conformation and AUG codon recognition also play a major role in ensuring translation initiation at the correct start site[406]. Furthermore, in eukaryotic cells, the transition from initiation to elongation is much slower than in bacteria and can take several seconds[81]. We observed that in the presence of ZNF598^{mut}, ribosomes accumulate at or shortly downstream of the start codon in a subset of mRNAs with short 5' UTRs in hiPSC. This suggests that ZNF598 can help prevent queuing and collisions of initiating ribosomes, which could occur if scanning 40S complexes catch up (**Figure 3.4**). If this occurs, it is possible that ZNF598 mediates the ubiquitylation only of the collided 40S subunit, which would enable the initiating 80S to proceed without being disassembled. Alternatively, both the scanning 40S and the initiating 80S could be ubiquitylated and removed from the transcript. Interestingly, recent studies suggested that only one 40S scans a single 5'UTR at the time and that ribosome queuing during initiation is not a common phenomenon in human cells[117]. In contrast, 40S and ribosome queuing have been observed in rabbit reticulocyte lysates[407], which naturally lack ZNF598[223].

One poignant example of the endogenous substrates of ZNF598 we identified are histone mRNAs, which have a very particular structure. They have very short 5'UTRs (15 – 30 nt), no introns, and no poly(A) tails. The regulation of histone mRNA levels is translation-dependent and tightly coupled to the cell cycle. An excess or reduction of histone levels is harmful to cells, and dysregulated histone synthesis alters the progression of the S phase[408,409]. We observed that many mRNAs encoding core histones, including the linker histone H1, accumulate ribosomes at the start codon in ZNF598^{mut}-expressing hiPSC, and we also found that a larger proportion of these cells are in S phase in comparison to controls (**Figure 2.36**). In addition to

histone mRNAs, we found ribosome accumulation on several mRNAs encoding proteins involved in RNA processing, protein folding and degradation, and protein targeting to the ER. Many of those transcripts and their protein products are highly abundant in cells, which suggests that they may also have high translation rates. Perturbed expression of these genes could induce proteostasis imbalance and trigger the ISR activation we observed in ZNF598-depleted hiPSC. These data suggest a new function for ribosome collision-sensing factors in preventing 40S collisions with initiating ribosomes.

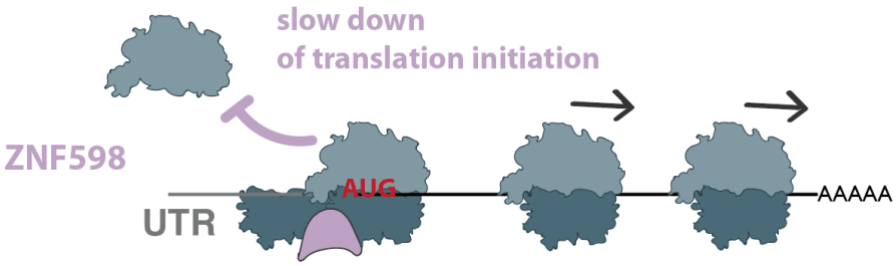

Figure 3.4. ZNF598 may prevent ribosome queuing during translation initiation on mRNAs with short 5'UTRs.

To directly test this hypothesis, it will be important to determine whether reducing translation initiation rates, e.g. with specific inhibitors, decreases ribosome pausing at start sites. It will also be important to investigate in more detail whether, in addition to short 5' UTRs, there are other sequence or structure determinants of ribosome pausing at start codons in ZNF598^{mut}-expressing cells. Another important open question is which pathways for ribosome disassembly act downstream of ZNF598 in this context. Our data show that in hiPSC, HBS1L and ZNF598 depletion led to highly similar cellular phenotypes (**Figure 2.17**), gene expression changes (**Figure 2.39**) and phenotypes in stalling reporter readthrough assays (**Figure 2.26**). Furthermore, our data suggested that GTPBP1 shares a function with HBS1L during ribosome disassembly in cells with normal karyotype. Therefore, it is conceivable that HBS1L and/ or GTPBP1, in concert with PELO, act downstream of ZNF598 during recognition of ribosome queues during translation initiation. Future experiments using ribosome profiling in cells expressing catalytic site mutants of HBS1L and GTPBP1, which cannot induce ribosome disassembly and remain bound to ribosomes[83], will be useful to test this hypothesis.

Chapter 4 – Materials and Methods

4.1. Materials

Table 4.1. Mammalian cell lines used in this study.
CRISPRi cell lines were further transduced with lentiviruses to stably integrate sgRNA constructs.

Cell line	Source	Identifier
cDN003_kucg_wt_ips	HipSci	HPSI0214i-kucg_2
cDN013_CRISPRi_kp6c2_ips	This study	N/A
cDN057_Lenti-X_293T	Takarabio	#632180
cDN075_CRISPRi_hek293c9	Dieter Edbauer Lab, DZNE	N/A
cDN257_CRISPRi_kp6c2_npc	This study	N/A

Table 4.2.Antibodies used in this study.

Antibody	Source	Identifier
Alpha-Tubulin	Sigma	T9026
ASCC3	Bethyl Laboratories Inc.	A304-015A-T
CHAT	Abcam	Ab6168
HA	Roche	11867423001
HBS1L	Atlas Antibodies	HPA029729
EDF1	Abcam	Ab97057
eIF2S1	Cell Signaling Technology	9722
eIF2S1-p (Ser51)	Cell Signaling Technology	9721
EIF4E2	Atlas Antibodies	HPA19253
GTPBP1	Bethyl Laboratories Inc.	A304-662A-M
GTPBP2	GeneTex	GTX122509
GIGYF2	Bethyl Laboratories Inc.	A303-732A
HB9	S Santa Cruz Biotechnology	SC-515769
Islet-1	R&D Systems	AF1837
Map2	Abcam	Ab92434
Nanog	Millipore	MABD24
Nestin	R&D Systems	MAB1259
P38	Cell Signaling Technology	9212
P38-p (Thr180/Tyr182)	Cell Signaling Technology	9211
Pax6	Abcam	Ab5790
PELO	Santa Cruz Biotechnology	SC-393418
RPS2	Bethyl Laboratories Inc.	A303-794A
Sox1	Santa Cruz Biotechnology	SC-365823
Sox2	Abcam	Ab87775
XBP1	Abcam	EPR22004
ZNF598	Abcam	Ab135921

Table 4.3. Plasmids used in this study.
pDN064, pDN115 and pDN292 served as template for sgRNA insertion. Single plasmids containing different sgRNAs are not listed (see Table 8.4 for sgRNA sequences)

Plasmid	Source	Identifier
pAAVS1-Ndi-CRISPRi Gen1	Mandegar et al. 2016	Addgene #73497
pAAVS1-TALEN-F	Mandegar et al. 2016	N/A
pAAVS1-TALEN-R	Mandegar et al. 2016	N/A
pMDLg/pRRE	Didier Trono Lab	Addgene #12251
pRSV-Rev	Didier Trono Lab	Addgene #12253
pMD2.G	Didier Trono Lab	Addgene #12259
pU6-sgRNA_EF1a-Puro-mKate	This study	pDN064
pU6-sgRNA_EF1a-Puro-GFP	This study	pDN115
pH7SK-sgRNA_hU6-sgRNA_EF1a-Puro-GFP	This study	pDN292
pUbC-BFP-T2A-FLAG-K0-P2A-mOrange	This study	pDN362
pUbC-BFP-T2A-FLAG-K20-P2A-mOrange	This study	pDN366
pUbC-BFP-T2A-FLAG-XBP1-P2A-mOrange	This study	pDN364
pUbC-BFP-T2A-FLAG-K0-P2A-mOrange-nonstop-malat	This study	pDN371
pUbC-BFP-T2A-FLAG-K0-P2A-mOrange-stop-malat	This study	pDN368
pA2UCOE-EF1a-ZNF598mut-P2A-BLC	This study	pDN415

Table 4.4. sgRNA sequences designed and used in this study.
sgRNA sequences were ordered with flanking sequences that overlap with cloning plasmids (pDN064, pDN115 and pDN292) for Gibson Assembly (also see methods section 8.2.2.).

sgRNA sequences	Source	Identifier
GAAGCCAAGATGGCGCATAG	This study	prDN1132_sgRNA_HBS1L
GCGTTGGCGCTGCAGCGGGG	This study	prDN1158_sgRNA_ASCC3
GGCCGGATCCCGGACCATGG	This study	prDN1160_sgRNA_ZNF598
GGGAACCTGAGGGTGAGCGG	This study	prDN1162_sgRNA_LTN1
GGGCCCGCGGGTCAGATCGG	This study	prDN1168_sgRNA_N4BP2
GAGCGCACGCTGAGGAGGAT	This study	prDN1321_sgRNA_EIF2S1
GCCAGCAAGGTAGGCCCGGG	This study	prDN1339_sgRNA_GTPBP1_1
GGAGAAGAACGGAAGGAACAG	This study	prDN1341_sgRNA_GTPBP2
GCGCCTGCGCGGAGGAGAAG	This study	prDN1412_sgRNA_NEMF
GGCCAGCGGGAACTGTGTAG	This study	prDN1426_sgRNA_PELO
GATCTCGGCGGGAGACGGGA	This study	prDN1428_sgRNA_GTPBP1_2
GCGGAACGGCTGGTTACCTG	This study	prDN1455_sgRNA_GIGYF2
GGCCATGGCCGAGAGCGACT	This study	prDN1459_sgRNA_EDF1
GCGGCGCGCAAGGAAAGATC	This study	prDN1564_sgRNA_EXOSC9

Table 4.5. Quantitative RT-PCR primers used in this study.
f = forward, r = reverse

Quantitative RT-PCR f	Quantitative RT-PCR r	Source	Identifier
TGCTGTCTCCATGTTTGATGTATCT	TCTCTGCTCCCCACCTCTAAGT	Vandesompele et al. 2002	N/A prDN335_B2M-qPCR-f prDN336_B2M-qPCR-r
CGGCATCGGAATGTTCGAG	GCTGTTGACGGCGAAATACAA	PrimerBank https://pga.mgh.harvard.edu/primerbank	#223633994c1 prDN1188_HBS1L_qPCR_f prDN1189_HBS1L_qPCR_r
AAAGTTTCCGCAGCACCATTC	ACAAGCAGCGAACTAAAGGGA	PrimerBank https://pga.mgh.harvard.edu/primerbank	#231573213c1 prDN1209_LTN1_qPCR_r prDN1210_LTN1_qPCR_f
GGGCCTTGAGGTCGATCTC	ACTACAGCGACTATGCCTACC	PrimerBank https://pga.mgh.harvard.edu/primerbank	#31342353c3 prDN1213_ZNF598_qPCR_r prDN1214_ZNF598_qPCR_f
TCGCCATGTTCTTTTTCTGTCAT	AAGTGGGGCTGCATTTCTCTT	PrimerBank https://pga.mgh.harvard.edu/primerbank	#24307917a1 prDN1215_ASCC3_qPCR_r prDN1216_ASCC3_qPCR_f
GGAAACGAGAGCCGGATTTATT	ACTATGTCCATTATGGCAGCTTC	PrimerBank https://pga.mgh.harvard.edu/primerbank	#284005480c3 prDN1248_qPCR-PERK_f prDN1249_qPCR-PERK_r
CCAAACCCACTTCGTTCAAGA	TCTCAATGAGCTAAACTCGTCAC	PrimerBank https://pga.mgh.harvard.edu/primerbank	#197245436c2 prDN1264_HRI_qPCR_f prDN1265_HRI_qPCR_r
ACGCTTTGGGGCTAATTCTTG	CCCGTAGGTCTGTGAAAAACTT	PrimerBank https://pga.mgh.harvard.edu/primerbank	#351542239c3 prDN1268_PKR_qPCR_f prDN1269_PKR_qPCR_r
AAATGCCCACCTACCTATCCA	CCTCCCCACAGTGTTTCTTGG	PrimerBank https://pga.mgh.harvard.edu/primerbank	#65287716c1 prDN1270_GCN2-qPCR_f prDN1271_GCN2-qPCR_r
CCGCAAGGTACAGACAGAGTC	CAGGCTTGAGAGTCGAAGTCG	PrimerBank https://pga.mgh.harvard.edu/primerbank	#31880782c1 prDN1347_qPCR_Pelo_f prDN1348_qPCR_Pelo_r
ATGGGCTGAGTGAAGCTGAC	CGGACCAGGTAATCACGCA	PrimerBank https://pga.mgh.harvard.edu/primerbank	#82546878c2 prDN1353_qPCR_gtpbp1_f prDN1354_qPCR_gtpbp1_r
GTGAGGCCGTCTACCAGATTG	GTGCAGGGTCTTGAGCGAA	PrimerBank https://pga.mgh.harvard.edu/primerbank	#45593139c1 prDN1355_qPCR_gtpbp2_f prDN1356_qPCR_gtpbp2_r
ATGAAGAGCCGCTTTAGCACC	GGCAAAACTAGACGGCATCATA	PrimerBank https://pga.mgh.harvard.edu/primerbank	#116642876c1 prDN1414_qPCR_NEMF_f prDN1415_qPCR_NEMF_r
CTCTGTCCAGTGGTGGGAGTA	CTGCCGTAACGATAATCTGCTAA	PrimerBank https://pga.mgh.harvard.edu/primerbank	#156766042c1 prDN1469_qPCR_GIGYF2_f prDN1470_qPCR_GIGYF2_r
ATCTTAGCGGCACAGAGACGA	GGCCGTGTTCTTGGTAATAGAAT	PrimerBank https://pga.mgh.harvard.edu/primerbank	#24497600c1 prDN1473_qPCR_EDF1_f prDN1474_qPCR_EDF1_r

CCAGAATCGTGC AAAAGAAGC	TACCCCATGAAT GTTACGCCT	PrimerBank https://pga.mgh.harv ard.edu/primerbank	#339275991c3 prDN1493_qPCR_N4BP2_f prDN1494_qPCR_N4BP2_r
TGGAACAGATTA CGGATGCTGC	GTTGCCCGATTG AGTTTTGGA	PrimerBank https://pga.mgh.harv ard.edu/primerbank	#77812669c2 prDN1553_qPCR_exosc9_f prDN1554_qPCR_exosc9_r
TGGTGAATGTCA GATCCATTGC	TAGAACGGATAC GCCTTCTGG	PrimerBank https://pga.mgh.harv ard.edu/primerbank	#77404353c1 prDN1323_qPCR_EIF2S1_f prDN1324_qPCR_EIF2S1_r
CAGACTACGTGC ACCTCTGC	CTGGGTCCAAGT TGTCCAGAAT	Yoon et al., 2019	N/A prDN866_XBP1-u_qPCR_f prDN867_XBP1-u_qPCR_r
GCTGAGTCCGCA GCAGGT	CTGGGTCCAAGT TGTCCAGAAT	Yoon et al., 2019	N/A prDN868_XBP1-s_qPCR_f prDN869_XBP1-s_qPCR_r
TGAAAAACAGAG TAGCAGCTCAGA	CCCAAGCGCTGT CTTAACTC	Yoon et al., 2019	N/A prDN864_XBP1-t-qPCR_f prDN865_XBP1-t-qPCR_r

Table 4.6. Oligonucleotides used for NGS library preparation after CRISPRi screens.
Two primer sets A and B were used to diversify NGS reads. PCR primer were ordered with a 3' phosphorothioate modification.

CRISPRi screen oligonucleotides	Source	Identifier
AATGATACGGCGACCACCGAGATCTACACGATCGGAAGA GCACACGTCTGAACTCCAGTCACATCACGGCACAAAAGG AAACTCACCCT	Weissman Lab	prDN846_A_I1
AATGATACGGCGACCACCGAGATCTACACGATCGGAAGA GCACACGTCTGAACTCCAGTCACCGATGTGCACAAAAGG AAACTCACCCT	Weissman Lab	prDN877_A_I2
AATGATACGGCGACCACCGAGATCTACACGATCGGAAGA GCACACGTCTGAACTCCAGTCACTTAGGCGCACAAAAGG AAACTCACCCT	Weissman Lab	prDN845_A_I3
AATGATACGGCGACCACCGAGATCTACACGATCGGAAGA GCACACGTCTGAACTCCAGTCACTGACCAGCACAAAAGG AAACTCACCCT	Weissman Lab	prDN851_A_I4
AATGATACGGCGACCACCGAGATCTACACGATCGGAAGA GCACACGTCTGAACTCCAGTCACACAGTGGCACAAAAGG AAACTCACCCT	Weissman Lab	prDN850_A_I5
AATGATACGGCGACCACCGAGATCTACACGATCGGAAGA GCACACGTCTGAACTCCAGTCACGCCAATGCACAAAAGG AAACTCACCCT	Weissman Lab	prDN842_A_I6
AATGATACGGCGACCACCGAGATCTACACGATCGGAAGA GCACACGTCTGAACTCCAGTCACCAGATCGCACAAAAGG AAACTCACCCT	Weissman Lab	prDN852_A_I7
AATGATACGGCGACCACCGAGATCTACACGATCGGAAGA GCACACGTCTGAACTCCAGTCACGATCAGGCACAAAAGG AAACTCACCCT	Weissman Lab	prDN876_A_I9

AATGATACGGCGACCACCGAGATCTACACGATCGGAAGAGCACACGTCTGAACTCCAGTCACTAGCTTGCACAAAAGGAAACTCACCCT	Weissman Lab	prDN844_A_I10
AATGATACGGCGACCACCGAGATCTACACGATCGGAAGAGCACACGTCTGAACTCCAGTCACGGCTACGCACAAAAGGAAACTCACCCT	Weissman Lab	prDN853_A_I11
AATGATACGGCGACCACCGAGATCTACACGATCGGAAGAGCACACGTCTGAACTCCAGTCACCTTGTAGCACAAAAGGAAACTCACCCT	Weissman Lab	prDN841_A_I12
AATGATACGGCGACCACCGAGATCTACACGATCGGAAGAGCACACGTCTGAACTCCAGTCACAGTCAAGCACAAAAGGAAACTCACCCT	Weissman Lab	prDN848_A_I13
AATGATACGGCGACCACCGAGATCTACACGATCGGAAGAGCACACGTCTGAACTCCAGTCACAGTTCCGCACAAAAGGAAACTCACCCT	Weissman Lab	prDN843_A_I14
AATGATACGGCGACCACCGAGATCTACACGATCGGAAGAGCACACGTCTGAACTCCAGTCACGTAGAGCGACTCGGTGCCACTTTTTC	Weissman Lab	prDN1085_B_I17
AATGATACGGCGACCACCGAGATCTACACGATCGGAAGAGCACACGTCTGAACTCCAGTCACGTCCGCGCACAAAAGGAAACTCACCCT	Weissman Lab	prDN879_A_I18
AATGATACGGCGACCACCGAGATCTACACGATCGGAAGAGCACACGTCTGAACTCCAGTCACGAGTGGGCACAAAAGGAAACTCACCCT	Weissman Lab	prDN847_A_I23
AATGATACGGCGACCACCGAGATCTACACGATCGGAAGAGCACACGTCTGAACTCCAGTCACGGTAGCCGACTCGGTGCCACTTTTTC	Weissman Lab	prDN1086_B_I24
AATGATACGGCGACCACCGAGATCTACACGATCGGAAGAGCACACGTCTGAACTCCAGTCACATGAGCCGACTCGGTGCCACTTTTTC	Weissman Lab	prDN1087_B_I26
AATGATACGGCGACCACCGAGATCTACACGATCGGAAGAGCACACGTCTGAACTCCAGTCACCAAAAGCGACTCGGTGCCACTTTTTC	Weissman Lab	prDN1088_B_I28
AATGATACGGCGACCACCGAGATCTACACGATCGGAAGAGCACACGTCTGAACTCCAGTCACCAACTACGACTCGGTGCCACTTTTTC	Weissman Lab	prDN1089_B_I29
AATGATACGGCGACCACCGAGATCTACACGATCGGAAGAGCACACGTCTGAACTCCAGTCACCACCGGCGACTCGGTGCCACTTTTTC	Weissman Lab	prDN1090_B_I30
CAAGCAGAAGACGGCATACGAGATGCACAAAAGGAAACTCACCCT	Weissman Lab	prDN1084_B_f
CAAGCAGAAGACGGCATACGAGATCGACTCGGTGCCACTTTTTC	Weissman Lab	prDN840_A_f
GTGTGTTTTGAGACTATAAGTATCCCTTGGAGAACCACCTTGTTG	Weissman Lab	prDN849_sgRNA-Illumina-5'
CCACTTTTTCAAGTTGATAACGGACTAGCCTTATTTAAACTTGCTATGCTGT	Weissman Lab	prDN1083_sgRNA-Illumina-3'

Table 4.7. Oligonucleotides used for ribosome footprint library preparation.
PCR primer were ordered with a 3' phosphorothioate modification.
*NI-811 had to be phosphorylated. All primer were pre-adenylated using the NEB Mth RNA ligase.

oligonucleotides	Source	Identifier
5′-/5Phos/NNNNNATCGTAGATCGGAAGAGCACACGTCTGAA/3ddC/	McGlincy and Ingolia, 2017	NI-810 prDN1794_3L_4N_B1
5'-NNNNNAGCTAAGATCGGAAGAGCACACGTCTGAA/3ddC/	McGlincy and Ingolia, 2017	NI-811 prDN017_3L_4N_B3*
5′-/5Phos/NNNNNCGTAAAGATCGGAAGAGCACACGTCTGAA/3ddC/	McGlincy and Ingolia, 2017	NI-812 prDN018_3L_4N_B3
5′-/5Phos/NNNNNCTAGAAGATCGGAAGAGCACACGTCTGAA/3ddC/	McGlincy and Ingolia, 2017	NI-813 prDN1795_3L_4N_B4
5′-/5Phos/NNNNNGATCAAGATCGGAAGAGCACACGTCTGAA/3ddC/	McGlincy and Ingolia, 2017	NI-814 prDN1796_3L_4N_B5
5′-/5Phos/NNNNNGCATAAGATCGGAAGAGCACACGTCTGAA/3ddC/	McGlincy and Ingolia, 2017	NI-815 prDN1797_3L_4N_B6
5′-/5Phos/NNNNNTAGACAGATCGGAAGAGCACACGTCTGAA/3ddC/	McGlincy and Ingolia, 2017	NI-816 prDN1798_3L_4N_B7
5′-/5Phos/NNNNNTCTAGAGATCGGAAGAGCACACGTCTGAA/3ddC/	McGlincy and Ingolia, 2017	NI-817 prDN1799_3L_4N_B8
5′-/5Phos/NNAGATCGGAAGAGCGTCGTGTAGGGAAAGAG/iSp18/GTGACTGGAGTTCAGACGTGTGCTC	McGlincy and Ingolia, 2017	NI-802 prDN021_RT_McI
CAAGCAGAAGACGGCATACGAGATCGTGATGTGACTGGAGTTCAGACGTGTG	McGlincy and Ingolia, 2017	NI-NI-798 prDN022_libPCR_fwd
CAAGCAGAAGACGGCATACGAGATCGTGATGTGACTGGAGTTCAGACGTGTG	McGlincy and Ingolia, 2017	NI-799 prDN023_RP_PCR_RI1
CAAGCAGAAGACGGCATACGAGATACATCGGTGACTGGAGTTCAGACGTGTG	McGlincy and Ingolia, 2017	NI-822 prDN024_RP_PCR_RI2
CAAGCAGAAGACGGCATACGAGATGCCTAAGTGACTGGAGTTCAGACGTGTG	McGlincy and Ingolia, 2017	NI-823 prDN025_ RP_PCR_RI3
CAAGCAGAAGACGGCATACGAGATTGGTCAGTGACTGGAGTTCAGACGTGTG	McGlincy and Ingolia, 2017	NI-824 prDN027_ RP_PCR_RI4
CAAGCAGAAGACGGCATACGAGATCACTGTGTGACTGGAGTTCAGACGTGTG	McGlincy and Ingolia, 2017	NI-825 prDN028_ RP_PCR_RI5
CAAGCAGAAGACGGCATACGAGATATTGGCGTGACTGGAGTTCAGACGTGTG	McGlincy and Ingolia, 2017	NI-826 prDN029_ RP_PCR_RI6
CAAGCAGAAGACGGCATACGAGATTACAAGGTGACTGGAGTTCAGACGTGTG	McGlincy and Ingolia, 2017	N/A prDN199_ RP_PCR_RI12
CAAGCAGAAGACGGCATACGAGATGCGGACGTGACTGGAGTTCAGACGTGTG	McGlincy and Ingolia, 2017	prDN204_ RP_PCR _RI18

4.2. Methods

4.2.1. Molecular Cloning

Digestion and fragment clean-up

Plasmid digestion was performed using NEB enzymes. Digestion was performed using 2-5 units of enzyme per 1 µg plasmid for 2-3 hours at 37°C, 5 units of Antarctic phosphatase were added for backbone dephosphorylation 30 minutes before end of incubation period. PCR products or small digestion products were generally cleaned up using Zymo DNA Clean& Concentrator kit. Plasmid digestions were generally cleaned up by agarose gel size selection, gel excision and gel extraction using Gel Extraction Kit (Analytics Jena).

Ethanol precipitation

RNA/ DNA samples were filled up to at least 200 µl using water. 1/10 times the volume 3 M NaOAc (pH 4.5), 2.5 to 3 times the volume cold 100% ethanol and 10 µl Glycogen were added to the sample. Samples were incubated for at least 30 minutes at -20°C before spinning for 30 minutes at 16,000xg/4°C. Pellets were dissolved in water.

Ligation

Ligation was performed using homemade T4 Ligase from the MPI Biochemistry Core Facility. Ligation of backbone to insert was generally performed in a 1:3 molar ratio for 2 hours at room temperature, followed by transformation of 2 µl ligation mix.

Gibson Assembly

Gibson assembly was performed using homemade Gibson Master Mix from the MPI Biochemistry Core Facility. Assembly of backbone to insert was generally performed in a 1:3 molar ratio for 2 hours at 50°C, followed by transformation of 2 µl Assembly mix.

Bacterial transformation

Top10 competent bacterial cells were thawed on ice. Meanwhile tubes containing plasmid DNA were prepared and pre-cooled on ice. 50 µl of thawed competent cells were added to plasmid DNA and incubated on ice for 10 minutes. Cells were heat shocked for 45 seconds at 42°C and set on ice for recovery for 5 minutes. 200 µl SOB medium was added to the cells and incubated at 37°C for an hour. Cells were plated on LB plates with Carbenicillin or Kanamycin antibiotics and incubated over night at 37°C.

Bacterial electroporation

MegaX electrocompetent bacterial cells were thawed on ice. Meanwhile tubes containing 100 ng plasmid DNA were prepared and pre-cooled on ice. 20 µl of thawed competent cells were added to plasmid DNA and incubated on ice for 20 minutes. Cell/ DNA mix was transferred to precooled 0.1 cm cuvettes, and electroporated at 2.0 kV, 200 ohms, 25 uF for 4.4-4.6 ms. The cuvette was immediately rinsed with warm SOC medium and cells were allowed to recover at 37°C for 2 hours. Cells were plated on LB plates with carbenicillin or kanamycin and incubated over night at 37°C.

4.2.2. Plasmid construction

sgRNA constructs

For the pooled screen the mU6-sgRNA_EF1A-Puro-mKate (pDN064) construct was used. To create this expression construct, the BFP cassette from the original plasmid (Addgene #60955; pDN022) was replaced by mKate2. For the single knockdown validation experiments we used a mU6-sgRNA_EF1A-Puro-GFP construct (pDN115, **Table 4.3**). The mKate2 expression cassette from pDN064 was therefore replaced by a GFP cassette. For sgRNA insertion, the expression vector pDN064/ pDN115 were digested with BstXI/ BlpI and assembled by Gibson assembly with oligos containing 30 bp overhangs to the backbone. The insertion was verified by Sanger sequencing.

sgRNA with mU6 promoter (overhangs for Gibson Assembly with pDN064/ pDN115):
5‘ taagtatcccttggagaaccaccttgttgg – 20 nt – gtttaagagctaagctggaaacagcatag 3’

For the dual sgRNA construct hS7K-sgRNA_hU6-sgRNA_EF1A-Puro-GFP (pDN292) construction we adapted the plasmid constructed in Tzelepis et al.[387], which for our single sgRNA plasmid (pDN115) served as a template. In short, the SapI site in the bacterial backbone and both BbsI sites in the WPRE was mutated by point mutations. The dual sgRNA cassette was amplified from plasmid pDN185 (Addgene #72666) and inserted into the plasmid backbone by Gibson assembly. The final plasmid (pDN292) is expressing sgRNA1 from a hS7K promoter followed by sgRNA2 expressed from a hU6 promoter; the EF1A-Puro-GFP cassette remained as for the single knockdown construct. For sgRNA insertion, the sgRNAs were inserted by Gibson assembly in two steps. First, the expression vector pDN292 was digested with SapI and assembled by Gibson assembly with oligos containing 30 bp overhangs to the backbone (**Table 4.4**). Second, the vector was digested with BbsI and

assembled by Gibson assembly with oligos containing 30 bp overhangs to the backbone. The final plasmids were verified by Sanger sequencing.

sgRNA1 with h7SK promoter (overhangs for Gibson Assembly with pDN292):
5‘ caggtttatatagcttgtgcgccgcttgggtacctc – 20 nt – gtttaagagctatgctggaaacagcatagcaagtt 3‘

sgRNA2 with hU6 promoter (overhangs for Gibson Assembly with pDN292):
5‘ tggctttatatatcttgtggaaaggacgaaacacc – 20 nt – gtttaagagctatgctggaaacagcatagcaagtt 3‘

Stalling constructs: UbC-BFP-T2A-FLAG-X-P2A-mOrange

For the expression of different stalling reporter, we adapted the reporter constructs from Hegde and Weissman lab[202,226,237]. We exchanged the promoter (CMV to UbC) and the fluorescent cassettes to fit our experimental set-up (GFP to BFP, and RFP to mOrange), further we replaced the first P2A sequence to T2A. For this, the UbC-BFP-T2A-FLAG-XBP1stall-P2A-mOrange cassette (XBP1 sequence from[226]) was synthesized by Twist Bioscience and inserted into a plasmid containing sequences for lentiviral packaging (Addgene #60955). The XBP1-SR (pDN364) was further exchanged by a non-stalling sequence (K0, Addgene #105686) and a poly-lysine sequence (K20-SR, Addgene #105688) to generate pDN362 and pDN366. We further generated a UbC-BFP-T2A-FLAG-K0-P2A-mOrange-nonstop-Malat and /-stop-Malat control (pDN368 and pDN371) by inserting the Malat structural sequence from Addgene plasmid #46834 into the “K0” plasmid (pDN362, Table 4.3).

Overexpression constructs: A2UCOE-EF1a-ZNF598^{mut}-2A-BLC

For gene overexpression, an A2UCOE-EF1a-ZNF598^{mut}-2A-BLC (mutation C29S/C32S)[229] cassette was synthesized by Twist Bioscience and inserted into a plasmid containing sequences for lentiviral packaging (Addgene #60955, **Table 4.3**).

Sanger Sequencing

Sanger sequencing was performed by Eurofins using the Tube-to-Seq service. For that, 15 µl of plasmid prep were prepared in a 50 ng/µl concentration, and 2 µl of 10 µM sequencing primer were added.

4.2.3. Cell culture

Storage and maintenance

For long term storage, cells were slowly frozen in 10% DMSO/ knockout serum replacement in isopropanol chambers at -80°C. After one day, cells were transferred to the vapor phase of the liquid nitrogen. Before thawing cells, plates were coated accordingly. Cells were quickly thawed in a 37°C waterbath for 1 minute. Cell suspension was transferred to 9 ml culture medium in a 15-ml falcon. Cells were spun down for 5 minutes at 200xg. The pellet was resuspended in fresh culture medium and transferred to the culture dish. For hiPSC, 10 µM ROCK inhibitor (Y-27632) was added while plating the cells.

HEK293 and HEK293T cells were maintained in somatic medium (DMEM high glucose + 10% FCS) at 37°C/5% CO_2 (**Table 4.1**). Cells were passaged every other day in a ratio of 1:10 to 1:20. For passaging, cells were washed with PBS, trypsinized for 3 minutes at 37°C using 0.25% Trypsin/EDTA and resuspended in fresh somatic medium.

hiPSC were maintained in mTeSR Plus medium on Geltrex coated plates at 37°C/ 5% CO_2 (**Table 4.1**). The medium was changed every other day. For maintenance, cells were passaged every five days in a ratio of 1:20 to 1:30 by cluster passaging. Cells were washed with PBS and incubated with 0.5 mM EDTA/ PBS for 5-7 minutes at room temperature. As soon as edges of cell colonies loosened, the EDTA/PBS was removed and the cells were carefully washed with PBS once. Cells were resuspended by pipetting fresh medium directly onto the cells, so clusters were washed off the plate. The cell suspension was pipetted up and down (not more than five times) until small clusters remained. Appropriate cell amount was transferred to a freshly coated plate containing fresh medium.

For single cell splitting, cells were washed with PBS, trypsinized for 3-5 minutes at 37°C using Accutase and resuspended in fresh mTeSR Plus medium. The appropriate number of cells was transferred to a 15-ml falcon and centrifuged for 5 minutes at 200xg. The cell pellet was resuspended in mTeSR Plus in addition of 10 µM ROCK inhibitor and transferred to a freshly coated plate. The next day, mTeSR Plus medium was changed to without ROCK inhibitor.

Cardiomyocyte derivation

The cardiomyocyte differentiation was adapted from Zhang et al. [354]. Plates for cardiomyocyte derivation were coated with Matrigel on the day before use. On day 0, hiPSC were singularized by single cell splitting, counted with the Countess (Thermo Fisher Scientific) and $5*10^6$ cells were seeded into a 6-well containing 8 ml T0-medium (Knockout DMEM with 1x L-Glutamine, 1x ITS, 10 ng/ml FGF2b, 1 µM CHIR99021, 1 ng/ml BMP4, 5 ng/ml Activin A). After 24 hours, medium was changed to TS medium (Knockout DMEM with 1x L-Glutamine, 1x TS, 250 µM

ascorbic acid). Cells were maintained in TS medium for 9 consecutive days, Wnt-inhibitor C59 (1x) was added on day 2 and 3. The medium was carefully changed daily. On day 9, cells were carefully washed twice with PBS to remove remaining media residues, and incubated in TS-Glc medium (Knockout DMEM without Glucose with 1x L-Glutamine, 2 mM lactic acid, 250 µM ascorbic acid (AA), 1x TS) for another 24 hours for CM enrichment. On day 10, cells were trypsinized for 10-15 minutes in Accutase at 37°C, resuspended in CM-maintenance medium (Knockout DMEM with 1x L-Glutamine, 2% FCS), centrifuged for 5 minutes at 200xg and transferred to a new plate in a 1:4 ratio. Cells were differentiated for a total of 15 days before experimental progression.

NPC derivation and culture

We established NPC and neuron differentiation protocols from Reinhardt et al. 2013[349]. hiPSC were grown to 90% confluency in 12-well plates. On day 0, colonies were cut by scratching a checkered pattern into the dish with a cannula. Cells were washed twice with PBS and pre-warmed Collagenase IV was added. Cells were incubated for 10-15 minutes at 37°C until borders of the colonies started detaching from the plate. Collagenase was removed and N2B27 (Neurobasal medium: DMEM/F12 50:50, 0.5x N2, 0.5x B27, 1x Glutamax) was carefully added to the plate. Cell cluster were carefully scaped of the plate using a cell scraper and transferred to a 15-ml tubes containing N2B27 medium. Cluster were pelleted by gravity and access medium was removed. Fresh N2B27 was added and cells were spun for 1 minute at 200xg. Cluster were resuspended in NPC-induction medium (NPC-IM; N2B27 with 200 µM ascorbic acid, 3 µM CHIR99021, 0.5 µM PMA, 150 nM Dorsomorphin, 10 µM SB) with 5 µM ROCK inhibitor. For embryoid body (EB) formation, cluster were transferred to a sterile p60 sterile dish (no tissue culture coating) and incubated at 37°C/ 5% CO_2 for six days. Medium was carefully changed every other day without ROCK inhibitor. On day 6, EBs were transferred to a 15-ml falcon and harshly pipetted up and down to dissociate EBs into single cells. Single cells were plated into a 6-well coated with Geltrex in NPC expansion medium (NPC-EM; N2B27 with 200 µM ascorbic acid, 3 µM CHIR99021, 0.5 µM PMA). Medium was changed every other day. The first rounds of passaging were performed in a sequential digest, where other non-NPCs were removed. For this, cells were washed with PBS and incubated for short time frames with Accutase. By checking under the microscope, we could observe detachment of non-NPCs before NPCs loosened up. By removing the first rounds of Accutase, those cells were removed before splitting the NPCs. Standard passaging was performed according to the hiPSC single cell passaging every 5 days.

Neuron derivation

Plates for neuron derivation were coated with Geltrex. On day 0, NPCs were singularized with Accutase, counted by the Countess and $1*10^6$ cells were seeded into a 6-well containing 2ml Patterning medium (PM; N2B27 with 200 µM ascorbic acid, 1 µM retinoic acid, 0.5 µM PMA and 10 ng/ml GDNF/ BDNF). The cells were maintained in PM for six days and the medium was changed every other day. On day 6, medium was changed to maturation medium (MM; N2B27 with 200 µM ascorbic acid, 100 µM dbcAMP, 5 ng/ml GDNF/ BDNF, 1 ng/ml TGF-b3) with 5 ng/µl Activin A. Activin A was removed from derived neurons after two days, and cells were maintained in plates for another ten days, the medium was changed every two to three days. During this period, 0.1 µM CompE was added for two days. On day 16, cells were trypsinized for 10-15 minutes in Accutase at 37°C, resuspended in MM, centrifuged for 5 minutes at 200xg and transferred to a new plate. Cells were maintained until day 21 before experimental progression.

Immunostaining of hiPSC/ NPC

Cells were seeded and grown on Ibidi glass bottom dishes. For staining, they were washed with PBS and fixed in 3.7% formaldehyde for 10 minutes at room temperature. Formaldehyde was exchanged stepwise with PBST (0.02% Tween-20), followed by three complete washes. Cells were permeabilized for 10 minutes in 0.5% Triton-X100 in PBST and blocked for one hour in blocking solution (3% BSA/ 0.1% Triton-X100 in PBS). Cells were incubated overnight with the primary antibody (**Table 4.2**) diluted in blocking solution at 4°C. Cells were washed three times in PBST, and incubated with the secondary antibody diluted in blocking solution for one hour at room temperature. Cells were washed again three times in PBST, DAPI was added during the second was step.

Immunostaining of neurons

Cells were seeded and grown on Ibidi glass bottom dishes. Cells were imaged on day 21 of neuron derivation. For staining, they were washed with PBS and fixed in 3.7% formaldehyde for 10 minutes at room temperature. Formaldehyde was exchanged stepwise with PBST (0.02% Tween), followed by three complete washes. Cells were permeabilized for 10 minutes in 0.7% Tween in PBS and blocked for one hour in neuron blocking solution (1% BSA/ 0.1% Triton-X100/ 10% FCS in PBS). Cells were washed once in 0.1% BSA/ PBS and incubated overnight with the primary antibody (**Table 4.2**) diluted in 1% BSA/ PBS at 4°C. Cells were washed three times in 0.1% BSA/ PBS, and incubated with the secondary antibody diluted in 1% BSA/ PBS for one hour at room temperature. Cells were washed again three times in 0.1% BSA/ PBST (0.05% Tween), DAPI was added during the second was step.

Mammalian cell nucleofection

Different electroporation programs were tested using the P3 Kit from Lonza. For hiPSC, CB-150 had highest efficiency, DN-100 for mESC. Cells were singularized using Accutase and counted. For nucleofection, $1.2*10^6$ cells were resuspended in 100 µl nucleofection reagent and nucleofected with 5 µg of plasmid DNA. Cells were immediately washed out of cuvettes with fresh medium and transferred to freshly coated 6-well plates. ROCK inhibitor (10 µM) was added during the procedure for hiPSC.

Transfection

Cells were transfected using TransIT LT1 (Mirus). 4 µg of plasmid DNA were mixed with 400 µl Optimem and 12 µl TransIT and incubated for 15 minutes at room temperature. Meanwhile, $2*10^6$ cells were prepared and seeded to a 6-well plate. Transfection reagent was added dropwise to the cells. ROCK inhibitor (10 µM) was added during the procedure for hiPSC. The medium was changed after 24 hours and the experiments were continued after additional 24 hours.

CRISPRi cassette engineering

2.5 µg of the CRISPRi construct pDN006 (#73497) were co-transfected with 1 µg of each TALENs homology arm targeting the AAVS1 locus (pDN032/033) into hiPSC (cDN003) by electroporation (**Table 4.3**). After three days, cells were reseeded in medium containing 10 µM ROCK inhibitor and 100 µg/ml G418 and selected until stable colonies appeared (~10 days). Single colonies were picked with a 20-µl pipette into 96-wells under the open laminar flow hood. After plate duplication, one was kept in culture, whereas the second plate was used for lysis. For lysis, cells were washed with PBS and lysed in the plate for 3 hours at 45°C using 50 µl lysis buffer (50 mM Tris pH 8.0, 10 mM CaCl2, 0.2 µg/ml Proteinase K, 0.05% SDS). Proteinase K was inactivated for 20 minutes at 80°C. Crude cell lysates were directly used for a screening PCR using the primer prDN210/ 211/ 212. After verification by gel electrophoresis, positive candidates were expanded, frozen away and verified by other assays.

Karyotyping

Cells were harvested at 60-80% confluency from a 6-well plate. 2 hours prior start, medium was changed to push cells into mitosis. Cells were incubated in medium containing 10 µg/ml colcemide for additional 90 minutes, detached, singularized, and resuspended in somatic medium (medium containing FCS). Cells were centrifuged for 5 minutes at 800xg, the pellet was loosened by flicking the tube several times. 1.5 ml of 75 mM KCl was carefully added to

the tube and incubated for 30 minutes at 37°C. 100 µl Carnoy's solution (three parts methanol and one part acetic acid) were added and incubated for 10 minutes at room temperature. As soon as fixative is added, the cells can clump together. It's important that the tube is immediately inverted after adding the fixative or that the tube is vortexed at a low speed while adding the fixative. After incubation, cells were centrifuged for 5 minutes at 800xg. The pellet was loosened by flicking the tube several times, and 2 ml Carnoy's solution was added. The suspension was incubated overnight at 4°C, and sent for analysis to the Institute of Medical Genetics and Applied Genomics in Tübingen.

Virus production

Per transfection, one p100 dish was coated with collagen solution for 10 minutes. HEK293-LentiX cells were trypsinized and counted and $6*10^6$ cells were seeded into the coated p100 with 10 ml HEK medium. Cells were incubated until the next day. For transduction, packaging plasmids were mixed in a ratio of 4:1:1 (Gag/Pol:Rev:VSV-G). Per p100 transfection, 5 µg of packaging plasmids were mixed with 5 µg of the transfer plasmid, 1 ml Optimem and 30 µl TransIt Lenti (Mirus). The mixture was incubated for 10 minutes at room temperature. Meanwhile the fresh medium was added to the cells and then transfected with the plasmid mix by dropwise pipetting it on the plate. After two days, the medium was collected and spun down for 10 minutes at 200xg to pellet cells. The supernatant was filtered through a 0.45 µm filter and 1 volume cold lentivirus precipitation solution was added to 4 volumes of supernatant. The suspension was vortexed and incubated over night at 4°C. The next day, the virus was precipitated by centrifugation for 30 minutes at 1500xg/4°C. The pellet was resuspended in 1 ml cold PBS and immediately aliquoted and frozen at -80°C.

Viral transduction

Lentiviral transduction was performed in a reverse transduction. For this, the virus was added to the plates first. For the transduction of a p100, 400 µl of concentrated lentivirus was thawed at room temperature. In the meantime, fresh medium was added to plates and cells were trypsinized and counted. The virus was added to the plates, followed by the addition of $3*10^6$ cells. Medium was exchanged on the next day.

4.2.4. RNA workflows

LiDS/Let RNA extraction

Cell medium was changed two hours prior to harvesting. For standard RNA extraction, cells were directly lysed in the plate using LiDS/LET buffer (5% LiDS in 20 mM Tris pH=7.4, 100 mM LiCl, 2 mM EDTA, 5 mM DTT pH7.4, 100 ng/ml Proteinase K) and stored at -80°C. RNA extracts in 400 µl LiDS/LET buffer were boiled at 60°C for 10 minutes. The lysates were triturated 10 times with a 26G syringe and vortexed for 20 seconds. Two times the volume acid phenol (pH 4.3), 1/10 BCP and 10 µl Glycogen were added and mixed vigorously. Samples were centrifuged for five minutes at 10,000xg/4°C. The aqueous phase was transferred to a new tube and the phenol step was repeated. The RNA was precipitated by the addition of three volumes of 100% ethanol and pellets were resuspended in water.

DNase treatment

10 µg of total RNA were digested for 30 minutes at 37°C/1500rpm using Turbo DNase (Thermo Fisher Scientific). To extract RNA, one volume of acid phenol (pH 4.3), 1/10 volume of BCP, 1/10 volume 3M NaO 1/10 NaOAc (pH4.5) and 10µl Glycogen were added and mixed vigorously. Samples were centrifuged for five minutes at 10,000xg/4°C. The aqueous phase was transferred to a new tube and washed once with one time the volume of BCP by mixing and centrifuging for five minutes at 10,000xg/4°C. The RNA was precipitated by the addition of three volumes of 100% ethanol and pellets were resuspended in water.

Quantitative RT-PCR

For the reverse transcription, 1 µg of DNase treated RNA was transcribed to cDNA using the Protoscript II First Strand cDNA Synthesis Kit (NEB). The 20-µl reaction volume was adjusted to 50 µl by the addition of water and stored at -20°C. Quantitative RT-PCR was performed with the KAPA SYBR Fast qPCR Mix (Roche). qPCR primer efficiency was tested with a serial dilution and only primer pairs with an efficiency between 1.9-2.1 were used for experiments (**Table 4.5**). For analysis, $\Delta\Delta$Ct values were calculated relative to control samples.

4.2.5. Ribosome profiling

Lysis

Ribosome footprint libraries were prepared essentially as described[410] with minor modifications. Cell medium was changed two hours prior to harvesting. Cells were quickly washed with ice cold PBS and snap frozen in liquid nitrogen. Snap frozen plates were thawed on ice and cells were scraped off the plate into polysome lysis buffer (20 mM Tris pH 7.4, 150 mM NaCl, 5 mM MgCl2, 1% Triton-X100, 1 mM DTT, 100 µg/ml CHX, 25 U/ml Turbo DNase, 0.1% NP-40). Samples were vortexed vigorously, triturated through a 26G gauge needle, and spun down for 7 minutes at 16,000xg/ 4°C. Supernatant was transferred to a new tube and RNA concentration was measured with the Qubit RNA HS Kit. Aliquots of 20 µg RNA in 200 µl polysome lysis buffer were snap-frozen and stored at -80°C.

RNase I digestion and sucrose cushion

20 µg RNA in 200 µl polysome lysis buffer were digested with 50 U RNase I (Ambion) for 45 minutes at 2000 rpm/22°C. Reaction was stopped by adding 100 U Superase In and extracts were loaded directly on a sucrose cushion. For this, 0.9 ml 1M sucrose in polysome lysis buffer was carefully inserted below the 200 µl digested extract, followed by centrifugation for 75 minutes at 120,000 rpm/4°C in a S120AT2 rotor. The pellet was dissolved in LiDS/LET lysis buffer and RNA was extracted by the standard LiDS/LET protocol.

Footprint size selection

RNA extracted after pelleting through a sucrose cushion were separated through a 15% PAA/ Urea gel to size-select ribosome footprints. 5 µg of total RNA were mixed with loading dye, boiled for three minutes at 90°C and loaded on the gel. 19-/32-nt oligos served as marker. Bands in the range of 19 to 32 nucleotides were excised from the gel, crushed with a pestle and eluted in gel elution buffer (GEB: 0.3 M NaOAc pH 4.5, 0.25% SDS, 1 mM EDTA pH 8). To enhance elution, gel slices were boiled for 10 minutes at 65°C, frozen on dry ice for 10 minutes, thawed at 65°C, and eluted on a rotating wheel overnight at room temperature. The next day, gel debris were removed by centrifuging samples through a Spin-X filter. RNA was pelleted by ethanol precipitation. Half of the size-selected product was used for 3' linker ligation.

3' Linker ligation

Size-selected RNA was dephosphorylated for 45 minutes at 37°C using T4 PNK. An oligo combination of the 19-/32-nucleotide marker was taken along as a control. The

dephosphorylated RNA was mixed with pre-adenylated linker (B1-B8, **Table 4.7**), 1x T4 RNA ligase buffer, 25% PEG-8000, Superase In and 1 µl T4 RNA Ligase 2 (trKQ). The mix was incubated for 3 hours at 25°C, and run on a 12% PAA/Urea gel. The ligation product (~50-60 nt) was excised and gel purified as in the step before. The concentration of the purified linker-ligated product was measured with the Nanodrop.

rRNA depletion

50 ng of the linker-ligated sample was used for rRNA depletion using the Ribo-Seq riboPOOL h/m/r depletion kit (siTOOLs) following the manufacturer's instructions. The RNA was mixed with 1 µl of the depletion oligos and 1 µl Superase In in 1x depletion buffer. The mix was incubated at 68°C for 10 minutes and annealed by turning off the thermoblock and slowly cooling down the samples to 37°C. The samples were mixed with 80 µl Streptavidin beads and incubated at 37°C for 15 minutes, followed by two minutes at 50°C. rRNA bound to the oligos were removed on a magnetic rack. The unbound nucleic acids were cleaned up and concentrated using the Zymo RNA Clean and Concentrator Kit.

RT and cDNA circularization

The rRNA-depleted footprints were annealed with the RT primer (prDN021, **Table 4.7**) at 65°C for 5 minutes and reverse transcribed for 30 minutes at 50°C in a RT master mix containing 1x Protoscript II Buffer, 0.5 mM dNTPs, 10 mM DTT, 20 U Superase In and 200 U Protoscript II. After reverse transcription, NaOH was added to 0.1 M and the RNA was hydrolysed by boiling the sample for 5 minutes at 90°C. Samples were run on a 10% PAA/ Urea gel. The RT product (~100-110 nt) was excised, gel slices were crushed with a pestle, and DNA was eluted for 60 minutes at 1500rpm/70°C in TE buffer. Gel remains were removed by centrifuging samples through a Spin-X filter and DNA was precipitated with ethanol. For cDNA circularization, a 20-µl reaction was prepared containing the gel-purified RT product mixed with 3µM CircLigase (TS2126 Rnl1, Homemade from MPI Biochemistry Core Facility) in circularization buffer (50 µM ATP, 2.5 mM MnCl2, 50 mM MOPS, pH 7.5, 10 mM KCl, 5 mM MgCl2, 1 mM DTT and 1mM Betaine) and incubated for three hours at 60°C, followed by heat inactivation for 10 minutes at 80°C.

Library PCR and Sequencing

4 µl of circularized cDNA was amplified using a common forward primer, a specific index reverse primer (**Table 4.7**), and the KAPA HiFi Polymerase with the High Fidelity buffer:

95°C/3min - [98°C/20sec - 62°C/20sec - 72°C/15sec] x12

The PCR product was run on an 8% PAA gel and bands in the range of ~165 nucleotides were excised. Gel slices were crushed with a pestle and DNA was eluted overnight in DNA elution buffer (300 nM NaCl, 10 mM Tris-Cl pH7.5, 0.2% Triton-X 100). The next day, gel debris were removed by centrifuging samples through a Spin-X filter. DNA was recovered by ethanol precipitation. The final library was quantified with the Qubit dsDNA High Sensitivity kit. Libraries were pooled and sequenced on a NextSeq 550 at 1.8 pM at the MPI Biochemistry Core Facility.

Sequencing data analysis

For analysis, samples were demultiplexed and trimmed using cutadapt v3.5. First, reads were demultiplexed by matching the barcode sequence to read 3' ends without allowance for indels in the match (*--no-indels*). Only reads containing adapter and that were >= 10bp after trimming were kept (*--trimmed-only -m 10*). Reads were also quality trimmed at both ends with a threshold quality score of 30 (*-q 30,30*). Following this, the two 5' random nucleotides introduced during circularization, and five random 3' nucleotides were removed (*-u 2 -u -5*). rRNA contaminants were quantified and removed using bowtie v1.2.2 with ---best to ensure that the best alignment is reported. Reads unmapped to the rRNA reference were aligned to the human genome (GRCh38/hg38) using STAR v2.6.1c allowing two mismatches (*--outFilterMismatchNmax2*), forced end-to-end alignment (--alignEndsType EndToEnd) and a maximum of one alignment per read (uniquely mapping reads only; *--outFilterMultimapNmax1*).

The ribosome occupancy was analyzed around the start and stop codon to identify specific changes in translation initiation and translation termination. All the analyses including statistics and plotting were performed in Python (3.8.2), using NumPy, Scipy, and Matplotlib. We considered 80 nucleotide positions upstream and 60 nucleotide positions downstream to the annotated start codons [411]. Similarly, we considered 60 nucleotide positions upstream and 80 nucleotide positions downstream to the annotated stop codons. We calculated the normalized ribosome occupancy at each position within the window[412]. Specifically, the coverage of A-site footprints was normalized by the average ribosome occupancy of all positions in that transcript:

$$D_{ij} = \frac{F_{ij}}{(\sum_{j=1}^{Li} F_{ij})/L_i}$$

where F_{ij} and are the ribosome footprints and density of position *j* of gene *i*, respectively. L_i is the length of genes. Then, the average ribosome densities at each position *j* within the window was calculated by averaging over all the well-expressed transcripts with a coverage > 0.1:

$$A_j = \frac{\sum_{i=1}^{N} D_{ij}}{N}$$

where A_j is the average of ribosome densities of position j within the window and *N* is the number of transcripts. Finally, we compared the averaged ribosome occupancy around the start and the stop codons between control (wild type, WT or non-targeting, NT) vs. knockdown or ZNF598^{mut} overexpression conditions.

To identify pause sites in each sample, the codon coverage per mRNA was transformed into z-scores. Pause sites were then identified as those positions in the transcript with a z-score higher than a certain threshold; we selected >5.0 to identify strong pause sites[413]. To further increase the confidence that the identified peaks are not a result of experimental or sequencing artefacts, the peak had to occur in both two replicates to be considered a pause site. If the pause site occurred at the same or adjacent codon (5 nucleotides upstream or downstream of the peak to account for possible minor differences in P-site footprint assignment) in datasets from WT and ZNF598^{mut}, then it was considered to be conserved. To identify positions at which ribosome pausing was increased upon ZNF598^{mut} expression, we followed the procedure by Stein et al[414]. We included genes that had an average sequencing coverage of ≥0.1 reads per codon in all the replicates (2 WT replicate + 2 ZNF598^{mut} replicates). Next, we used two-tailed Fisher's exact tests to identify positions at which there were statistically significant changes in ribosome pausing between the WT and ZNF598^{mut}. In brief, reads at each position and for each transcript were averaged between replicates and rounded to the nearest integer. At each position of a transcript, 2 × 2 contingency tables were generated to perform a two-tailed Fisher's exact test to compare the ratio of reads in samples from WT and ZNF598^{mut} expressing cells at a given position to the ratio at all other positions in that transcript (i.e. the summed reads in each fraction for the entire transcript minus the position of interest). Together, this compares the observed ratio of ribosome reads from WT and ZNF598^{mut} samples at a given position to the expected ratio based on the total number of reads that map to the transcript.

RNA-sequencing

Samples for RNA sequencing were extracted from LiDS/LET harvested samples that were treated the same ways as for ribosome profiling. RNA was extracted by phenol extraction using the standard LiDS/LET extraction protocol. Extracted RNA was subjected to an RNA integrity check on a tageStation (MPI Biochemistry Core Facility) and target knockdown was validated by quantitative RT-PCR. 250 ng of RNA extract were used for library preparation with the Universal Plus RNA-seq with NuQuant kit (Tecan). Optionally, 2.5 ng SequinA or SequinB spike-in was mixed to the total RNA samples before library preparation. Libraries were pooled and loaded at a 2 pM on a NextSeq 550 at the MPI Biochemistry Core Facility. For analysis, reads were aligned to the human genome (GRCh38/hg38) using STAR v2.6.1c allowing one mismatch *(--outFilterMismatchNmax1*) and a maximum of one alignment per read (uniquely mapping reads only; *--outFilterMultimapNmax1*). BAM outputs were also generated with coordinates relative to the gene feature in the transcriptome *(--quantMode TranscriptomeSAM*). Data were further analyzed and visualized using DESeq2 and ClusterProfiler in R with an adjusted p-value of 0.05.

4.2.6. Protein workflows

RIPA protein lysis

Cell medium was changed two hours prior to harvesting. For standard protein extraction, cells were directly lysed in the plate using RIPA buffer (20 mM Tris pH 7.5, 150 mM NaCl, 1% NP-40, 0.5% sodium deoxycholate, 0.1% SDS, 10 µg/ml aprotinin, 20 µM leupeptin, 2.5 µM pepstatin A, 0.5 mM AEBSF, 1x phosphatase inhibitor) and scraped off the plate. The lysate was incubated on ice for 20 minutes and mixed by vortexing in between. The lysate was spun down for 10 minutes at 10,000xg/4°C and the supernatant was transferred to a new tube. EDTA was added to a final concentration of 5 mM and protein concentration was quantified using a BCA assay. Sample concentration was adjusted to 1 µg/µl by the addition of Laemmli buffer. Samples were shortly boiled at 90°C, and stored at -20°C.

Polysome profiling for protein extraction

Cell medium was changed two hours prior to harvesting. Cells were quickly washed with ice cold PBS and snap frozen in liquid nitrogen. Snap frozen plates (p100) were thawed on ice and cells were scraped off the plate into polysome lysis buffer (50 mM HEPES pH 7.4, 150 mM KCl, 15 mM MgCl2, 1% Triton-X100, 1 mM DTT, 1x protease and phosphatase inhibitor). Samples were vortexed vigorously, triturated through a 26G gauge needle and spun down for 7 minutes at 16,000xg/ 4°C. Supernatant was transferred to a new tube, snap frozen in liquid

nitrogen and stored at -80°C. Samples were loaded on a 10-50% sucrose gradient in gradient buffer (50 mM HEPES pH 7.5, 150 mM KCL, 15 mM MgCl2, 1 mM DTT) and centrifuged for 3 hours at 40,000rpm in a SW41 rotor. 10 fractions of 1.1 ml were collected on the Piston Fractionator (Biocomp), snap-frozen and stored at -80°C.

Protein extraction from sucrose fractions

Polysome fractions were thawed, sodium deoxycholate was added to 0.02%, samples were vortexed and incubated for 30 minutes on ice. Next, 20% TCA was added 1:1, the samples were vortexed and again incubated for 30 minutes on ice. Proteins were pelleted for 30 minutes at 13,000xg/4°C, washed once with 100% ice-cold acetone, and again centrifuged for 30 minutes at 13,000xg/4°C. Pellets were resuspended in 4x Laemmli, boiled and loaded on an SDS-PAGE gel. From a p100 starting material, 1/3 of the resuspended sample was loaded.

Western Blotting

15 µg protein sample were loaded on 4-12% Bis-Tris gels and run in 1x MOPS or MES running buffer. Proteins were transferred to 0.2 µm nitrocellulose membranes in the NEB Trans-Blot Turbo device using 1x semi-dry blotting buffer (10% ethanol, 48 mM Tris base, 39 mM glycine, 0.075% SDS) for 45 min at 25 V. The membrane was stained with Ponceau (5% acetic acid, 0.1% Ponceau S) for 5 minutes, washed with water and imaged for total protein assessment. After de-staining with PBS-T (0.05% Tween), membranes were blocked for an hour in 5% milk in PBST and incubated overnight with the primary antibody in 5% milk/ PBST at 4°C (**Table 4.2**). The next day, the membranes were washed three times with PBST, incubated with the secondary antibody diluted in 5%milk/ PBST for an hour at room temperature and washed again three times. Blots were incubated for 5 minutes in Supersignal West Pico Plus ECL substrate and imaged on the iBright. When necessary, membranes were stripped using Restore Western Blot stripping buffer (Thermo Fisher Scientific) for 30 minutes at room temperature, blocked for another hour, and re-probed with another antibody were applied as described above.

4.2.7. Pooled CRISPRi screening

Library design

The 262 gene candidates were selected based on gene ontology searches and current literature. For sgRNA selection, the CRISPRia Design pipeline and supplemented files[345] were used. Additionally, we included publicly available H1 cell DNase and FAIRE-seq data (ENCSR794OFW, ENCSR000DCD) as well as SNP data from the kucg-2 hiPSC line (https://www.hipsci.org/lines/#/lines/HPSI0214i-kucg_2). Using the standard settings, sequences within -25 and 500bp of the transcriptional start site are scanned for PAM motifs (NGG), and sgRNA activity scores are predicted by inclusion of chromatin accessibility data and off-target scoring. Each sgRNA was standardized to 19 base pairs and a 5' G was added to enhance U6 promoter dependent transcription. The final list included 9 sgRNAs per gene and 10% non-targeting controls, resulting in a pool of 3000 sgRNAs. 5' and 3' overhangs were added to each sgRNA sequence for library construction and oligo pools were synthesized by Twist Bioscience.

5' overhang:
TGTGTGTTTTGAGACTATAAGTATCCCTTGGAGAACCACCTTGTTG
3'overhang:
GTTTAAGAGCTAAGCTGGAAACAGCATAGCAAGTTTAAATAAGGCTAGTCCG

Library cloning

The sgRNA pool was amplified using KAPA HiFi Hotstart polymerase with the High-Fidelity buffer:

95°C/3min - [98°C/20sec - 56°C/15sec - 72°C/15sec] x12 – 72°C/1min

and cleaned up using the Zymo DNA Clean & Concentrator Kit. pDN064, which served as a backbone, was digested with BstXI/BlpI. Both components were assembled by Gibson assembly in a 3:1 ratio (insert:backbone) by standard protocol. The assembled plasmids were precipitated with ethanol, and transformed into MegaX competent cells. Colonies were scraped of the plate and the plasmid DNA was extracted by Plasmid Plus Midi Kit (Qiagen). The resulting plasmid pool was checked for a normal sgRNA distribution by NGS sequencing and packed into lentiviruses using the standard protocol.

Pooled growth screens

Growth screens were performed on dividing cell (hiPSC, HEK293 cells and NPC). 10^7 hiPSC and HEK293 cells were transduced in replicates with the sgRNA pool in the absence of doxycycline with an initial transduction rate of 30%, reseeded after two days in puromycin with 2 and 1 µg/ml and selected for two passages. After 3 days recovery without puromycin, $3*10^6$ cells, which equals a 1000x coverage, were seeded either without or with 2 µM doxycycline. hiPSC were passaged after five days, whereas HEK293 cells were passaged every three days. Cells were harvested after ten days, which corresponds to approximately ten cell divisions. $8*10^6$ NPCs were transduced in the presence of doxycycline with an initial transduction rate of 50%, reseeded in 2.5 µg puromycin the next day, and selected for two days. $3*10^6$ cells were seeded either without or with 2 µM doxycycline. Cells were passaged every five days and harvested after 15 and 25 days, which corresponds to approximately ten and seventeen cell divisions.

Pooled survival screens

Survival screens were performed on post-mitotic cells, i.e. CM and neurons, and knockdown was induced with $3*10^6$ cells, which corresponds to a 1000 coverage. Virus transductions ewre performed in two biologigal replicates for CM and three biological replicates for neurons. For CM, hiPSC were transduced and selected with puromycin as for the growth screens, and CM derivation was initialized after hiPSC selection. CM were split at the reseeding step to two wells either without or with 2 µM doxycycline and cultured for additional 25 days before harvesting. For neurons, NPC were transduced and selected with puromycin as for growth screens, and neuron derivation was initialized after NPC selection. Neurons were split at the reseeding step to two wells either without or with 2 µM doxycycline and cultured for additional 20 days before harvesting.

Pooled differentiation screens

Differentiation screens were performed during the derivation of CM or NPC from hiPSC and neurons from NPC.

Library preparation and sequencing

$5*10^6$ cells were harvested per screen and gDNA was extracted using the Nucleospin Blood Kit (Macherey&Nagel). Per screening condition, 20 µg of DNA was amplified using NEBNext Ultra II Q5 Mix. Two different primer sets were used to maximize read variety during next

generation sequencing (**Table 4.6**). Each PCR mix contained 5 µg DNA and was amplified with the standard program:

98°C/2min - [98°C/10sec - 60°C/30sec - 65°C/45sec] x22 - 65°C/5min

PCR mixes for the same samples were pooled and concentrated using the Zymo DNA Clean and Concentrator Kit. The product was run on an 8% PAA gel. The PCR product was excised, the gel slices were crushed with a pestle and eluted in water overnight at room temperature on a rotating wheel. The next day, gel debris were removed by Spin-X filter and the DNA was recovered by ethanol precipitation. The final library concentration was measured with the Qubit dsDNA HS kit. Libraries were pooled and loaded at 2 pM on a NextSeq 550 at the MPI Biochemistry Core Facility with custom primer (**Table 4.6**).

Analysis

Sequencing reads were aligned to the expected library sequences and read counts were analyzed using ScreenProcessing[345]. sgRNAs that had less than 50 reads were excluded from the analysis. Growth phenotypes were calculated by normalizing sgRNA $\log_2$ enrichment of the average top three sgRNAs from T0 to endpoint samples. Mann-Whitney P-value was calculated using the average phenotype from all nine sgRNAs per target.

4.2.8. Single sgRNA validation experiments

Single and double knockdown growth assays

Single KD experiments were performed using the pDN115 construct, mU6-sgRNA_EF1A-Puro-GFP (**Table 4.3**). The plasmid was digested using BstXI/BlpI. Primer pairs containing the 20 nt sgRNA sequence were annealed and both were assembled by Gibson Assembly in a 3:1 ratio (insert:backbone) by a standard protocol. sgRNA insertion was verified by Sanger sequencing. Cells were transduced with an initial transduction efficiency of 40-60%. After two days, cells were either used for a growth assay or selected with puromycin for protein and RNA extraction. For the growth assay, cells were seeded with and without doxycycline in replicates. Cells were passaged every four days, where percentage of GFP-positive cells was measured by flow cytometry. hiPSC and HEK293 cells were passaged for up to 20 days, NPC for up to 28 days.

Sampling for Western blotting and quantitative RT-PCR

Cells were selected in puromycin after transduction. For RNA extraction cells were cultured for zero, one and five days and harvested in LiDS/LET buffer. For protein extraction, cells were cultured for zero and five cell doublings and harvested in RIPA buffer.

Cell cycle analysis by propidium iodide staining

Puromycin-selected cells were cultured with or without doxycycline for the indicated period of time. Fresh medium was added two hours prior to harvesting. Cells were collected by trypsinization, washed once in PBS, and fixed by slowly adding 70% ethanol. Cells were stored at -20°C until use. For PI staining, ethanol was removed, and cells were washed once with 0.1% Triton-X100/ PBS. Cells were stained in 0.1% Triton-X100/ PBS with 20 µg/ml PI and 50 µg/ml RNase A for at least one hour at 4°C. Cells were then directly analyzed on the Attune flow cytometer. Samples were compared to an induced non-targeting control, which was harvested at the same time point as the tested KD samples.

Global protein synthesis assay by HPG incorporation

Puromycin selected cells were cultured with 2 µM doxycycline for the indicated period of time. Fresh medium was added two hours prior harvesting. Cells were washed twice with PBS and starved for methionine for 30 minutes at 37°C in somatic medium without methionine. As a control, we included a sample in which translation is inhibited by CHX. For this, after 30 minutes starvation, we added 100 µg/ml CHX and incubated cells for another 15 minutes at 37°C. Finally, 0.2 mM HPG was added to the culture for 30 minutes and incubated at 37°C. Cells were harvested by trypsinization, washed once in PBS and fixed for 10 minutes in 3.7% formaldehyde. Cells were washed once in TBS, permeabilized in 0.5% TBST for 15 minutes and washed again in TBS. Click reaction was performed for 30 minutes in 100 mM Tris pH 8.5, 1 mM $CuSO_4$, 20 µM picolyl azide A647, 100 mM ascorbic acid. Cells were washed three times in 0.2% TBST and analyzed on the Attune flow cytometer. We subtracted the background signal from the +CHX control from the A647 signal and compared knockdown HPG incorporation to an induced non-targeting control, treated and harvested the same as the tested samples.

LDH assay

Puromycin selected cells were cultured with 2 µM doxycycline for the indicated period of time. The supernatant was collected to assess cytotoxicity using the CytoTox 96 Non-Radioactive Cytotoxicity Assay kit (Promega). Cytotoxicity levels were quantified relative to an induced non-targeting control.

Stalling experiments

hiPSC and HEK293 cells that already contained the mU6-sgRNA_EF1A-Puro-GFP (pDN115, **Table 4.3**) construct were used. Before transduction with the stalling constructs (pDN362, 364, 366, 368 and 371), gene knockdown was induced for 3 days with 2 µM doxycycline. For samples with a very early phenotype, i.e. LTN1 and GTPBP1, the knockdown was induced during transduction with the stalling constructs. Cells were transduced and allowed to recover for 2 days before analysis. Cells were harvested and analyzed on the Attune flow cytometer. Fluorescent signals were compensated by cells expressing each fluorophore by itself expressed under the same promoter (UbC). The median fluorescent intensity of samples expressing a stalling construct were normalized to the corresponding non-stalling control construct with the same knockdown condition.

Overexpression experiments

hiPSC and HEK293 cells that already contained the mU6-ZNF598_EF1A-Puro-GFP construct were used. Before transduction with the ZNF598^{mut} construct (pDN415, **Table 4.3**), gene knockdown was induced for 2 cell doublings by doxycycline treatment for HEK293 cells. Cells were transduced and allowed to recover 2 cell doublings before analysis. Cells were harvested for Western Blot, quantitative RT-PCR and ribosome profiling analysis.

Chapter 5 – Supplemental Data

5.1. Abbreviations

40S	small ribosomal subunit
60S	large ribosomal subunit
80S	assembled ribosome
A site	aminoacyl site
ATP	adenosine tri-phosphate
BMP	bone morphogenic protein
Cas9	CRISPR associated system 9
CAT tails	c-terminal alanine threonine tails
CDS	coding sequence
CM	cardiomyocytes
CRISPR	clustered regularly interspaced short palindromic repeats
CRISPRi	CRISPR interference
crRNA	CRISPR RNA
dCas9	dead Cas9
DNA	desoxyribonucleic acid
DOX	doxycycline
DSB	double-strand break
E site	exit site
E1	ubiquitin-conjugating enzyme 1
E2	ubiquitin-conjugating enzyme 2
E3	ubiquitin-conjugating enzyme 3
eIF	eukaryotic translation initiation factor
eEF	eukaryotic translation elongation factor
eRF	eukaryotic translation release factor
ER	endoplasmic reticulum
FGF	fibroblast growth factors
GCN2	control nonderepressible 2 kinase
GDP	guanosine di-phosphate
GFP	green fluorescent protein
GTP	guanosine tri-phosphate
hiPSC	human induced pluripotent stem cells
HipSci	Human Induced Pluripotent Stem Cells Initiative
HRI	heme-regulated inhibitor
tRNA-iMet-CAT	initiator Methionine
ISR	integrated stress response
JNK	c-Jun N-terminal kinase
KD	knockdown
KRAB	krüppel-associated box
M7G cap	5’ 7-methylguanosine cap
MAPK	mitogen-activated kinase
MAP2K	mitogen-activated kinase kinase
MAP3K	mitogen-activated kinase kinase kinase
mRNA	messenger ribonucleic acid

NGD	no-go decay
NGS	next generation sequencing
NMD	nonsense-mediated decay
NPC	neuronal progenitor cell
NSD	non-stop decay
NT	non-targeting
ORF	open reading frame
P	phosphorylation
P site	peptidyl site
PAM	protospacer adjacent motif
PERK	PKR-like endoplasmatic reticulum kinase
PIC	pre-initiation complex
RNA	ribonucleic acid
RNAi	RNA interference
RP	ribosomal protein
RPL	ribosomal protein of the large subunit
RPS	ribosomal protein of the small subunit
RQC	ribosome-associated quality control
rRNA	ribosomal ribonucleic acid
RSR	ribotoxic stress response
RT-PCR	reverse transcription – polymerase chain reaction
sgRNA	short guide RNA
SR	stralling reporter
TGFb	transforming growth factors
TM	tunicamycin
tracrRNA	transactivating CRISPR RNA
tRNA	transfer ribonucleic acid
TSS	transcriptional start site
uORF	upstream open reading frame
UPR	unfolded protein response
UPS	ubiquitin-proteasome system
UTR	untranslated region
XBP1-u/s	XBP1-unspliced/spliced
$ZNF598^{mut}$	ZNF598 C29S/C32S RING mutant

5.2. Supplementary Figures

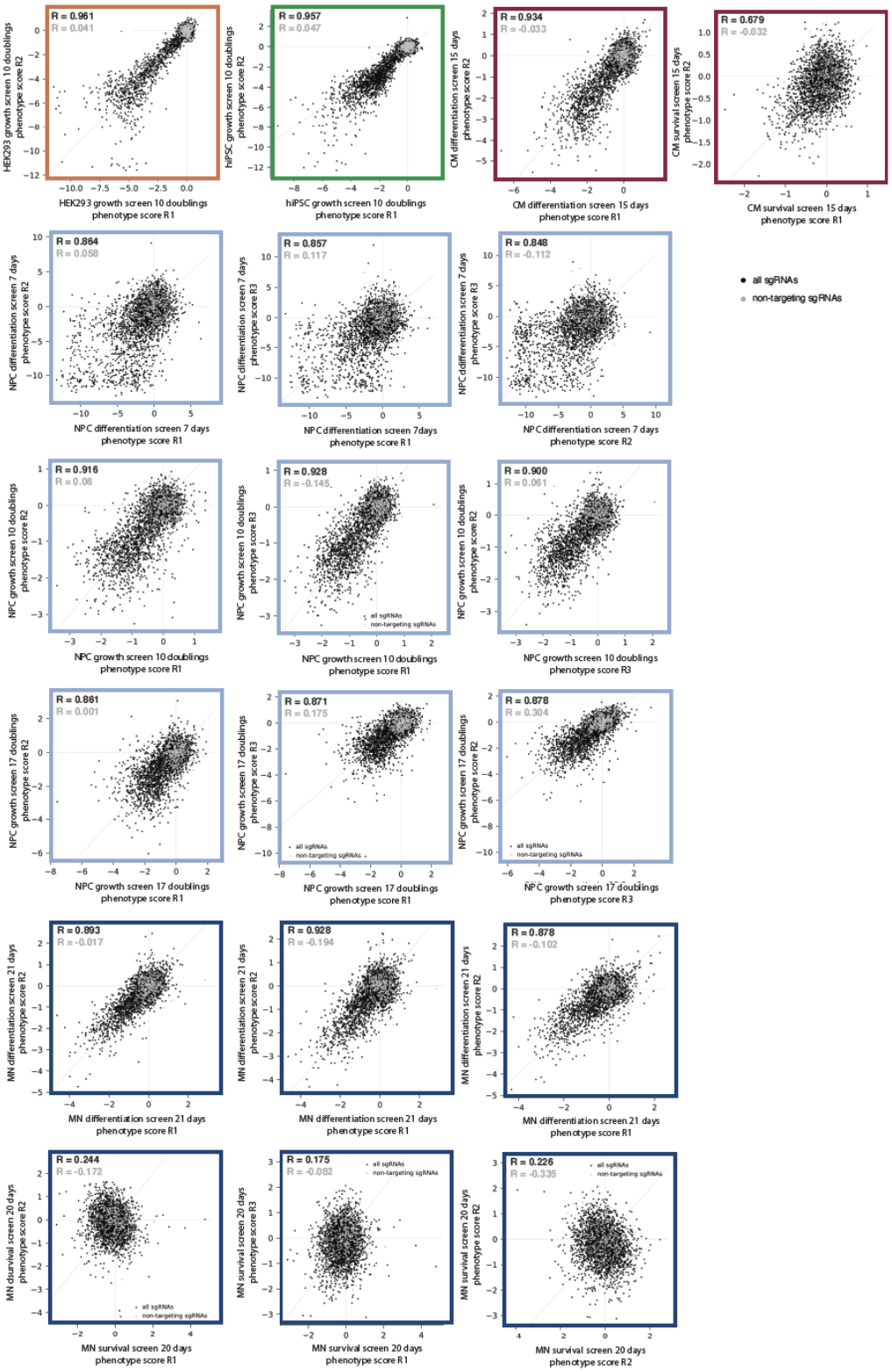

Figure S 5.1. CRISPRi screen phenotypes scatter plot.
Correlation plots of two independent biological replicates for growth, differentiation and survival screens (black: targeting sgRNAs; gray: non-targeting sgRNAs). R = Pearson correlation. CRISPRi phenotype scores for every sgRNA were plotted against biological replicates within the same cell line. Data were analyzed using the Screen Processing pipeline.

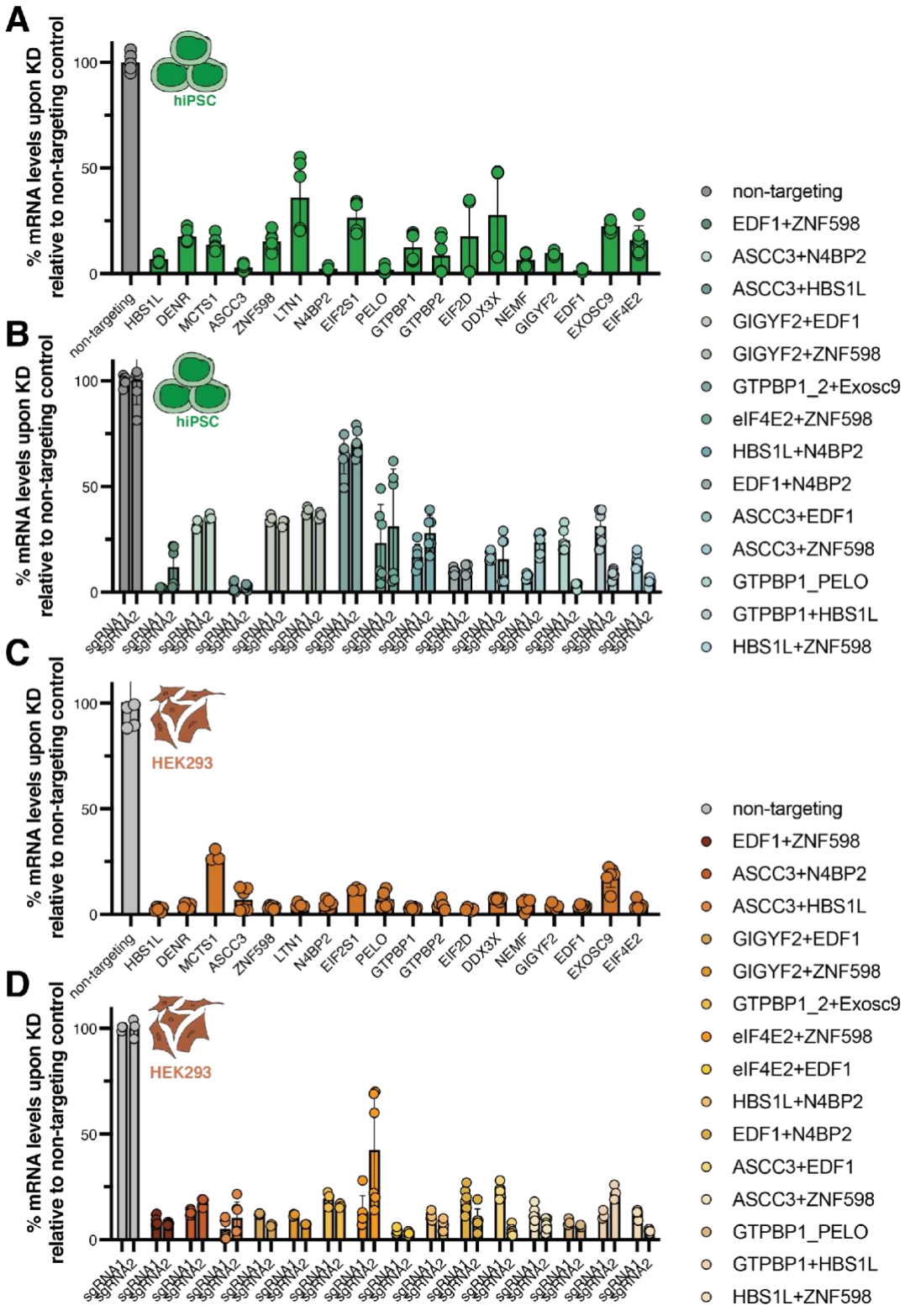

Figure S 5.2 mRNA levels are downregulated upon target knockdown.
To measure remaining mRNA levels, gene knockdown was induced for three cell doublings before RNA extraction. B2M was used as a reference gene for relative mRNA quantification. mRNA levels were normalized to the levels in corresponding non-targeting control (n=2) with three technical replicates.

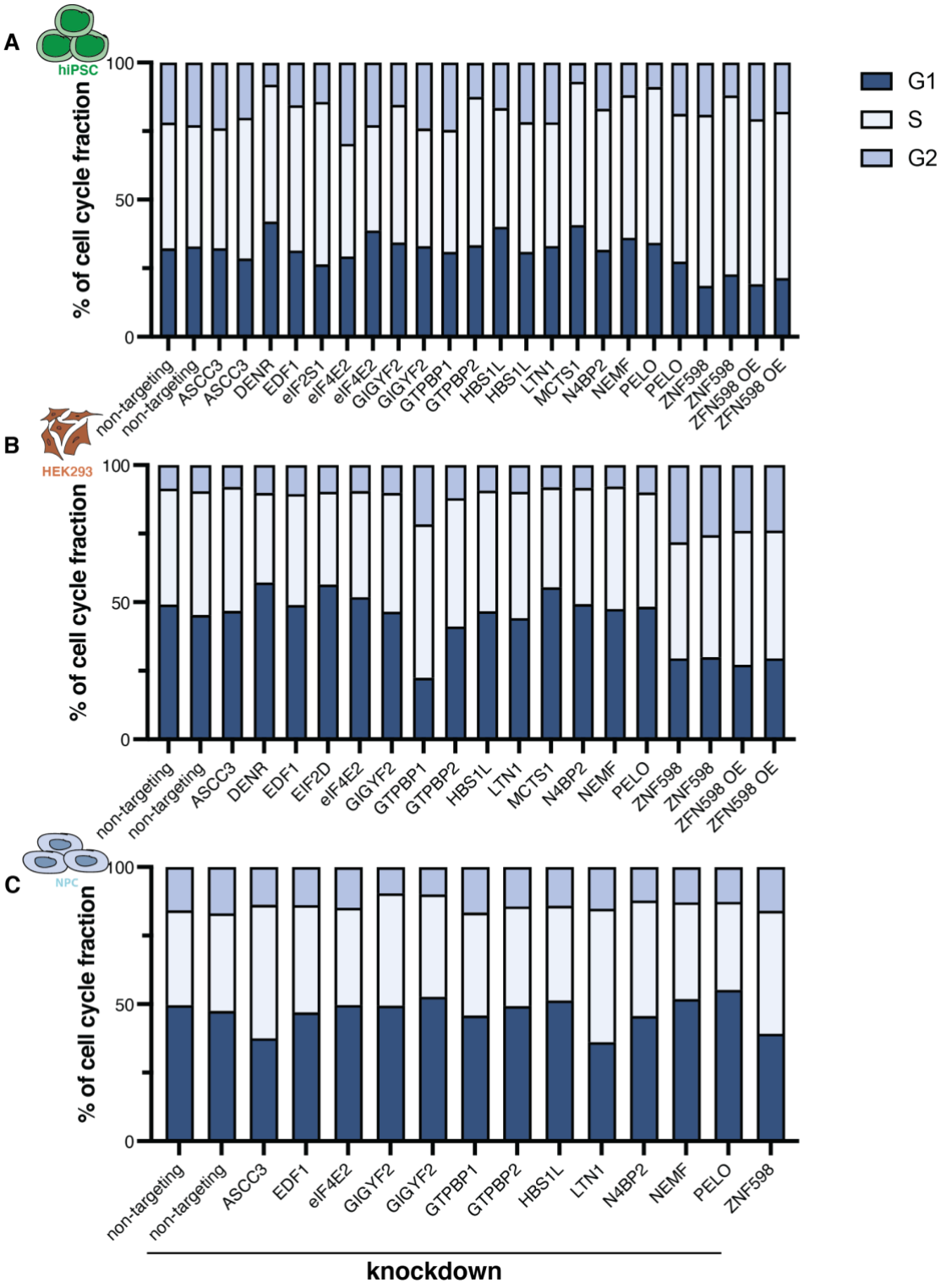

Figure S 5.3. Cell cycle progression is exclusively affected by ZNF598 KD and ZNF598mut OE in hiPSC and HEK293.
Gene knockdown (KD) was induced for two (GTPBP1, LTN1), and five cell doublings (others) in biological replicates. Cells were harvested at 75% viability after knockdown, stained with propidium iodide and analyzed by flow cytometry. Proportions of cells per cell cycle phase (G1, S and G2) were determined with the Watson Pragmatic Algorithm. Fraction of cells in G1, S and G2 phase upon knockdown of ribosome collision factors with different screening phenotype strengths in (A) HEK293 cells, (B) hiPSC and (C) NPC. At least 10,000 cells were analyzed per biological replicate. Experiments were performed in two biological replicates. Color of gene label indicates pooled screening phenotypes.

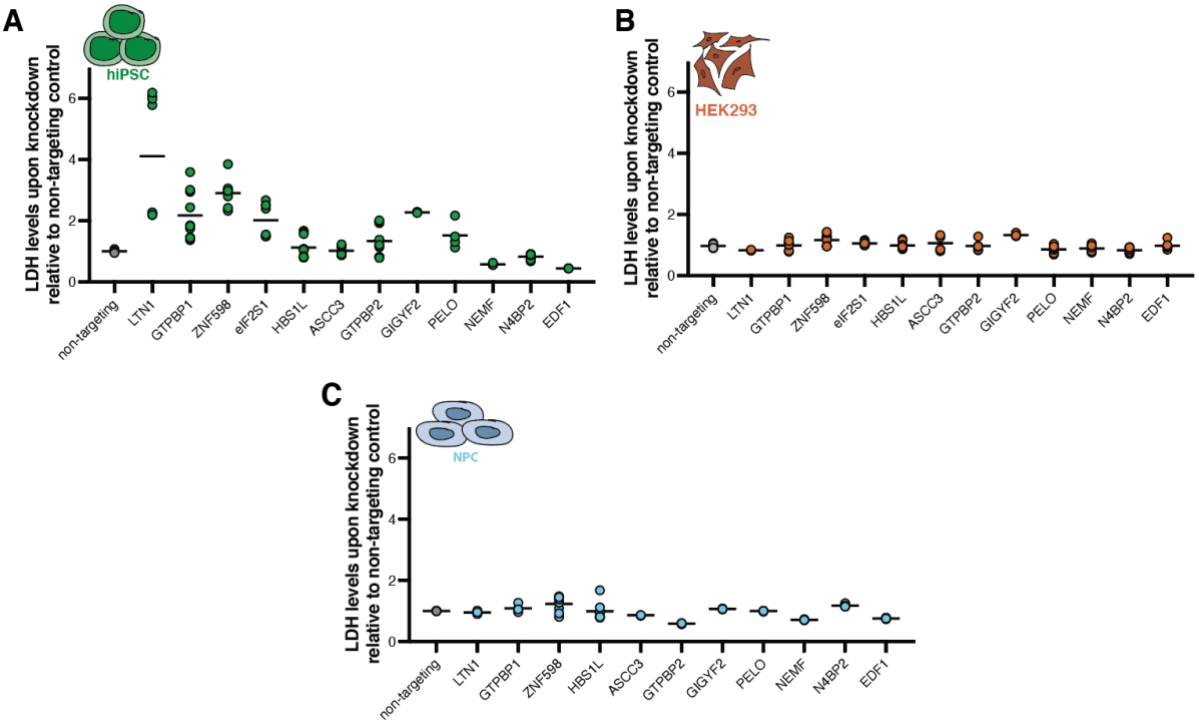

Figure S 5.4. Cytotoxicity levels increase upon RQC factor knockdown in hiPSC.
Gene knockdown (KD) was induced for two (GTPBP1, LTN1), and five cell doublings (others) in biological replicates before measuring cytotoxicity with LDH. LDH levels in the medium of four technical replicates were measured by a colorimetric quantification using a CytoTox Assay Kit (Promega) and normalized to a non-targeting sgRNA control cell population (A) HEK293 (B) hiPSC, (C) NPC.

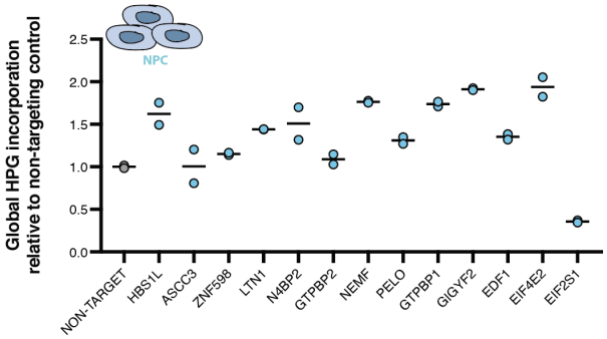

Figure S 5.5. Global translation generally increases upon target knockdown in NPCs.
Gene knockdown (KD) was induced for two (GTPBP1, LTN1), and five cell doublings (others) in biological replicates before HPG incorporation into the nascent chain. HPG was incorporated for 30 minutes in the nascent chain and a picolyl-azide was added by click chemistry after fixation. At least 10,000 cells were analyzed by flow cytometry and HPG incorporation changes were normalized to a non-targeting control.

Figure on the next page:

Figure S 5.6. Fluorescent intensity of stalling constructs expression is knockdown and cell context-dependent.
Reporter constructs used in this thesis: no stalling control (K0), poly-lysine stretch (K20), XBP1 stalling, stop codon-containing control and non-stop construct. Fluorescent intensity of BFP and mOrange was measured in 30,000 cells by flow cytometry and the resulting ratio was plotted using Flowjo. Gray histograms = non-targeting control, orange lines = HEK293 cells, green lines = hiPSC, blue lines = NPC. Experiments were performed in biological replicates, solid and dotted line.

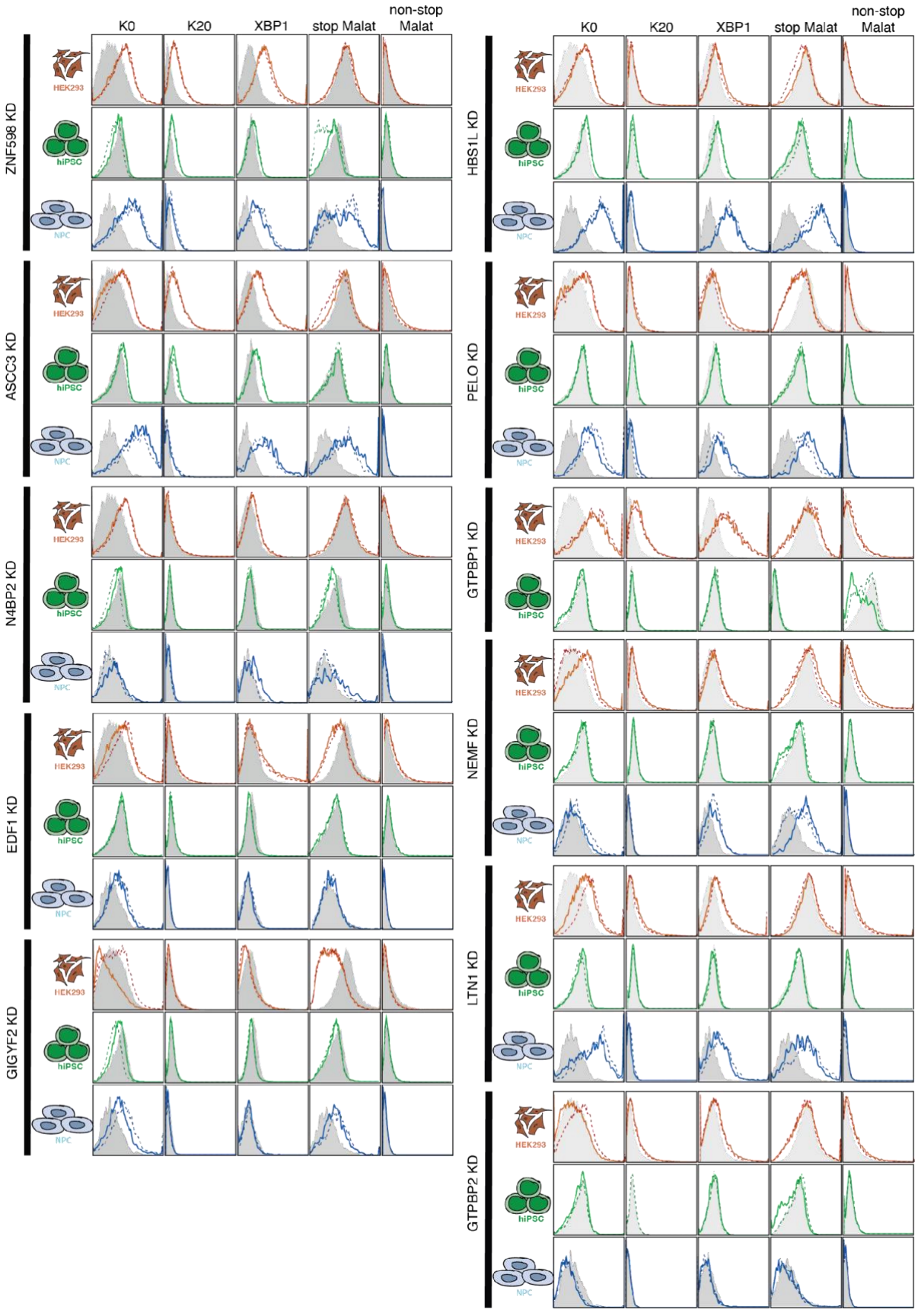
K0
K20
XBP1
stop Malat
non-stop Malat
ZNF598 KD
HBS1L KD
ASCC3 KD
PELO KD
N4BP2 KD
GTPBP1 KD
EDF1 KD
NEMF KD
GIGYF2 KD
LTN1 KD
GTPBP2 KD
HEK293
hiPSC
NPC

5.3. Supplementary Tables

Table S 5.1. Individual phenotype scores per sgRNA in mitotic cell contexts.
Evaluation of individual sgRNA phenotypes of the nine sgRNAs that were investigated in this work and as an average (Av) of the two screen replicates (R1 and R2).

sgRNA-ID	HEK293_R1	HEK293_R2	HEK293_Av	hiPSC_R1	hiPSC_R2	hiPSC_av	NPC_R1	NPC_R2	NPC_R3	NPC_av
GTPBP1_-_39102123.23-P1P2	-0.17	0.23	0.03	0.10	0.02	0.06	0.04	0.12	-0.03	0.04
GTPBP1_-_39102165.23-P1P2	-3.10	-4.04	-3.57	-3.46	-2.47	-2.97	-1.32	-0.72	-1.08	-1.04
GTPBP1_+_39101982.23-P1P2	0.00	-0.24	-0.12	0.12	-0.24	-0.06	-0.23	0.16	0.14	0.03
GTPBP1_+_39101996.23-P1P2	-0.48	-0.18	-0.33	-0.01	-0.33	-0.17	-0.12	-0.76	-0.03	-0.30
GTPBP1_+_39102002.23-P1P2	-0.29	-0.13	-0.21	-0.47	0.38	-0.05	0.16	-0.91	-0.02	-0.26
GTPBP1_+_39102006.23-P1P2	0.15	0.23	0.19	0.06	0.07	0.07	0.08	-0.18	-0.06	-0.05
GTPBP1_+_39102026.23-P1P2	0.25	0.09	0.17	0.24	-0.17	0.03	-0.01	0.06	0.14	0.06
GTPBP1_+_39102063.23-P1P2	0.03	-0.22	-0.09	-0.32	-0.08	-0.20	-0.08	0.03	0.17	0.04
GTPBP1_+_39102388.23-P1P2	-2.67	-4.17	-3.42	-2.18	-2.32	-2.25	-0.53	-0.72	-0.10	-0.45
GTPBP2_-_43597002.23-P1P2	0.32	-0.14	0.09	0.10	-0.11	0.00	-0.26	0.23	0.01	-0.01
GTPBP2_+_43596689.23-P1P2	0.34	-0.10	0.12	-0.60	0.14	-0.23	0.43	0.23	0.40	0.35
GTPBP2_+_43596694.23-P1P2	0.33	-0.05	0.14	0.51	-0.02	0.24	0.02	0.10	-0.04	0.03
GTPBP2_+_43596750.23-P1P2	-0.20	-0.21	-0.21	-0.70	-0.19	-0.44	-0.32	-0.04	-0.09	-0.15
GTPBP2_+_43596820.23-P1P2	-0.03	-0.10	-0.07	0.27	0.30	0.28	0.04	0.22	0.34	0.20
GTPBP2_+_43596867.23-P1P2	0.34	-0.61	-0.13	0.56	0.41	0.48	0.11	-0.52	-0.02	-0.14
GTPBP2_+_43596957.23-P1P2	0.08	-0.26	-0.09	0.05	0.42	0.23	0.06	0.03	-0.04	0.02
GTPBP2_+_43596960.23-P1P2	-0.09	0.51	0.21	0.08	0.40	0.24	0.39	-0.01	-0.28	0.03
GTPBP2_+_43596975.23-P1P2	0.06	0.16	0.11	0.28	0.08	0.18	0.27	0.16	-0.02	0.13
HBS1L_-_135375685.23-P1P2	-0.15	-0.02	-0.08	-2.47	-2.90	-2.69	-0.73	0.30	-0.41	-0.28
HBS1L_-_135375767.23-P1P2	-0.09	-0.29	-0.19	0.24	0.09	0.16	0.49	0.04	0.49	0.34
HBS1L_-_135375767.23-P1P2_ref	-0.25	-0.04	-0.15	-1.07	-2.54	-1.81	-0.10	-1.13	-0.47	-0.57
HBS1L_-_135375915.23-P1P2	0.05	-0.21	-0.08	-1.69	-3.16	-2.43	-0.64	-0.74	-0.13	-0.50
HBS1L_-_135375938.23-P1P2	-0.07	0.41	0.17	-1.67	-0.96	-1.31	-0.04	0.26	-0.62	-0.13
HBS1L_-_135375949.23-P1P2	-0.21	0.48	0.14	-0.24	0.00	-0.12	-0.04	0.13	0.15	0.08
HBS1L_+_135375722.23-P1P2	-0.32	-0.07	-0.19	-1.85	-3.30	-2.58	-0.71	-0.34	-0.50	-0.51
HBS1L_+_135375911.23-P1P2	0.26	-0.19	0.04	-2.06	-2.69	-2.37	-1.34	-1.27	-1.29	-1.30
HBS1L_+_135375920.23-P1P2	-0.25	0.09	-0.08	-2.25	-4.52	-3.39	-0.74	-0.77	-0.99	-0.83
HBS1L_+_135375943.23-P1P2	-0.21	0.15	-0.03	-1.69	-1.43	-1.56	-0.43	-0.81	-0.60	-0.61
PELO_-_52083773.23-P2	-0.05	0.10	0.03	-0.08	-0.43	-0.25	0.15	0.15	-0.37	-0.02
PELO_-_52083812.23-P2	0.24	-0.20	0.02	-0.11	-0.30	-0.20	-0.24	-0.11	-0.18	-0.18
PELO_-_52083849.23-P2	-0.15	-0.41	-0.28	0.38	0.25	0.31	0.01	-0.15	0.31	0.06

PELO_-_52083980.23-P2	-0.22	0.34	0.06	0.12	0.41	0.26	0.38	0.07	-0.33	0.04
PELO_-_52084090.23-P2	-2.07	-0.98	-1.53	-2.20	-2.73	-2.47	-0.72	-0.34	-0.19	-0.42
PELO_-_52095976.23-P1	-0.51	-1.11	-0.81	-2.14	-1.98	-2.06	-0.80	-0.36	0.00	-0.38
PELO_-_52096039.23-P1	-1.08	-0.95	-1.01	-1.52	-1.69	-1.61	-0.39	-0.25	-0.03	-0.23
PELO_-_52096308.23-P1	-0.18	0.19	0.01	0.23	0.14	0.18	-0.13	0.19	-0.13	-0.02
PELO_+_52083762.23-P2	-0.01	-0.02	-0.01	0.21	0.31	0.26	0.59	0.42	0.06	0.36
PELO_+_52083798.23-P2	0.14	0.09	0.12	-0.25	-0.21	-0.23	-0.14	0.25	-0.10	0.00
PELO_+_52083820.23-P2	0.60	-0.12	0.24	-0.13	-0.13	-0.13	0.21	-0.15	-0.23	-0.06
PELO_+_52083843.23-P2	0.01	0.11	0.06	0.07	-0.25	-0.09	-0.06	-0.07	0.13	0.00
PELO_+_52095940.23-P1	-1.05	-0.73	-0.89	-1.77	-1.61	-1.69	-0.46	-0.71	-0.79	-0.65
PELO_+_52095956.23-P1	-0.52	-1.29	-0.90	-1.01	-1.35	-1.18	-0.93	-0.66	-1.03	-0.87
PELO_+_52095998.23-P1	-1.01	-1.26	-1.14	-1.18	-1.49	-1.33	-0.38	-0.36	-0.62	-0.45
PELO_+_52096004.23-P1	-0.48	-0.63	-0.55	-1.04	-0.36	-0.70	-0.11	-0.65	-0.27	-0.34
PELO_+_52096186.23-P1	-0.60	-0.33	-0.47	-1.15	-1.09	-1.12	-0.08	-0.25	0.27	-0.02
PELO_+_52096194.23-P1	-0.67	-0.68	-0.68	-1.45	-0.96	-1.20	-0.37	0.27	-0.27	-0.12
ASCC3_-_101329132.23-P1P2	-1.19	-0.85	-1.02	-2.63	-3.85	-3.24	-2.18	-2.24	-2.05	-2.16
ASCC3_-_101329188.23-P1P2	-2.23	-2.53	-2.38	-2.55	-5.63	-4.09	-2.01	-0.55	-2.01	-1.52
ASCC3_-_101329188.23-P1P2_ref	-0.86	-0.75	-0.80	-1.89	-3.24	-2.56	-1.72	-1.25	-2.10	-1.69
ASCC3_-_101329193.23-P1P2	-2.34	-1.73	-2.04	-2.92	-4.14	-3.53	-2.07	-1.71	-2.20	-1.99
ASCC3_-_101329193.23-P1P2_ref	-1.41	-0.91	-1.16	-3.37	-3.52	-3.45	-2.50	-2.55	-2.12	-2.39
ASCC3_-_101329197.23-P1P2	-1.83	-1.02	-1.43	-2.95	-4.72	-3.83	-1.88	-1.91	-2.71	-2.17
ASCC3_+_101328981.23-P1P2	-0.58	-0.65	-0.61	-2.83	-4.91	-3.87	-2.01	-2.18	-2.65	-2.28
ASCC3_+_101329019.23-P1P2	-0.67	-0.35	-0.51	-2.28	-4.95	-3.62	-2.02	-1.85	-2.64	-2.17
ASCC3_+_101329184.23-P1P2	-0.27	-0.02	-0.14	-1.99	-2.12	-2.06	-0.31	-0.38	-0.22	-0.30
ASCC3_+_101329219.23-P1P2	-0.15	-0.30	-0.22	-2.39	-3.30	-2.84	-2.13	-1.90	-1.63	-1.89
ASCC3_+_101329230.23-P1P2	-2.17	-1.96	-2.06	-2.37	-3.74	-3.05	-1.90	-1.63	-1.98	-1.84
ZNF598_-_2059607.23-P1P2	-0.38	0.08	-0.15	-0.25	-0.88	-0.57	0.18	0.05	-0.68	-0.15
ZNF598_-_2059754.23-P1P2	-0.17	-0.63	-0.40	-0.26	-0.06	-0.16	0.08	-0.26	0.21	0.01
ZNF598_-_2059761.23-P1P2	-0.26	-0.18	-0.22	-0.88	-0.89	-0.89	-0.33	-0.11	-0.48	-0.31
ZNF598_-_2059773.23-P1P2	-0.18	-0.04	-0.11	0.14	0.32	0.23	-0.23	-0.32	-0.82	-0.46
ZNF598_-_2059777.23-P1P2	-0.27	0.26	0.00	-0.19	-0.47	-0.33	-0.16	0.05	-0.46	-0.19
ZNF598_+_2059741.23-P1P2	-0.20	-0.21	-0.20	-2.42	-3.19	-2.80	-0.36	-0.26	-0.46	-0.36
ZNF598_+_2059762.23-P1P2	-0.42	-0.08	-0.25	-1.38	-2.47	-1.93	-0.59	0.04	-0.68	-0.41
ZNF598_+_2059765.23-P1P2	-0.28	-0.07	-0.17	-0.30	-0.40	-0.35	-0.11	0.56	0.03	0.16
EIF2S1_-_67827054.23-P1P2	-0.37	0.13	-0.12	-1.24	-1.93	-1.59	-0.52	-0.49	-0.28	-0.43

EIF2S1_-_67827080.23-P1P2	-5.33	-6.78	-6.05	-4.01	-2.97	-3.49	-1.71	-2.40	-1.61	-1.91
EIF2S1_-_67827085.23-P1P2	-10.75	-10.92	-10.84	-5.83	-8.62	-7.23	-2.08	-1.14	-0.88	-1.37
EIF2S1_-_67827098.23-P1P2	-6.87	-5.08	-5.98	-4.18	-5.07	-4.63	-1.78	-1.46	-2.46	-1.90
EIF2S1_-_67827140.23-P1P2	-0.55	0.00	-0.27	-0.07	-0.23	-0.15	0.14	0.27	-0.23	0.06
EIF2S1_+_67827089.23-P1P2	-5.16	-7.38	-6.27	-2.85	-4.81	-3.83	-2.21	-1.90	-1.01	-1.70
EIF2S1_+_67827270.23-P1P2	-1.24	-1.94	-1.59	-2.52	-3.22	-2.87	-0.22	0.14	-0.06	-0.05
EIF2S1_+_67827307.23-P1P2	-1.14	-0.78	-0.96	-2.11	-3.12	-2.62	0.07	-0.63	-0.10	-0.22
EIF2S1_+_67827313.23-P1P2	-1.12	-1.00	-1.06	-2.70	-2.66	-2.68	-0.97	-0.82	-0.67	-0.82

Table S 5.2. Growth assays of gene knockdowns validate screening phenotypes in hiPSC.
Growth phenotypes upon target knockdown were assessed by measuring GFP fluorescence and normalization to the corresponding non-induced sgRNA. Cells were split every four cell divisions (T) and GFP fluorescence was measured using flow cytometry. Experiments were performed in biological replicates.

Gene	Rep	T0	T4	T8	T12	T16	T20
HBS1L	R1	100	101.7	13.9	1.5	2.8	0.0
HBS1L	R2	100	120.0	14.8	2.7	2.9	0.0
HSPA14	R1	100	119.7	56.9	9.6	4.8	0.0
HSPA14	R2	100	93.7	59.6	9.1	2.9	0.0
HSPA2	R1	100	159.7	100.0	96.3	95.7	96.2
HSPA2	R2	100	113.2	94.4	93.5	85.2	90.3
DNAJC2	R1	100	88.9	22.9	6.7	2.8	0.0
DNAJC2	R2	100	100.7	22.2	1.5	1.7	0.0
DENR	R1	100	98.8	18.2	4.2	1.0	0.0
DENR	R2	100	95.2	27.3	2.8	0.9	0.0
MCTS1	R1	100	86.0	79.5	44.6	19.1	7.2
MCTS1	R2	100	88.5	83.3	46.1	20.0	8.5
ASCC3	R1	100	99.6	42.9	0.4	0.0	0.0
ASCC3	R2	100	104.4	61.0	1.6	0.0	0.0
ZNF598	R1	100	84.4	29.6	1.1	0.0	0.0
ZNF598	R2	100	114.5	16.5	2.6	0.0	0.0
LTN1	R1	100	46.3	6.0	1.4	0.0	0.0
LTN1	R2	100	41.8	7.3	1.9	0.0	0.0
N4BP2	R1	100	118.6	95.2	88.1	90.2	94.1
N4BP2	R2	100	106.3	96.0	89.6	81.4	90.7
ctrl_50	R1	100	104.4	110.3	79.6	96.1	94.7
ctrl_50	R2	100	103.7	100.4	94.5	102.8	92.0
PERK	R1	100	96.5	107.8	94.0	93.0	78.3
PERK	R2	100	109.3	113.7	94.4	93.0	100.0
HRI	R1	100	97.5	93.8	97.6	98.1	100.0
HRI	R2	100	97.3	120.0	97.4	94.4	92.5
PKR	R1	100	92.9	73.7	41.4	100.0	94.6
PKR	R2	100	88.2	77.0	46.2	90.5	90.0
GCN2	R1	100	102.5	98.7	97.5	96.0	95.9
GCN2	R2	100	98.4	109.0	98.8	100.0	100.0
EIF2S1	R1	100	0.5	0.0	0.0	0.0	0.0
EIF2S1	R2	100	1.8	0.0	0.0	0.0	0.0
PELO	R1	100	96.6	100.0	31.8	15.0	2.6
PELO	R2	100	111.7	73.2	29.1	10.2	2.1
GTPBP1_ips	R1	100	76.9	17.4	7.3	2.6	0.0
GTPBP1_ips	R2	100	87.7	13.1	7.1	0.0	0.0
GTPBP2	R1	100	96.4	68.0	50.7	28.1	38.5
GTPBP2	R2	100	97.6	70.3	49.3	22.4	34.4
EIF2D	R1	100	100.0	104.6	57.4	34.0	14.5
EIF2D	R2	100	100.0	100.0	51.0	26.3	10.9
DDX3X	R1	100	100.0	62.2	85.9	71.2	48.5
DDX3X	R2	100	98.8	91.9	82.6	66.7	49.2
NEMF	R1	100	98.2	89.4	77.8	63.4	45.0
NEMF	R2	100	95.2	96.3	69.8	61.7	55.1
EDF1	R1	100	94.7	110.1	82.8	85.7	78.2

EDF1	R2	100	98.7	114.7	96.9	108.6	98.2
EXOSC9	R1	100	64.5	8.6	5.8	8.9	0.0
EXOSC9	R2	100	39.4	0.0	6.7	6.3	0.0
EIF4E2	R1	100	102.0	68.2	25.0	21.4	12.0
EIF4E2	R2	100	100.0	78.7	47.3	0.0	58.8
GIGYF2	R1	100	69.7	42.6	28.0	9.9	0.0
GIGYF2	R2	100	94.3	61.1	37.4	11.3	0.0

Table S 5.3. Growth assays of gene knockdowns validate screening phenotypes in HEK293 cells. Growth phenotypes upon target knockdown were assessed by measuring GFP fluorescence and normalization to the corresponding non-induced sgRNA. Cells were split every four cell divisions (T) and GFP fluorescence was measured using flow cytometry. Experiments were performed in biological replicates.

Genet	Rep	T0	T4	T8	T12	T16	T20
HBS1L	R1	100	97.1	94.4	95.0	90.5	94.7
HBS1L	R2	100	102.7	100.0	100.0	100.0	100.0
HSPA14	R1	100	96.3	100.0	100.0	90.6	80.6
HSPA14	R2	100	102.0	95.0	92.7	87.8	84.2
HSPA2	R1	100	85.3	100.0	94.1	100.0	93.3
HSPA2	R2	100	90.9	107.1	100.0	100.0	100.0
DENR	R1	100	79.4	100.0	82.1	76.9	73.9
DENR	R2	100	71.8	86.2	77.8	76.0	62.5
MCTS1	R1	100	96.1	94.0	82.4	74.2	63.1
MCTS1	R2	100	93.8	95.2	87.3	79.0	68.3
N4BP2	R1	100	97.2	100.0	106.1	104.1	113.0
N4BP2	R2	100	110.1	97.4	97.5	97.4	91.9
ASCC3	R1	100	102.5	97.6	92.9	75.7	67.1
ASCC3	R2	100	98.4	93.2	87.5	73.0	64.0
ZNF598	R1	100	94.8	76.4	48.8	41.3	41.9
ZNF598	R2	100	91.6	74.0	58.5	47.6	39.5
LTN1	R1	100	98.7	89.3	104.7	97.9	93.3
LTN1	R2	100	109.1	126.3	93.0	88.9	88.4
ctrl	R1	100	101.9	84.7	100.0	102.0	100.0
ctrl	R2	100	95.5	80.0	102.2	102.1	102.1
PERK	R1	100	90.2	118.2	123.1	172.7	148.4
PERK	R2	100	82.0	115.7	116.1	111.8	120.5
HRI	R1	100	98.4	114.6	98.1	98.1	100.0
HRI	R2	100	91.5	137.3	98.1	94.4	92.5
PKR	R1	100	112.6	115.3	100.0	100.0	94.6
PKR	R2	100	102.0	72.3	95.0	90.5	90.0
GCN2	R1	100	84.5	134.6	100.0	96.0	95.9
GCN2	R2	100	88.9	113.5	100.0	100.0	100.0
EIF2S1	R1	100	46.7	2.7	5.0	0.0	0.0
EIF2S1	R2	100	62.5	14.5	6.5	1.8	0.0
PELO	R1	100	96.9	88.6	81.0	66.0	75.8
PELO	R2	100	97.2	91.9	90.1	76.2	86.3
GTPBP1_hek	R1	100	85.7	19.0	13.2	11.0	10.0
GTPBP1_hek	R2	100	81.8	13.9	7.7	5.2	6.6
GTPBP1_ips	R1	100	105.5	74.1	13.0	14.9	10.9
GTPBP1_ips	R2	100	98.3	36.6	17.3	10.0	8.3
GTPBP2	R1	100	98.8	97.7	106.4	91.8	92.8
GTPBP2	R2	100	102.6	102.5	101.3	100.0	100.0
EIF2D	R1	100	101.3	95.0	87.3	78.4	76.7
EIF2D	R2	100	100.0	95.1	87.7	75.6	71.4
DDX3X	R1	100	96.3	79.8	63.6	61.8	54.5
DDX3X	R2	100	80.7	67.1	42.0	26.6	20.8
NEMF	R1	100	102.3	96.3	87.8	97.9	93.9
NEMF	R2	100	98.1	96.7	91.8	96.6	95.2
GIGYF2	R1	100	100.0	105.6	73.5	46.3	35.8
GIGYF2	R2	100	94.4	98.3	79.6	48.1	28.8
EDF1	R1	100	94.2	98.6	95.9	98.5	94.4
EDF1	R2	100	89.7	98.6	113.6	101.8	89.4
EXOSC9	R1	100	92.5	17.9	20.0	13.3	13.3
EXOSC9	R2	100	82.9	17.5	19.2	12.5	10.0
DNAJC2	R1	100	120.7	100.0	88.7	66.7	66.7
DNAJC2	R2	100	97.3	92.4	92.7	-	107.1
EIF4E2	R1	100	102.5	100.7	115.0	136.8	152.2
EIF4E2	R2	100	103.6	108.9	108.9	114.8	108.6

Table S 5.4. Growth assays of gene knockdowns validate screening phenotypes in NPCs.
Growth phenotypes upon target knockdown were assessed by measuring GFP fluorescence and normalization to the corresponding non-induced sgRNA. Cells were split every four cell divisions (T) and GFP fluorescence was measured using flow cytometry. Experiments were performed in biological replicates.

Gene	Rep	T0	T4	T8	T12	T16	T20
HBS1L	R1	100	95.3	68.3	35.9	15.6	5.6
HBS1L	R2	100	94.4	75.4	45.6	35.1	20.2
DENR	R1	100	96.1	82.6	46.4	40.0	0.0
DENR	R2	100	82.8	58.3	34.4	31.6	0.0
MCTS1	R1	100	93.1	83.5	76.9	137.2	116.3
MCTS1	R2	100	93.8	87.6	80.4	87.1	53.2
ASCC3	R1	100	94.7	46.2	51.2	0.0	0.0
ASCC3	R2	100	93.1	46.2	31.2	0.0	0.0
ZNF598	R1	100	96.9	90.3	82.8	48.4	25.4
ZNF598	R2	100	95.2	80.3	83.8	49.7	28.6
LTN1	R1	100	81.1	56.5	21.5	0.0	0.0
LTN1	R2	100	69.2	51.1	24.7	0.0	0.0
N4BP2	R1	100	98.6	103.6	130.5	53.0	33.0
N4BP2	R2	100	85.7	89.8	79.2	46.0	27.0
ctrl	R1	100	91.5	91.1	100.7	102.4	93.6
ctrl	R2	100	96.9	86.5	93.8	63.3	48.5
PERK	R1	100	87.8	81.8	86.6	79.3	57.2
PERK	R2	100	95.7	89.9	100.6	112.9	80.2
HRI	R1	100	93.3	81.1	88.1	222.7	120.5
HRI	R2	100	77.9	84.2	102.3	103.4	70.8
PKR	R1	100	97.9	84.3	90.3	313.2	250.0
PKR	R2	100	86.8	84.2	78.0	72.6	48.8
GCN2	R1	100	109.4	90.0	95.7	112.8	107.7
GCN2	R2	100	81.4	92.3	121.4	128.2	102.6
EIF2S1	R1	100	54.1	27.8	0.0	0.0	0.0
EIF2S1	R2	100	40.0	32.7	0.0	0.0	0.0
PELO	R1	100	92.7	80.0	47.5	32.9	21.2
PELO	R2	100	82.2	65.0	40.5	42.1	23.7
GTPBP1	R1	100	96.6	63.8	43.5	34.0	17.0
GTPBP1	R2	100	94.9	60.2	42.9	22.2	11.1
GTPBP2	R1	100	93.1	79.3	69.2	46.4	34.0
GTPBP2	R2	100	83.1	75.2	67.1	45.3	25.5
EIF2D	R1	100	101.1	88.1	85.1	69.0	40.8
EIF2D	R2	100	94.9	97.3	91.9	71.1	35.1
DDX3X	R1	100	98.7	61.6	42.6	23.9	8.7
DDX3X	R2	100	84.3	53.4	45.5	26.6	8.6
NEMF	R1	100	96.2	82.9	80.6	121.9	92.4
NEMF	R2	100	88.5	87.6	82.1	102.9	78.3
GIGYF2	R1	100	93	90	97.7	112.9	152.2
GIGYF2	R2	100	100	98.2	103.3	124.4	113.9
EDF1	R1	100	92.2	86.1	91.9	127.4	99.1
EDF1	R2	100	87.7	86.7	78.5	113.3	97.3
EXOSC9	R1	100	65.4	24.8	9.0	0.0	0.0
EXOSC9	R2	100	68.3	26.5	9.3	0.0	0.0
EIF4E2	R1	100	97.6	88.9	88.1	54.2	38.9
EIF4E2	R2	100	89.4	76.6	73.8	45.3	24.7

Table S 5.5. Genetic interactions in hiPSC.
Summary of single and double knockdown growth phenotypes and the expected growth (expected growth = observed phenotype of sgRNA1 * sgRNA2). Percent of GFP-positive cells was analyzed by flow cytometry analysis of 10,000 cells in biological replicates and normalized to non-induced control. Green coloring indicates representative values that are used in the main text.

Genes	Rep	T0	T4	T8	T12	T16	T20
EIF4E2	1	100.0	102.0	68.2	25.0	21.4	12.0
EIF4E2	2	100.0	100.0	78.7	47.3	0.0	0.0
ZNF598	1	100.0	84.4	29.6	1.1	0.0	0.0
ZNF598	2	100.0	114.5	16.5	2.6	0.0	0.0
EIF4E2+ZNF98	1	100.0	103.2	39.0	0.0	0.0	0.0
EIF4E2+ZNF98	2	100.0	66.9	22.9	0.0	0.0	0.0
Growth_expect		**100.0**	**100.5**	**16.9**	**0.7**	**0.0**	**0.0**
EIF4E2	1	100.0	102.0	68.2	25.0	21.4	12.0
EIF4E2	2	100.0	100.0	78.7	47.3	0.0	0.0
EDF1	1	100.0	94.7	110.1	82.8	85.7	78.2
EDF1	2	100.0	98.7	114.7	96.9	108.6	98.2
EIF4E2+EDF1	1	100.0	97.1	56.2	15.6	2.5	3.3
EIF4E2+EDF1	2	100.0	93.7	31.3	13.8	13.5	1.7
Growth_expect		**100.0**	**97.7**	**82.6**	**32.5**	**10.4**	**5.3**
HBS1L	1	100.0	101.7	13.9	1.5	2.8	0.0
HBS1L	2	100.0	100.6	10.6	0.8	2.3	0.0
N4BP2	1	100.0	118.6	95.2	88.1	90.2	94.1
N4BP2	2	100.0	106.3	96.0	89.6	81.4	90.7
HBS1L+N4BP2	1	100.0	92.7	1	0.0	0.0	0.0
HBS1L+N4BP2	2	100.0	93.1	0.5	0.0	0.0	0.0
Growth_expect		**100.0**	**113.7**	**11.7**	**1.0**	**2.2**	**0.0**
EDF1	1	100.0	94.7	110.1	82.8	85.7	78.2
EDF1	2	100.0	98.7	114.7	96.9	108.6	98.2
N4BP2	1	100.0	118.6	95.2	88.1	90.2	94.1
N4BP2	2	100.0	106.3	96.0	89.6	81.4	90.7
EDF1+N4BP2	1	100.0	71.3	33.7	23.5	0.0	0.0
EDF1+N4BP2	2	100.0	78.4	63.7	66.1	0.0	0.0
Growth_expect		**100.0**	**108.7**	**107.5**	**79.8**	**83.4**	**81.5**
ASCC3	1	100.0	99.6	42.9	0.4	0.0	0.0
ASCC3	2	100.0	104.4	61.0	1.6	0.0	0.0
EDF1	1	100.0	94.7	110.1	82.8	85.7	78.2
EDF1	2	100.0	98.7	114.7	96.9	108.6	98.2
ASCC3+EDF1	1	100.0	72.5	0.0	0.0	0.0	0.0
ASCC3+EDF1	2	100.0	67.6	0.0	0.0	0.0	0.0
Growth_expect		**100.0**	**98.7**	**58.4**	**0.9**	**0.0**	**0.0**
ASCC3	1	100.0	99.6	42.9	0.4	0.0	0.0
ASCC3	2	100.0	104.4	61.0	1.6	0.0	0.0
ZNF598	1	100.0	84.4	29.6	1.1	0.0	0.0
ZNF598	2	100.0	114.5	16.5	2.6	0.0	0.0
ASCC3+ZNF598	1	100.0	57.9	0.0	0.0	0.0	0.0
ASCC3+ZNF598	2	100.0	82.6	0.0	0.0	0.0	0.0
Growth_expect		**100.0**	**101.5**	**12.0**	**0.0**	**0.0**	**0.0**
EDF1	1	100.0	94.7	110.1	82.8	85.7	78.2
EDF1	2	100.0	98.7	114.7	96.9	108.6	98.2
ZNF598	1	100.0	84.4	29.6	1.1	0.0	0.0
ZNF598	2	100.0	114.5	16.5	2.6	0.0	0.0
EDF1+ZNF598	1	100.0	69.4	14.3	0.0	0.0	0.0
EDF1+ZNF598	2	100.0	66.7	30.8	0.0	0.0	0.0
Growth_expect		**100.0**	**96.2**	**25.9**	**1.7**	**0.0**	**0.0**
ASCC3	1	100.0	99.6	42.9	0.4	0.0	0.0
ASCC3	2	100.0	104.4	61.0	1.6	0.0	0.0
N4BP2	1	100.0	118.6	95.2	88.1	90.2	94.1
N4BP2	2	100.0	106.3	96.0	89.6	81.4	90.7
ASCC3+N4BP2	1	100.0	73.7	27.3	0.0	0.0	0.0
ASCC3+N4BP2	2	100.0	78.3	27.3	0.0	0.0	0.0
Growth_expect		**100.0**	**114.7**	**49.6**	**0.9**	**0.0**	**0.0**
ASCC3	1	100.0	99.6	42.9	0.4	0.0	0.0
ASCC3	2	100.0	104.4	61.0	1.6	0.0	0.0
HBS1L	1	100.0	101.7	13.9	1.5	2.8	0.0
HBS1L	2	100.0	100.6	10.6	0.8	2.3	0.0
ASCC3+HBS1L	1	100.0	94.1	36.4	0.0	0.0	0.0
ASCC3+HBS1L	2	100.0	65.5	25.0	0.0	0.0	0.0

Growth_expect		**100.0**	**103.2**	**6.4**	**0.0**	**0.0**	**0.0**
GIGYF2	1	100.0	98.4	74.5	63.3	31.0	15.0
GIGYF2	2	100.0	98.6	89.1	55.6	28.1	12.5
EDF1	1	100.0	94.7	110.1	82.8	85.7	78.2
EDF1	2	100.0	98.7	114.7	96.9	108.6	98.2
GIGYF2+EDF1	1	100.0	87.5	64.3	0.0	0.0	0.0
GIGYF2+EDF1	2	100.0	73.1	62.5	0.0	0.0	0.0
Growth_expect		**100.0**	**95.3**	**92.0**	**53.4**	**28.7**	**12.1**
GIGYF2	1	100.0	98.4	74.5	63.3	31.0	15.0
GIGYF2	2	100.0	98.6	89.1	55.6	28.1	12.5
ZNF598	1	100.0	84.4	29.6	1.1	0.0	0.0
ZNF598	2	100.0	114.5	16.5	2.6	0.0	0.0
GIGYF2+ZNF598	1	100.0	73.9	37.5	0.0	0.0	0.0
GIGYF2+ZNF598	2	100.0	80.0	33.3	0.0	0.0	0.0
Growth_expect		**100.0**	**98.0**	**18.9**	**1.1**	**0.0**	**0.0**
GTPBP1	1	100.0	76.9	17.4	7.3	2.6	0.0
GTPBP1	2	100.0	87.7	13.1	7.1	0.0	0.0
EXOSC9	1	100.0	64.5	3.0	0.0	0.0	0.0
EXOSC9	2	100.0	39.4	0.0	0.0	0.0	0.0
GTPBP1+EXOSC	1	100.0	42.3	41.2	0.0	0.0	0.0
GTPBP1+EXOSC	2	100.0	37.0	31.3	0.0	0.0	0.0
Growth_expect		**100.0**	**42.8**	**0.2**	**0.0**	**0.0**	**0.0**
GTPBP1	1	100.0	76.9	17.4	7.3	2.6	0.0
GTPBP1	2	100.0	87.7	13.1	7.1	0.0	0.0
PELO	1	100.0	96.6	100.0	31.8	15.0	2.6
PELO	2	100.0	112.0	73.0	29.1	10.2	2.1
GTPBP1+PELO	1	100.0	98.8	32.7	11.4	0.0	0.0
GTPBP1+PELO	2	100.0	129.3	52.8	24.5	16.7	0.0
Growth_expect		**100.0**	**85.8**	**13.2**	**2.2**	**0.2**	**0.0**
GTPBP1	1	100.0	76.9	17.4	7.3	2.6	0.0
GTPBP1	2	100.0	87.7	13.1	7.1	0.0	0.0
HBS1L	1	100.0	101.7	13.9	1.5	2.8	0.0
HBS1L	2	100.0	100.6	10.6	0.8	2.3	0.0
GTPBP1+HBS1L	1	100.0	60.0	6.9	13.5	0.0	0.0
GTPBP1+HBS1L	2	100.0	50.9	9.2	19.3	0.0	0.0
Growth_expect		**100.0**	**83.3**	**1.9**	**0.1**	**0.0**	**0.0**
HBS1L	1	100.0	101.7	13.9	1.5	2.8	0.0
HBS1L	2	100.0	100.6	10.6	0.8	2.3	0.0
ZNF598	1	100.0	84.4	29.6	1.1	0.0	0.0
ZNF598	2	100.0	114.5	16.5	2.6	0.0	0.0
HBS1L+ZNF598	1	100.0	60.4	16.0	21.4	0.0	0.0
HBS1L+ZNF598	2	100.0	50.5	19.4	24.0	0.0	0.0
Growth_expect		**100.0**	**100.6**	**2.8**	**0.0**	**0.0**	**0.0**

Table S 5.6. Genetic interactions in HEK293 cells.
Summary of single and double knockdown growth phenotypes and the expected growth (expected growth = observed phenotype of sgRNA1 * sgRNA2). Percent of GFP-positive cells was analyzed by flow cytometry analysis of 10,000 cells in biological replicates and normalized to non-induced control. Orange coloring indicates representative values that are used in the main text.

Genes	Rep	T0	T4	T8	T12	T16	T20
EIF4E2	1	100.0	102.5	100.7	115.0	136.8	152.2
EIF4E2	2	100.0	103.6	108.9	108.9	114.8	108.6
ZNF598	1	100.0	94.8	76.4	48.8	41.3	41.9
ZNF598	2	100.0	91.6	74.0	58.5	47.6	39.5
EIF4E2+ZNF98	1	100.0	91.7	71.4	120.1	44.2	45.3
EIF4E2+ZNF98	2	100.0	92.3	92.3	95.5	68.5	76.2
Growth_expect		**100.0**	**96.0**	**78.8**	**60.1**	**55.9**	**53.1**
EIF4E2	1	100.0	102.5	100.7	115.0	136.8	152.2
EIF4E2	2	100.0	103.6	108.9	108.9	114.8	108.6
EDF1	1	100.0	94.2	98.6	95.9	98.5	94.4
EDF1	2	100.0	89.7	98.6	113.6	101.8	89.4
EIF4E2+EDF1	1	100.0		97.2	74.9	66.9	92.4
EIF4E2+EDF1	2	100.0	103.1	94.6	85.5	74.9	42.3
Growth_expect		**100.0**	**94.8**	**103.3**	**117.3**	**126.0**	**119.8**
HBS1L	1	100.0	97.1	94.4	95.0	90.5	94.7
HBS1L	2	100.0	102.7	100.0	100.0	100.0	100.0
N4BP2	1	100.0	97.2	100.0	106.1	104.1	113.0
N4BP2	2	100.0	110.1	97.4	97.5	97.4	91.9
HBS1L+N4BP2	1	100.0	104.8	97.6	87.0	64.6	78.7
HBS1L+N4BP2	2	100.0	102.6	87.5	75.9	57.9	52.2
Growth_expect		**100.0**	**103.5**	**95.9**	**99.3**	**95.9**	**99.8**
EDF1	1	100.0	94.2	98.6	95.9	98.5	94.4
EDF1	2	100.0	89.7	98.6	113.6	101.8	89.4
N4BP2	1	100.0	97.2	100.0	106.1	104.1	113.0
N4BP2	2	100.0	110.1	97.4	97.5	97.4	91.9
EDF1+N4BP2	1	100.0	88.5	80.6	83.4	87.3	0.0
EDF1+N4BP2	2	100.0	103.0	99.4	97.5	97.5	0.0
Growth_expect		**100.0**	**95.3**	**97.3**	**106.6**	**100.9**	**94.1**
ASCC3	1	100.0	102.5	97.6	92.9	75.7	67.1
ASCC3	2	100.0	98.4	93.2	87.5	73.0	64.0
EDF1	1	100.0	94.2	98.6	95.9	98.5	94.4
EDF1	2	100.0	89.7	98.6	113.6	101.8	89.4
ASCC3+EDF1	1	100.0	91.2	83.2	65.1	60.8	0.0
ASCC3+EDF1	2	100.0	97.7	91.6	65.9	63.3	0.0
Growth_expect		**100.0**	**92.4**	**94.0**	**94.5**	**74.4**	**60.2**
ASCC3	1	100.0	102.5	97.6	92.9	75.7	67.1
ASCC3	2	100.0	98.4	93.2	87.5	73.0	64.0
ZNF598	1	100.0	94.8	76.4	48.8	41.3	41.9
ZNF598	2	100.0	91.6	74.0	58.5	47.6	39.5
ASCC3+ZNF598	1	100.0	96.4	85.4	73.1	62.5	0.0
ASCC3+ZNF598	2	100.0	96.2	82.1	68.1	61.6	0.0
Growth_expect		**100.0**	**93.6**	**71.7**	**48.4**	**33.0**	**26.7**
EDF1	1	100.0	94.2	98.6	95.9	98.5	94.4
EDF1	2	100.0	89.7	98.6	113.6	101.8	89.4
ZNF598	1	100.0	94.8	76.4	48.8	41.3	41.9
ZNF598	2	100.0	91.6	74.0	58.5	47.6	39.5
EDF1+ZNF598	1	100.0	97.1	76.5	53.1	48.6	43.2
EDF1+ZNF598	2	100.0	86.8	70.3	56.8	69.7	104.2
Growth_expect		**100.0**	**85.7**	**74.2**	**56.2**	**44.5**	**37.4**
ASCC3	1	100.0	102.5	97.6	92.9	75.7	67.1
ASCC3	2	100.0	98.4	93.2	87.5	73.0	64.0
N4BP2	1	100.0	97.2	100.0	106.1	104.1	113.0
N4BP2	2	100.0	110.1	97.4	97.5	97.4	91.9
ASCC3+N4BP2	1	100.0	100.0	90.0	78.6	75.0	74.1
ASCC3+N4BP2	2	100.0	100.0	90.0	70.0	60.6	53.1
Growth_expect		**100.0**	**104.1**	**94.1**	**91.8**	**74.9**	**67.2**
ASCC3	1	100.0	102.5	97.6	92.9	75.7	67.1
ASCC3	2	100.0	98.4	93.2	87.5	73.0	64.0
HBS1L	1	100.0	97.1	94.4	95.0	90.5	94.7
HBS1L	2	100.0	102.7	100.0	100.0	100.0	100.0
ASCC3+HBS1L	1	100.0	100.0	97.3	74.3	67.6	63.9
ASCC3+HBS1L	2	100.0	110.8	100.0	79.4	54.5	52.4

Growth_expect		**100.0**	**100.4**	**92.7**	**87.9**	**70.8**	**63.8**
GIGYF2	1	100.0	107.4	71.9	83.0	50.0	25.8
GIGYF2	2	100.0	95.2	101.8	76.4	51.9	41.4
EDF1	1	100.0	94.2	98.6	95.9	98.5	94.4
EDF1	2	100.0	89.7	98.6	113.6	101.8	89.4
GIGYF2+EDF1	1	100.0	89.2	60.0	40.6	40.6	38.7
GIGYF2+EDF1	2	100.0	89.2	65.7	47.1	42.4	35.5
Growth_expect		**100.0**	**93.1**	**85.6**	**83.5**	**51.0**	**30.8**
GIGYF2	1	100.0	107.4	71.9	83.0	50.0	25.8
GIGYF2	2	100.0	95.2	101.8	76.4	51.9	41.4
ZNF598	1	100.0	94.8	76.4	48.8	41.3	41.9
ZNF598	2	100.0	91.6	74.0	58.5	47.6	39.5
GIGYF2+ZNF598	1	100.0	95.0	59.0	35.1	35.1	40.0
GIGYF2+ZNF598	2	100.0	91.3	59.6	41.3	40.4	36.2
Growth_expect		**100.0**	**94.4**	**65.3**	**42.8**	**22.7**	**13.7**
GTPBP1	1	100.0	85.7	19.0	13.2	11.0	10.0
GTPBP1	2	100.0	81.8	13.9	7.7	5.2	6.6
EXOSC9	1	100.0	92.5	17.9	20.0	13.3	13.3
EXOSC9	2	100.0	82.0	17.5	19.2	12.5	10.0
GTPBP1+EXOSC9	1	100.0	47.8	16.7	14.3	16.7	0.0
GTPBP1+EXOSC9	2	100.0	50.0	30.0	33.3	25.0	0.0
Growth_expect		**100.0**	**73.1**	**2.9**	**2.0**	**1.0**	**1.0**
GTPBP1	1	100.0	85.7	19.0	13.2	11.0	10.0
GTPBP1	2	100.0	81.8	13.9	7.7	5.2	6.6
PELO	1	100.0	108.5	91.0	79.6	81.3	64.3
PELO	2	100.0	96.7	101.8	90.4	82.9	68.0
GTPBP1+PELO	1	100.0	81.1	81.1	63.5	66.7	44.0
GTPBP1+PELO	2	100.0	78.6	78.6	74.9	28.6	33.3
Growth_expect		**100.0**	**85.9**	**15.9**	**8.9**	**6.6**	**5.5**
GTPBP1	1	100.0	85.7	19.0	13.2	11.0	10.0
GTPBP1	2	100.0	81.8	13.9	7.7	5.2	6.6
HBS1L	1	100.0	97.1	94.4	95.0	90.5	94.7
HBS1L	2	100.0	102.7	100.0	100.0	100.0	100.0
GTPBP1+HBS1L	1	100.0	89.8	80.4	100.0	54.2	49.6
GTPBP1+HBS1L	2	100.0	107.6	91.6	96.7	48.3	45.5
Growth_expect		**100.0**	**83.7**	**16.0**	**10.2**	**7.7**	**8.1**
HBS1L	1	100.0	97.1	94.4	95.0	90.5	94.7
HBS1L	2	100.0	102.7	100.0	100.0	100.0	100.0
ZNF598	1	100.0	94.8	76.4	48.8	41.3	41.9
ZNF598	2	100.0	91.6	74.0	58.5	47.6	39.5
HBS1L+ZNF598	1	100.0	100.0	86.2	83.6	79.0	60.3
HBS1L+ZNF598	2	100.0	99.3	91.4	92.6	80.0	77.4
Growth_expect		**100.0**	**93.1**	**73.1**	**52.3**	**42.3**	**39.6**

Table S 5.7. Genetic interactions in NPC.
Summary of single and double knockdown growth phenotypes and the expected growth (expected growth = observed phenotype of sgRNA1 * sgRNA2). Percent of GFP-positive cells was analyzed by flow cytometry analysis of 10,000 cells in biological replicates and normalized to non-induced control. Blue coloring indicates representative values that are used in the main text.

Genes	Rep	T0	T4	T8	T12	T16	T20
EIF4E2	1	100.0	97.6	88.9	88.1	54.2	38.9
EIF4E2	2	100.0	89.4	76.6	73.8	45.3	24.7
ZNF598	1	100.0	96.9	90.3	82.8	48.4	25.4
ZNF598	2	100.0	95.2	80.3	83.8	49.7	28.6
EIF4E2+ZNF98	1	100.0	96.3	72.4	79.0	84.7	97.3
EIF4E2+ZNF98	2	100.0	105.8	92.9	90.3	87.4	66.7
exprected_growth		**100.0**	**89.8**	**70.6**	**67.4**	**24.4**	**8.6**
EIF4E2	1	100.0	97.6	88.9	88.1	54.2	38.9
EIF4E2	2	100.0	89.4	76.6	73.8	45.3	24.7
EDF1	1	100.0	92.2	86.1	91.9	127.4	99.1
EDF1	2	100.0	87.7	86.7	78.5	113.3	97.3
EIF4E2+EDF1	1	100.0	97.5	87.3	93.3	82.4	37.6
EIF4E2+EDF1	2	100.0	94.9	89.7	97.8	100.0	65.1
exprected_growth		**100.0**	**84.1**	**71.5**	**69.0**	**59.9**	**31.3**
HBS1L	1	100.0	95.3	68.3	35.9	15.6	5.6
HBS1L	2	100.0	94.4	75.4	45.6	35.1	20.2
N4BP2	1	100.0	98.6	104.0	131.0	53.0	33.0
N4BP2	2	100.0	85.7	89.8	79.2	46.0	27.0
HBS1L+N4BP2	1	100.0	99.0	63.2	48.9	22.4	15.7
HBS1L+N4BP2	2	100.0	84.2	62.1	37.3	19.4	14.2
exprected_growth		**100.0**	**87.4**	**69.6**	**42.8**	**12.5**	**3.9**
EDF1	1	100.0	92.2	86.1	91.9	127.4	99.1
EDF1	2	100.0	87.7	86.7	78.5	113.3	97.3
N4BP2	1	100.0	98.6	104.0	131.0	53.0	33.0
N4BP2	2	100.0	85.7	89.8	79.2	46.0	27.0
EDF1+N4BP2	1	100.0	86.3	73.8	84.8	90.2	65.9
EDF1+N4BP2	2	100.0	86.0	85.0	118.6	114.3	64.3
exprected_growth		**100.0**	**82.9**	**83.7**	**89.5**	**59.6**	**29.5**
ASCC3	1	100.0	94.7	46.2	51.2	0.0	0.0
ASCC3	2	100.0	93.1	46.2	31.2	0.0	0.0
EDF1	1	100.0	92.2	86.1	91.9	127.4	99.1
EDF1	2	100.0	87.7	86.7	78.5	113.3	97.3
ASCC3+EDF1	1	100.0	77.3	21.1	0.0	0.0	0.0
ASCC3+EDF1	2	100.0	74.2	17.8	0.0	0.0	0.0
exprected_growth		**100.0**	**84.5**	**39.9**	**35.1**	**0.0**	**0.0**
ASCC3	1	100.0	94.7	46.2	51.2	0.0	0.0
ASCC3	2	100.0	93.1	46.2	31.2	0.0	0.0
ZNF598	1	100.0	96.9	90.3	82.8	48.4	25.4
ZNF598	2	100.0	95.2	80.3	83.8	49.7	28.6
ASCC3+ZNF598	1	100.0	100.0	27.3	0.0	0.0	0.0
ASCC3+ZNF598	2	100.0	81.8	31.3	0.0	0.0	0.0
exprected_growth		**100.0**	**90.2**	**39.4**	**34.3**	**0.0**	**0.0**
EDF1	1	100.0	92.2	86.1	91.9	127.4	99.1
EDF1	2	100.0	87.7	86.7	78.5	113.3	97.3
ZNF598	1	100.0	96.9	90.3	82.8	48.4	25.4
ZNF598	2	100.0	95.2	80.3	83.8	49.7	28.6
EDF1+ZNF598	1	100.0	110.5	98.0	77.9	77.4	48.4
EDF1+ZNF598	2	100.0	101.5	85.2	65.6	79.5	35.9
exprected_growth		**100.0**	**86.4**	**73.7**	**71.0**	**59.0**	**26.5**
ASCC3	1	100.0	94.7	46.2	51.2	0.0	0.0
ASCC3	2	100.0	93.1	46.2	31.2	0.0	0.0
N4BP2	1	100.0	98.6	104.0	131.0	53.0	33.0
N4BP2	2	100.0	85.7	89.8	79.2	46.0	27.0
ASCC3+N4BP2	1	100.0	85.3	25.4	0.0	0.0	0.0
ASCC3+N4BP2	2	100.0	86.8	23.7	0.0	0.0	0.0
exprected_growth		**100.0**	**86.5**	**44.8**	**43.3**	**0.0**	**0.0**
ASCC3	1	100.0	94.7	46.2	51.2	0.0	0.0
ASCC3	2	100.0	93.1	46.2	31.2	0.0	0.0
HBS1L	1	100.0	95.3	68.3	35.9	15.6	5.6
HBS1L	2	100.0	94.4	75.4	45.6	35.1	20.2
ASCC3+HBS1L	1	100.0	89.0	20.8	0.0	0.0	0.0
ASCC3+HBS1L	2	100.0	85.6	21.7	0.0	0.0	0.0
exprected_growth		**100.0**	**89.1**	**33.2**	**16.8**	**0.0**	**0.0**

GIGYF2	1	100.0	93.0	90.0	97.7	112.9	152.2
GIGYF2	2	100.0	100.0	98.2	103.3	124.4	113.9
EDF1	1	100.0	92.2	86.1	91.9	127.4	99.1
EDF1	2	100.0	87.7	86.7	78.5	113.3	97.3
GIGYF2+EDF1	1	100.0	101.5	66.2	92.9	72.9	68.6
GIGYF2+EDF1	2	100.0	100.0	73.7	78.8	65.7	38.6
exprected_growth		**100.0**	**86.8**	**81.3**	**85.6**	**142.8**	**130.7**
GIGYF2	1	100.0	93.0	90.0	97.7	112.9	152.2
GIGYF2	2	100.0	100.0	98.2	103.3	124.4	113.9
ZNF598	1	100.0	96.9	90.3	82.8	48.4	25.4
ZNF598	2	100.0	95.2	80.3	83.8	49.7	28.6
GIGYF2+ZNF598	1	100.0	104.4	118.4	139.6	181.3	143.8
GIGYF2+ZNF598	2	100.0	91.3	90.0	163.6	208.6	128.6
exprected_growth		**100.0**	**92.7**	**80.3**	**83.7**	**58.2**	**35.9**
GTPBP1	1	100.0	96.6	63.8	43.5	34.0	17.0
GTPBP1	2	100.0	94.9	60.2	42.9	22.2	11.1
EXOSC9	1	100.0	65.4	24.8	9.0	0.0	0.0
EXOSC9	2	100.0	68.3	26.5	9.3	0.0	0.0
GTPBP1+EXOSC9	1	100.0	60.4	15.2	0.0	0.0	0.0
GTPBP1+EXOSC9	2	100.0	57.1	10.1	0.0	0.0	0.0
exprected_growth		**100.0**	**64.0**	**15.9**	**3.9**	**0.0**	**0.0**
GTPBP1	1	100.0	96.6	63.8	43.5	34.0	17.0
GTPBP1	2	100.0	94.9	60.2	42.9	22.2	11.1
PELO	1	100.0	92.7	80.0	47.5	32.9	21.2
PELO	2	100.0	82.2	65.0	40.5	42.1	23.7
GTPBP1+PELO	1	100.0	90.1	39.7	0.0	0.0	0.0
GTPBP1+PELO	2	100.0	81.8	21.0	0.0	0.0	0.0
exprected_growth		**100.0**	**83.7**	**45.0**	**19.0**	**10.6**	**3.2**
GTPBP1	1	100.0	96.6	63.8	43.5	34.0	17.0
GTPBP1	2	100.0	94.9	60.2	42.9	22.2	11.1
HBS1L	1	100.0	95.3	68.3	35.9	15.6	5.6
HBS1L	2	100.0	94.4	75.4	45.6	35.1	20.2
GTPBP1+HBS1L	1	100.0	76.8	45.0	0.0	0.0	0.0
GTPBP1+HBS1L	2	100.0	80.0	37.0	0.0	0.0	0.0
exprected_growth		**100.0**	**90.8**	**44.5**	**17.6**	**7.1**	**1.8**
HBS1L	1	100.0	95.3	68.3	35.9	15.6	5.6
HBS1L	2	100.0	94.4	75.4	45.6	35.1	20.2
ZNF598	1	100.0	96.9	90.3	82.8	48.4	25.4
ZNF598	2	100.0	95.2	80.3	83.8	49.7	28.6
HBS1L+ZNF598	1	100.0	96.0	60.0	39.1	34.9	17.5
HBS1L+ZNF598	2	100.0	86.4	49.3	34.9	41.8	25.5
exprected_growth		**100.0**	**91.1**	**61.3**	**33.9**	**12.4**	**3.5**

Table S 5.8. Genes with sensitive pauses upon ZNF598^{mut} expression in hiPSC.

	Gene
1	AAR2
2	ACO2
3	ACOT13
4	ADSS2
5	AHCY
6	AIMP2
7	ALYREF
8	AP2S1
9	ARCN1
10	ARL6IP1
11	ARL6IP5
12	ARPC4
13	ATIC
14	ATP1A1
15	ATP5F1B
16	ATP5MG
17	ATP5PO
18	ATP6V0C
19	ATP6V1E1
20	ATP6V1G1
21	AURKB
22	BCCIP
23	C11orf58
24	C1QBP
25	CALM1
26	CAPZA1
27	CCDC58
28	CCND2
29	CCT4
30	CCT7
31	CD9
32	CDC123
33	CDC23
34	CDKAL1
35	CEBPZ
36	CHD8
37	CLDN6
38	CNIH1
39	COPB1
40	COPG1
41	COPS3
42	COX4I1
43	COX5A
44	COX5B
45	CRABP2
46	CSTB
47	CTNNB1
48	CXADR
49	DARS1
50	DCAF15
51	DDX18
52	DDX27
53	DDX5
54	DEGS1
55	DHX15
56	DHX36
57	DLST
58	DMAC2
59	DPM1
60	DPPA4
61	DYNLL1
62	EARS2
63	EEF1E1
64	EEF2
65	EIF1
66	EIF2A
67	EIF2S1
68	EIF3E
69	EIF3H
70	EIF3K
71	EIF3L
72	EIF4A1
73	EIF4E
74	EMC4
75	EMG1
76	ENO1
77	EPB41L2
78	ERLIN2
79	EXOSC10
80	EXOSC3
81	FAM98A
82	FARSB
83	FASN
84	FASTKD5
85	FKBP1A
86	FLNA
87	FSCN1
88	FTO
89	FXYD5
90	G3BP1
91	G3BP2
92	GADD45GIP1
93	GARS1
94	GFM1
95	GHITM
96	GINS1
97	GLYR1
98	GMNN
99	GNG5
100	GPX1
101	GSTP1
102	GTF3C1
103	GTPBP4
104	H1-10
105	H1-2
106	H1-4
107	H1-5
108	H2AC12
109	H2AC14
110	H2AC20
111	H2AC7
112	H2AX
113	H2BC12
114	H2BC13
115	H2BC14
116	H2BC5
117	H2BC7
118	H2BC8
119	H2BC9
120	H3C1
121	H3C11
122	H3C2
123	H3C4
124	H3C7
125	H3C8
126	H4C3
127	H4C9
128	HADHB
129	HMGN1
130	HMGN2
131	HNRNPDL
132	HNRNPU
133	HSD17B12
134	HSD17B4
135	HSPA8
136	HSPA9
137	IARS1
138	ID3
139	IDH1
140	IGFBP2
141	ILF2
142	KARS1
143	KDM5B
144	KHDRBS1
145	KLF10
146	L1TD1
147	LARP7
148	LDHA
149	LIN28A
150	LONP1
151	LRPPRC
152	LSM3
153	LUC7L2
154	MACROH2A1
155	MALSU1
156	MARCKSL1
157	MARS1
158	MAT2A
159	MED29
160	MGST1
161	MRM3
162	MRPL18
163	MRPL27
164	MRPL34
165	MRPL58
166	MRPS14
167	MRPS18A
168	MRPS18C
169	MRPS2
170	MRPS25
171	MRPS27
172	MRPS28
173	MRPS30
174	MRPS35
175	MRPS9
176	MSH2
177	MTHFD1L
178	MYADM
179	MYL12A
180	NACA2
181	NAP1L4
182	NAT10
183	NCKAP1
184	NCL
185	NDUFA4
186	NDUFB2
187	NDUFB3
188	NDUFB6
189	NDUFS6
190	NELFA
191	NELFE
192	NIPSNAP1
193	NME4
194	NOB1
195	NOP16
196	NUP107
197	NVL
198	PABPC1
199	PCNA
200	PEF1
201	PELP1
202	PEX19
203	PFAS
204	PFDN4
205	PFN2
206	PLD3
207	PLK1
208	PMF1
209	PNPT1
210	PPA1
211	PPA2
212	PPM1G
213	PPT1
214	PRDX3
215	PRDX6
216	PSAP
217	PSMB3
218	PSMB5
219	PSMB7
220	PSMG2
221	PTCD3
222	RAB11A
223	RAB1A
224	RAB8A
225	RAC1
226	RACK1
227	RAD23B
228	RANBP2
229	RANGAP1
230	REEP5
231	RPA3
232	RPL11
233	RPL13
234	RPL19
235	RPL23
236	RPL32
237	RPL4
238	RPN1
239	RPS12
240	RPS13
241	RPS15A
242	RPS16
243	RPS17
244	RPS21
245	RPS27L
246	RRBP1
247	RRM1
248	RRM2
249	RRP36
250	RRP7A
251	RSL24D1
252	RUVBL2
253	SAFB
254	SARNP
255	SEC13
256	SELENOF
257	SERPINH1
258	SF3A1
259	SF3A2
260	SF3B1
261	SF3B4
262	SFPQ
263	SHMT2
264	SLC29A1
265	SLC39A14
266	SLIRP
267	SMC4
268	SMU1
269	SNRNP200
270	SNW1
271	SPAG7
272	SPATS2L
273	SPIN4
274	SQSTM1
275	SRP14
276	SRP54
277	SRP68
278	SRRT
279	SRSF1
280	SRSF10
281	SSB
282	SSR3
283	STRAP
284	STT3A
285	SUB1
286	SUCLG1
287	SUMO2
288	SUPT4H1
289	SYNCRIP
290	TIMM50
291	TMEM11
292	TMEM126A
293	TMX2
294	TOMM22
295	TOMM6
296	TOMM7
297	TOP2A
298	TPX2
299	TRAP1
300	TRIR
301	TRMT112
302	TSR1
303	TUBA1B
304	TUBB2A
305	TXNDC17
306	TXNDC5
307	U2SURP
308	UBE2C
309	UBE2E3
310	UBE2V2
311	UBQLN2
312	UFC1
313	UQCR11
314	UQCRB
315	VCL
316	WDR43
317	XPNPEP1
318	YAE1
319	YTHDF3
320	ZIC3
321	ZNF24
322	ZNRD2
323	ZRANB2

References

1 Collart, M. A. & Weiss, B. Ribosome pausing, a dangerous necessity for co-translational events. *Nucleic Acids Res* 48, 1043-1055, doi:10.1093/nar/gkz763 (2020).
2 de Sousa Abreu, R., Penalva, L. O., Marcotte, E. M. & Vogel, C. Global signatures of protein and mRNA expression levels. *Mol Biosyst* 5, 1512-1526, doi:10.1039/b908315d (2009).
3 Schwanhausser, B. *et al.* Global quantification of mammalian gene expression control. *Nature* 473, 337-342, doi:10.1038/nature10098 (2011).
4 Kristensen, A. R., Gsponer, J. & Foster, L. J. Protein synthesis rate is the predominant regulator of protein expression during differentiation. *Mol Syst Biol* 9, 689, doi:10.1038/msb.2013.47 (2013).
5 Liu, Y., Beyer, A. & Aebersold, R. On the Dependency of Cellular Protein Levels on mRNA Abundance. *Cell* 165, 535-550, doi:10.1016/j.cell.2016.03.014 (2016).
6 Maier, T., Guell, M. & Serrano, L. Correlation of mRNA and protein in complex biological samples. *FEBS Lett* 583, 3966-3973, doi:10.1016/j.febslet.2009.10.036 (2009).
7 Fujii, K., Shi, Z., Zhulyn, O., Denans, N. & Barna, M. Pervasive translational regulation of the cell signalling circuitry underlies mammalian development. *Nat Commun* 8, 14443, doi:10.1038/ncomms14443 (2017).
8 Gabut, M., Bourdelais, F. & Durand, S. Ribosome and Translational Control in Stem Cells. *Cells* 9, doi:10.3390/cells9020497 (2020).
9 Rodrigues, D. C. *et al.* Shifts in Ribosome Engagement Impact Key Gene Sets in Neurodevelopment and Ubiquitination in Rett Syndrome. *Cell Rep* 30, 4179-4196 e4111, doi:10.1016/j.celrep.2020.02.107 (2020).
10 Tahmasebi, S., Amiri, M. & Sonenberg, N. Translational Control in Stem Cells. *Front Genet* 9, 709, doi:10.3389/fgene.2018.00709 (2018).
11 Bekker-Jensen, D. B. *et al.* An Optimized Shotgun Strategy for the Rapid Generation of Comprehensive Human Proteomes. *Cell Syst* 4, 587-599 e584, doi:10.1016/j.cels.2017.05.009 (2017).
12 Kulak, N. A., Geyer, P. E. & Mann, M. Loss-less Nano-fractionator for High Sensitivity, High Coverage Proteomics. *Mol Cell Proteomics* 16, 694-705, doi:10.1074/mcp.O116.065136 (2017).
13 Uhlen, M. *et al.* Proteomics. Tissue-based map of the human proteome. *Science* 347, 1260419, doi:10.1126/science.1260419 (2015).
14 Wilhelm, M. *et al.* Mass-spectrometry-based draft of the human proteome. *Nature* 509, 582-587, doi:10.1038/nature13319 (2014).
15 Balch, W. E., Morimoto, R. I., Dillin, A. & Kelly, J. W. Adapting proteostasis for disease intervention. *Science* 319, 916-919, doi:10.1126/science.1141448 (2008).
16 Balchin, D., Hayer-Hartl, M. & Hartl, F. U. In vivo aspects of protein folding and quality control. *Science* 353, aac4354, doi:10.1126/science.aac4354 (2016).
17 Klaips, C. L., Jayaraj, G. G. & Hartl, F. U. Pathways of cellular proteostasis in aging and disease. *J Cell Biol* 217, 51-63, doi:10.1083/jcb.201709072 (2018).
18 Taylor, R. C. & Dillin, A. Aging as an event of proteostasis collapse. *Cold Spring Harb Perspect Biol* 3, doi:10.1101/cshperspect.a004440 (2011).
19 Labbadia, J. & Morimoto, R. I. The biology of proteostasis in aging and disease. *Annu Rev Biochem* 84, 435-464, doi:10.1146/annurev-biochem-060614-033955 (2015).
20 Higuchi-Sanabria, R., Frankino, P. A., Paul, J. W., 3rd, Tronnes, S. U. & Dillin, A. A Futile Battle? Protein Quality Control and the Stress of Aging. *Dev Cell* 44, 139-163, doi:10.1016/j.devcel.2017.12.020 (2018).
21 Jayaraj, G. G., Hipp, M. S. & Hartl, F. U. Functional Modules of the Proteostasis Network. *Cold Spring Harb Perspect Biol* 12, doi:10.1101/cshperspect.a033951 (2020).
22 Hetz, C., Chevet, E. & Oakes, S. A. Proteostasis control by the unfolded protein response. *Nat Cell Biol* 17, 829-838, doi:10.1038/ncb3184 (2015).
23 Moehle, E. A., Shen, K. & Dillin, A. Mitochondrial proteostasis in the context of cellular and organismal health and aging. *J Biol Chem* 294, 5396-5407, doi:10.1074/jbc.TM117.000893 (2019).
24 Holtkamp, W. *et al.* Cotranslational protein folding on the ribosome monitored in real time. *Science* 350, 1104-1107, doi:10.1126/science.aad0344 (2015).
25 Nilsson, O. B. *et al.* Cotranslational Protein Folding inside the Ribosome Exit Tunnel. *Cell Rep* 12, 1533-1540, doi:10.1016/j.celrep.2015.07.065 (2015).
26 Kim, Y. E., Hipp, M. S., Bracher, A., Hayer-Hartl, M. & Hartl, F. U. Molecular chaperone functions in protein folding and proteostasis. *Annu Rev Biochem* 82, 323-355, doi:10.1146/annurev-biochem-060208-092442 (2013).
27 Hartl, F. U. Molecular chaperones in cellular protein folding. *Nature* 381, 571-579, doi:10.1038/381571a0 (1996).
28 Brehme, M. & Voisine, C. Model systems of protein-misfolding diseases reveal chaperone modifiers of proteotoxicity. *Dis Model Mech* 9, 823-838, doi:10.1242/dmm.024703 (2016).

29 Brehme, M. *et al.* A chaperome subnetwork safeguards proteostasis in aging and neurodegenerative disease. *Cell Rep* 9, 1135-1150, doi:10.1016/j.celrep.2014.09.042 (2014).
30 Gong, Y. *et al.* An atlas of chaperone-protein interactions in Saccharomyces cerevisiae: implications to protein folding pathways in the cell. *Mol Syst Biol* 5, 275, doi:10.1038/msb.2009.26 (2009).
31 O'Brien, D. & van Oosten-Hawle, P. Regulation of cell-non-autonomous proteostasis in metazoans. *Essays Biochem* 60, 133-142, doi:10.1042/EBC20160006 (2016).
32 Forster, F., Unverdorben, P., Sledz, P. & Baumeister, W. Unveiling the long-held secrets of the 26S proteasome. *Structure* 21, 1551-1562, doi:10.1016/j.str.2013.08.010 (2013).
33 Cohen-Kaplan, V., Livneh, I., Avni, N., Cohen-Rosenzweig, C. & Ciechanover, A. The ubiquitin-proteasome system and autophagy: Coordinated and independent activities. *Int J Biochem Cell Biol* 79, 403-418, doi:10.1016/j.biocel.2016.07.019 (2016).
34 Dikic, I. Proteasomal and Autophagic Degradation Systems. *Annu Rev Biochem* 86, 193-224, doi:10.1146/annurev-biochem-061516-044908 (2017).
35 Varshavsky, A. The Ubiquitin System, Autophagy, and Regulated Protein Degradation. *Annu Rev Biochem* 86, 123-128, doi:10.1146/annurev-biochem-061516-044859 (2017).
36 Zhao, J., Zhai, B., Gygi, S. P. & Goldberg, A. L. mTOR inhibition activates overall protein degradation by the ubiquitin proteasome system as well as by autophagy. *Proc Natl Acad Sci U S A* 112, 15790-15797, doi:10.1073/pnas.1521919112 (2015).
37 Collins, G. A. & Goldberg, A. L. The Logic of the 26S Proteasome. *Cell* 169, 792-806, doi:10.1016/j.cell.2017.04.023 (2017).
38 Finley, D. Recognition and processing of ubiquitin-protein conjugates by the proteasome. *Annu Rev Biochem* 78, 477-513, doi:10.1146/annurev.biochem.78.081507.101607 (2009).
39 Zheng, N. & Shabek, N. Ubiquitin Ligases: Structure, Function, and Regulation. *Annu Rev Biochem* 86, 129-157, doi:10.1146/annurev-biochem-060815-014922 (2017).
40 Bhattacharyya, S., Yu, H., Mim, C. & Matouschek, A. Regulated protein turnover: snapshots of the proteasome in action. *Nat Rev Mol Cell Biol* 15, 122-133, doi:10.1038/nrm3741 (2014).
41 de la Pena, A. H., Goodall, E. A., Gates, S. N., Lander, G. C. & Martin, A. Substrate-engaged 26S proteasome structures reveal mechanisms for ATP-hydrolysis-driven translocation. *Science* 362, doi:10.1126/science.aav0725 (2018).
42 Dong, Y. *et al.* Cryo-EM structures and dynamics of substrate-engaged human 26S proteasome. *Nature* 565, 49-55, doi:10.1038/s41586-018-0736-4 (2019).
43 Beck, F. *et al.* Near-atomic resolution structural model of the yeast 26S proteasome. *Proc Natl Acad Sci U S A* 109, 14870-14875, doi:10.1073/pnas.1213333109 (2012).
44 Esser, C., Alberti, S. & Hohfeld, J. Cooperation of molecular chaperones with the ubiquitin/proteasome system. *Biochim Biophys Acta* 1695, 171-188, doi:10.1016/j.bbamcr.2004.09.020 (2004).
45 Carra, S., Seguin, S. J., Lambert, H. & Landry, J. HspB8 chaperone activity toward poly(Q)-containing proteins depends on its association with Bag3, a stimulator of macroautophagy. *J Biol Chem* 283, 1437-1444, doi:10.1074/jbc.M706304200 (2008).
46 Gamerdinger, M. *et al.* Protein quality control during aging involves recruitment of the macroautophagy pathway by BAG3. *EMBO J* 28, 889-901, doi:10.1038/emboj.2009.29 (2009).
47 Arndt, V. *et al.* Chaperone-assisted selective autophagy is essential for muscle maintenance. *Curr Biol* 20, 143-148, doi:10.1016/j.cub.2009.11.022 (2010).
48 Galluzzi, L. *et al.* Molecular definitions of autophagy and related processes. *EMBO J* 36, 1811-1836, doi:10.15252/embj.201796697 (2017).
49 Suraweera, A., Munch, C., Hanssum, A. & Bertolotti, A. Failure of amino acid homeostasis causes cell death following proteasome inhibition. *Mol Cell* 48, 242-253, doi:10.1016/j.molcel.2012.08.003 (2012).
50 Wilson, D. N. & Doudna Cate, J. H. The structure and function of the eukaryotic ribosome. *Cold Spring Harb Perspect Biol* 4, doi:10.1101/cshperspect.a011536 (2012).
51 Yoshihama, M. *et al.* The human ribosomal protein genes: sequencing and comparative analysis of 73 genes. *Genome Res* 12, 379-390, doi:10.1101/gr.214202 (2002).
52 Milo, R. What is the total number of protein molecules per cell volume? A call to rethink some published values. *Bioessays* 35, 1050-1055, doi:10.1002/bies.201300066 (2013).
53 Ingolia, N. T., Lareau, L. F. & Weissman, J. S. Ribosome profiling of mouse embryonic stem cells reveals the complexity and dynamics of mammalian proteomes. *Cell* 147, 789-802, doi:10.1016/j.cell.2011.10.002 (2011).
54 Plescia, O. J., Palczuk, N. C., Cora-Figueroa, E., Mukherjee, A. & Braun, W. Production of antibodies to soluble RNA (sRNA). *Proc Natl Acad Sci U S A* 54, 1281-1285, doi:10.1073/pnas.54.4.1281 (1965).
55 Crick, F. H. The origin of the genetic code. *J Mol Biol* 38, 367-379, doi:10.1016/0022-2836(68)90392-6 (1968).
56 Schimmel, P. The emerging complexity of the tRNA world: mammalian tRNAs beyond protein synthesis. *Nat Rev Mol Cell Biol* 19, 45-58, doi:10.1038/nrm.2017.77 (2018).
57 Yusupov, M. M. *et al.* Crystal structure of the ribosome at 5.5 A resolution. *Science* 292, 883-896, doi:10.1126/science.1060089 (2001).
58 Selmer, M. *et al.* Structure of the 70S ribosome complexed with mRNA and tRNA. *Science* 313, 1935-1942, doi:10.1126/science.1131127 (2006).

59 Wilson, D. N. & Beckmann, R. The ribosomal tunnel as a functional environment for nascent polypeptide folding and translational stalling. *Curr Opin Struct Biol* 21, 274-282, doi:10.1016/j.sbi.2011.01.007 (2011).

60 Gautschi, M., Mun, A., Ross, S. & Rospert, S. A functional chaperone triad on the yeast ribosome. *Proc Natl Acad Sci U S A* 99, 4209-4214, doi:10.1073/pnas.062048599 (2002).

61 Merrick, W. C. & Pavitt, G. D. Protein Synthesis Initiation in Eukaryotic Cells. *Cold Spring Harb Perspect Biol* 10, doi:10.1101/cshperspect.a033092 (2018).

62 Erdmann-Pham, D. D., Dao Duc, K. & Song, Y. S. The Key Parameters that Govern Translation Efficiency. *Cell Syst* 10, 183-192 e186, doi:10.1016/j.cels.2019.12.003 (2020).

63 Altmann, M. & Linder, P. Power of yeast for analysis of eukaryotic translation initiation. *J Biol Chem* 285, 31907-31912, doi:10.1074/jbc.R110.144196 (2010).

64 Rowlands, A. G., Panniers, R. & Henshaw, E. C. The catalytic mechanism of guanine nucleotide exchange factor action and competitive inhibition by phosphorylated eukaryotic initiation factor 2. *J Biol Chem* 263, 5526-5533 (1988).

65 Erickson, F. L. & Hannig, E. M. Ligand interactions with eukaryotic translation initiation factor 2: role of the gamma-subunit. *EMBO J* 15, 6311-6320 (1996).

66 Pisarev, A. V., Hellen, C. U. & Pestova, T. V. Recycling of eukaryotic posttermination ribosomal complexes. *Cell* 131, 286-299, doi:10.1016/j.cell.2007.08.041 (2007).

67 Asano, K., Clayton, J., Shalev, A. & Hinnebusch, A. G. A multifactor complex of eukaryotic initiation factors, eIF1, eIF2, eIF3, eIF5, and initiator tRNA(Met) is an important translation initiation intermediate in vivo. *Genes Dev* 14, 2534-2546, doi:10.1101/gad.831800 (2000).

68 Sokabe, M., Fraser, C. S. & Hershey, J. W. The human translation initiation multi-factor complex promotes methionyl-tRNAi binding to the 40S ribosomal subunit. *Nucleic Acids Res* 40, 905-913, doi:10.1093/nar/gkr772 (2012).

69 Jackson, R. J., Hellen, C. U. & Pestova, T. V. The mechanism of eukaryotic translation initiation and principles of its regulation. *Nat Rev Mol Cell Biol* 11, 113-127, doi:10.1038/nrm2838 (2010).

70 Kumar, P., Hellen, C. U. & Pestova, T. V. Toward the mechanism of eIF4F-mediated ribosomal attachment to mammalian capped mRNAs. *Genes Dev* 30, 1573-1588, doi:10.1101/gad.282418.116 (2016).

71 Villa, N., Do, A., Hershey, J. W. & Fraser, C. S. Human eukaryotic initiation factor 4G (eIF4G) protein binds to eIF3c, -d, and -e to promote mRNA recruitment to the ribosome. *J Biol Chem* 288, 32932-32940, doi:10.1074/jbc.M113.517011 (2013).

72 Kozak, M. An analysis of 5'-noncoding sequences from 699 vertebrate messenger RNAs. *Nucleic Acids Res* 15, 8125-8148, doi:10.1093/nar/15.20.8125 (1987).

73 Ivanov, I. P., Loughran, G., Sachs, M. S. & Atkins, J. F. Initiation context modulates autoregulation of eukaryotic translation initiation factor 1 (eIF1). *Proc Natl Acad Sci U S A* 107, 18056-18060, doi:10.1073/pnas.1009269107 (2010).

74 Martin-Marcos, P., Cheung, Y. N. & Hinnebusch, A. G. Functional elements in initiation factors 1, 1A, and 2beta discriminate against poor AUG context and non-AUG start codons. *Mol Cell Biol* 31, 4814-4831, doi:10.1128/MCB.05819-11 (2011).

75 Loughran, G., Sachs, M. S., Atkins, J. F. & Ivanov, I. P. Stringency of start codon selection modulates autoregulation of translation initiation factor eIF5. *Nucleic Acids Res* 40, 2898-2906, doi:10.1093/nar/gkr1192 (2012).

76 Hinnebusch, A. G., Ivanov, I. P. & Sonenberg, N. Translational control by 5'-untranslated regions of eukaryotic mRNAs. *Science* 352, 1413-1416, doi:10.1126/science.aad9868 (2016).

77 Slusher, L. B., Gillman, E. C., Martin, N. C. & Hopper, A. K. mRNA leader length and initiation codon context determine alternative AUG selection for the yeast gene MOD5. *Proc Natl Acad Sci U S A* 88, 9789-9793, doi:10.1073/pnas.88.21.9789 (1991).

78 Algire, M. A., Maag, D. & Lorsch, J. R. Pi release from eIF2, not GTP hydrolysis, is the step controlled by start-site selection during eukaryotic translation initiation. *Mol Cell* 20, 251-262, doi:10.1016/j.molcel.2005.09.008 (2005).

79 Majumdar, R. & Maitra, U. Regulation of GTP hydrolysis prior to ribosomal AUG selection during eukaryotic translation initiation. *EMBO J* 24, 3737-3746, doi:10.1038/sj.emboj.7600844 (2005).

80 Yamamoto, H. *et al.* Structure of the mammalian 80S initiation complex with initiation factor 5B on HCV-IRES RNA. *Nat Struct Mol Biol* 21, 721-727, doi:10.1038/nsmb.2859 (2014).

81 Wang, J. *et al.* eIF5B gates the transition from translation initiation to elongation. *Nature* 573, 605-608, doi:10.1038/s41586-019-1561-0 (2019).

82 Ogle, J. M. *et al.* Recognition of cognate transfer RNA by the 30S ribosomal subunit. *Science* 292, 897-902, doi:10.1126/science.1060612 (2001).

83 Shao, S. *et al.* Decoding Mammalian Ribosome-mRNA States by Translational GTPase Complexes. *Cell* 167, 1229-1240 e1215, doi:10.1016/j.cell.2016.10.046 (2016).

84 Loveland, A. B., Demo, G., Grigorieff, N. & Korostelev, A. A. Ensemble cryo-EM elucidates the mechanism of translation fidelity. *Nature* 546, 113-117, doi:10.1038/nature22397 (2017).

85 Moazed, D. & Noller, H. F. Intermediate states in the movement of transfer RNA in the ribosome. *Nature* 342, 142-148, doi:10.1038/342142a0 (1989).

86 Gutierrez, E. *et al.* eIF5A promotes translation of polyproline motifs. *Mol Cell* 51, 35-45, doi:10.1016/j.molcel.2013.04.021 (2013).
87 Melnikov, S. *et al.* Molecular insights into protein synthesis with proline residues. *EMBO Rep* 17, 1776-1784, doi:10.15252/embr.201642943 (2016).
88 Melnikov, S. *et al.* Crystal Structure of Hypusine-Containing Translation Factor eIF5A Bound to a Rotated Eukaryotic Ribosome. *J Mol Biol* 428, 3570-3576, doi:10.1016/j.jmb.2016.05.011 (2016).
89 Schmidt, C. *et al.* Structure of the hypusinylated eukaryotic translation factor eIF-5A bound to the ribosome. *Nucleic Acids Res* 44, 1944-1951, doi:10.1093/nar/gkv1517 (2016).
90 Shin, B. S. *et al.* Amino acid substrates impose polyamine, eIF5A, or hypusine requirement for peptide synthesis. *Nucleic Acids Res* 45, 8392-8402, doi:10.1093/nar/gkx532 (2017).
91 Spahn, C. M. *et al.* Domain movements of elongation factor eEF2 and the eukaryotic 80S ribosome facilitate tRNA translocation. *EMBO J* 23, 1008-1019, doi:10.1038/sj.emboj.7600102 (2004).
92 Taylor, D. J. *et al.* Structures of modified eEF2 80S ribosome complexes reveal the role of GTP hydrolysis in translocation. *EMBO J* 26, 2421-2431, doi:10.1038/sj.emboj.7601677 (2007).
93 Abeyrathne, P. D., Koh, C. S., Grant, T., Grigorieff, N. & Korostelev, A. A. Ensemble cryo-EM uncovers inchworm-like translocation of a viral IRES through the ribosome. *Elife* 5, doi:10.7554/eLife.14874 (2016).
94 Murray, J. *et al.* Structural characterization of ribosome recruitment and translocation by type IV IRES. *Elife* 5, doi:10.7554/eLife.13567 (2016).
95 Budkevich, T. *et al.* Structure and dynamics of the mammalian ribosomal pretranslocation complex. *Mol Cell* 44, 214-224, doi:10.1016/j.molcel.2011.07.040 (2011).
96 Behrmann, E. *et al.* Structural snapshots of actively translating human ribosomes. *Cell* 161, 845-857, doi:10.1016/j.cell.2015.03.052 (2015).
97 Atkinson, G. C., Baldauf, S. L. & Hauryliuk, V. Evolution of nonstop, no-go and nonsense-mediated mRNA decay and their termination factor-derived components. *BMC Evol Biol* 8, 290, doi:10.1186/1471-2148-8-290 (2008).
98 Pisareva, V. P., Skabkin, M. A., Hellen, C. U., Pestova, T. V. & Pisarev, A. V. Dissociation by Pelota, Hbs1 and ABCE1 of mammalian vacant 80S ribosomes and stalled elongation complexes. *EMBO J* 30, 1804-1817, doi:10.1038/emboj.2011.93 (2011).
99 Dever, T. E. & Green, R. The elongation, termination, and recycling phases of translation in eukaryotes. *Cold Spring Harb Perspect Biol* 4, a013706, doi:10.1101/cshperspect.a013706 (2012).
100 Nierhaus, K. H. The allosteric three-site model for the ribosomal elongation cycle: features and future. *Biochemistry* 29, 4997-5008, doi:10.1021/bi00473a001 (1990).
101 Bertram, G., Bell, H. A., Ritchie, D. W., Fullerton, G. & Stansfield, I. Terminating eukaryote translation: domain 1 of release factor eRF1 functions in stop codon recognition. *RNA* 6, 1236-1247, doi:10.1017/s1355838200000777 (2000).
102 Song, H. *et al.* The crystal structure of human eukaryotic release factor eRF1--mechanism of stop codon recognition and peptidyl-tRNA hydrolysis. *Cell* 100, 311-321, doi:10.1016/s0092-8674(00)80667-4 (2000).
103 Wada, M. & Ito, K. A genetic approach for analyzing the co-operative function of the tRNA mimicry complex, eRF1/eRF3, in translation termination on the ribosome. *Nucleic Acids Res* 42, 7851-7866, doi:10.1093/nar/gku493 (2014).
104 Frolova, L. *et al.* Eukaryotic polypeptide chain release factor eRF3 is an eRF1- and ribosome-dependent guanosine triphosphatase. *RNA* 2, 334-341 (1996).
105 Kononenko, A. V. *et al.* Role of the individual domains of translation termination factor eRF1 in GTP binding to eRF3. *Proteins* 70, 388-393, doi:10.1002/prot.21544 (2008).
106 Mantsyzov, A. B. *et al.* NMR solution structure and function of the C-terminal domain of eukaryotic class 1 polypeptide chain release factor. *FEBS J* 277, 2611-2627, doi:10.1111/j.1742-464X.2010.07672.x (2010).
107 Rees, D. C., Johnson, E. & Lewinson, O. ABC transporters: the power to change. *Nat Rev Mol Cell Biol* 10, 218-227, doi:10.1038/nrm2646 (2009).
108 Becker, T. *et al.* Structural basis of highly conserved ribosome recycling in eukaryotes and archaea. *Nature* 482, 501-506, doi:10.1038/nature10829 (2012).
109 Shoemaker, C. J. & Green, R. Translation drives mRNA quality control. *Nat Struct Mol Biol* 19, 594-601, doi:10.1038/nsmb.2301 (2012).
110 des Georges, A. *et al.* Structure of mammalian eIF3 in the context of the 43S preinitiation complex. *Nature* 525, 491-495, doi:10.1038/nature14891 (2015).
111 Lomakin, I. B., Shirokikh, N. E., Yusupov, M. M., Hellen, C. U. & Pestova, T. V. The fidelity of translation initiation: reciprocal activities of eIF1, IF3 and YciH. *EMBO J* 25, 196-210, doi:10.1038/sj.emboj.7600904 (2006).
112 Skabkin, M. A. *et al.* Activities of Ligatin and MCT-1/DENR in eukaryotic translation initiation and ribosomal recycling. *Genes Dev* 24, 1787-1801, doi:10.1101/gad.1957510 (2010).
113 Tempel, W., Dimov, S., Tong, Y., Park, H. W. & Hong, B. S. Crystal structure of human multiple copies in T-cell lymphoma-1 oncoprotein. *Proteins* 81, 519-525, doi:10.1002/prot.24198 (2013).

114 Vaidya, A. T., Lomakin, I. B., Joseph, N. N., Dmitriev, S. E. & Steitz, T. A. Crystal Structure of the C-terminal Domain of Human eIF2D and Its Implications on Eukaryotic Translation Initiation. *J Mol Biol* 429, 2765-2771, doi:10.1016/j.jmb.2017.07.015 (2017).

115 Weisser, M. *et al.* Structural and Functional Insights into Human Re-initiation Complexes. *Mol Cell* 67, 447-456 e447, doi:10.1016/j.molcel.2017.06.032 (2017).

116 Johnstone, T. G., Bazzini, A. A. & Giraldez, A. J. Upstream ORFs are prevalent translational repressors in vertebrates. *EMBO J* 35, 706-723, doi:10.15252/embj.201592759 (2016).

117 Bohlen, J., Fenzl, K., Kramer, G., Bukau, B. & Teleman, A. A. Selective 40S Footprinting Reveals Cap-Tethered Ribosome Scanning in Human Cells. *Mol Cell* 79, 561-574 e565, doi:10.1016/j.molcel.2020.06.005 (2020).

118 Hinnebusch, A. G. The scanning mechanism of eukaryotic translation initiation. *Annu Rev Biochem* 83, 779-812, doi:10.1146/annurev-biochem-060713-035802 (2014).

119 Pakos-Zebrucka, K. *et al.* The integrated stress response. *EMBO Rep* 17, 1374-1395, doi:10.15252/embr.201642195 (2016).

120 Schleich, S. *et al.* DENR-MCT-1 promotes translation re-initiation downstream of uORFs to control tissue growth. *Nature* 512, 208-212, doi:10.1038/nature13401 (2014).

121 Morris, D. R. & Geballe, A. P. Upstream open reading frames as regulators of mRNA translation. *Mol Cell Biol* 20, 8635-8642, doi:10.1128/MCB.20.23.8635-8642.2000 (2000).

122 Luukkonen, B. G., Tan, W. & Schwartz, S. Efficiency of reinitiation of translation on human immunodeficiency virus type 1 mRNAs is determined by the length of the upstream open reading frame and by intercistronic distance. *J Virol* 69, 4086-4094, doi:10.1128/JVI.69.7.4086-4094.1995 (1995).

123 Kozak, M. Constraints on reinitiation of translation in mammals. *Nucleic Acids Res* 29, 5226-5232, doi:10.1093/nar/29.24.5226 (2001).

124 Carvunis, A. R. *et al.* Proto-genes and de novo gene birth. *Nature* 487, 370-374, doi:10.1038/nature11184 (2012).

125 Poyry, T. A., Kaminski, A. & Jackson, R. J. What determines whether mammalian ribosomes resume scanning after translation of a short upstream open reading frame? *Genes Dev* 18, 62-75, doi:10.1101/gad.276504 (2004).

126 Hinnebusch, A. G. Translational regulation of GCN4 and the general amino acid control of yeast. *Annu Rev Microbiol* 59, 407-450, doi:10.1146/annurev.micro.59.031805.133833 (2005).

127 Skabkin, M. A., Skabkina, O. V., Hellen, C. U. & Pestova, T. V. Reinitiation and other unconventional posttermination events during eukaryotic translation. *Mol Cell* 51, 249-264, doi:10.1016/j.molcel.2013.05.026 (2013).

128 Schleich, S., Acevedo, J. M., Clemm von Hohenberg, K. & Teleman, A. A. Identification of transcripts with short stuORFs as targets for DENR*MCTS1-dependent translation in human cells. *Sci Rep* 7, 3722, doi:10.1038/s41598-017-03949-6 (2017).

129 Young, D. J. *et al.* Tma64/eIF2D, Tma20/MCT-1, and Tma22/DENR Recycle Post-termination 40S Subunits In Vivo. *Mol Cell* 71, 761-774 e765, doi:10.1016/j.molcel.2018.07.028 (2018).

130 Young, D. J., Meydan, S. & Guydosh, N. R. 40S ribosome profiling reveals distinct roles for Tma20/Tma22 (MCT-1/DENR) and Tma64 (eIF2D) in 40S subunit recycling. *Nat Commun* 12, 2976, doi:10.1038/s41467-021-23223-8 (2021).

131 Green, K. M., Miller, S. L., Malik, I. & Todd, P. K. Non-canonical initiation factors modulate repeat-associated non-AUG translation. *Hum Mol Genet*, doi:10.1093/hmg/ddac021 (2022).

132 Genuth, N. R. & Barna, M. The Discovery of Ribosome Heterogeneity and Its Implications for Gene Regulation and Organismal Life. *Mol Cell* 71, 364-374, doi:10.1016/j.molcel.2018.07.018 (2018).

133 Draptchinskaia, N. *et al.* The gene encoding ribosomal protein S19 is mutated in Diamond-Blackfan anaemia. *Nat Genet* 21, 169-175, doi:10.1038/5951 (1999).

134 Gupta, V. & Warner, J. R. Ribosome-omics of the human ribosome. *RNA* 20, 1004-1013, doi:10.1261/rna.043653.113 (2014).

135 Wong, Q. W. *et al.* RPL39L is an example of a recently evolved ribosomal protein paralog that shows highly specific tissue expression patterns and is upregulated in ESCs and HCC tumors. *RNA Biol* 11, 33-41, doi:10.4161/rna.27427 (2014).

136 O'Leary, M. N. *et al.* The ribosomal protein Rpl22 controls ribosome composition by directly repressing expression of its own paralog, Rpl22l1. *PLoS Genet* 9, e1003708, doi:10.1371/journal.pgen.1003708 (2013).

137 Fahl, S. P., Wang, M., Zhang, Y., Duc, A. C. & Wiest, D. L. Regulatory Roles of Rpl22 in Hematopoiesis: An Old Dog with New Tricks. *Crit Rev Immunol* 35, 379-400, doi:10.1615/critrevimmunol.v35.i5.30 (2015).

138 Fahl, S. P., Harris, B., Coffey, F. & Wiest, D. L. Rpl22 Loss Impairs the Development of B Lymphocytes by Activating a p53-Dependent Checkpoint. *J Immunol* 194, 200-209, doi:10.4049/jimmunol.1402242 (2015).

139 Milenkovic, I. *et al.* RPL3L-containing ribosomes modulate mitochondrial activity in the mammalian heart. *BiorXiv*, doi:https://doi.org/10.1101/2021.12.04.471171 (2021).

140 Landon, A. L. *et al.* MNKs act as a regulatory switch for eIF4E1 and eIF4E3 driven mRNA translation in DLBCL. *Nat Commun* 5, 5413, doi:10.1038/ncomms6413 (2014).

141 Joshi, B., Cameron, A. & Jagus, R. Characterization of mammalian eIF4E-family members. *Eur J Biochem* 271, 2189-2203, doi:10.1111/j.1432-1033.2004.04149.x (2004).
142 Hernandez, G. & Vazquez-Pianzola, P. Functional diversity of the eukaryotic translation initiation factors belonging to eIF4 families. *Mech Dev* 122, 865-876, doi:10.1016/j.mod.2005.04.002 (2005).
143 Sun, F., Palmer, K. & Handel, M. A. Mutation of Eif4g3, encoding a eukaryotic translation initiation factor, causes male infertility and meiotic arrest of mouse spermatocytes. *Development* 137, 1699-1707, doi:10.1242/dev.043125 (2010).
144 Morita, M. *et al.* A novel 4EHP-GIGYF2 translational repressor complex is essential for mammalian development. *Mol Cell Biol* 32, 3585-3593, doi:10.1128/MCB.00455-12 (2012).
145 Heck, A. M. & Wilusz, J. The Interplay between the RNA Decay and Translation Machinery in Eukaryotes. *Cold Spring Harb Perspect Biol* 10, doi:10.1101/cshperspect.a032839 (2018).
146 Doma, M. K. & Parker, R. Endonucleolytic cleavage of eukaryotic mRNAs with stalls in translation elongation. *Nature* 440, 561-564, doi:10.1038/nature04530 (2006).
147 Tsuboi, T. *et al.* Dom34:hbs1 plays a general role in quality-control systems by dissociation of a stalled ribosome at the 3' end of aberrant mRNA. *Mol Cell* 46, 518-529, doi:10.1016/j.molcel.2012.03.013 (2012).
148 Frischmeyer, P. A. *et al.* An mRNA surveillance mechanism that eliminates transcripts lacking termination codons. *Science* 295, 2258-2261, doi:10.1126/science.1067338 (2002).
149 Simms, C. L., Thomas, E. N. & Zaher, H. S. Ribosome-based quality control of mRNA and nascent peptides. *Wiley Interdiscip Rev RNA* 8, doi:10.1002/wrna.1366 (2017).
150 Passos, D. O. *et al.* Analysis of Dom34 and its function in no-go decay. *Mol Biol Cell* 20, 3025-3032, doi:10.1091/mbc.E09-01-0028 (2009).
151 Chen, L. *et al.* Structure of the Dom34-Hbs1 complex and implications for no-go decay. *Nat Struct Mol Biol* 17, 1233-1240, doi:10.1038/nsmb.1922 (2010).
152 Shoemaker, C. J., Eyler, D. E. & Green, R. Dom34:Hbs1 promotes subunit dissociation and peptidyl-tRNA drop-off to initiate no-go decay. *Science* 330, 369-372, doi:10.1126/science.1192430 (2010).
153 Shao, S., von der Malsburg, K. & Hegde, R. S. Listerin-dependent nascent protein ubiquitination relies on ribosome subunit dissociation. *Mol Cell* 50, 637-648, doi:10.1016/j.molcel.2013.04.015 (2013).
154 Verma, R., Oania, R. S., Kolawa, N. J. & Deshaies, R. J. Cdc48/p97 promotes degradation of aberrant nascent polypeptides bound to the ribosome. *Elife* 2, e00308, doi:10.7554/eLife.00308 (2013).
155 van den Elzen, A. M. *et al.* Dissection of Dom34-Hbs1 reveals independent functions in two RNA quality control pathways. *Nat Struct Mol Biol* 17, 1446-1452, doi:10.1038/nsmb.1963 (2010).
156 Kobayashi, K. *et al.* Structural basis for mRNA surveillance by archaeal Pelota and GTP-bound EF1alpha complex. *Proc Natl Acad Sci U S A* 107, 17575-17579, doi:10.1073/pnas.1009598107 (2010).
157 Carr-Schmid, A., Pfund, C., Craig, E. A. & Kinzy, T. G. Novel G-protein complex whose requirement is linked to the translational status of the cell. *Mol Cell Biol* 22, 2564-2574, doi:10.1128/MCB.22.8.2564-2574.2002 (2002).
158 Adham, I. M. *et al.* Disruption of the pelota gene causes early embryonic lethality and defects in cell cycle progression. *Mol Cell Biol* 23, 1470-1476, doi:10.1128/MCB.23.4.1470-1476.2003 (2003).
159 Nyamsuren, G. *et al.* Pelota regulates the development of extraembryonic endoderm through activation of bone morphogenetic protein (BMP) signaling. *Stem Cell Res* 13, 61-74, doi:10.1016/j.scr.2014.04.011 (2014).
160 Unterholzner, L. & Izaurralde, E. SMG7 acts as a molecular link between mRNA surveillance and mRNA decay. *Mol Cell* 16, 587-596, doi:10.1016/j.molcel.2004.10.013 (2004).
161 Gatfield, D. & Izaurralde, E. Nonsense-mediated messenger RNA decay is initiated by endonucleolytic cleavage in Drosophila. *Nature* 429, 575-578, doi:10.1038/nature02559 (2004).
162 Huntzinger, E., Kashima, I., Fauser, M., Sauliere, J. & Izaurralde, E. SMG6 is the catalytic endonuclease that cleaves mRNAs containing nonsense codons in metazoan. *RNA* 14, 2609-2617, doi:10.1261/rna.1386208 (2008).
163 Loh, B., Jonas, S. & Izaurralde, E. The SMG5-SMG7 heterodimer directly recruits the CCR4-NOT deadenylase complex to mRNAs containing nonsense codons via interaction with POP2. *Genes Dev* 27, 2125-2138, doi:10.1101/gad.226951.113 (2013).
164 Eberle, A. B., Lykke-Andersen, S., Muhlemann, O. & Jensen, T. H. SMG6 promotes endonucleolytic cleavage of nonsense mRNA in human cells. *Nat Struct Mol Biol* 16, 49-55, doi:10.1038/nsmb.1530 (2009).
165 Boehm, V., Haberman, N., Ottens, F., Ule, J. & Gehring, N. H. 3' UTR length and messenger ribonucleoprotein composition determine endocleavage efficiencies at termination codons. *Cell Rep* 9, 555-568, doi:10.1016/j.celrep.2014.09.012 (2014).
166 Lykke-Andersen, S. *et al.* Human nonsense-mediated RNA decay initiates widely by endonucleolysis and targets snoRNA host genes. *Genes Dev* 28, 2498-2517, doi:10.1101/gad.246538.114 (2014).
167 Schmidt, S. A. *et al.* Identification of SMG6 cleavage sites and a preferred RNA cleavage motif by global analysis of endogenous NMD targets in human cells. *Nucleic Acids Res* 43, 309-323, doi:10.1093/nar/gku1258 (2015).
168 Czaplinski, K. *et al.* The surveillance complex interacts with the translation release factors to enhance termination and degrade aberrant mRNAs. *Genes Dev* 12, 1665-1677, doi:10.1101/gad.12.11.1665 (1998).

169 Wang, W., Czaplinski, K., Rao, Y. & Peltz, S. W. The role of Upf proteins in modulating the translation read-through of nonsense-containing transcripts. *EMBO J* 20, 880-890, doi:10.1093/emboj/20.4.880 (2001).

170 Kashima, I. *et al.* Binding of a novel SMG-1-Upf1-eRF1-eRF3 complex (SURF) to the exon junction complex triggers Upf1 phosphorylation and nonsense-mediated mRNA decay. *Genes Dev* 20, 355-367, doi:10.1101/gad.1389006 (2006).

171 He, F. & Jacobson, A. Nonsense-Mediated mRNA Decay: Degradation of Defective Transcripts Is Only Part of the Story. *Annu Rev Genet* 49, 339-366, doi:10.1146/annurev-genet-112414-054639 (2015).

172 Amrani, N. *et al.* A faux 3'-UTR promotes aberrant termination and triggers nonsense-mediated mRNA decay. *Nature* 432, 112-118, doi:10.1038/nature03060 (2004).

173 Behm-Ansmant, I., Gatfield, D., Rehwinkel, J., Hilgers, V. & Izaurralde, E. A conserved role for cytoplasmic poly(A)-binding protein 1 (PABPC1) in nonsense-mediated mRNA decay. *EMBO J* 26, 1591-1601, doi:10.1038/sj.emboj.7601588 (2007).

174 Ivanov, P. V., Gehring, N. H., Kunz, J. B., Hentze, M. W. & Kulozik, A. E. Interactions between UPF1, eRFs, PABP and the exon junction complex suggest an integrated model for mammalian NMD pathways. *EMBO J* 27, 736-747, doi:10.1038/emboj.2008.17 (2008).

175 Silva, A. L., Ribeiro, P., Inacio, A., Liebhaber, S. A. & Romao, L. Proximity of the poly(A)-binding protein to a premature termination codon inhibits mammalian nonsense-mediated mRNA decay. *RNA* 14, 563-576, doi:10.1261/rna.815108 (2008).

176 Singh, G., Rebbapragada, I. & Lykke-Andersen, J. A competition between stimulators and antagonists of Upf complex recruitment governs human nonsense-mediated mRNA decay. *PLoS Biol* 6, e111, doi:10.1371/journal.pbio.0060111 (2008).

177 Serin, G., Gersappe, A., Black, J. D., Aronoff, R. & Maquat, L. E. Identification and characterization of human orthologues to Saccharomyces cerevisiae Upf2 protein and Upf3 protein (Caenorhabditis elegans SMG-4). *Mol Cell Biol* 21, 209-223, doi:10.1128/MCB.21.1.209-223.2001 (2001).

178 Chamieh, H., Ballut, L., Bonneau, F. & Le Hir, H. NMD factors UPF2 and UPF3 bridge UPF1 to the exon junction complex and stimulate its RNA helicase activity. *Nat Struct Mol Biol* 15, 85-93, doi:10.1038/nsmb1330 (2008).

179 Melero, R. *et al.* The cryo-EM structure of the UPF-EJC complex shows UPF1 poised toward the RNA 3' end. *Nat Struct Mol Biol* 19, 498-505, S491-492, doi:10.1038/nsmb.2287 (2012).

180 Yamashita, A. Role of SMG-1-mediated Upf1 phosphorylation in mammalian nonsense-mediated mRNA decay. *Genes Cells* 18, 161-175, doi:10.1111/gtc.12033 (2013).

181 Yamashita, A. *et al.* SMG-8 and SMG-9, two novel subunits of the SMG-1 complex, regulate remodeling of the mRNA surveillance complex during nonsense-mediated mRNA decay. *Genes Dev* 23, 1091-1105, doi:10.1101/gad.1767209 (2009).

182 Okada-Katsuhata, Y. *et al.* N- and C-terminal Upf1 phosphorylations create binding platforms for SMG-6 and SMG-5:SMG-7 during NMD. *Nucleic Acids Res* 40, 1251-1266, doi:10.1093/nar/gkr791 (2012).

183 Arias-Palomo, E. *et al.* The nonsense-mediated mRNA decay SMG-1 kinase is regulated by large-scale conformational changes controlled by SMG-8. *Genes Dev* 25, 153-164, doi:10.1101/gad.606911 (2011).

184 Fernandez, I. S. *et al.* Characterization of SMG-9, an essential component of the nonsense-mediated mRNA decay SMG1C complex. *Nucleic Acids Res* 39, 347-358, doi:10.1093/nar/gkq749 (2011).

185 Melero, R. *et al.* Structures of SMG1-UPFs complexes: SMG1 contributes to regulate UPF2-dependent activation of UPF1 in NMD. *Structure* 22, 1105-1119, doi:10.1016/j.str.2014.05.015 (2014).

186 Chakrabarti, S. *et al.* Molecular mechanisms for the RNA-dependent ATPase activity of Upf1 and its regulation by Upf2. *Mol Cell* 41, 693-703, doi:10.1016/j.molcel.2011.02.010 (2011).

187 Ghosh, S., Ganesan, R., Amrani, N. & Jacobson, A. Translational competence of ribosomes released from a premature termination codon is modulated by NMD factors. *RNA* 16, 1832-1847, doi:10.1261/rna.1987710 (2010).

188 Franks, T. M., Singh, G. & Lykke-Andersen, J. Upf1 ATPase-dependent mRNP disassembly is required for completion of nonsense- mediated mRNA decay. *Cell* 143, 938-950, doi:10.1016/j.cell.2010.11.043 (2010).

189 Bhattacharya, A. *et al.* Characterization of the biochemical properties of the human Upf1 gene product that is involved in nonsense-mediated mRNA decay. *RNA* 6, 1226-1235, doi:10.1017/s1355838200000546 (2000).

190 Cheng, Z., Muhlrad, D., Lim, M. K., Parker, R. & Song, H. Structural and functional insights into the human Upf1 helicase core. *EMBO J* 26, 253-264, doi:10.1038/sj.emboj.7601464 (2007).

191 Karousis, E. D. & Muhlemann, O. Nonsense-Mediated mRNA Decay Begins Where Translation Ends. *Cold Spring Harb Perspect Biol* 11, doi:10.1101/cshperspect.a032862 (2019).

192 Buhler, M., Steiner, S., Mohn, F., Paillusson, A. & Muhlemann, O. EJC-independent degradation of nonsense immunoglobulin-mu mRNA depends on 3' UTR length. *Nat Struct Mol Biol* 13, 462-464, doi:10.1038/nsmb1081 (2006).

193 Metze, S., Herzog, V. A., Ruepp, M. D. & Muhlemann, O. Comparison of EJC-enhanced and EJC-independent NMD in human cells reveals two partially redundant degradation pathways. *RNA* 19, 1432-1448, doi:10.1261/rna.038893.113 (2013).

194 Lopez-Perrote, A. *et al.* Human nonsense-mediated mRNA decay factor UPF2 interacts directly with eRF3 and the SURF complex. *Nucleic Acids Res* 44, 1909-1923, doi:10.1093/nar/gkv1527 (2016).

195 Colombo, M., Karousis, E. D., Bourquin, J., Bruggmann, R. & Muhlemann, O. Transcriptome-wide identification of NMD-targeted human mRNAs reveals extensive redundancy between SMG6- and SMG7-mediated degradation pathways. *RNA* 23, 189-201, doi:10.1261/rna.059055.116 (2017).

196 Lykke-Andersen, J., Shu, M. D. & Steitz, J. A. Human Upf proteins target an mRNA for nonsense-mediated decay when bound downstream of a termination codon. *Cell* 103, 1121-1131, doi:10.1016/s0092-8674(00)00214-2 (2000).

197 Gehring, N. H., Neu-Yilik, G., Schell, T., Hentze, M. W. & Kulozik, A. E. Y14 and hUpf3b form an NMD-activating complex. *Mol Cell* 11, 939-949, doi:10.1016/s1097-2765(03)00142-4 (2003).

198 Palacios, I. M., Gatfield, D., St Johnston, D. & Izaurralde, E. An eIF4AIII-containing complex required for mRNA localization and nonsense-mediated mRNA decay. *Nature* 427, 753-757, doi:10.1038/nature02351 (2004).

199 Joazeiro, C. A. P. Mechanisms and functions of ribosome-associated protein quality control. *Nat Rev Mol Cell Biol* 20, 368-383, doi:10.1038/s41580-019-0118-2 (2019).

200 Arthur, L. *et al.* Translational control by lysine-encoding A-rich sequences. *Sci Adv* 1, doi:10.1126/sciadv.1500154 (2015).

201 Koutmou, K. S. *et al.* Ribosomes slide on lysine-encoding homopolymeric A stretches. *Elife* 4, doi:10.7554/eLife.05534 (2015).

202 Juszkiewicz, S. & Hegde, R. S. Initiation of Quality Control during Poly(A) Translation Requires Site-Specific Ribosome Ubiquitination. *Mol Cell* 65, 743-750 e744, doi:10.1016/j.molcel.2016.11.039 (2017).

203 Dimitrova, L. N., Kuroha, K., Tatematsu, T. & Inada, T. Nascent peptide-dependent translation arrest leads to Not4p-mediated protein degradation by the proteasome. *J Biol Chem* 284, 10343-10352, doi:10.1074/jbc.M808840200 (2009).

204 Letzring, D. P., Wolf, A. S., Brule, C. E. & Grayhack, E. J. Translation of CGA codon repeats in yeast involves quality control components and ribosomal protein L1. *RNA* 19, 1208-1217, doi:10.1261/rna.039446.113 (2013).

205 Sundaramoorthy, E. *et al.* ZNF598 and RACK1 Regulate Mammalian Ribosome-Associated Quality Control Function by Mediating Regulatory 40S Ribosomal Ubiquitylation. *Mol Cell* 65, 751-760 e754, doi:10.1016/j.molcel.2016.12.026 (2017).

206 Yoshida, H. *et al.* XBP1 mRNA Is Induced by ATF6 and Spliced by IRE1 in Response to ER Stress to Produce a Highly Active Transcription Factor phorylation, the activated Ire1p specifically cleaves HAC1 precursor mRNA to remove an intron of 252 nucle-otides. The cleaved 5 and 3 halves of mature HAC1 mRNA are ligated by Rlg1p (tRNA ligase). HAC1 mRNA encodes the basic leucine zipper (bZIP). 107, 881-891 (2001).

207 Lee, A.-H., Iwakoshi, N. N., Glimcher, L. H. & XBP-1 Regulates a Subset of Endoplasmic Reticulum Resident Chaperone Genes in the Unfolded Protein Response. 23, 7448-7459, doi:10.1128/mcb.23.21.7448-7459.2003 (2003).

208 Brandman, O. *et al.* A ribosome-bound quality control complex triggers degradation of nascent peptides and signals translation stress. *Cell* 151, 1042-1054, doi:10.1016/j.cell.2012.10.044 (2012).

209 Defenouillere, Q. *et al.* Cdc48-associated complex bound to 60S particles is required for the clearance of aberrant translation products. *Proc Natl Acad Sci U S A* 110, 5046-5051, doi:10.1073/pnas.1221724110 (2013).

210 Lyumkis, D. *et al.* Structural basis for translational surveillance by the large ribosomal subunit-associated protein quality control complex. *Proc Natl Acad Sci U S A* 111, 15981-15986, doi:10.1073/pnas.1413882111 (2014).

211 Shen, P. S. *et al.* Protein synthesis. Rqc2p and 60S ribosomal subunits mediate mRNA-independent elongation of nascent chains. *Science* 347, 75-78, doi:10.1126/science.1259724 (2015).

212 Shao, S., Brown, A., Santhanam, B. & Hegde, R. S. Structure and assembly pathway of the ribosome quality control complex. *Mol Cell* 57, 433-444, doi:10.1016/j.molcel.2014.12.015 (2015).

213 Bengtson, M. H. & Joazeiro, C. A. Role of a ribosome-associated E3 ubiquitin ligase in protein quality control. *Nature* 467, 470-473, doi:10.1038/nature09371 (2010).

214 Verma, R. *et al.* Vms1 and ANKZF1 peptidyl-tRNA hydrolases release nascent chains from stalled ribosomes. *Nature* 557, 446-451, doi:10.1038/s41586-018-0022-5 (2018).

215 Zurita Rendon, O. *et al.* Vms1p is a release factor for the ribosome-associated quality control complex. *Nat Commun* 9, 2197, doi:10.1038/s41467-018-04564-3 (2018).

216 Kostova, K. K. *et al.* CAT-tailing as a fail-safe mechanism for efficient degradation of stalled nascent polypeptides. *Science* 357, 414-417, doi:10.1126/science.aam7787 (2017).

217 Yonashiro, R. *et al.* The Rqc2/Tae2 subunit of the ribosome-associated quality control (RQC) complex marks ribosome-stalled nascent polypeptide chains for aggregation. *Elife* 5, e11794, doi:10.7554/eLife.11794 (2016).

218 Choe, Y. J. *et al.* Failure of RQC machinery causes protein aggregation and proteotoxic stress. *Nature* 531, 191-195, doi:10.1038/nature16973 (2016).

219 Defenouillere, Q. *et al.* Rqc1 and Ltn1 Prevent C-terminal Alanine-Threonine Tail (CAT-tail)-induced Protein Aggregation by Efficient Recruitment of Cdc48 on Stalled 60S Subunits. *J Biol Chem* 291, 12245-12253, doi:10.1074/jbc.M116.722264 (2016).

220 Sitron, C. S. & Brandman, O. CAT tails drive degradation of stalled polypeptides on and off the ribosome. *Nat Struct Mol Biol* 26, 450-459, doi:10.1038/s41594-019-0230-1 (2019).

221 Udagawa, T. *et al.* Failure to Degrade CAT-Tailed Proteins Disrupts Neuronal Morphogenesis and Cell Survival. *Cell Rep* 34, 108599, doi:10.1016/j.celrep.2020.108599 (2021).
222 Ikeuchi, K. *et al.* Collided ribosomes form a unique structural interface to induce Hel2-driven quality control pathways. *EMBO J* 38, doi:10.15252/embj.2018100276 (2019).
223 Juszkiewicz, S. *et al.* ZNF598 Is a Quality Control Sensor of Collided Ribosomes. *Mol Cell* 72, 469-481 e467, doi:10.1016/j.molcel.2018.08.037 (2018).
224 Singh, R. K., Gonzalez, M., Kabbaj, M. H. & Gunjan, A. Novel E3 ubiquitin ligases that regulate histone protein levels in the budding yeast Saccharomyces cerevisiae. *PLoS One* 7, e36295, doi:10.1371/journal.pone.0036295 (2012).
225 Matsuo, Y. *et al.* Ubiquitination of stalled ribosome triggers ribosome-associated quality control. *Nat Commun* 8, 159, doi:10.1038/s41467-017-00188-1 (2017).
226 Juszkiewicz, S., Speldewinde, S. H., Wan, L., Svejstrup, J. Q. & Hegde, R. S. The ASC-1 Complex Disassembles Collided Ribosomes. *Mol Cell* 79, 603-614 e608, doi:10.1016/j.molcel.2020.06.006 (2020).
227 Jung, D. J. *et al.* Novel transcription coactivator complex containing activating signal cointegrator 1. *Mol Cell Biol* 22, 5203-5211, doi:10.1128/MCB.22.14.5203-5211.2002 (2002).
228 Dango, S. *et al.* DNA unwinding by ASCC3 helicase is coupled to ALKBH3-dependent DNA alkylation repair and cancer cell proliferation. *Mol Cell* 44, 373-384, doi:10.1016/j.molcel.2011.08.039 (2011).
229 Hashimoto, S., Sugiyama, T., Yamazaki, R., Nobuta, R. & Inada, T. Identification of a novel trigger complex that facilitates ribosome-associated quality control in mammalian cells. *Sci Rep* 10, 3422, doi:10.1038/s41598-020-60241-w (2020).
230 Liaud, N. *et al.* Cellular response to small molecules that selectively stall protein synthesis by the ribosome. *PLoS Genet* 15, e1008057, doi:10.1371/journal.pgen.1008057 (2019).
231 D'Orazio, K. N. *et al.* The endonuclease Cue2 cleaves mRNAs at stalled ribosomes during No Go Decay. *Elife* 8, doi:10.7554/eLife.49117 (2019).
232 Saito, K. *et al.* Ribosome collisions induce mRNA cleavage and ribosome rescue in bacteria. *Nature* 603, 503-508, doi:10.1038/s41586-022-04416-7 (2022).
233 Cerullo, F. *et al.* Bacterial ribosome collision sensing by a MutS DNA repair ATPase paralogue. *Nature* 603, 509-514, doi:10.1038/s41586-022-04487-6 (2022).
234 Glover, M. L. *et al.* NONU-1 Encodes a Conserved Endonuclease Required for mRNA Translation Surveillance. *Cell Rep* 30, 4321-4331 e4324, doi:10.1016/j.celrep.2020.03.023 (2020).
235 Juszkiewicz, S. *et al.* Ribosome collisions trigger cis-acting feedback inhibition of translation initiation. *Elife* 9, doi:10.7554/eLife.60038 (2020).
236 Sinha, N. K. *et al.* EDF1 coordinates cellular responses to ribosome collisions. *Elife* 9, doi:10.7554/eLife.58828 (2020).
237 Hickey, K. L. *et al.* GIGYF2 and 4EHP Inhibit Translation Initiation of Defective Messenger RNAs to Assist Ribosome-Associated Quality Control. *Mol Cell* 79, 950-962 e956, doi:10.1016/j.molcel.2020.07.007 (2020).
238 Chapat, C. *et al.* Cap-binding protein 4EHP effects translation silencing by microRNAs. *Proc Natl Acad Sci U S A* 114, 5425-5430, doi:10.1073/pnas.1701488114 (2017).
239 Veltri, A. J. *et al.* Distinct elongation stalls during translation are linked with distinct pathways for mRNA degradation. *Elife* 11, doi:10.7554/eLife.76038 (2022).
240 Giovannone, B. *et al.* GIGYF2 gene disruption in mice results in neurodegeneration and altered insulin-like growth factor signaling. *Hum Mol Genet* 18, 4629-4639, doi:10.1093/hmg/ddp430 (2009).
241 Ash, M. R. *et al.* Conserved beta-hairpin recognition by the GYF domains of Smy2 and GIGYF2 in mRNA surveillance and vesicular transport complexes. *Structure* 18, 944-954, doi:10.1016/j.str.2010.04.020 (2010).
242 Terrey, M. *et al.* GTPBP1 resolves paused ribosomes to maintain neuronal homeostasis. *Elife* 9, doi:10.7554/eLife.62731 (2020).
243 Senju, S., Iyama, K., Kudo, H., Aizawa, S. & Nishimura, Y. Immunocytochemical analyses and targeted gene disruption of GTPBP1. *Mol Cell Biol* 20, 6195-6200, doi:10.1128/MCB.20.17.6195-6200.2000 (2000).
244 Zinoviev, A. *et al.* Functions of unconventional mammalian translational GTPases GTPBP1 and GTPBP2. *Genes Dev* 32, 1226-1241, doi:10.1101/gad.314724.118 (2018).
245 Yan, L. L., Zaher, H. S. & Ribosome quality control antagonizes the activation of the integrated stress response on colliding ribosomes. 81, 614-628.e614, doi:10.1016/j.molcel.2020.11.033 (2021).
246 Liakath-Ali, K. *et al.* An evolutionarily conserved ribosome-rescue pathway maintains epidermal homeostasis. *Nature* 556, 376-380, doi:10.1038/s41586-018-0032-3 (2018).
247 Terrey, M., Adamson, S. I., Chuang, J. H. & Ackerman, S. L. Defects in translation-dependent quality control pathways lead to convergent molecular and neurodevelopmental pathology. *Elife* 10, doi:10.7554/eLife.66904 (2021).
248 Buszczak, M., Signer, R. A. & Morrison, S. J. Cellular differences in protein synthesis regulate tissue homeostasis. *Cell* 159, 242-251, doi:10.1016/j.cell.2014.09.016 (2014).
249 Blair, J. D., Hockemeyer, D., Doudna, J. A., Bateup, H. S. & Floor, S. N. Widespread Translational Remodeling during Human Neuronal Differentiation. *Cell Rep* 21, 2005-2016, doi:10.1016/j.celrep.2017.10.095 (2017).

250 Gonzalez, F. *et al.* An iCRISPR platform for rapid, multiplexable, and inducible genome editing in human pluripotent stem cells. *Cell Stem Cell* 15, 215-226, doi:10.1016/j.stem.2014.05.018 (2014).

251 Matsuo, Y. & Inada, T. The ribosome collision sensor Hel2 functions as preventive quality control in the secretory pathway. *Cell Rep* 34, 108877, doi:10.1016/j.celrep.2021.108877 (2021).

252 Winz, M. L., Peil, L., Turowski, T. W., Rappsilber, J. & Tollervey, D. Molecular interactions between Hel2 and RNA supporting ribosome-associated quality control. *Nat Commun* 10, 563, doi:10.1038/s41467-019-08382-z (2019).

253 Meydan, S. & Guydosh, N. R. A cellular handbook for collided ribosomes: surveillance pathways and collision types. *Curr Genet* 67, 19-26, doi:10.1007/s00294-020-01111-w (2021).

254 Vattem, K. M. & Wek, R. C. Reinitiation involving upstream ORFs regulates ATF4 mRNA translation in mammalian cells. *Proc Natl Acad Sci U S A* 101, 11269-11274, doi:10.1073/pnas.0400541101 (2004).

255 Pavitt, G. D., Ramaiah, K. V., Kimball, S. R. & Hinnebusch, A. G. eIF2 independently binds two distinct eIF2B subcomplexes that catalyze and regulate guanine-nucleotide exchange. *Genes Dev* 12, 514-526, doi:10.1101/gad.12.4.514 (1998).

256 Dever, T. E. *et al.* Phosphorylation of initiation factor 2 alpha by protein kinase GCN2 mediates gene-specific translational control of GCN4 in yeast. *Cell* 68, 585-596, doi:10.1016/0092-8674(92)90193-g (1992).

257 Dong, J., Qiu, H., Garcia-Barrio, M., Anderson, J. & Hinnebusch, A. G. Uncharged tRNA activates GCN2 by displacing the protein kinase moiety from a bipartite tRNA-binding domain. *Mol Cell* 6, 269-279, doi:10.1016/s1097-2765(00)00028-9 (2000).

258 Wek, S. A., Zhu, S. & Wek, R. C. The histidyl-tRNA synthetase-related sequence in the eIF-2 alpha protein kinase GCN2 interacts with tRNA and is required for activation in response to starvation for different amino acids. *Mol Cell Biol* 15, 4497-4506, doi:10.1128/MCB.15.8.4497 (1995).

259 Walter, P. & Ron, D. The unfolded protein response: from stress pathway to homeostatic regulation. *Science* 334, 1081-1086, doi:10.1126/science.1209038 (2011).

260 Harding, H. P. *et al.* An integrated stress response regulates amino acid metabolism and resistance to oxidative stress. *Mol Cell* 11, 619-633, doi:10.1016/s1097-2765(03)00105-9 (2003).

261 Lu, P. D., Harding, H. P. & Ron, D. Translation reinitiation at alternative open reading frames regulates gene expression in an integrated stress response. *J Cell Biol* 167, 27-33, doi:10.1083/jcb.200408003 (2004).

262 Hetz, C. & Papa, F. R. The Unfolded Protein Response and Cell Fate Control. *Mol Cell* 69, 169-181, doi:10.1016/j.molcel.2017.06.017 (2018).

263 Rouse, J. *et al.* A novel kinase cascade triggered by stress and heat shock that stimulates MAPKAP kinase-2 and phosphorylation of the small heat shock proteins. *Cell* 78, 1027-1037, doi:10.1016/0092-8674(94)90277-1 (1994).

264 Vind, A. C., Genzor, A. V. & Bekker-Jensen, S. Ribosomal stress-surveillance: three pathways is a magic number. *Nucleic Acids Res* 48, 10648-10661, doi:10.1093/nar/gkaa757 (2020).

265 Wu, C. C., Peterson, A., Zinshteyn, B., Regot, S. & Green, R. Ribosome Collisions Trigger General Stress Responses to Regulate Cell Fate. *Cell* 182, 404-416 e414, doi:10.1016/j.cell.2020.06.006 (2020).

266 Davis, R. J. Signal transduction by the JNK group of MAP kinases. *Cell* 103, 239-252, doi:10.1016/s0092-8674(00)00116-1 (2000).

267 Xia, Z., Dickens, M., Raingeaud, J., Davis, R. J. & Greenberg, M. E. Opposing effects of ERK and JNK-p38 MAP kinases on apoptosis. *Science* 270, 1326-1331, doi:10.1126/science.270.5240.1326 (1995).

268 Cuenda, A. & Rousseau, S. p38 MAP-kinases pathway regulation, function and role in human diseases. *Biochim Biophys Acta* 1773, 1358-1375, doi:10.1016/j.bbamcr.2007.03.010 (2007).

269 Borisova, M. E. *et al.* p38-MK2 signaling axis regulates RNA metabolism after UV-light-induced DNA damage. *Nat Commun* 9, 1017, doi:10.1038/s41467-018-03417-3 (2018).

270 Gupta, S. *et al.* Selective interaction of JNK protein kinase isoforms with transcription factors. *EMBO J* 15, 2760-2770 (1996).

271 Yang, D. D. *et al.* Absence of excitotoxicity-induced apoptosis in the hippocampus of mice lacking the Jnk3 gene. *Nature* 389, 865-870, doi:10.1038/39899 (1997).

272 Sabapathy, K. *et al.* Defective neural tube morphogenesis and altered apoptosis in the absence of both JNK1 and JNK2. *Mech Dev* 89, 115-124, doi:10.1016/s0925-4773(99)00213-0 (1999).

273 Kuan, C. Y. *et al.* The Jnk1 and Jnk2 protein kinases are required for regional specific apoptosis during early brain development. *Neuron* 22, 667-676, doi:10.1016/s0896-6273(00)80727-8 (1999).

274 Lamb, J. A., Ventura, J. J., Hess, P., Flavell, R. A. & Davis, R. J. JunD mediates survival signaling by the JNK signal transduction pathway. *Mol Cell* 11, 1479-1489, doi:10.1016/s1097-2765(03)00203-x (2003).

275 Ventura, J. J., Kennedy, N. J., Lamb, J. A., Flavell, R. A. & Davis, R. J. c-Jun NH(2)-terminal kinase is essential for the regulation of AP-1 by tumor necrosis factor. *Mol Cell Biol* 23, 2871-2882, doi:10.1128/MCB.23.8.2871-2882.2003 (2003).

276 Read, M. A. *et al.* Tumor necrosis factor alpha-induced E-selectin expression is activated by the nuclear factor-kappaB and c-JUN N-terminal kinase/p38 mitogen-activated protein kinase pathways. *J Biol Chem* 272, 2753-2761, doi:10.1074/jbc.272.5.2753 (1997).

277 Zeke, A., Misheva, M., Remenyi, A. & Bogoyevitch, M. A. JNK Signaling: Regulation and Functions Based on Complex Protein-Protein Partnerships. *Microbiol Mol Biol Rev* 80, 793-835, doi:10.1128/MMBR.00043-14 (2016).
278 Wang, X. *et al.* Complete inhibition of anisomycin and UV radiation but not cytokine induced JNK and p38 activation by an aryl-substituted dihydropyrrolopyrazole quinoline and mixed lineage kinase 7 small interfering RNA. *J Biol Chem* 280, 19298-19305, doi:10.1074/jbc.M413059200 (2005).
279 Jandhyala, D. M., Ahluwalia, A., Obrig, T. & Thorpe, C. M. ZAK: a MAP3Kinase that transduces Shiga toxin- and ricin-induced proinflammatory cytokine expression. *Cell Microbiol* 10, 1468-1477, doi:10.1111/j.1462-5822.2008.01139.x (2008).
280 Vind, A. C. *et al.* ZAKalpha Recognizes Stalled Ribosomes through Partially Redundant Sensor Domains. *Mol Cell* 78, 700-713 e707, doi:10.1016/j.molcel.2020.03.021 (2020).
281 Sauter, K. A., Magun, E. A., Iordanov, M. S. & Magun, B. E. ZAK is required for doxorubicin, a novel ribotoxic stressor, to induce SAPK activation and apoptosis in HaCaT cells. *Cancer Biol Ther* 10, 258-266, doi:10.4161/cbt.10.3.12367 (2010).
282 Vin, H. *et al.* Sorafenib suppresses JNK-dependent apoptosis through inhibition of ZAK. *Mol Cancer Ther* 13, 221-229, doi:10.1158/1535-7163.MCT-13-0561 (2014).
283 Derijard, B. *et al.* Independent human MAP-kinase signal transduction pathways defined by MEK and MKK isoforms. *Science* 267, 682-685, doi:10.1126/science.7839144 (1995).
284 Raingeaud, J., Whitmarsh, A. J., Barrett, T., Derijard, B. & Davis, R. J. MKK3- and MKK6-regulated gene expression is mediated by the p38 mitogen-activated protein kinase signal transduction pathway. *Mol Cell Biol* 16, 1247-1255, doi:10.1128/MCB.16.3.1247 (1996).
285 Han, J. *et al.* Characterization of the structure and function of a novel MAP kinase kinase (MKK6). *J Biol Chem* 271, 2886-2891, doi:10.1074/jbc.271.6.2886 (1996).
286 Brancho, D. *et al.* Mechanism of p38 MAP kinase activation in vivo. *Genes Dev* 17, 1969-1978, doi:10.1101/gad.1107303 (2003).
287 Tournier, C. *et al.* MKK7 is an essential component of the JNK signal transduction pathway activated by proinflammatory cytokines. *Genes Dev* 15, 1419-1426, doi:10.1101/gad.888501 (2001).
288 Iordanov, M. S. *et al.* Ribotoxic stress response: activation of the stress-activated protein kinase JNK1 by inhibitors of the peptidyl transferase reaction and by sequence-specific RNA damage to the alpha-sarcin/ricin loop in the 28S rRNA. *Mol Cell Biol* 17, 3373-3381, doi:10.1128/MCB.17.6.3373 (1997).
289 Lucas, C. L., Chandra, A., Nejentsev, S., Condliffe, A. M. & Okkenhaug, K. PI3Kdelta and primary immunodeficiencies. *Nat Rev Immunol* 16, 702-714, doi:10.1038/nri.2016.93 (2016).
290 Piccirillo, C. A., Bjur, E., Topisirovic, I., Sonenberg, N. & Larsson, O. Translational control of immune responses: from transcripts to translatomes. *Nat Immunol* 15, 503-511, doi:10.1038/ni.2891 (2014).
291 Morita, M. *et al.* mTORC1 controls mitochondrial activity and biogenesis through 4E-BP-dependent translational regulation. *Cell Metab* 18, 698-711, doi:10.1016/j.cmet.2013.10.001 (2013).
292 Buffington, S. A., Huang, W. & Costa-Mattioli, M. Translational control in synaptic plasticity and cognitive dysfunction. *Annu Rev Neurosci* 37, 17-38, doi:10.1146/annurev-neuro-071013-014100 (2014).
293 Tahmasebi, S., Khoutorsky, A., Mathews, M. B. & Sonenberg, N. Translation deregulation in human disease. *Nat Rev Mol Cell Biol* 19, 791-807, doi:10.1038/s41580-018-0034-x (2018).
294 Narla, A. & Ebert, B. L. Ribosomopathies: human disorders of ribosome dysfunction. *Blood* 115, 3196-3205, doi:10.1182/blood-2009-10-178129 (2010).
295 Yelick, P. C. & Trainor, P. A. Ribosomopathies: Global process, tissue specific defects. *Rare Dis* 3, e1025185, doi:10.1080/21675511.2015.1025185 (2015).
296 Mills, E. W. & Green, R. Ribosomopathies: There's strength in numbers. *Science* 358, doi:10.1126/science.aan2755 (2017).
297 Shwachman, H., Diamond, L. K., Oski, F. A. & Khaw, K. T. The Syndrome of Pancreatic Insufficiency and Bone Marrow Dysfunction. *J Pediatr* 65, 645-663, doi:10.1016/s0022-3476(64)80150-5 (1964).
298 Trainor, P. A., Dixon, J. & Dixon, M. J. Treacher Collins syndrome: etiology, pathogenesis and prevention. *Eur J Hum Genet* 17, 275-283, doi:10.1038/ejhg.2008.221 (2009).
299 Ebert, B. L. *et al.* Identification of RPS14 as a 5q- syndrome gene by RNA interference screen. *Nature* 451, 335-339, doi:10.1038/nature06494 (2008).
300 Chagnon, P. *et al.* A missense mutation (R565W) in cirhin (FLJ14728) in North American Indian childhood cirrhosis. *Am J Hum Genet* 71, 1443-1449, doi:10.1086/344580 (2002).
301 Ludwig, L. S. *et al.* Altered translation of GATA1 in Diamond-Blackfan anemia. *Nat Med* 20, 748-753, doi:10.1038/nm.3557 (2014).
302 Simsek, D. *et al.* The Mammalian Ribo-interactome Reveals Ribosome Functional Diversity and Heterogeneity. *Cell* 169, 1051-1065 e1018, doi:10.1016/j.cell.2017.05.022 (2017).
303 Parks, M. M. *et al.* Variant ribosomal RNA alleles are conserved and exhibit tissue-specific expression. *Sci Adv* 4, eaao0665, doi:10.1126/sciadv.aao0665 (2018).
304 Dai, M. S. & Lu, H. Inhibition of MDM2-mediated p53 ubiquitination and degradation by ribosomal protein L5. *J Biol Chem* 279, 44475-44482, doi:10.1074/jbc.M403722200 (2004).
305 Dai, M. S. *et al.* Ribosomal protein L23 activates p53 by inhibiting MDM2 function in response to ribosomal perturbation but not to translation inhibition. *Mol Cell Biol* 24, 7654-7668, doi:10.1128/MCB.24.17.7654-7668.2004 (2004).

306 Donati, G., Montanaro, L. & Derenzini, M. Ribosome biogenesis and control of cell proliferation: p53 is not alone. *Cancer Res* 72, 1602-1607, doi:10.1158/0008-5472.CAN-11-3992 (2012).
307 Jones, N. C. *et al.* Prevention of the neurocristopathy Treacher Collins syndrome through inhibition of p53 function. *Nat Med* 14, 125-133, doi:10.1038/nm1725 (2008).
308 Chartier-Harlin, M. C. *et al.* Translation initiator EIF4G1 mutations in familial Parkinson disease. *Am J Hum Genet* 89, 398-406, doi:10.1016/j.ajhg.2011.08.009 (2011).
309 Dhungel, N. *et al.* Parkinson's disease genes VPS35 and EIF4G1 interact genetically and converge on alpha-synuclein. *Neuron* 85, 76-87, doi:10.1016/j.neuron.2014.11.027 (2015).
310 Nichols, N. *et al.* EIF4G1 mutations do not cause Parkinson's disease. *Neurobiol Aging* 36, 2444 e2441-2444, doi:10.1016/j.neurobiolaging.2015.04.017 (2015).
311 Chu, J. *et al.* A mouse forward genetics screen identifies LISTERIN as an E3 ubiquitin ligase involved in neurodegeneration. *Proc Natl Acad Sci U S A* 106, 2097-2103, doi:10.1073/pnas.0812819106 (2009).
312 Steward, O. & Levy, W. B. Preferential localization of polyribosomes under the base of dendritic spines in granule cells of the dentate gyrus. *J Neurosci* 2, 284-291 (1982).
313 Ostroff, L. E., Fiala, J. C., Allwardt, B. & Harris, K. M. Polyribosomes redistribute from dendritic shafts into spines with enlarged synapses during LTP in developing rat hippocampal slices. *Neuron* 35, 535-545, doi:10.1016/s0896-6273(02)00785-7 (2002).
314 Blanco, S. *et al.* Stem cell function and stress response are controlled by protein synthesis. *Nature* 534, 335-340, doi:10.1038/nature18282 (2016).
315 Dorrbaum, A. R., Kochen, L., Langer, J. D. & Schuman, E. M. Local and global influences on protein turnover in neurons and glia. *Elife* 7, doi:10.7554/eLife.34202 (2018).
316 Dastidar, S. G. & Nair, D. A Ribosomal Perspective on Neuronal Local Protein Synthesis. *Front Mol Neurosci* 15, 823135, doi:10.3389/fnmol.2022.823135 (2022).
317 Hanahan, D. & Weinberg, R. A. Hallmarks of cancer: the next generation. *Cell* 144, 646-674, doi:10.1016/j.cell.2011.02.013 (2011).
318 Drubin, D. G. & Hyman, A. A. Stem cells: the new "model organism". *Mol Biol Cell* 28, 1409-1411, doi:10.1091/mbc.E17-03-0183 (2017).
319 Knoblich, J. A. Mechanisms of asymmetric stem cell division. *Cell* 132, 583-597, doi:10.1016/j.cell.2008.02.007 (2008).
320 Takahashi, K. & Yamanaka, S. Induction of pluripotent stem cells from mouse embryonic and adult fibroblast cultures by defined factors. *Cell* 126, 663-676, doi:10.1016/j.cell.2006.07.024 (2006).
321 Zakrzewski, W., Dobrzynski, M., Szymonowicz, M. & Rybak, Z. Stem cells: past, present, and future. *Stem Cell Res Ther* 10, 68, doi:10.1186/s13287-019-1165-5 (2019).
322 Turner, N. & Grose, R. Fibroblast growth factor signalling: from development to cancer. *Nat Rev Cancer* 10, 116-129, doi:10.1038/nrc2780 (2010).
323 Rao, T. P. & Kuhl, M. An updated overview on Wnt signaling pathways: a prelude for more. *Circ Res* 106, 1798-1806, doi:10.1161/CIRCRESAHA.110.219840 (2010).
324 Moustakas, A. & Heldin, C. H. The regulation of TGFbeta signal transduction. *Development* 136, 3699-3714, doi:10.1242/dev.030338 (2009).
325 Kilpinen, H. *et al.* Common genetic variation drives molecular heterogeneity in human iPSCs. *Nature* 546, 370-375, doi:10.1038/nature22403 (2017).
326 Barrangou, R. *et al.* CRISPR provides acquired resistance against viruses in prokaryotes. *Science* 315, 1709-1712, doi:10.1126/science.1138140 (2007).
327 Mojica, F. J., Diez-Villasenor, C., Garcia-Martinez, J. & Soria, E. Intervening sequences of regularly spaced prokaryotic repeats derive from foreign genetic elements. *J Mol Evol* 60, 174-182, doi:10.1007/s00239-004-0046-3 (2005).
328 Hsu, P. D. *et al.* DNA targeting specificity of RNA-guided Cas9 nucleases. *Nat Biotechnol* 31, 827-832, doi:10.1038/nbt.2647 (2013).
329 Deltcheva, E. *et al.* CRISPR RNA maturation by trans-encoded small RNA and host factor RNase III. *Nature* 471, 602-607, doi:10.1038/nature09886 (2011).
330 Sternberg, S. H., Redding, S., Jinek, M., Greene, E. C. & Doudna, J. A. DNA interrogation by the CRISPR RNA-guided endonuclease Cas9. *Nature* 507, 62-67, doi:10.1038/nature13011 (2014).
331 Cong, L. *et al.* Multiplex genome engineering using CRISPR/Cas systems. *Science* 339, 819-823, doi:10.1126/science.1231143 (2013).
332 Mali, P. *et al.* RNA-guided human genome engineering via Cas9. *Science* 339, 823-826, doi:10.1126/science.1232033 (2013).
333 Boettcher, M. & McManus, M. T. Choosing the Right Tool for the Job: RNAi, TALEN, or CRISPR. *Mol Cell* 58, 575-585, doi:10.1016/j.molcel.2015.04.028 (2015).
334 Breunig, C. T. *et al.* CRISPR Tools for Physiology and Cell State Changes: Potential of Transcriptional Engineering and Epigenome Editing. *Physiol Rev* 101, 177-211, doi:10.1152/physrev.00034.2019 (2021).
335 Gilbert, L. A. *et al.* CRISPR-mediated modular RNA-guided regulation of transcription in eukaryotes. *Cell* 154, 442-451, doi:10.1016/j.cell.2013.06.044 (2013).
336 Qi, L. S. *et al.* Repurposing CRISPR as an RNA-guided platform for sequence-specific control of gene expression. *Cell* 152, 1173-1183, doi:10.1016/j.cell.2013.02.022 (2013).

337 Groner, A. C. *et al.* KRAB-zinc finger proteins and KAP1 can mediate long-range transcriptional repression through heterochromatin spreading. *PLoS Genet* 6, e1000869, doi:10.1371/journal.pgen.1000869 (2010).

338 Gilbert, L. A. *et al.* Genome-Scale CRISPR-Mediated Control of Gene Repression and Activation. *Cell* 159, 647-661, doi:10.1016/j.cell.2014.09.029 (2014).

339 Riepe, C. *et al.* Double stranded DNA breaks and genome editing trigger loss of ribosomal protein RPS27A. *FEBS J*, doi:10.1111/febs.16321 (2021).

340 Mandegar, M. A. *et al.* CRISPR Interference Efficiently Induces Specific and Reversible Gene Silencing in Human iPSCs. *Cell Stem Cell* 18, 541-553, doi:10.1016/j.stem.2016.01.022 (2016).

341 Tian, R. *et al.* CRISPR Interference-Based Platform for Multimodal Genetic Screens in Human iPSC-Derived Neurons. *Neuron* 104, 239-255 e212, doi:10.1016/j.neuron.2019.07.014 (2019).

342 Tian, R. *et al.* Genome-wide CRISPRi/a screens in human neurons link lysosomal failure to ferroptosis. *Nat Neurosci* 24, 1020-1034, doi:10.1038/s41593-021-00862-0 (2021).

343 Zhang, Y. *et al.* Rapid single-step induction of functional neurons from human pluripotent stem cells. *Neuron* 78, 785-798, doi:10.1016/j.neuron.2013.05.029 (2013).

344 Wang, C. *et al.* Scalable Production of iPSC-Derived Human Neurons to Identify Tau-Lowering Compounds by High-Content Screening. *Stem Cell Reports* 9, 1221-1233, doi:10.1016/j.stemcr.2017.08.019 (2017).

345 Horlbeck, M. A. *et al.* Compact and highly active next-generation libraries for CRISPR-mediated gene repression and activation. *Elife* 5, doi:10.7554/eLife.19760 (2016).

346 Ruggero, D. Translational control in cancer etiology. *Cold Spring Harb Perspect Biol* 5, doi:10.1101/cshperspect.a012336 (2013).

347 Donnelly, N. & Storchova, Z. Causes and consequences of protein folding stress in aneuploid cells. *Cell Cycle* 14, 495-501, doi:10.1080/15384101.2015.1006043 (2015).

348 Martins-Taylor, K. & Xu, R. H. Concise review: Genomic stability of human induced pluripotent stem cells. *Stem Cells* 30, 22-27, doi:10.1002/stem.705 (2012).

349 Reinhardt, P. *et al.* Derivation and expansion using only small molecules of human neural progenitors for neurodegenerative disease modeling. *PLoS One* 8, e59252, doi:10.1371/journal.pone.0059252 (2013).

350 Marrone, L. *et al.* FUS pathology in ALS is linked to alterations in multiple ALS-associated proteins and rescued by drugs stimulating autophagy. *Acta Neuropathol* 138, 67-84, doi:10.1007/s00401-019-01998-x (2019).

351 Kim, U. K. *et al.* Expression of TGF-beta1, osteonectin, and BMP-4 in mandibular distraction osteogenesis with compression stimulation: reverse transcriptase-polymerase chain reaction study and biomechanical test. *J Oral Maxillofac Surg* 68, 2076-2084, doi:10.1016/j.joms.2009.09.070 (2010).

352 Chambers, S. M. *et al.* Highly efficient neural conversion of human ES and iPS cells by dual inhibition of SMAD signaling. *Nat Biotechnol* 27, 275-280, doi:10.1038/nbt.1529 (2009).

353 Reinhardt, L. *et al.* Dual Inhibition of GSK3beta and CDK5 Protects the Cytoskeleton of Neurons from Neuroinflammatory-Mediated Degeneration In Vitro and In Vivo. *Stem Cell Reports* 12, 502-517, doi:10.1016/j.stemcr.2019.01.015 (2019).

354 Zhang, M. *et al.* Universal cardiac induction of human pluripotent stem cells in two and three-dimensional formats: implications for in vitro maturation. *Stem Cells* 33, 1456-1469, doi:10.1002/stem.1964 (2015).

355 Tohyama, S. *et al.* Distinct metabolic flow enables large-scale purification of mouse and human pluripotent stem cell-derived cardiomyocytes. *Cell Stem Cell* 12, 127-137, doi:10.1016/j.stem.2012.09.013 (2013).

356 Zhu, P. *et al.* Silencing and un-silencing of tetracycline-controlled genes in neurons. *PLoS One* 2, e533, doi:10.1371/journal.pone.0000533 (2007).

357 Noormohammadi, A. *et al.* Somatic increase of CCT8 mimics proteostasis of human pluripotent stem cells and extends C. elegans lifespan. *Nat Commun* 7, 13649, doi:10.1038/ncomms13649 (2016).

358 Mair, B. *et al.* Essential Gene Profiles for Human Pluripotent Stem Cells Identify Uncharacterized Genes and Substrate Dependencies. *Cell Rep* 27, 599-615 e512, doi:10.1016/j.celrep.2019.02.041 (2019).

359 Hillenmeyer, M. E. *et al.* The chemical genomic portrait of yeast: uncovering a phenotype for all genes. *Science* 320, 362-365, doi:10.1126/science.1150021 (2008).

360 Wang, A. *et al.* Ribosomal protein RPL41 induces rapid degradation of ATF4, a transcription factor critical for tumour cell survival in stress. *J Pathol* 225, 285-292, doi:10.1002/path.2918 (2011).

361 Wang, S. *et al.* RPL41, a small ribosomal peptide deregulated in tumors, is essential for mitosis and centrosome integrity. *Neoplasia* 12, 284-293, doi:10.1593/neo.91610 (2010).

362 Hoshino, S., Imai, M., Kobayashi, T., Uchida, N. & Katada, T. The eukaryotic polypeptide chain releasing factor (eRF3/GSPT) carrying the translation termination signal to the 3'-Poly(A) tail of mRNA. Direct association of erf3/GSPT with polyadenylate-binding protein. *J Biol Chem* 274, 16677-16680, doi:10.1074/jbc.274.24.16677 (1999).

363 Schepens, B. *et al.* A role for hnRNP C1/C2 and Unr in internal initiation of translation during mitosis. *EMBO J* 26, 158-169, doi:10.1038/sj.emboj.7601468 (2007).

364 Elatmani, H. *et al.* The RNA-binding protein Unr prevents mouse embryonic stem cells differentiation toward the primitive endoderm lineage. *Stem Cells* 29, 1504-1516, doi:10.1002/stem.712 (2011).

365 Kuspert, M. *et al.* LARP4B is an AU-rich sequence associated factor that promotes mRNA accumulation and translation. *RNA* 21, 1294-1305, doi:10.1261/rna.051441.115 (2015).

366 Horos, R. *et al.* Ribosomal deficiencies in Diamond-Blackfan anemia impair translation of transcripts essential for differentiation of murine and human erythroblasts. *Blood* 119, 262-272, doi:10.1182/blood-2011-06-358200 (2012).

367 Xia, K. *et al.* Common genetic variants on 1p13.2 associate with risk of autism. *Mol Psychiatry* 19, 1212-1219, doi:10.1038/mp.2013.146 (2014).

368 Piazzon, N. *et al.* Implication of the SMN complex in the biogenesis and steady state level of the signal recognition particle. *Nucleic Acids Res* 41, 1255-1272, doi:10.1093/nar/gks1224 (2013).

369 Jin, W. *et al.* Structural basis for snRNA recognition by the double-WD40 repeat domain of Gemin5. *Genes Dev* 30, 2391-2403, doi:10.1101/gad.291377.116 (2016).

370 Lau, C. K., Bachorik, J. L. & Dreyfuss, G. Gemin5-snRNA interaction reveals an RNA binding function for WD repeat domains. *Nat Struct Mol Biol* 16, 486-491, doi:10.1038/nsmb.1584 (2009).

371 Vrotsos, E. G., Kolattukudy, P. E. & Sugaya, K. MCP-1 involvement in glial differentiation of neuroprogenitor cells through APP signaling. *Brain Res Bull* 79, 97-103, doi:10.1016/j.brainresbull.2009.01.004 (2009).

372 Zhou, L. *et al.* Monocyte chemoattractant protein-1 induces a novel transcription factor that causes cardiac myocyte apoptosis and ventricular dysfunction. *Circ Res* 98, 1177-1185, doi:10.1161/01.RES.0000220106.64661.71 (2006).

373 Mullen, J. R. *et al.* Identification and characterization of genes and mutants for an N-terminal acetyltransferase from yeast. *EMBO J* 8, 2067-2075, doi:10.1002/j.1460-2075.1989.tb03615.x (1989).

374 Arnesen, T. *et al.* Interaction between HIF-1 alpha (ODD) and hARD1 does not induce acetylation and destabilization of HIF-1 alpha. *FEBS Lett* 579, 6428-6432, doi:10.1016/j.febslet.2005.10.036 (2005).

375 Arnesen, T. *et al.* Cloning and characterization of hNAT5/hSAN: an evolutionarily conserved component of the NatA protein N-alpha-acetyltransferase complex. *Gene* 371, 291-295, doi:10.1016/j.gene.2005.12.008 (2006).

376 Pang, A. L., Clark, J., Chan, W. Y. & Rennert, O. M. Expression of human NAA11 (ARD1B) gene is tissue-specific and is regulated by DNA methylation. *Epigenetics* 6, 1391-1399, doi:10.4161/epi.6.11.18125 (2011).

377 Hsieh, A. C. *et al.* The translational landscape of mTOR signalling steers cancer initiation and metastasis. *Nature* 485, 55-61, doi:10.1038/nature10912 (2012).

378 Krishna, K. H. & Kumar, M. S. Molecular evolution and functional divergence of eukaryotic translation initiation factor 2-alpha kinases. *PLoS One* 13, e0194335, doi:10.1371/journal.pone.0194335 (2018).

379 Mills, E. W., Wangen, J., Green, R. & Ingolia, N. T. Dynamic Regulation of a Ribosome Rescue Pathway in Erythroid Cells and Platelets. *Cell Rep* 17, 1-10, doi:10.1016/j.celrep.2016.08.088 (2016).

380 Watson, J. V., Chambers, S. H. & Smith, P. J. A pragmatic approach to the analysis of DNA histograms with a definable G1 peak. *Cytometry* 8, 1-8, doi:10.1002/cyto.990080101 (1987).

381 Burd, J. F. & Usategui-Gomez, M. Immunochemical studies on lactate dehydrogenase. *Biochim Biophys Acta* 310, 238-247, doi:10.1016/0005-2795(73)90026-3 (1973).

382 Jiang, H. *et al.* Monitoring dynamic glycosylation in vivo using supersensitive click chemistry. *Bioconjug Chem* 25, 698-706, doi:10.1021/bc400502d (2014).

383 Lin, Y. J., Huang, L. H. & Huang, C. T. Enhancement of heterologous gene expression in Flammulina velutipes using polycistronic vectors containing a viral 2A cleavage sequence. *PLoS One* 8, e59099, doi:10.1371/journal.pone.0059099 (2013).

384 Liu, Z. *et al.* Systematic comparison of 2A peptides for cloning multi-genes in a polycistronic vector. *Sci Rep* 7, 2193, doi:10.1038/s41598-017-02460-2 (2017).

385 Qin, J. Y. *et al.* Systematic comparison of constitutive promoters and the doxycycline-inducible promoter. *PLoS One* 5, e10611, doi:10.1371/journal.pone.0010611 (2010).

386 Norrman, K. *et al.* Quantitative comparison of constitutive promoters in human ES cells. *PLoS One* 5, e12413, doi:10.1371/journal.pone.0012413 (2010).

387 Tzelepis, K. *et al.* A CRISPR Dropout Screen Identifies Genetic Vulnerabilities and Therapeutic Targets in Acute Myeloid Leukemia. *Cell Rep* 17, 1193-1205, doi:10.1016/j.celrep.2016.09.079 (2016).

388 Mani, R., St Onge, R. P., Hartman, J. L. t., Giaever, G. & Roth, F. P. Defining genetic interaction. *Proc Natl Acad Sci U S A* 105, 3461-3466, doi:10.1073/pnas.0712255105 (2008).

389 Woo, K. C. *et al.* Modulation of exosome-mediated mRNA turnover by interaction of GTP-binding protein 1 (GTPBP1) with its target mRNAs. *FASEB J* 25, 2757-2769, doi:10.1096/fj.10-178715 (2011).

390 Harding, H. P., Zhang, Y. & Ron, D. Protein translation and folding are coupled by an endoplasmic-reticulum-resident kinase. *Nature* 397, 271-274, doi:10.1038/16729 (1999).

391 Tabas, I. & Ron, D. Integrating the mechanisms of apoptosis induced by endoplasmic reticulum stress. *Nat Cell Biol* 13, 184-190, doi:10.1038/ncb0311-184 (2011).

392 Haze, K., Yoshida, H., Yanagi, H., Yura, T. & Mori, K. Mammalian transcription factor ATF6 is synthesized as a transmembrane protein and activated by proteolysis in response to endoplasmic reticulum stress. *Mol Biol Cell* 10, 3787-3799, doi:10.1091/mbc.10.11.3787 (1999).

393 Liu, C. Y., Wong, H. N., Schauerte, J. A. & Kaufman, R. J. The protein kinase/endoribonuclease IRE1alpha that signals the unfolded protein response has a luminal N-terminal ligand-independent dimerization domain. *J Biol Chem* 277, 18346-18356, doi:10.1074/jbc.M112454200 (2002).

394 Yanagitani, K. *et al.* Cotranslational targeting of XBP1 protein to the membrane promotes cytoplasmic splicing of its own mRNA. *Mol Cell* 34, 191-200, doi:10.1016/j.molcel.2009.02.033 (2009).

395 Calfon, M. *et al.* IRE1 couples endoplasmic reticulum load to secretory capacity by processing the XBP-1 mRNA. *Nature* 415, 92-96, doi:10.1038/415092a (2002).

396 Garzia, A. *et al.* The E3 ubiquitin ligase and RNA-binding protein ZNF598 orchestrates ribosome quality control of premature polyadenylated mRNAs. *Nat Commun* 8, 16056, doi:10.1038/ncomms16056 (2017).

397 Matthews, H. K., Bertoli, C. & de Bruin, R. A. M. Cell cycle control in cancer. *Nat Rev Mol Cell Biol* 23, 74-88, doi:10.1038/s41580-021-00404-3 (2022).

398 Wu, C. C. C. *et al.* Ribosome Collisions Trigger General Stress Responses to Regulate Cell Fate. 182, 404-416.e414, doi:10.1016/j.cell.2020.06.006 (2020).

399 Adamson, B. *et al.* A Multiplexed Single-Cell CRISPR Screening Platform Enables Systematic Dissection of the Unfolded Protein Response. *Cell* 167, 1867-1882 e1821, doi:10.1016/j.cell.2016.11.048 (2016).

400 Metzger, M. B., Pruneda, J. N., Klevit, R. E. & Weissman, A. M. RING-type E3 ligases: master manipulators of E2 ubiquitin-conjugating enzymes and ubiquitination. *Biochim Biophys Acta* 1843, 47-60, doi:10.1016/j.bbamcr.2013.05.026 (2014).

401 Thoreen, C. C. *et al.* A unifying model for mTORC1-mediated regulation of mRNA translation. *Nature* 485, 109-113, doi:10.1038/nature11083 (2012).

402 Shah, P., Ding, Y., Niemczyk, M., Kudla, G. & Plotkin, J. B. Rate-limiting steps in yeast protein translation. *Cell* 153, 1589-1601, doi:10.1016/j.cell.2013.05.049 (2013).

403 Wang, C., Han, B., Zhou, R. & Zhuang, X. Real-Time Imaging of Translation on Single mRNA Transcripts in Live Cells. *Cell* 165, 990-1001, doi:10.1016/j.cell.2016.04.040 (2016).

404 Yan, X., Hoek, T. A., Vale, R. D. & Tanenbaum, M. E. Dynamics of Translation of Single mRNA Molecules In Vivo. *Cell* 165, 976-989, doi:10.1016/j.cell.2016.04.034 (2016).

405 Leppek, K., Das, R. & Barna, M. Functional 5' UTR mRNA structures in eukaryotic translation regulation and how to find them. *Nat Rev Mol Cell Biol* 19, 158-174, doi:10.1038/nrm.2017.103 (2018).

406 Basu, I., Gorai, B., Chandran, T., Maiti, P. K. & Hussain, T. Selection of start codon during mRNA scanning in eukaryotic translation initiation. *Commun Biol* 5, 587, doi:10.1038/s42003-022-03534-2 (2022).

407 Kozak, M. Effects of long 5' leader sequences on initiation by eukaryotic ribosomes in vitro. *Gene Expr* 1, 117-125 (1991).

408 Jasencakova, Z. & Groth, A. Restoring chromatin after replication: how new and old histone marks come together. *Semin Cell Dev Biol* 21, 231-237, doi:10.1016/j.semcdb.2009.09.018 (2010).

409 Haimov, O., Sinvani, H. & Dikstein, R. Cap-dependent, scanning-free translation initiation mechanisms. *Biochim Biophys Acta* 1849, 1313-1318, doi:10.1016/j.bbagrm.2015.09.006 (2015).

410 McGlincy, N. J. & Ingolia, N. T. Transcriptome-wide measurement of translation by ribosome profiling. *Methods* 126, 112-129, doi:10.1016/j.ymeth.2017.05.028 (2017).

411 Young, D. J., Guydosh, N. R., Zhang, F., Hinnebusch, A. G. & Green, R. Rli1/ABCE1 Recycles Terminating Ribosomes and Controls Translation Reinitiation in 3'UTRs In Vivo. *Cell* 162, 872-884, doi:10.1016/j.cell.2015.07.041 (2015).

412 Sharma, P., Wu, J., Nilges, B. S. & Leidel, S. A. Humans and other commonly used model organisms are resistant to cycloheximide-mediated biases in ribosome profiling experiments. *Nat Commun* 12, 5094, doi:10.1038/s41467-021-25411-y (2021).

413 Chyzynska, K., Labun, K., Jones, C., Grellscheid, S. N. & Valen, E. Deep conservation of ribosome stall sites across RNA processing genes. *NAR Genom Bioinform* 3, lqab038, doi:10.1093/nargab/lqab038 (2021).

414 Stein, K. C., Morales-Polanco, F., van der Lienden, J., Rainbolt, T. K. & Frydman, J. Ageing exacerbates ribosome pausing to disrupt cotranslational proteostasis. *Nature* 601, 637-642, doi:10.1038/s41586-021-04295-4 (2022).

Acknowledgements

I'm grateful for everyone who supported me on my PhD journey.

Most of all, I am grateful to have Danny as my mentor. You gave me the opportunity to experience science and the scientific community in every detail. Your trust and support over the years were fundamental for my success. Your many ideas and guidance not only developed a great project, but also helped me to grow personally to become a great scientist. I will never forget that you believed in me from the beginning on; we started a new journey together, as you started your own first lab and let me be part of it. Thank you for your scientific and personal support throughout these years!

Thank you to the members of my thesis advisory committee, Peter Murray, Sebastian Bultmann, and Dieter Edbauer. I am thankful for the time you invested to discuss and improve the progress of my PhD project.

Thank you to the IMPRS-LS graduate school. Your numerous courses and social activities made it easy to be part of the campus and PhD life. With the program, we could meet fellow PhD candidates and learn from their experience. But most importantly, I met people who became close friends. To Laura and Jasmin: bars and clubs might end, but not our friendship.

I am grateful for everyone in Danny's lab – a supportive group of young scientists that slowly but steadily grew in number. Although Covid made it tricky sometimes, I always enjoyed your company. I hope you continue and honor the "timer-cake" in the future, so that there will always be regular cake sessions in the lab. A special thank you to Drew, who started the PhD with me as my computational counterpart in the lab (I think it was the better choice we both stuck to what we are best in!). Many thanks also to Sergio who helped me with my analysis. I cannot believe you are both still friendly with me and that we came through my initial lack of understanding and skepticisms. Thank you for your patience!

I am very grateful to Bianca, who supported me with all the coffee I needed. Thank you for being the go-to person for scientific and personal problems. The LM department was a great environment for science and for meeting people alike. I met great scientists who kept me sane at work by having a coffee or a beer break on the terrace and discussing science, among other things. Thommy, you were my center of calmness and stability. Kalle, you became a retreat from science during countless nights at work. Lorenzo, you were always there for me when I needed a break and listened when I needed an open ear. Barbara, you always had my back; you were always up for a chat, honest, and persistent. Thank you all for being there as my friends and motivating me to go on!

But also outside of work, I had so many people supporting me, even though this sometimes meant dragging me out of the lab. Thank you to the "Süß & Fruchtig" crew and my friends from my studies – Jakob, Krisi, and Roman – for always listening to and advising me. And if not advising me, just being there and distracting me. I'm grateful that even after our academic paths drifted apart, I can rely on your friendship and count on your comfort. A major thank you to Yanina and Sabrina! Even though my science talk was not understandable so many times, you kept believing in me and motivated me over and over again!

Lastly, I want to thank my family, who always supported me in every possible way. Mom and Dad thank you for always being there, I wouldn't have managed all of this without you. I love you.